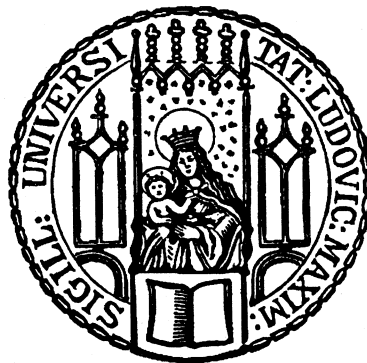


# Proteomic characterization of microglial dysfunction and repair mechanisms in Alzheimer's disease

Laura Sebastián Monasor



Graduate School of  
Systemic Neurosciences  
LMU Munich



Dissertation der Graduate School of Systemic Neurosciences  
der Ludwig-Maximilians-Universität München

October 2020



**Supervisor:** Dr. Sabina Tahirovic  
Ex vivo Models  
Deutsches Zentrum für Neurodegenerative Erkrankungen  
e. V. (DZNE), Munich

**First Reviewer:** Dr. Sabina Tahirovic  
**Second Reviewer:** Prof. Dr. Dieter Edbauer  
**Third Reviewer:** Prof. Dr. Arthur Liesz  
**External Reviewer:** Dr. Annett Halle

**Date of Submission:** 2<sup>nd</sup> of October 2020  
**Date of Defense:** 9<sup>th</sup> of February 2021



*To my grandparents, Valentín and Puri,  
who I wish, never had to inspire me to study this disease*

*A mis abuelos, Valentín y Puri,  
quienes ojalá nunca me hubieran inspirado a estudiar esta enfermedad*

# Table of Contents

Table of Contents .....	6
Abstract.....	9
Introduction.....	11
<b>1. Alzheimer’s disease .....</b>	<b>11</b>
1.1. Pathophysiology of AD .....	11
1.1.1. The A $\beta$ peptide.....	12
1.1.2. A $\beta$ pathology.....	14
1.1.3. Neurofibrillary tangles and dystrophic neurites .....	15
1.1.4. Neuroinflammation.....	16
1.2. The amyloid cascade hypothesis.....	18
1.3. Etiology of AD.....	19
1.4. Mouse models of AD .....	20
<b>2. Microglia as central player in health and disease .....</b>	<b>22</b>
2.1. Microglial ontogeny .....	22
2.2. Physiological role of microglia in the CNS .....	23
2.2.1. Molecular characterization of homeostatic microglia .....	25
2.3. Microglia in AD: “a double-edge sword” .....	26
2.3.1. Mechanisms A $\beta$ clearance in the CNS .....	27
2.3.2. Microglial deficiency of A $\beta$ clearance in AD.....	28
2.3.3. Molecular characterization of AD microglia .....	30
<b>3. Modulation of microglia as therapeutic approach for AD .....</b>	<b>32</b>
3.1. Anti-A $\beta$ therapies: active and passive immunization .....	32
3.2. Other microglial immunomodulation approaches .....	33
3.3. GM-CSF as potential immunomodulator of AD microglia .....	34
<b>Aims of the study .....</b>	<b>37</b>
<b>Materials and Methods.....</b>	<b>38</b>
<b>1. Materials .....</b>	<b>38</b>
1.1. Laboratory equipment and general consumables.....	38
1.2. Cell culture equipment and consumables.....	38
1.3. Surgical instruments .....	39
1.4. Microscopy equipment.....	39
1.5. Mass spectrometry and FACS equipment .....	39
1.6. Mouse lines .....	39
1.7. Reagents, solutions and consumables for different applications.....	40
1.7.1. Genotyping of transgenic mouse lines.....	40
1.7.2. Microglia isolation, in vitro and ex vivo assays.....	41
1.7.3. Mouse procedures: <i>in vivo</i> treatments and histology.....	43
1.7.4. Biochemistry: Western blotting.....	46
1.8. Software.....	49
<b>2. Methods .....</b>	<b>50</b>

2.1.	Genotyping of transgenic mouse lines .....	50
2.1.1.	PCR program for APPPS1 genotyping .....	50
2.1.2.	PCR program for APP <sup>NL-G-F</sup> genotyping .....	51
2.2.	Microglia isolation, <i>in vitro</i> and <i>ex vivo</i> assays.....	51
2.2.1.	Microglia isolation .....	51
2.2.2.	Microglial phagocytosis of labelled- <i>E.coli</i> particles.....	52
2.2.3.	FACS analysis.....	52
2.2.4.	Preparation of organotypic brain slices and GM-CSF treatments.....	53
2.3.	Mouse procedures .....	54
2.3.1.	GM-CSF treatments of APP-KI mice .....	54
2.3.2.	Histology.....	56
2.4.	Immunofluorescence analyses: image acquisition and quantifications .....	58
2.4.1.	Analysis of plaque load and proliferation upon GM-CSF treatments <i>in vivo</i> and <i>ex vivo</i> .....	59
2.4.2.	Analysis of microglia recruitment, plaque size, dystrophic neurites and CD68 coverage area in APPPS1 and APP-KI mice .....	60
2.4.3.	Analysis of A $\beta$ and pE3-A $\beta$ coverage area in APPPS1 and APP-KI mice.....	60
2.5.	Biochemistry .....	61
2.5.1.	Western blotting analysis for microglial proteome validation .....	61
2.5.2.	Western blotting using mouse tissue for A $\beta$ quantification.....	62
2.6.	Proteomic analysis .....	63
2.6.1.	Sample processing .....	63
2.6.2.	Mass spectrometry analysis.....	63
2.6.3.	Data analysis.....	64
2.7.	Statistical analysis.....	65
<b>Results .....</b>		<b>66</b>
<b>1. Characterization of microglial proteome dynamics along AD progression.....</b>		<b>66</b>
1.1.	Amyloid plaque burden in APPPS1 and APP-KI mouse models: definition of pathological stages.. ..	66
1.2.	MACS microglial isolation enables proteomic analysis of AD microglia .....	67
1.3.	Microglial proteome changes appear earlier in APPPS1 than in APP-KI mice.....	68
1.4.	Identification of Microglial A $\beta$ Response Proteins (MARPs).....	72
1.5.	Microglial proteomic and transcriptomic changes in response to A $\beta$ only partially overlap... ..	75
1.6.	Gene ontology analysis of MARP signatures .....	77
1.7.	Microglial AD risk genes are altered in APPPS1 and APP-KI proteomes .....	80
1.8.	MARPs are detected in microglia recruited at amyloid plaques .....	81
1.9.	APPPS1 and APP-KI plaques show different structural properties.....	90
1.10.	Microglial recruitment is triggered by fibrillar A $\beta$ .....	92
1.11.	Phagocytic deficiency correlates with the presence of fibrillar A $\beta$ and acquisition of MARP signatures .....	96
<b>2. Testing the potential of GM-CSF for microglial repair .....</b>		<b>97</b>
2.1.	GM-CSF induces A $\beta$ plaque clearance in APP-KI organotypic brain slices .....	97
2.2.	Short-term GM-CSF treatment does not modulate microglial A $\beta$ clearance <i>in vivo</i> .....	98

2.3. Long-term GM-CSF treatment is not sufficient to enhance microglial A $\beta$ clearance <i>in vivo</i> .....	103
<b>Discussion.....</b>	<b>107</b>
<b>1. MARP signatures characterize microglial response to A<math>\beta</math> along AD progression.....</b>	<b>107</b>
1.1. Early-MARPs reflect a protective but frustrated microglial response to A $\beta$ .....	108
1.1.1. Increase of immune-response mechanisms.....	108
1.1.2. Stimulation of the endo-lysosomal system.....	109
1.2. Middle-MARPs show a metabolic switch and loss of microglial homeostatic functions.....	111
1.2.1. Increase of lipid and glucose metabolism.....	111
1.2.2. Increment of exosome biogenesis and pro-inflammatory signaling.....	112
1.2.3. Progressive loss of microglial homeostatic functions.....	113
1.3. Advanced-MARPs reflect an aged and dysfunctional microglial phenotype.....	115
1.3.1. Continued increase in glucose and lipid metabolism.....	116
1.3.2. Alterations in endo-lysosomal system and oxidative stress.....	116
1.3.3. Enhanced reduction of homeostatic signatures.....	117
1.3.4. DNA destabilization and senescence.....	118
1.4. MARP signatures reflect a continuum of microglial changes along AD pathology.....	119
<b>2. A<math>\beta</math> conformation determines microglial recruitment and acquisition of MARP signatures.....</b>	<b>119</b>
<b>3. Fibrillar A<math>\beta</math> is associated to acquisition of MARP signatures and phagocytic impairment.....</b>	<b>120</b>
<b>4. The challenge of microglial immunomodulation in AD.....</b>	<b>122</b>
<b>5. Conclusions.....</b>	<b>124</b>
<b>Appendix.....</b>	<b>125</b>
1. Microglial proteomic analysis from GM-CSF-treated APP-KI mice (raw data).....	125
2. Step-by-step mouse microglia isolation protocol.....	135
3. Self-programmed ImageJ macro for analysis of A $\beta$ load.....	138
<b>References.....</b>	<b>140</b>
<b>List of Figures.....</b>	<b>162</b>
<b>List of Tables.....</b>	<b>164</b>
<b>List of Abbreviations.....</b>	<b>165</b>
<b>Acknowledgements.....</b>	<b>172</b>
<b>Affidavit/Eidesstattliche Versicherung.....</b>	<b>174</b>
<b>Author contributions.....</b>	<b>175</b>

## Abstract

Alzheimer's disease (AD) is a progressive neurodegenerative disease and it is the most common cause of dementia in the elderly. It is characterized by the presence of extracellular A $\beta$  plaques, intracellular neurofibrillary tangles and neuroinflammation. Despite the incessant efforts to find effective treatments, to date, there is no cure for AD. Microglia, as the brain resident immune cells, are the first line of defense in the brain and contribute to A $\beta$  plaque clearance. Numerous genetic alterations have been identified in microglial genes that confer risk to develop late-onset AD, mainly associated to the deficiency of microglia to clear A $\beta$  plaques. Therefore, the molecular characterization of microglia has become a priority to find novel therapeutic options for AD patients. Different studies have analyzed microglia at the transcriptome level in AD, but this characterization has not been thoroughly performed at the proteome level. In addition, various approaches have been directed to modulate or repair microglial function in AD. However, the molecular signatures of repaired microglia have not been elucidated, which would facilitate the design of more effective microglial immunomodulatory strategies for AD.

Thus, in this study, I aimed to characterize microglial proteomic fingerprints along AD progression and to reveal the proteomic signatures of functionally repaired microglia. For the first aim, I analyzed microglia from two different amyloidosis mouse models, the APPPS1 and the APP<sup>NL-G-F</sup> (APP-KI), at different stages of AD. Mass spectrometry-based proteomic analysis revealed a panel of time-resolved microglial A $\beta$ -response protein changes or MARP signatures, that were commonly regulated in both mouse models, and reflected the molecular changes occurring in microglia during different phases of amyloid accumulation (early, middle and advanced). Interestingly, despite the similar amyloid load observed in both AD models, APPPS1 microglia showed earlier proteomic changes than APP-KI microglia, which correlated with the presence of fibrillar A $\beta$  and phagocytic impairment. This study provides a valuable resource of time-resolved microglial proteome changes along with their functional consequences, which will help to identify novel molecular targets for microglial repair and AD biomarkers.

In order to reveal the proteomic signatures of functionally repaired microglia, I used the hematopoietic growth factor GM-CSF, as a microglial immunomodulatory tool, which showed the potential to reduce A $\beta$  load *ex vivo* and *in vivo*. Although GM-CSF treatment stimulated microglial phagocytosis and led to a strong reduction of A $\beta$  burden in organotypic brain slices from APP-KI mice, this effect could not be recapitulated *in vivo*. Accordingly, I could not detect major changes in the microglial proteome upon GM-CSF treatment. Thus, new strategies are

needed to unravel the molecular fingerprints of repaired microglia. Despite the challenges to significantly reduce amyloid plaque burden in amyloidosis mouse models, microglia immunomodulation still holds a great potential for the development of effective treatments for AD patients.

# Introduction

## 1. Alzheimer's disease

Alzheimer's disease (AD) is the most prevalent cause of dementia in the elderly that accounts for 60-80% of all cases. It is a neurodegenerative disease that progressively affects memory, language, reasoning and movement, which interfere with the person's daily life and ultimately leads to death (Association, 2020). AD is thought to start affecting the brain around 20 years before the first symptoms are noticeable and has an average duration of 8 to 10 years (Masters *et al*, 2015; Association, 2020). Worldwide, there are 47 million people living with AD and this number is expected to rise to 76 million by 2030. For this reason, AD is considered a global epidemic ([www.alz.org](http://www.alz.org)) with an enormous socioeconomic impact. Despite the ceaseless efforts to understand the disease and find a cure, to date there are no effective treatments to stop or delay AD progression. Therefore, the World Health Organization has acknowledged AD as a public health priority (Lane *et al*, 2018).

### 1.1. Pathophysiology of AD

Alzheimer's disease was first identified in 1906 by the German psychiatrist and neuropathologist, Alois Alzheimer, from a 51-year-old female patient, Auguste Dieter, that exhibited an unusual dementia. Auguste Dieter suffered from progressive memory loss, disorientation and hallucinations as main symptoms and was hospitalized into mental institution (Irrenschloss) in Frankfurt am Main (Germany). After she died, Alzheimer's post-mortem neuropathological examination revealed the presence of brain atrophy (Figure 1), arteriosclerotic vasculature, neurofibrillary tangles, cortical neuronal loss, gliosis and abundant cortical deposits ("military foci") of what he described as "an unknown" substance (Alzheimer, 1907; Alzheimer *et al*, 1995). This unknown substance was later identified as Amyloid- $\beta$  peptide (A $\beta$ ), the major component of amyloid deposits found in the brain parenchyma and vasculature of AD and Down's syndrome patients, who also develop AD pathology (Masters *et al*, 1985; Glenner, 1989). Although AD has been studied for over 100 years and major progress has been made in understanding the disease, especially at the molecular level, the main pathological features were already characterized in Alzheimer's case report (Alzheimer *et al*, 1995; Holtzman *et al*, 2011). Extracellular A $\beta$  plaques (amyloid plaques) and neurofibrillary tangles are the two hallmarks required for the pathological post-mortem diagnosis of AD and to date, the most accurate way to diagnose AD (DeTure & Dickson, 2019).

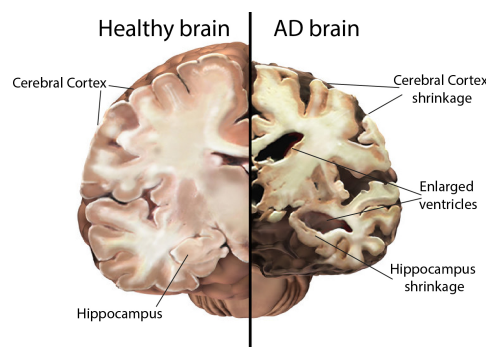


**Figure 1. AD brain atrophy compared to healthy brain.**

Brain slice from an advanced-stage AD patient showing different signs of brain atrophy like hippocampus and cortical shrinkage and enlarged ventricles compared to a healthy brain architecture. Modified from <https://www.alz.org/>

### 1.1.1. The A $\beta$ peptide

#### 1.1.1.1. APP processing

The amyloid precursor protein (APP), is a type I single-pass transmembrane protein, which presents three major isoforms of different length generated by alternative splicing. The APP<sub>695</sub> isoform is predominantly expressed by neurons, while APP<sub>751</sub> and APP<sub>770</sub> isoforms can be found in peripheral tissues (Muller *et al.*, 2017). Although the physiological role of APP has still not been fully elucidated, it has been ascribed to neuronal- and synapto-trophic properties, axonal growth and guidance, synaptogenesis, and learning and memory, among other functions (Muller & Zheng, 2012; Dawkins & Small, 2014; Muller *et al.*, 2017).

In AD, amyloid plaques are found as extracellular aggregates of A $\beta$  peptide that aberrantly accumulate in the brain parenchyma (Holtzman *et al.*, 2011). A $\beta$  is a ~4 kDa peptide generated by sequential proteolytic cleavage from APP by two proteases, the  $\beta$ - and  $\gamma$ -secretases (Figure 2) (Haass & Selkoe, 1993; Selkoe, 2001). The mechanism of APP processing that leads to A $\beta$  formation is known as the amyloidogenic pathway and starts with the cleavage of APP in its extracellular region by the  $\beta$ -secretase BACE1 ( $\beta$ -site APP-cleaving enzyme), giving rise to a soluble APP fragment (APP $\beta$ ) and a membrane-bound C-terminal fragment (CTF $\beta$  or C99) (Figure 2). The CTF $\beta$  fragment is subsequently cleaved by the tetrameric  $\gamma$ -secretase complex (APH1, PEN2, nicastrin and presenilin-PS1 or PS2-), that depending on the exact location of this cleavage, can generate A $\beta$  species of different length (37-43 amino acids or longer) and the APP intracellular domain (AICD) (Figure 2) (Haass & Selkoe, 1993; Selkoe, 2001; Edbauer *et al.*, 2003; Haass, 2004; Steiner *et al.*, 2018). The most abundant A $\beta$  species are A $\beta$ 40 (~80-90%) and A $\beta$ 42 (~5-10%) (Murphy & LeVine, 2010). The A $\beta$ 42 are the major species found in amyloid plaques (also known as senile plaques), which are more hydrophobic and prone to aggregate and fibrillarize

(Iwatsubo *et al*, 1994; Haass, 2004; Murphy & LeVine, 2010). Modified (N-terminally truncated) A $\beta$  species, such as Pyroglutamate (pE3-A $\beta$ ), have also been found in great amounts in human AD plaques (Saido *et al*, 1995). These modified species show a high aggregation propensity and neurotoxicity and have been reported to appear in early AD pathology in human patients and at advanced pathological stages in AD mouse models (Frost *et al*, 2013). A third secretase, the  $\alpha$ -secretase, impedes A $\beta$  generation by cleaving APP within the A $\beta$  amino acid sequence and generates a soluble APP fragment (APP $\alpha$ ) and a transmembrane C-terminal fragment (CTF $\alpha$  or C83) (Figure 2) (Sisodia *et al*, 1990; De Strooper *et al*, 1993). The CTF $\alpha$  fragment can be further cleaved by the  $\gamma$ -secretase complex, generating a 3 KDa peptide (p3) and an AICD (Haass *et al*, 1993; Cao & Sudhof, 2001). This alternative mechanism of APP processing is known as non-amyloidogenic pathway (Kojro & Fahrenholz, 2005) (Figure 2).

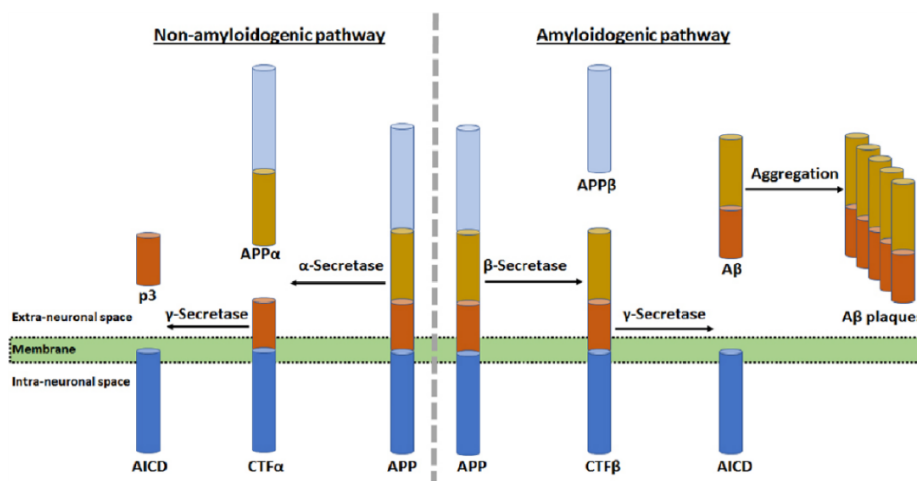


**Figure 2. APP processing and A $\beta$  plaque formation.**

Scheme showing the two alternative pathways of APP processing. The amyloidogenic pathway involves a first cleavage of APP by a  $\beta$ -secretase generating a soluble APP $\beta$  fragment and membrane-bound CTF $\beta$  fragment. A second cleavage by the  $\gamma$ -secretase complex generates an AICD and the A $\beta$  peptide, which after aggregation leads to the formation of amyloid plaques. The non-amyloidogenic pathway precludes A $\beta$  generation and involves the cleavage of APP by an  $\alpha$ -secretase, leading to the generation of a soluble APP $\alpha$  fragment and a membrane-bound CTF $\alpha$ , which can be further cleaved by the  $\gamma$ -secretase complex producing an AICD and the soluble peptide p3. Scheme retrieved from (Das *et al*, 2019), <http://creativecommons.org/licenses/by-sa/4.0/>.

### 1.1.1.2. Physiological and pathogenic roles of A $\beta$ peptide

Despite the pathogenicity associated to A $\beta$  in AD, this peptide is generated under physiological conditions throughout the lifespan of an individual, and can be detected in body fluids like cerebrospinal fluid (CSF) and plasma (Selkoe & Schenk, 2003) (Brothers *et al*, 2018; Holtzman *et al*, 2011; Puig & Combs, 2013). The physiological function of A $\beta$  has been associated to different mechanisms such as protection against infections, modulation of synaptic activity, neuronal

survival or memory enhancement (Morley *et al*, 2010; Puzzo *et al*, 2011; Brothers *et al*, 2018). However, while low (physiological) levels of A $\beta$  might have beneficial functions, high levels (pathological) lead to detrimental effects (Morley & Farr, 2012; Morley *et al*, 2019). The imbalance between A $\beta$  production and clearance mechanisms is thought to be the cause of A $\beta$  accumulation and amyloid pathology (Mawuenyega *et al*, 2010; Saido & Leissring, 2012).

Secreted soluble monomeric A $\beta$  peptides can self-assemble into oligomers, which aggregate to form proto-fibrils and finally fibrils that present a typical  $\beta$ -sheet structure (Finder & Glockshuber, 2007; Ahmed *et al*, 2010). Both A $\beta$ 40 and A $\beta$ 42 are capable of forming different aggregate conformations (Friedrich *et al*, 2010). However, A $\beta$ 42 has shown a higher propensity to oligomerize and aggregate than A $\beta$ 40 (Bitan *et al*, 2003). Neurotoxicity associated to A $\beta$  has been linked to induction of oxidative stress, membrane disruption, apoptosis or inflammation (Soto, 2003). Although some studies have shown evidence of the neuronal toxicity associated to fibrillar A $\beta$  (Geula *et al*, 1998; Yankner & Lu, 2009), soluble oligomers have been proposed as the most harmful A $\beta$  form, linked to synaptic dysfunction and cognitive decline. In fact, the levels of A $\beta$  oligomers showed a better correlation with AD symptoms and synapse loss than fibrillar deposits (Finder & Glockshuber, 2007). Nevertheless, insoluble deposits might act as a reservoir of oligomeric forms (Haass & Selkoe, 2007; Koffie *et al*, 2009). The pathogenicity associated to the A $\beta$  oligomers led to the creation of the “A $\beta$  oligomer hypothesis”, which postulates oligomeric A $\beta$  forms as the major contributors to AD pathogenesis (Lambert *et al*, 1998; Cline *et al*, 2018). Overall, changes driven by aging or genetic modifications can cause an increase in A $\beta$  generation and/or reduced degradation and clearance that result in A $\beta$  accumulation and aggregation in amyloid plaques (Haass, 2004; Pearson & Peers, 2006).

### 1.1.2. A $\beta$ pathology

The main types of extracellular A $\beta$  plaques, which are most frequently observed in the brain parenchyma of AD patients, are dense-core and diffuse plaques (Holtzman *et al*, 2011; DeTure & Dickson, 2019). Dense-core plaques present a compacted fibrillar ( $\beta$ -sheet conformation) amyloid core that strongly stains with amyloid dyes (bind to  $\beta$ -sheet structures) such as Thioflavin S, Congo red or Thiazine red, and a surrounding halo of less compacted A $\beta$ , where A $\beta$  oligomers can be found (Figure 3A) (Selkoe, 2001; Koffie *et al*, 2009; van Groen *et al*, 2011; DeTure & Dickson, 2019). These dense-core plaques are usually associated with reactive microglia and astrocytes as well as dystrophic neurites and synaptic loss (Selkoe, 2001; DeTure & Dickson, 2019). Diffuse amyloid plaques are composed of uncompacted and non-fibrillar A $\beta$  that present an amorphous

structure and are stained weakly with amyloid-specific dyes (Figure 3B). These plaques do not seem to trigger glial reactivity in AD brains (Selkoe, 2001; Holtzman *et al.*, 2011; van Groen *et al.*, 2011; DeTure & Dickson, 2019) and have been suggested to represent an early, immature stage of amyloid plaques that can be also found during normal aging (Selkoe, 2001; DeTure & Dickson, 2019). Another type of extracellular deposits are the ones found in cerebral blood vessels, which can impair blood flow and cause ischemic lesions (Figure 3C). This pathological feature is known as cerebral amyloid angiopathy (CAA) and it is present in 85-95% of AD cases (DeTure & Dickson, 2019).

The gradual distribution and extension of A $\beta$  pathology with aging and AD progression in the human brain, has been classified in amyloid stages or phases. Initially, the Braak system defined 3 stages of amyloid deposition: in the stage A, the basal frontal and temporal lobes are affected, followed by neocortices and hippocampus in the stage B, and finally, extending into the cortices, subcortical nuclei and cerebellum in the stage C. Additionally, they defined different stages (I-VI) for the classification of neurofibrillary pathology (Braak & Braak, 1997). A more recent staging system was proposed by Dietmar Thal, who defined 5 phases: the neocortex is affected in the Thal phase 1, extending into the allocortex in the phase 2, then, to the subcortical nuclei and the striatum in the phase 3, and finally reaching into the brainstem in the phase 4 and the cerebellum in the phase 5 (Thal *et al.*, 2002).

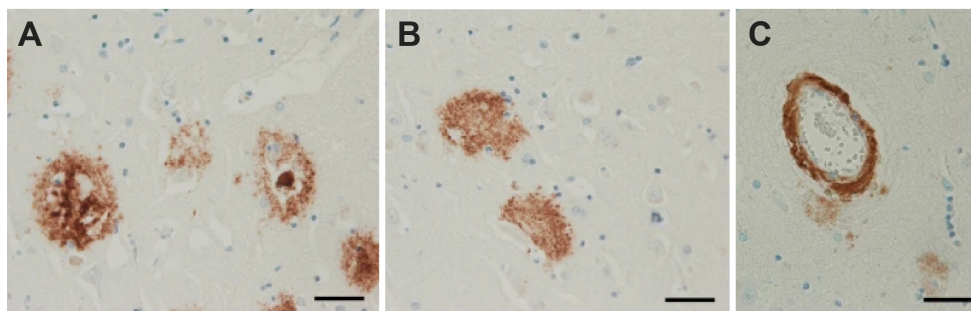


**Figure 3. Main types of extracellular A $\beta$  deposits in human AD brains.**

Immunohistochemical visualization of A $\beta$  plaques from human AD patients showing dense core plaques (A), diffuse plaques (B) and CAA deposits (C). Scale bars: 40  $\mu$ m. Modified from (DeTure & Dickson, 2019) <http://creativecommons.org/licenses/by-sa/4.0/>

### 1.1.3. Neurofibrillary tangles and dystrophic neurites

TAU is the main microtubule associated protein (MAP) in mature neurons, mostly found in the neuronal axon. It is involved in the assembly and stability of microtubules and its function is regulated by phosphorylation (Iqbal *et al.*, 2005; Spires-Jones & Hyman, 2014). In AD, TAU is

aberrantly hyperphosphorylated (p-TAU) and aggregates in the somatodendritic compartment forming intraneuronal paired helical filaments (PHF) and occasionally, also straight filaments, that give rise to neurofibrillary tangles (NFT) (Figure 4A and B) (Wisniewski *et al*, 1976; Iqbal *et al.*, 2005; Spires-Jones & Hyman, 2014). Extracellular NFT can remain in the brain parenchyma after neurons have died and are known as ghost tangles (Figure 4A) (Spires-Jones & Hyman, 2014). Hyperphosphorylated TAU filaments are also found in dystrophic neurites occurring at amyloid plaques and in the neuropil (neuropil threads) (Grundke-Iqbal *et al*, 1986; Iqbal *et al*, 2010). Dystrophic neurites are described as bulbous swellings of mainly axonal origin that are found associated to senile plaques and form, the so called, neuritic plaques (Figure 4B) (Benzing *et al*, 1993; DeTure & Dickson, 2019). Besides TAU aggregates, dystrophic neurites can accumulate APP, synaptic, neurofilament and ubiquitin proteins, but also, lysosomal vesicles and degenerating mitochondria, indicative of impaired neuronal function that affects cytoskeleton integrity, intracellular trafficking and degradation processes (DeTure & Dickson, 2019). NFT pathology and neuritic plaques have shown to correlate well with cognitive decline and neuronal loss in AD (Spires-Jones & Hyman, 2014; DeTure & Dickson, 2019).

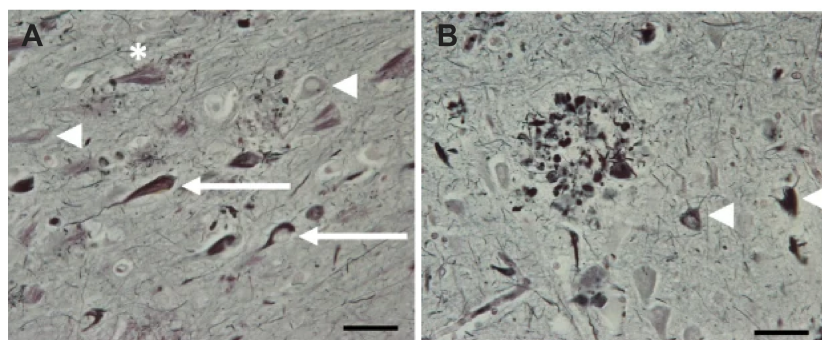


**Figure 4. Neurofibrillary tangles and dystrophic neurite pathology in AD brains.**

Silver staining showing NFT (A) and dystrophic neurites from a neuritic plaque (B). In A, arrows indicate mature tangles, arrowheads pre-tangles and asterisk ghost tangles. In B, arrowheads indicate NFT. Scale bars: 40  $\mu\text{m}$ . Modified from (DeTure & Dickson, 2019) <http://creativecommons.org/licenses/by-sa/4.0/>.

#### 1.1.4. Neuroinflammation

Neuroinflammation has been defined as the activation of the brain innate immune system to protect the central nervous system (CNS) from damage (Zhang & Jiang, 2015). Alois Alzheimer was probably the first to observe signs of neuroinflammation in AD when he described the presence of more fibrous glia (likely astrocytes), and glia containing adipose saccules (probably microglia), in the brain of Auguste Dieter (Alzheimer, 1907; Alzheimer *et al.*, 1995). In fact, the presence of reactive microglia and astroglia associated to A $\beta$  plaques, and increased levels of inflammatory factors, have been consistently observed in AD patients and mouse models

(McGeer *et al*, 1987; Benzing *et al*, 1999; Akiyama *et al*, 2000; Wyss-Coray, 2006; Motta *et al*, 2007; Saito & Saido, 2018), feature that is considered as an important hallmark of AD (Zhang & Jiang, 2015). Astrocytes and microglia are some of the main glial cell types in the CNS, which play important functions. Astrocytes are key in maintaining brain homeostasis by providing trophic support to neurons, regulating synapses and maintaining the blood-brain-barrier (BBB) integrity and permeability. Instead, microglia are the brain resident immune cells and represent the first line of defense in the CNS protecting it against different insults and promoting tissue repair (Zhang & Jiang, 2015; Fakhoury, 2018) (microglial role in the CNS and AD is described in depth in section 2). In response to stimulation, such as A $\beta$ , both astrocytes and microglia transform morphologically (hypertrophic cell body and processes) and can release inflammatory factors such as cytokines, chemokines and reactive oxygen species (Zhang & Jiang, 2015). In AD, both glial cell types are found surrounding senile plaques (Figure 5). However, while microglial cell bodies are in close contact to the plaque cores (Figure 5A), astrocytes cell somas are located further away from them (Figure 5B). It has been shown that activated microglia in AD and other neurodegenerative diseases, induce reactivity of a subtype of astrocytes through the release of pro-inflammatory cytokines such as IL-1 $\alpha$ , TNF and C1q. Moreover these reactive astrocytes lose their beneficial functions and become toxic to neurons and oligodendrocytes (Liddelow *et al*, 2017). Besides their association to A $\beta$  plaques, astro- and microgliosis have also been found in the vicinity of NFT (Serrano-Pozo *et al*, 2011).

The role of neuroinflammation in AD, like in other neurodegenerative diseases, is complex, as both beneficial and detrimental effects have been associated to glial responses. It is being discussed if neuroinflammation might be the driving force or just a consequence of the disease process (Wyss-Coray, 2006). On one hand, microglia and astrocytes are involved in A $\beta$  clearance, thereby conferring protection. (Ries & Sastre, 2016; Kaur *et al*, 2019). On the other hand, reactive microglia and astrocytes can release pro-inflammatory factors such as IL-1 $\beta$ , IL-6 or TNF- $\alpha$ , that can lead to neurotoxicity (Kaur *et al.*, 2019). In addition, microglial reactivity might contribute to Tau pathology and spreading (Metcalf & Figueiredo-Pereira, 2010; Asai *et al*, 2015; Maphis *et al*, 2015), but also, to A $\beta$  plaques seeding (Parhizkar *et al*, 2019; Spangenberg *et al*, 2019).

It has been proposed that microglia and astrocytes may have a protective role in early disease stages by promoting A $\beta$  clearance, but their response becomes inefficient (decreased clearance) and even detrimental (neurotoxicity) as disease progresses (Wyss-Coray, 2006; Kaur *et al.*, 2019).

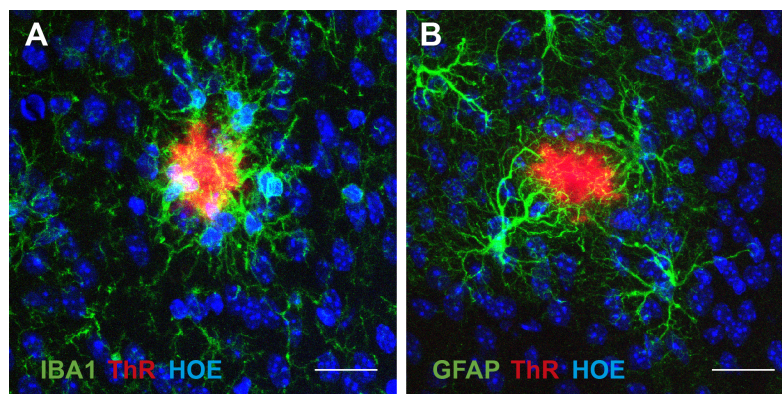


**Figure 5. Microglia and astrocytes cluster around A $\beta$  plaques.**

**A.** Microglia (IBA1, green) in close contact to the fibrillar plaque core stained with Thiazine-red (ThR, red). **B.** Astrocytes (GFAP, green) with cell soma located away from the plaque core (ThR, red). Scale bar: 20  $\mu$ m. Both images were generated using 3-month-old APPPS1 mice.

## 1.2. The amyloid cascade hypothesis

The amyloid cascade hypothesis, initially formulated by Hardy and Higgins in 1992 (Hardy & Higgins, 1992) and later updated in 2016 (Selkoe & Hardy, 2016), proposed that the accumulation and deposition of A $\beta$  peptide, is the first pathogenic event that triggers a cascade of pathological insults observed in AD, such as neurofibrillary tangles, cell loss, vasculature damage, neuroinflammation and ultimately dementia (Hardy & Higgins, 1992; Selkoe & Hardy, 2016). This hypothesis was grounded on the findings that mutations in either *APP* itself or *PSEN* lead to higher A $\beta$  generation and cause early onset AD. Moreover, Down syndrome patients, which present a trisomy in the chromosome 21, where *APP* gene is located, irrevocably develop A $\beta$  pathology at an early age (Hardy & Higgins, 1992; Selkoe & Hardy, 2016). Another piece of evidence that supports this hypothesis, is the presence of an *APP* missense mutation (A673T-Icelandic), that leads to a lifetime reduction of A $\beta$  production and aggregation and is protective against AD and cognitive decline (Jonsson *et al*, 2012). In addition, several neurotoxic effects have been directly attributed to A $\beta$  (Hardy & Higgins, 1992; Selkoe & Hardy, 2016). However, this hypothesis also received some criticism due to the fact that amyloid plaque load does not seem to correlate with cognitive impairment and neuronal loss, and non-demented individuals show substantial amyloid plaque load by Positron Emission Tomography (PET) imaging. In addition, although this hypothesis opened a window of optimism regarding the therapeutic targeting of A $\beta$  production (by  $\beta$ - and  $\gamma$ -secretase inhibitors) or A $\beta$  clearance (by active or passive immunization), so far, none of the clinical trials succeeded in stopping the development of AD (Ricciarelli & Fedele, 2017; Makin, 2018). Therefore, new intervention approaches to tackle AD are urgently needed.

### 1.3. Etiology of AD

There are two forms of AD, the rarest one, which accounts for 1-6% of all AD cases, is a familial form called FAD (familial AD). It is also known as early-onset AD (EOAD) due to the early presentation of the symptoms (30 to 60 years) (Bekris *et al.*, 2010; Holtzman *et al.*, 2011). FAD can be caused by mutations in *APP*, *PSEN1* or *PSEN2*, that are inherited in an autosomal dominant manner, reason why this AD form has also been described as autosomal-dominant AD (ADAD) (Bateman *et al.*, 2011). Over 32 different *APP* pathogenic mutations have been identified among 85 families, and most of these mutations are located surrounding the secretases cleavage sites on exons 16 and 17 (Bekris *et al.*, 2010; Bateman *et al.*, 2011). *APP* mutations alter the structural and biophysical properties of A $\beta$  and lead to higher aggregation capacity (Bateman *et al.*, 2011). The most common mutations affect the  $\gamma$ -secretase cleavage site and increase the ratio of A $\beta$ 42 to A $\beta$ 40, enhancing the aggregation and fibrillization properties of A $\beta$  and thereby, its A $\beta$  pathogenicity. However, some *APP* mutations like the Swedish, are located close to the  $\beta$ -secretase cleavage site and result in an increased generation of all A $\beta$  species. *PSEN* mutations also lead to the higher generation of A $\beta$ 42, or to the increase in the A $\beta$ 42 to A $\beta$ 40 ratio (Bateman *et al.*, 2011; Holtzman *et al.*, 2011).

The second and most common form of AD, which accounts for around 99% of all cases, is the “sporadic” (SAD) or “late onset” AD (LOAD). Although the clinical presentation of the disease is very similar to the FAD, the symptoms for LOAD usually start after 65 years of age and the incidence raises with age (Bateman *et al.*, 2011; Holtzman *et al.*, 2011). The cause for developing LOAD is thought to be driven by the interaction between genetic and environmental factors. Indeed, approximately 70% of the risk to develop LOAD may be associated to genetic factors (Lane *et al.*, 2018). The biggest genetic risk known for sporadic AD is the  $\epsilon$ 4 variant of the *APOE* gene, while  $\epsilon$ 2 variant is protective. Bearing one  $\epsilon$ 4 allele increases the risk for AD at around 3-fold, whereas carrying two alleles increases it by approximately 12-fold (Slooter *et al.*, 1998). In addition, the presence of the  $\epsilon$ 4 variant also decreases the age of onset by approximately 5 years per  $\epsilon$ 4 copy (Corder *et al.*, 1993). *APOE* is a plasma high density lipoprotein produced in high levels in the CNS, especially by astrocytes under physiological conditions. Although it is still not clear how *APOE* affects AD pathogenesis, different studies suggest that *APOE*, by binding to A $\beta$ , might influence the clearance and the aggregation of this peptide (Kim *et al.*, 2009a). Besides *APOE*, genome-wide association-studies (GWAS), whole genome sequencing analyses and gene-expression network analysis have identified novel genetic polymorphisms in or near more than 20 genes associated to LOAD risk, which are mainly involved in lipid metabolism, endocytosis

and immune response pathways (Bertram *et al.*, 2008; Harold *et al.*, 2009; Hollingworth *et al.*, 2011; Naj *et al.*, 2011; Lambert *et al.*, 2013; Karch & Goate, 2015; Sims *et al.*, 2017). Strikingly, some of those polymorphisms were found in genes that are expressed, in some cases exclusively, by microglia, including *SPI1*, *CR1*, *CD33*, *ABCA7*, *MS4A4s*, *TREM2* and *INPP5D*, among others (Efthymiou & Goate, 2017; McQuade & Blurton-Jones, 2019). It has been proposed that one of the main drivers of LOAD is the reduced A $\beta$  clearance that leads to the accumulation of A $\beta$  in the brain (Mawuenyega *et al.*, 2010; Lane *et al.*, 2018). In fact, some of the identified polymorphisms occur in genes implicated in microglial phagocytosis, such as *CD33*, *TREM2* and *ABCA7* (Efthymiou & Goate, 2017), which point to the involvement of microglia in AD etiology.

#### 1.4. Mouse models of AD

Animal mouse models represent important tools to understand the pathological mechanisms underlying diseases like AD, or to carry out pre-clinical testing of novel candidate drugs (Drummond & Wisniewski, 2017). Transgenic mice are the most used animal model for AD research with over 100 different genetically modified mouse lines available, that recapitulate some aspects of AD pathology. However, the majority of mouse models only mimic a specific pathological feature of AD, like amyloidosis or Tau pathology, but not both (Hall & Roberson, 2012; Drummond & Wisniewski, 2017). Although the mouse *App* gene shares 97% of the sequence with its human homologue, wild type (WT) mice do not develop A $\beta$  pathology due the differences in 3 amino acids within the mouse A $\beta$  sequence, that prevent A $\beta$  aggregation and formation of extracellular plaques (Xu *et al.*, 2015; Drummond & Wisniewski, 2017). The first successful mouse line (PDAPP) able to recapitulate consistent A $\beta$  pathology, was generated by the overexpression of the human *APP* (under the PDGF- $\beta$  promoter) bearing the Indiana human *APP* mutation (V717F) (Games *et al.*, 1995). Today many different transgenic lines exist expressing the human *APP* and/or *PSEN* with one or several FAD mutations. The onset and extent of A $\beta$  pathology largely depend on the specific mutation/s, the number of mutations, and the promoter that controls the expression of the transgene (physiological or constitutive) (Hall & Roberson, 2012; Drummond & Wisniewski, 2017). The most common promoters used to drive transgene overexpression in mouse lines are the PDGF- $\beta$  and Thy-1, which are specifically expressed in neurons, and the PrP, that is expressed in neurons and glia (Hall & Roberson, 2012). Some of the most frequently used transgenic mouse lines such as APP23, APPPS1 and 5XFAD, overexpress *APP* with one or several FAD mutations alone, or in combination with *PSEN* mutations (Table 1) (Hall & Roberson, 2012; Drummond & Wisniewski, 2017). Although these lines show a robust A $\beta$  pathology, gene overexpression might cause artificial effects. The more recent knock-in (KI)

mouse models ( $APP^{NL-F}$  and  $APP^{NL-G-F}$ ), avoid transgene overexpression and are generated by humanizing the mouse  $A\beta$  sequence and including FAD mutations, thereby enabling amyloid deposition, but maintaining the physiological  $APP$  expression (Table 1) (Saito *et al*, 2014; Drummond & Wisniewski, 2017).

Contrary to  $A\beta$  pathology, which is well recapitulated in AD mouse models, Tau pathology is not well mimicked in transgenic mice. Most mouse models of Tau pathology are generated by overexpression of mutated human Tau ( $MAPT$ ) (Table 1), using mutations that occur in another disease, frontotemporal dementia. However, Tau mutations have not been associated with AD (Hall & Roberson, 2012; Jankowsky & Zheng, 2017; King, 2018). Nevertheless, Tau models such as rTg4510 and PS19 develop p-TAU, NFT and neurodegeneration enabling studies of these pathological features in AD (Table 1) (Jankowsky & Zheng, 2017). In addition, few mouse models overexpressing both human  $MAPT$  and  $APP$  or  $PSEN$  mutations have been created in order to recapitulate both key AD pathological hallmarks,  $A\beta$  plaques and NFT. This is the case of the 3xTg line (Table 1).

Finally, another neurodegenerative feature of AD, dystrophic neurites, have been found in transgenic mice that present  $A\beta$  pathology, and thus, are also well recapitulated in AD mouse models (Li *et al*, 2016; Sadleir *et al*, 2016).

Overall, transgenic mouse models of AD mimic better  $A\beta$  than Tau pathology. Although amyloidosis mouse models are useful tools to study  $A\beta$  pathology and associated alterations, their strengths and limitations should be considered when using them for research.

Transgene	Mouse line	Mutation	Promoter	Plaques (months)	Reference
hAPP	Tg2576	APP-Swe	hamPrP	11	(Hsiao <i>et al</i> , 1996)
	APP23	APP-Swe	mThy-1	6	(Sturchler-Pierrat <i>et al</i> , 1997)
	J20	APP-Swe, Ind	hPDGF- $\beta$	6	(Mucke <i>et al</i> , 2000)
	$APP^{NL-F}$	APP-Swe, Iber	mApp	2	(Saito <i>et al</i> , 2014)
	$APP^{NL-G-F}$	APP-Swe, Art, Iber	mApp	2	(Saito <i>et al</i> , 2014)
hAPP/PSEN	APPPS1 (APPPS1-21)	APP-Swe PSEN1-L166P	mThy-1 mThy-1	1.5	(Radde <i>et al</i> , 2006)
	APP/PS1 (PS/APP)	APP-Swe PSEN1-M146L	hamPrP hPDGF- $\beta$	6	(Holcomb <i>et al</i> , 1998)

	5XFAD	<i>APP</i> -Swe, Lon, Flo <i>PSEN1</i> -M146L, L28V	mThy-1 mThy-1	2	(Oakley <i>et al</i> , 2006)
hTAU	rTg4510	<i>MAPT</i> -P301L	mPrP	-	(Ramsden <i>et al</i> , 2005; Santacruz <i>et al</i> , 2005)
	PS19	<i>MAPT</i> -P301S	mPrP	-	(Yoshiyama <i>et al</i> , 2007)
hTAU/ <i>APP</i> / <i>PSEN1</i>	3xTg	<i>MAPT</i> -P301L	mThy-1	6	(Oddo <i>et al</i> , 2003)
		<i>APP</i> -Swe <i>PSEN1</i> -M146L	mThy-1 mPs1		

**Table 1. Transgenic mouse models of AD.**

Examples of mouse lines commonly used in AD research. Abbreviations: Swe: Swedish, Ind: Indiana, Iber: Iberian, Lon: London, Flo: Florida, h: human, m: mouse, ham: hamster.

## 2. Microglia as central player in health and disease

Microglia are the brain resident immune cells and account for around 10% of all brain cells. In physiological conditions, they play important functions in the maintenance of brain homeostasis. Under neurodegenerating conditions, including AD, microglia mediate neuroprotective and neuroinflammatory responses, that -when sustained-, can lead to neurotoxicity (Colonna & Butovsky, 2017; Hansen *et al*, 2018).

### 2.1. Microglial ontogeny

Microglia were first discovered in 1919 by the Spanish neuroscientist Pío del Río Hortega, who named and characterized these glial cells based on their small soma, in a series of four papers “El Tercer Elemento de los Centros Nerviosos” (The Third Element of Neural Centers) (Río-Hortega, 1919c). Del Río Hortega described microglia as the brain phagocytic cells with mesodermal origin (Río-Hortega, 1919c, a, d, b; Sierra *et al*, 2016).

Since its first discovery 100 years ago, microglia have been deeply studied. The mesodermal origin of microglia proposed by Del Río Hortega, was confirmed in mice thanks to *in vivo* fate mapping studies. These studies showed that differing from the other brain cells of neuroectodermal origin (Stark, 2014), microglia originate from early primitive erythromyeloid progenitors (distinct from the one that give rise to peripheral monocytes) at embryonic day 7.5 (E7.5) in the yolk sac. Then, by E9.5 they migrate into the developing brain where they proliferate and colonize the whole brain parenchyma (Ginhoux *et al*, 2010; Ginhoux *et al*, 2013; Kierdorf *et al*, 2013; Hoeffel *et al*, 2015). Important transcription factors for the differentiation of microglia from the erythromyeloid progenitors are RUNX1, PU.1 and IRF8. Moreover, CSF1R, IL-34 and TGF- $\beta$

are also essential factors for microglial terminal differentiation (Crotti & Ransohoff, 2016). In addition, microglial maintenance largely depends on the presence and activation of CSF1R. The genetic or chemical inhibition of this receptor dramatically influences microglia survival, approach that has been used for microglial depletion studies (Dai *et al*, 2002; Elmore *et al*, 2014). Ligands for CSF1R are CSF1 (also known as M-CSF) and IL-34. Although they are both produced by neurons, CSF1 can also be released by glial cells, including microglia (Lin *et al*, 2008; Ma *et al*, 2012; Colonna & Butovsky, 2017). Phenotypically, microglia from the developing brain present an ameboid morphology until the postnatal period, when they adopt a ramified morphology (Lenz & Nelson, 2018).

Mouse microglia, like peripheral macrophages, can self-renew during the lifespan of an animal. Under physiological conditions, microglial renewal does not depend on infiltrating peripheral monocytes (Ajami *et al*, 2007). Microglia seem to proliferate randomly in healthy conditions, but when exposed to pathological conditions they expand clonally (Tay *et al*, 2017). Studies about murine microglial turnover rates have retrieved conflicting results, from fast turnover rates of around 3 months (Askew *et al*, 2017), to rather slow of 15-28 (Fuger *et al*, 2017) and 41 months (Tay *et al*, 2017).

In human, ameboid microglia have been detected as early as gestational week 5.5 in the brain (Monier *et al*, 2006). However it is not until gestational week 35, that differentiated microglia can be seen throughout the embryonic human brain (Ginhoux & Prinz, 2015).

Similar to mouse microglia, reports about microglial self-renewing rates in human are controversial. One study estimated that microglia population can self-renew around 100 times along an average person's lifetime of 80 years (Askew *et al*, 2017), while another study showed that they renew at a slow pace with an average microglial life of 4.2 years (Reu *et al*, 2017).

## **2.2. Physiological role of microglia in the CNS**

Microglia play important functions during brain development and throughout adulthood. However these functions seem to be specific for every stage, defined by unique molecular programs (Matcovitch-Natan *et al*, 2016; Prinz *et al*, 2019). During embryonic development and early postnatal stage, microglia show an "macrophage-like" ameboid morphology, suggesting cell activation and phagocytic activity (Lawson *et al*, 1990; Matcovitch-Natan *et al*, 2016). In fact, microglia from the developing brain have been shown to clear apoptotic or excessive neuronal precursor cells, and can regulate their numbers by inducing apoptosis (Marin-Teva *et al*, 2004; Askew *et al*, 2017). In addition, microglia regulate neurogenesis by promoting neuronal

precursors proliferation, survival and maturation (Frost & Schafer, 2016). Furthermore, in the developing brain, microglia play an essential function in shaping synapses, for the correct establishment of neuronal networks (Stevens *et al*, 2007). Besides neurons, microglia have been reported to support the development and function of other brain cells like oligodendrocytes, and seem to be essential for normal myelination during postnatal development (Hagemeyer *et al*, 2017; Wlodarczyk *et al*, 2017). Studies performed in CSF1R-deficient mice that lead to microglial depletion in the developing brain, have revealed numerous brain abnormalities that result in premature death, further supporting the importance of microglia during brain development (Erblich *et al*, 2011).

In the adult brain, microglia are homogeneously distributed throughout the brain in a density of approximately  $6.5 \times 10^3$  cells/mm<sup>3</sup> (Nimmerjahn *et al*, 2005), although regional differences have also been reported (Lawson *et al.*, 1990). Unlike microglia from the developing brain, adult microglia in a steady state show a ramified morphology, with highly motile processes that enable them to survey the brain environment and monitor synapses (Figure 6). It has been estimated, that microglia scan the whole brain once every few hours (Nimmerjahn *et al.*, 2005; Wake *et al*, 2009). In the mature CNS, microglia-synapse interactions are regulated by neuronal activity, suggesting a highly controlled mechanism of neurons over microglial function (Wake *et al.*, 2009). Microglia can also secrete neurotrophic factors such as brain-derived neurotrophic factor (BDNF) and contribute to the formation of new synapses (Parkhurst *et al*, 2013). Besides shaping and clearing non-required synapses, they are also involved in the clearance of apoptotic cells and cell debris by phagocytosis, for example during neurogenesis in the adult hippocampus (Sierra *et al*, 2010). In addition, microglia can rapidly react to infections or injury in order to protect the brain and maintain homeostasis (Kreutzberg, 1996).

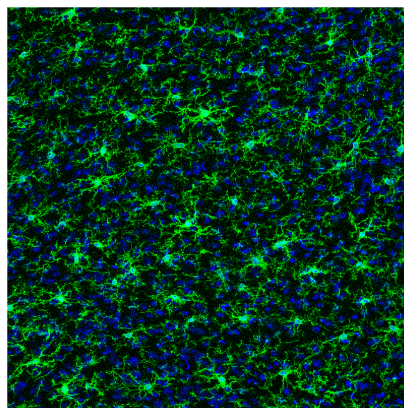


**Figure 6. Microglia present a ramified morphology in the adult healthy brain.** Microglia labelled with IBA1 (green) from the cortex of a 3-month-old WT mouse. Nuclei are visualized with Hoechst (blue).

### 2.2.1. Molecular characterization of homeostatic microglia

As key regulators of the CNS, microglia have been deeply characterized at the molecular level. Although microglial profiles are highly dependent on the local environmental cues (Gosselin *et al.*, 2014; Thion & Garel, 2020), common homeostatic microglial signatures from healthy mice, have been consistently reported by multiple studies, especially at the transcriptomic level. These homeostatic signatures enriched in microglia, include genes like *Fcrls*, *P2ry12*, *P2ry13*, *Tmem119*, *Cx3cr1*, *Csf1r*, *Hexb*, *Olfml3*, *Sall1*, *Tgfbr1*, *Siglech* and *Gpr34*, among others (Gautier *et al.*, 2012; Beutner *et al.*, 2013; Chiu *et al.*, 2013; Hickman *et al.*, 2013; Butovsky *et al.*, 2014; Zhang *et al.*, 2014; Crotti & Ransohoff, 2016; Butovsky & Weiner, 2018). Some of these microglial homeostatic signatures, have also been identified in healthy human brains (Galatro *et al.*, 2017; Olah *et al.*, 2018). In fact, Galatro and colleagues showed that human and mice healthy microglia present a large overlap in their expression profile with common genes like *CX3CR1* and *P2RY12* (Galatro *et al.*, 2017). However, they also observed differences, especially when focusing on age-dependent changes (Galatro *et al.*, 2017). Interestingly, age-related microglial changes in human seem to resemble an AD phenotype with the up-regulation of AD risk genes like *TREM2*, *MS4A4A*, *SORL1* or *CD33* (Olah *et al.*, 2018).

Additional studies have also revealed a plethora of molecules that reflect microglial function. Specifically, microglia are equipped with a repertoire of receptors used to “sense” the environment and identify invading pathogens, misfolded or aggregated proteins, chemokines and cytokines, etc. (Hickman *et al.*, 2013). These receptors are known as the microglial sensome and include: pattern-recognition receptors (PRRs), which detect pathogen-associated molecular patterns (PAMPs) and damage-associated molecular patterns (DAMPs), such as toll like receptors (TLR) (*Tlr2*, *Tlr7*, *Tlr4*, *Tlr13*), scavenger receptors (SR) (*Cd36*, *Cd47*, *Cd14*) and C-type lectin receptors (*Clec5a*, *Clec7a* and *Clec4a3*) (Hickman *et al.*, 2013; Colonna & Butovsky, 2017). Other sensome receptors include purinergic receptors (*P2ry12*, *P2ry13*, *P2ry6*), which sense ATP released by apoptotic neurons and promote migration and phagocytosis, and cytokine and chemokine receptors (*Cx3cr1*, *Ccr5*, *Csf1r*, *Tgfbr1*, *Tgfbr2*), among others (Hickman *et al.*, 2013; Colonna & Butovsky, 2017). As immune cells of the CNS, microglia respond to changes in the brain environment by releasing pro-inflammatory cytokines such as IL-1 $\beta$ , IL-6 and TNF- $\alpha$  that promote an inflammatory reaction that activates other glial cells like astrocytes (Prinz *et al.*, 2019). However, microglia are very plastic cells and can respond differently depending on the insult. For example, they respond with the secretion of pro-inflammatory factors upon a bacterial infection, whereas by phagocytosis of apoptotic cells or myelin debris, microglia release anti-

inflammatory factors (Hanisch & Kettenmann, 2007). Microglia can also act as antigen-presenting cells (APCs). They are equipped with the machinery to process antigens in the lysosomes and express major histocompatibility complex (MHC) class II (MHC II) and costimulatory molecules required for the presentation of antigens to T cells (Colonna & Butovsky, 2017). In addition, microglia present checkpoint mechanisms, or what has been defined as “off signals”, mainly by their interaction with neurons, that keep them in a “calm” non-reactive state (Hanisch & Kettenmann, 2007). Some of the molecules involved in this mechanism are CD200-CD200R, and CX3CL1-CX3CR1, with the receptors expressed by microglia and the ligands by neurons (Hanisch & Kettenmann, 2007; Rogers *et al*, 2011; Walker & Lue, 2013). The disruption of these signaling interactions, leads to microglial activation (Hanisch & Kettenmann, 2007).

Apart from microglial markers such as TMEM119, CX3CR1 or P2RY12 (Butovsky *et al.*, 2014), microglia in a “resting or surveying” (non-activated) state can be visualized by immunohistochemical techniques, with other markers like the commonly used Ionized calcium binding adaptor molecule 1 (IBA1) (Figure 6), which binds to actin and is involved in membrane ruffling and phagocytosis (Sasaki *et al*, 2001; Hopperton *et al*, 2018); CD11b, that is part of the complement receptor 3 (CR3) and binds to antigens for their phagocytosis; and the Cluster of differentiation 68 (CD68), which labels lysosomes and is considered a marker for activated microglia. (Hopperton *et al.*, 2018). Those markers can be detected in homeostatic and activated microglia, although they increase their levels upon activation (Hopperton *et al.*, 2018).

Overall, microglia are highly dynamic and motile cells, that are equipped with a large variety of receptors and molecules in order to rapidly respond to changes in their surrounding brain environment, and defend it from endogenous or exogenous harmful factors, to ultimately maintain brain homeostasis and a healthy neuronal architecture.

### **2.3. Microglia in AD: “a double-edge sword”**

The role of microglia in AD is still controversial, due to studies pointing to both beneficial and deleterious effects mediated by microglia. For this reason, the function of microglia in AD and other neurodegenerative diseases has been defined as a “double-edge sword” (Schlachetzki & Hull, 2009). As discussed earlier (section 1.1.4), microglia in AD are found surrounding A $\beta$  plaques showing an activated phenotype (Figure 5A) (Hickman *et al*, 2018). *In vivo* two-photon imaging studies have reported, that microglia react rapidly to forming plaques, by polarizing their processes and migrating towards them (Bolmont *et al*, 2008). As our brain sentinels, microglia intend to eliminate the toxic insult. In fact, they express several receptors to identify

and bind A $\beta$ , which facilitate its clearance (Lee & Landreth, 2010; Hansen *et al.*, 2018). At the same time, microglia initiate an inflammatory response in an attempt to enhance A $\beta$  clearance (Sarlus & Heneka, 2017). However, microglial phagocytic capacity has been shown to be compromised in AD (Hellwig *et al.*, 2015). As AD progresses and A $\beta$  pathology is not resolved, inflammation becomes chronic. This leads to neurotoxic effects mediated by pro-inflammatory cytokines and uncontrolled phagocytosis of synapses by microglia, that eventually, may result in neuronal death (Sarlus & Heneka, 2017; Hansen *et al.*, 2018). Indeed, microglial depletion studies in amyloidosis mouse models, prevented spine and neuronal loss and reduced neuroinflammation, pointing to the detrimental function of microglia in the chronic phase of the disease (Spangenberg *et al.*, 2016; Spangenberg & Green, 2017).

Overall, microglia seem to have a beneficial effect in the clearance of A $\beta$  deposits, but their role may become detrimental as disease progresses due to impaired or insufficient A $\beta$  clearance and sustained inflammation. Thus, identifying the molecular mechanisms that are responsible for microglial failure to clear A $\beta$ , is vital to find novel therapeutic targets for the repair and enhancement of microglial protective functions.

### 2.3.1. Mechanisms A $\beta$ clearance in the CNS

Two main general mechanisms have been reported for A $\beta$  clearance in the brain, which include its transport or drainage to the peripheral blood and lymphatic systems and its degradation within the CNS (Zuroff *et al.*, 2017). The principal mechanism of A $\beta$  clearance from the brain into the blood stream involves LRP1, which is mainly located in the cerebral endothelium and by binding to A $\beta$ , it facilitates its transport by transcytosis across the BBB (Deane *et al.*, 2009). The expression of LRP1 has been found to be reduced during ageing and AD, which contributes to the accumulation of A $\beta$  in the brain parenchyma (Deane *et al.*, 2009). In addition, some evidence suggests that APOE might be required for LRP1-mediated transport through the BBB (Shibata *et al.*, 2000).

Within the brain parenchyma, A $\beta$  -mainly its soluble form-, can be extracellularly cleared by degrading proteases such as NEP, IDE, MMP9, ECE1, ACE and PreP. However, NEP and IDE are considered the major A $\beta$  degrading proteases (Lee & Landreth, 2010). NEP is an integral membrane protein with its active site facing the extracellular space. It is mainly expressed by microglia, astrocytes and neurons and it is believed to be the most potent A $\beta$ -degrading protease (Zuroff *et al.*, 2017). Decreased levels of NEP have been found in AD brains inversely correlating with A $\beta$  accumulation and clinical diagnosis (Wang *et al.*, 2010b). IDE is mainly found as a

cytosolic protein in glial cells like microglia, but they can also secrete it, while in neurons it is found at the cell surface (Zuroff *et al.*, 2017).

In addition, A $\beta$  can be internalized and intracellularly degraded by microglia and astrocytes (Ries & Sastre, 2016). However, these processes have been better described in microglia. Mechanisms of A $\beta$  uptake include pinocytosis and receptor-mediated phagocytosis and endocytosis (Mohamed & Posse de Chaves, 2011; Ries & Sastre, 2016; Sole-Domenech *et al.*, 2016). Microglia clear soluble A $\beta$  through fluidic phase macropinocytosis, which involves the formation of pinosomes or macropinocytic vesicles through the closure of membrane ruffles. This process depends on actin cytoskeleton, that is critical for microglial clearance (Mandrekar *et al.*, 2009). In turn, fibrillar A $\beta$  has been shown to be cleared by microglia through receptor-mediated phagocytosis and endocytosis (Mohamed & Posse de Chaves, 2011). These processes involve different receptors such as SR (SR-A, SR-B, CD36, CD40 or CD47); TLR (TLR-2, TLR-4) and co-receptor CD14, receptors for Advanced Glycation End Products (RAGE), Fc receptors (FcRs) (Fc $\gamma$ RI, Fc $\gamma$ RII and Fc $\gamma$ RIII), the Triggering Receptor Expressed on Myeloid Cells 2 (TREM2), and the complement system (C1q and C3b) (Mohamed & Posse de Chaves, 2011; Ries & Sastre, 2016). Once fibrillar A $\beta$  is bound to the receptor, a signaling cascade is initiated and phagocytosis of A $\beta$  takes place (Lee & Landreth, 2010). The formation of the phagocytic vesicle (phagosome) involves actin rearrangement. In turn, the process of receptor-mediated endocytosis requires clathrin-coated pits and additional accessory proteins (Sole-Domenech *et al.*, 2016). Engulfed A $\beta$  passes through multivesicular bodies before it reaches the lysosome for degradation. In the lysosome, degradation of internalized material is facilitated by hydrolytic enzymes such as Cathepsins (Sole-Domenech *et al.*, 2016; Zuroff *et al.*, 2017).

### 2.3.2. Microglial deficiency of A $\beta$ clearance in AD

Several mechanisms involved in the binding, uptake and degradation of A $\beta$  have been reported to fail in AD microglia. Hickman and colleagues reported that microglial levels of SR-A, CD36 and RAGE and NEP, IDE and MMP9 progressively decreased as AD mice aged, while pro-inflammatory cytokines increased. TNF- $\alpha$  triggered the down-regulation of *Sra* and *Cd36* gene expression and reduced A $\beta$  uptake, suggesting that inflammation may impair A $\beta$  clearance by inducing the downregulation of A $\beta$  receptors (Hickman *et al.*, 2008). Moreover, as previously mentioned (section 1.3), some of the identified genetic variants in microglial genes that confer risk to develop LOAD, are implicated in A $\beta$  clearance. This is the case of *CD33*, *ABCA7*, *SORL1*, *BIN1* or *TREM2* among others (Hansen *et al.*, 2018). The most common *TREM2* variant known as

R47H, which results in a partial loss of function of this protein, increases the risk for LOAD by approximately 4-fold (Guerreiro *et al*, 2013; Jonsson *et al*, 2013). As A $\beta$  receptor, the loss of function of *TREM2* due to genetic alterations, impairs A $\beta$  recognition and phagocytosis increasing A $\beta$  load and therefore the risk to develop AD. In fact, different studies support this notion. For example, *Trem2* deficiency in primary microglia, reduced microglial phagocytosis of A $\beta$  plaques (Xiang *et al*, 2016). In addition, *Trem2* deficient AD mice showed a significant decrease in microglia recruitment to A $\beta$  plaques and increase in A $\beta$  load (Wang *et al*, 2015; Parhizkar *et al.*, 2019), while overexpression of *Trem2* increased A $\beta$  phagocytosis and reduced neuroinflammation and synapse loss (Jiang *et al*, 2014). In turn, the *CD33* single nucleotide polymorphism (SNP) rs3865444, was shown to confer protection against AD and is associated with lower *CD33* levels in microglia and reduced insoluble A $\beta$ 42 in the brain. Conversely, the number of *CD33* positive microglia are increased in AD brains compared to controls and correlate with the levels of insoluble A $\beta$ 42 and A $\beta$  load. In addition, *CD33* was able to inhibit A $\beta$ 42 clearance in a microglial culture, and knocking out *Cd33* in a mouse model of AD, resulted in a significant reduction of insoluble A $\beta$ 42 levels and A $\beta$  plaque load (Griciuc *et al*, 2013). Thus, *CD33* has an inhibitory function in microglial A $\beta$  uptake, further supporting the involvement of microglia in A $\beta$  clearance and AD pathogenesis.

Deficiency in the clearance rates of A $\beta$ 40 and A $\beta$ 42 has also been reported in AD patients compared to healthy individuals (Mawuenyega *et al.*, 2010). Furthermore, insufficient lysosomal acidification has been linked to deficient fibrillar A $\beta$  clearance by microglia (Majumdar *et al*, 2007), and autophagic and lysosomal defects were observed in microglia upon chronic A $\beta$  exposure in AD mouse models and patients (Pomilio *et al*, 2020). Importantly, aging is considered the main risk factor to develop AD (Guerreiro & Bras, 2015). Microglia loses its homeostatic functions and present a pro-inflammatory reactive phenotype as they age, which correlate with the deficiency in phagocytosis of cell debris and immune surveillance (Koellhoffer *et al*, 2017). Along these lines, microglial phagocytosis of A $\beta$  fibrils has been shown to be reduced with normal aging (Floden & Combs, 2011).

Taken together, there is substantial evidence that supports microglial deficiency in A $\beta$  clearance as underlying cause for AD pathogenesis, especially for LOAD. Thus, a deep characterization of the molecular changes in microglia triggered by A $\beta$ , and the identification of the mechanisms that lead to impaired A $\beta$  clearance, is necessary to find new and more promising therapeutic options for AD patients.

### 2.3.3. Molecular characterization of AD microglia

As discussed earlier, the large amount of data provided by GWAS and sequencing studies linking microglial-specific genes with the risk to develop AD, has placed microglia in the center of AD research. For this reason, in the last decade there was an exponential increase in the number of studies characterizing microglia in the context of AD pathogenesis. Especially, numerous transcriptome studies, have made a great contribution to our understanding of microglial changes in AD.

#### 2.3.3.1. Transcriptomic profiling of mouse AD microglia

Microglia from AD mouse models have been extensively studied at the transcriptome level using the bulk population, but also, at the single cell level. Keren-Shaul and colleagues, performed single-cell RNA sequencing with microglia isolated from the 5XFAD amyloidosis mouse model. They discovered a disease-associated microglia (DAM) population with a unique transcriptomic signature that suggested protective functions (Keren-Shaul *et al.*, 2017). The acquisition of the DAM state by microglia, required a two-step activation: an initial TREM2-independent step that included the upregulation of genes like *Tyrobp* (Trem2 adaptor), *ApoE*, *Ctsb*, *Ctsd* and *B2m* and the downregulation of microglial homeostatic markers such as *Cx3cr1*, *Tmem119*, *P2ry12/13* and *Csf1r*; and a second TREM2-dependent step, which drove the upregulation of genes involved in lipid metabolism and phagocytosis such as *Trem2*, *Cd9*, *Cst7*, *Clec7a*, *Itgax* (CD11c) and *Lpl*. Of note, the DAM signature was also found in an amyotrophic lateral sclerosis (ALS) mouse model (Keren-Shaul *et al.*, 2017). Interestingly, Krasemann and colleagues, by analyzing the transcriptome of bulk microglia from APPPS1 mice, multiple sclerosis (MS) and ALS mouse models, found a signature that largely overlapped with the DAM signature (Keren-Shaul *et al.*, 2017; Krasemann *et al.*, 2017). However, as they found these microglial changes to be associated with neuritic plaques and induced upon phagocytosis of apoptotic neurons, Krasemann and colleagues termed this signature microglial neurogenerative phenotype (MGnD), that represented in this case, a neurotoxic microglial response (Krasemann *et al.*, 2017). Similar to the DAM signature, they observed the up-regulation of immune response-related genes and the downregulation homeostatic markers, which were controlled by two major axes: TGF $\beta$  and TREM2-APOE signaling, that regulated the expression of the homeostatic and the MGnD signatures, respectively (Keren-Shaul *et al.*, 2017; Krasemann *et al.*, 2017).

Overall, these transcriptomic studies, and others (Mathys *et al.*, 2017; Sala Frigerio *et al.*, 2019), reported common markers expressed by microglia in a disease state, which was coupled with the repression of microglial homeostatic markers. However, the authors interpreted the functional

involvement of these signatures in an opposite manner, with the expression of DAM being protective and the MGnD being detrimental (Keren-Shaul *et al.*, 2017; Krasemann *et al.*, 2017). Functional studies are needed to determine the specific molecular mechanisms that are critical for microglial protective performance in AD, and the ones that underscore dysfunctional or detrimental outcomes.

### 2.3.3.2. Transcriptomic profiling of human AD microglia

Human microglia from AD postmortem brains have also been recently characterized at the transcriptome level by different studies using frozen brain samples. Mathys and colleagues analyzed brain cells by single-nucleus RNA sequencing (snRNA) from the prefrontal cortex of 48 individuals (24 with varying degree of AD pathology and 24 non-AD subjects). They found an AD-associated microglial subpopulation that showed a partial overlap with the DAM signature (28 genes out of 229 upregulated DAM), including *CD74*, *APOE*, *SPP1* and MHC-II genes (Keren-Shaul *et al.*, 2017; Mathys *et al.*, 2019). However, human AD microglia also showed alteration in genes that were not identified in mouse models, such as *C1QB* and *CD14* (Mathys *et al.*, 2019).

In a more recent study, Zhou and colleagues also performed snRNA-seq using brains from human AD patients that carried WT *TREM2* or its AD risk variants, R47H and R62H, and compared it to control individuals (Zhou *et al.*, 2020). They showed that human AD microglia without *TREM2* mutations presented an upregulation of few DAM markers like *APOE*, *TREM2*, *CD68* and *MHCII*, but also, a significant increase of homeostatic genes such as *TMEM119*, *CX3CR1* and *P2RY12*. In addition, they presented an up-regulation of other genes like *A2M*, *CHI3L1*, *AIF1* (IBA1) and *IRF8*. The authors suggested that *IRF8* might be the main driver for the upregulation of the homeostatic signature in AD microglia. Moreover, they showed that *TREM2*-variant carriers had a reduced microglial activation profile (specially prominent in the *TREM2*-R47H cases) compared to non-carriers, which was in line with previous reports indicating that *TREM2* function is necessary for the acquisition of a reactive microglial phenotype in AD (Wang *et al.*, 2015; Keren-Shaul *et al.*, 2017; Zhou *et al.*, 2020).

Few months ago, Srinivasan and colleagues reported a RNA sequencing analysis of sorted CD11b positive myeloid cells from AD and control brains (Srinivasan *et al.*, 2020). They also revealed a poor overlap between the expression profile of human and mouse AD microglia, with the exception of the DAM marker *APOE* (Keren-Shaul *et al.*, 2017). They termed their identified human AD microglia signature as “Human AD Microglia” (HAM), which displayed a rather enhanced aging profile (Srinivasan *et al.*, 2020).

Taken together, to date, human AD microglia characterization has revealed a low overlap with the microglial signatures retrieved from mouse studies, with the exception of *APOE* and *TREM2* genes. Although the three abovementioned studies reported limitations in their analysis, mostly based on the usage of frozen tissue, one has to keep in mind the differences between mouse models and human AD in terms of AD pathology. While most used AD mouse models mimic almost exclusively an amyloid pathology, that at best, would recapitulate an early human pathology, the analyzed human cases were mostly in late-stage AD, which include Tau alterations and neuronal loss, among other pathological features not present in mouse models (Hall & Roberson, 2012; King, 2018). Thus, it is not meaningful to make a one to one comparison of these studies. However, it is necessary to obtain further insights into the characterization human AD microglia, especially at different AD stages, in order to find clinically relevant AD markers that can be properly modeled and further studied in animal models or explored as biomarkers.

### **3. Modulation of microglia as therapeutic approach for AD**

As discussed earlier, there is plenty of evidence that points to a microglial deficiency in A $\beta$  clearance as underlying cause of AD, especially for sporadic cases. Therefore, modulation of microglia has been considered a promising therapeutic approach to enhance microglial clearance function and thus, reduce A $\beta$  load. Several strategies have been developed over the past years for this purpose. I will describe some of the most recent and clinically relevant approaches that may hold therapeutic potential.

#### **3.1. Anti-A $\beta$ therapies: active and passive immunization**

Immunotherapies aiming at A $\beta$  targeting include A $\beta$  vaccines and anti-A $\beta$  antibodies, which represent active and passive immunization, respectively. Studies of active and passive immunization in animal models have retrieved good results in terms of reduction of A $\beta$  load and associated pathologies (Schenk *et al.*, 1999; Bard *et al.*, 2000; Bacskai *et al.*, 2002; Wilcock *et al.*, 2004). These studies suggested that A $\beta$  clearance is mediated by the stimulation and engagement of microglial Fc receptors that bind to A $\beta$  and lead to receptor-mediated phagocytosis (Schenk *et al.*, 1999; Bard *et al.*, 2000; Bacskai *et al.*, 2002; Wilcock *et al.*, 2004). However, other mechanisms of A $\beta$  removal may also play a role (Das *et al.*, 2003). For the last two decades, lots of efforts and resources have been invested into the development of A $\beta$  vaccines and antibodies for the treatment of AD patients. The first clinical trial of active immunization using an A $\beta$ 42 vaccine (AN1792, from Janssen and Pfizer) in mild to moderate-stage AD patients, was terminated due to the appearance

of meningoencephalitis and micro-hemorrhages in immunized subjects (Gilman *et al*, 2005). A follow-up study of the AN1792-treated patients, revealed a significant decrease of A $\beta$  load but did not correlate with cognitive improvement or overall prolonged survival (Holmes *et al*, 2008). Some of the adverse reactions associated to the AN1792 immunization were found to be associated to T-cell inflammatory responses (Cacabelos, 2020). Second-generation vaccines such as ACC-001 and CAD106 have aimed to avoid the engagement of T-cell response. CAD106 (Amilomotide, from Novartis) was the only vaccine accepted to move to a clinical trial phase III and was combined with a BACE1 inhibitor (CNP520) (van Dyck, 2018). However, the trial was recently terminated due to worsening of cognitive function (<https://clinicaltrials.gov; ID: NCT02565511>).

Regarding A $\beta$ -antibody therapies (passive immunization), Bapineuzumab (from Janssen and Pfizer) was the first monoclonal antibody used to target A $\beta$  in AD. However, after two phase III trials, the study was stopped due to the lack of effect (Salloway *et al*, 2014). Another monoclonal antibody, Aducanumab (from Biogen and Neuroimmune), was proved successful in reducing A $\beta$  load and improving cognitive decline in phase I clinical trials (Sevigny *et al*, 2016). Unfortunately, efficacy could not be reproduced in following phases, and trials were finally discontinued in Phase III (<https://www.alzforum.org/news/research-news/biogeneisai-halt-phase-3-aducanumab-trials>). Today, some A $\beta$ -antibodies still remain in clinical trials. This is the case of Gantenerumab (from Hoffman-La Roche, [NCT03443973](#); [NCT03444870](#)) and Solanezumab (from Eli Lilly & Co., [NCT02760602](#)), which are in phase III clinical trials (Huang *et al*, 2020).

Despite the promising pre-clinical results of the anti-A $\beta$  immunotherapies and the enormous efforts at human and economic level, so far, all clinical trials have failed to achieve significant cognitive improvement for AD patients (Cacabelos, 2020). However, learning from past errors might help to improve the design of these therapies in the future, and this approach may still hold promise for AD patients.

### 3.2. Other microglial immunomodulation approaches

Due to the failure of the abovementioned anti-A $\beta$  therapies and others targeting A $\beta$  production, such as the secretase inhibitors (Huang *et al*, 2020), novel therapeutic options are being explored in order to enhance microglial clearance function and ultimately reduce A $\beta$  load and improve cognition.

TREM2 has been identified as an important regulator of microglial function. Especially when microglia are exposed to a challenge like A $\beta$ , TREM2 is necessary for microglial transition to a

disease-associated or reactive state (Keren-Shaul *et al.*, 2017), exhibiting a protective role in AD (Jiang *et al.*, 2014). On the contrary, loss-of-function *TREM2* variants increase the risk to develop LOAD due to reduced microglial function (Zhou *et al.*, 2018). Full-length *TREM2* associates with its adaptor DAP12, to trigger a signaling cascade that involves SYK phosphorylation and promotes survival, migration and phagocytosis in myeloid cells (Konishi & Kiyama, 2018). *TREM2* ectodomain shedding by a  $\alpha$ -secretase seems to abolish this signaling (Kleinberger *et al.*, 2014). Several studies have succeeded in the stimulation of *TREM2* signaling through the development of agonistic antibodies (Cheng *et al.*, 2018; Schlepckow *et al.*, 2020). One study used an antibody that boosted proximal signaling and improved microglial survival, proliferation and migration (Cheng *et al.*, 2018). A second study developed an antibody (4D9) that inhibited the  $\alpha$ -secretase cleavage in the *TREM2* ectodomain and stabilized the cell-surface *TREM2*, which led to increased macrophage viability, enhanced microglial phagocytosis of myelin and A $\beta$  *in vitro*, but also, reduced A $\beta$  load *in vivo* (Schlepckow *et al.*, 2020). To date, this therapeutic approach appears promising, although further research is still required to assess its safety, due to the inevitable reduction of soluble *TREM2*, which might also play important functions in the CNS (Zhong *et al.*, 2017; Zhong *et al.*, 2019).

Lysosomal function is essential for microglial degradation ability of dead cells or protein aggregates like A $\beta$ , among other waste products (Zuroff *et al.*, 2017). It has been reported that microglia in a steady state, presents a deficient acidification of lysosomes required for degradation of fibrillar A $\beta$ , due to the mislocalization of a chloride transporter (CIC-7) in the lysosome (Majumdar *et al.*, 2011). Activation of microglia with Macrophage stimulating factor (M-CSF) resulted in the proper localization of the CIC-7 transporter and lysosomal acidification necessary for fibrillar A $\beta$  degradation (Majumdar *et al.*, 2011). Moreover, increasing lysosomal biogenesis by the overexpression of the lysosomal master regulator TFEB in its deacetylated form, led to increased fibrillar A $\beta$  degradation (Bao *et al.*, 2016). Therefore, enhancement of lysosomal function might represent a therapeutic strategy for microglia immunomodulation in AD.

### **3.3. GM-CSF as potential immunomodulator of AD microglia**

Microglial functional decline due to aging and AD has been shown to be reversible when exposed to factors secreted by their younger counterparts (Daria *et al.*, 2017). In this study performed in my laboratory, organotypic brain slices from aged APPPS1 and postnatal WT mice were co-cultured *ex vivo*. Co-culturing the old AD and young WT tissue, led to the rejuvenation of the old AD microglia, which was manifested by increased proliferation and A $\beta$  phagocytosis, resulting in a significant reduction of the A $\beta$  load. This study demonstrated that the factors secreted by the

young slices, and in particular, by young microglia, repaired AD microglial phagocytic function. Interestingly, Granulocyte macrophage colony-stimulating factor (GM-CSF) was identified as one of the factors able to rejuvenate or repair AD microglia (Daria *et al.*, 2017).

GM-CSF is a secreted glycoprotein that binds to a heteromeric cell-surface receptor composed of alpha (GM-CSFR $\alpha$ ) and beta (GM-CSFR $\beta$ ) subunits, through which it mediates intracellular signaling. It has been considered a pleiotropic cytokine due to its various functions in the immune system (Hansen *et al.*, 2008). GM-CSF is also well known as a hematopoietic growth factor, since it induces the proliferation and differentiation of hematopoietic progenitor cells from the myeloid lineage (Ridwan *et al.*, 2012). As a drug, it has been largely used in the clinic to mobilize myeloid progenitor cells from the bone marrow into the bloodstream, in immunosuppressed patients after chemotherapy or transplantation (Buchsel *et al.*, 2002). In the CNS, microglia/macrophages are the main source of GM-CSF (Zhang *et al.*, 2014), although both, GM-CSF and its receptor (GM-CSFR), can be also expressed by neurons and astrocytes (Ridwan *et al.*, 2012). Of note, a substantial reduction of the GM-CSFR $\alpha$  in hippocampal neurons of AD patients has been reported (Ridwan *et al.*, 2012). Moreover, GM-CSF has been shown to induce proliferation of cultured human fetal and adult microglia (Lee *et al.*, 1994) and stimulate microglial phagocytosis *in vivo* (Giulian & Ingeman, 1988). Importantly, GM-CSF was proven to cross the BBB (McLay *et al.*, 1997), and when administered systemically in a model of Alzheimer's disease, was able to induce a significant reduction of A $\beta$  load and improve cognition, which was accompanied by increased synaptic area and microglial density (Boyd *et al.*, 2010). However, the molecular mechanism by which GM-CSF mediates the stimulation of microglial A $\beta$  clearance remains unknown.

In sum, GM-CSF was shown to increase microglial A $\beta$  phagocytosis *ex vivo* and *in vivo* and therefore, holds potential as a rejuvenation or repair factor for AD microglia. However, due to its functions in the peripheral immune system, its use as a drug for the treatment of neurodegenerative diseases should be carefully considered. Nevertheless, the mechanisms by which GM-CSF induces microglial rejuvenation in the context of AD should be dissected, in order to find more direct molecular targets for microglial repair in AD.

Taken together, microglial function can be modulated through different mechanisms that have resulted in enhanced microglial phagocytic performance and reduction of A $\beta$  load. Although microglial targeting still represents a challenge due to the dynamic nature of these glial cells, immunomodulation strategies have opened a window of new therapeutic opportunities for the treatment of AD. However, a deep understanding of the molecular fingerprints of microglia at

different disease stages is necessary, to design optimal therapeutic windows and targeting approaches, that enhance microglial protective functions and prevent the detrimental ones.

## Aims of the study

The discovery of genetic AD risk variants in microglial genes, along with functional studies pointing to microglial A $\beta$  deficiency in AD, have directly implicated microglia in the etiology of AD. Therefore, the characterization of AD microglia has become a priority for the identification of the molecular mechanisms that lead to microglial dysfunction. Although many studies have characterized microglia at the transcriptome level, microglial proteome has not been deeply studied in the context of AD. Thus, the first aim of my PhD project focused on characterizing microglial proteomic fingerprints during the course of AD using two different AD mouse models. With this study, I intended to elucidate the molecular mechanisms of microglial response to A $\beta$  pathology and identify signaling pathways that underscore microglial dysfunction in AD. In addition, my goal was to discover the triggering factors for microglial response in AD and the functional outcome of microglial proteomic alterations during AD progression.

The second objective of my PhD project was to reveal the proteomic signatures of repaired microglia *in vivo* using GM-CSF as an immunomodulatory factor. GM-CSF was shown capable of restoring microglial phagocytic capacity *ex vivo* and *in vivo*, but the molecular mechanism behind this effect was not investigated. Therefore, I used GM-CSF as a tool to understand the mechanism by which this hematopoietic factor restores microglial phagocytic function and to characterize the signatures of functionally repaired microglia.

# Materials and Methods

## 1. Materials

### 1.1. Laboratory equipment and general consumables

Instrument	Company
Analytical balance (0.0001-200g)	Denver Instrument
Balance (0.01-2000g)	Sartorius
Cryostat (CryS1AR NX70)	Thermo Fisher Scientific
DNA electrophoresis gel system	Bio-Rad
Electrophoresis system Mini-Protean	Bio-Rad
Electrophoresis System, XCell SureLock Mini-Cell	Thermo Fisher Scientific
Embedding Molds, Peel-A-Way® (Square - S22)	Polysciences, Inc
Heating and stirring plate	IKA RH
Imager agarose gels	INTAS Science Imaging
Luminescent image analyzer (ImageQuant LAS-4000) (developer Western blot)	GE Healthcare
MilliQ plus filtration system	Merck Millipore
NanoQuant Infinite M200 PRO (plate reader for protein quantification)	TECAN
Parafilm "M" roll	Bemis
PCR tubes	Neolab
pH meter (Seven easy)	Mettler Toledo
Pipette controller accu-jet pro	BrandTech
Pipette set	Gilson, Eppendorf
Pipette tips (10, 200, 300 and 1000 µL)	Sarstedt
Peristaltic pump	World Precision Instruments
Precellys tissue homogenizer	Bertin Instruments
Protein electrophoresis and transfer systems	Bio-Rad
Serological pipettes (2, 5, 10 and 25 mL)	Sarstedt
Tabletop centrifuge (Heraeus Fresco 17)	Thermo Fisher Scientific
Thermocycler (Biometra)	Analytik-Jena
Thermomixer compact	Eppendorf
Tubes (0.5, 1.5, 2, 15 and 50 mL)	Sarstedt
Ultracentrifuge Optima Max-up	Beckman Coulter
Ultrasonic bath (Sonorex Super)	Brandelin
Vortex mixer (Vortex-2 genie)	Scientific industries

Table 2. List of laboratory equipment and consumables used in this study

### 1.2. Cell culture equipment and consumables

Instrument	Company
Cell culture dishes Nunc (3.5, 6, and 10 mL)	Thermo Fisher Scientific
Cell culture well plates (6, 12 and 24 wells)	Thermo Fisher Scientific
Centrifuge (5810R)	Thermo Fisher Scientific
CO <sub>2</sub> incubator	Binder, Thermo Fisher Scientific

Laminar flow hood	Thermo Fisher Scientific
QuadroMACS separator	Miltenyi Biotec
Pasteur glass pipettes	VWR
Stericup filter bottle (250 mL)	Millipore
Tubes (0.5, 1.5, 2, 15 and 50 mL)	Sarstedt
Tissue chopper (TC752)	Mickle Laboratory Engineering Company

**Table 3. List of cell culture equipment and consumables used in this study**

### 1.3. Surgical instruments

Instrument	Company
Dumont #2, Laminectomy Forceps (11223-20)	Fine Science Tools
Dumont #5, straight fine forceps (11252-20)	Fine Science Tools
Hardened fine scissors straight (14090-11)	Fine Science Tools
Large spatula, double, one round end	Heathrow Scientific
Thin spatula, double, one round end	Heathrow Scientific

**Table 4. Surgical tools used for the preparation of organotypic brain slices and microglia isolation**

### 1.4. Microscopy equipment

Instrument	Company
Confocal microscope TCS SP5	Leica Microsystems
Dissection microscope (SZ61)	Olympus
Epifluorescence microscope (AxioImager A2)	Zeiss

**Table 5. List of microscopes used in this study**

### 1.5. Mass spectrometry and FACS equipment

Instrument	Company
Flow cytometer BD FACSVerser	BDBiosciences
Ion source NanoFlex with PRSO-V1 column oven	Sonation
Mass spectrometer Q-Exactive HF	Thermo Fisher Scientific
Liquid chromatograph EASY-nLC 1000/1200	Thermo Fisher Scientific

**Table 6. List of mass spectrometry and FACS instruments, consumables and reagents**

### 1.6. Mouse lines

Both male and female mice were used in this study and housed in groups under specific pathogen-free conditions. They had access to water and standard mouse chow (Ssniff® Ms-H, Ssniff Spezialdiäten GmbH, Soest, Germany) *ad libitum* and were kept under a 12/12 h light-dark cycle. All animal studies were conducted according to the German animal welfare law and approved by the government of Upper Bavaria.

Designation	Genetic modifications	Reference/Source	Identifier	Additional information
C57BL/6J	No genetic modifications were introduced in these mice	The Jackson laboratory	RRID:IMSR_JAX:000664	This line was used for the cross breeding of the APPPS1 and APP-KI lines
APPPS1	Constitutive expression of human mutated <i>APP</i> (Swedish) and <i>PS1</i> (L166P) under the neuronal Thy-1 mouse promoter	(Radde <i>et al.</i> , 2006)	RRID:MGI:5313568	Heterozygous (C57BL/6 background)
APP <sup>NL-G-F</sup> (APP-KI)	Humanized mutated A $\beta$ sequence ( <i>APP</i> Swedish-NL, Artic-G and Iberian-F) expressed under the mouse promoter	(Saito <i>et al.</i> , 2014)	RRID:MGI:6160916	Homozygous (C57BL/6 background)

Table 7. List of mouse lines utilized in this study

## 1.7. Reagents, solutions and consumables for different applications

### 1.7.1. Genotyping of transgenic mouse lines

#### 1.7.1.1. Primers

Oligonucleotide primers were purchased from Sigma Aldrich.

Mouse line	Primer	Sequence (5'-->3')
APPPS1	APP-forward	GAATTCCGACATGACTCAGG
	APP-reverse	GTTCTGCTGCATCTTGGACA
	PS1-forward	CAGGTGCTATAAGGTCATCC
	PS1-reverse	ATCACAGCCAAGATGAGCCA
APP <sup>NL-G-F</sup> (APP-KI)	WT-forward	ATCTCGGAAGTGAAGATG
	WT-reverse	TGTAGATGAGAACTTAAC
	KI-forward	ATCTCGGAAGTGAATCTA
	KI-reverse	CGTATAATGTATGCTATACGAAG

Table 8. Primers used for genotyping of transgenic mouse lines

#### 1.7.1.2. Other reagents

Reagent	Company
Agarose Ultrapure	Life Technologies
Deoxyribonucleotides (dNTPs)	Roche
DNA Ladder 1kb Plus	Invitrogen
DNA Polymerase (GoTaq G2)	Promega
GelRed Nucleic Acid Stain	Biotium
GoTaq buffer (5x)	Promega
NaOH (1M)	Millipore
Tris base	AppliChem

Table 9. Reagents used for genotypic of transgenic mouse lines

### 1.7.1.3. Solutions

Solution	Composition
1-1.5% Agarose gel	1-1.5% Agarose in 1x TAE buffer 5/10 $\mu$ L GelRed stain (10/20 well gel)
Alkaline lysis buffer for DNA extraction	50mM NaOH (from NaOH 1M stock) in distilled water (dH <sub>2</sub> O)
Neutralization buffer (after tissue lysis, for genotyping)	1.5 M Tris in dH <sub>2</sub> O, pH 8.8
TAE buffer (1x)	40 mM Tris 20 mM Acetic acid 1mM EDTA in dH <sub>2</sub> O, pH 8.0

Table 10. Solutions used for genotyping of transgenic mouse lines

## 1.7.2. Microglia isolation, in vitro and ex vivo assays

### 1.7.2.1. Reagents and key consumables

Reagent	Company
Bovine serum albumin (BSA)	Sigma Aldrich
CD11b (Microglia) MicroBeads (130-093-634)	Miltenyi Biotec
Cell strainer (40 $\mu$ m)	NeoLab
Centrifuge tubes Corning (15 mL)	Sigma Aldrich
Ethylenediaminetetraacetic Acid (EDTA)	Thermo Fisher Scientific
CD11b-APC-Cy7 antibody, rat monoclonal (Cat#:557657, RRID: <a href="#">AB_396772</a> )	BDBiosciences
Cell scrapers (16 cm)	Starstedt
Cytochalasin D (CytoD)	Sigma Aldrich
Dimethylsulfoxide (DMSO)	Roth
Dulbecco's modified eagle medium 1x (DMEM/F12, 1:1), (11320-033)	Gibco
Fetal calf serum (FCS)	Sigma Aldrich
GM-CSF, recombinant mouse (415-ML-010)	R&D Systems
Hanks's buffered salt solution (HBSS) 1x (14025-050)	Gibco
HEPES (1M)	Gibco
Horse serum (heat inactivated)	Stem Cell Technologies/ Gibco
L-Glutamine	Gibco
MACS columns LS	Miltenyi Biotec

Neural Tissue Dissociation Kit (P) (130-092-628)	Miltenyi Biotec
Membrane inserts (PICM ORG 050)	Millipore
Minimum essential medium (MEM) (32360-026)	Gibco
Pasteur glass pipettes (with cotton)	VWR
Phosphate-buffered saline (PBS) 1x, pH 7	Gibco
Penicillin-Streptomycin (Pen-Strep)	Invitrogen
pHrodo™ Green <i>E.coli</i> BioParticles™ (P35366)	Invitrogen
Potassium chloride (KCl)	Merck
Potassium Dihydrogen Phosphate (KH <sub>2</sub> PO <sub>4</sub> )	Merck
Propidium iodide (PI)	Sigma Aldrich
Sodium chloride (NaCl)	Roth
Tissue chopper blades	Gillette
Trypan blue	Life Technologies
Tris base	AppliChem

Table 11. Reagents and consumables utilized for *in vitro* and *ex vitro* procedures

## 1.7.2.2. Microglia isolation and culture, phagocytosis assay and FACS solutions

Solution	Composition
BSA solution (for coating Pasteur glass pipettes)	4% BSA in dH <sub>2</sub> O
CytoD stock solution	10 mM CytoD in DMSO
FACS buffer	1% FCS 2mM EDTA in 0.01 M PBS
GM-CSF stock solution	10 µg/mL GM-CSF in 0.1% BSA-PBS
HBSS buffer	7mM HEPES in HBSS 1x
MACS buffer	0.5% BSA 2 mM EDTA in PBS 1x
Microglia culture medium	10% FCS (heat inactivated) 1% Pen-Strep 10 ng/mL GM-CSF (for adult microglia, added freshly) in DMEM/F12 medium

PBS 1x (0.01M)	137 mM NaCl 2.7 mM KCl 1.8 mM KH <sub>2</sub> PO <sub>4</sub> 10 mM Na <sub>2</sub> HPO <sub>4</sub> × 2H <sub>2</sub> O in dH <sub>2</sub> O, pH 7.4
----------------	---

Table 12. Solutions used for microglia isolation, culture and phagocytosis assay

### 1.7.2.3. Organotypic brain slices solutions

Solution	Composition
Dissection media	1% Pen-Strep 10 mM Tris pH 7.2 in MEM medium
GM-CSF stock solution	1 µg/mL GM-CSF in 0.1% BSA-PBS
Slice culture media	25% horse serum (heat inactivated) 25% HBSS 1 mM L-Glutamine 50% MEM medium pH 7.4

Table 13. Solutions used for preparing, culturing and treating organotypic brain slices

### 1.7.3. Mouse procedures: *in vivo* treatments and histology

#### 1.7.3.1. Reagents and key consumables

Reagent	Company
5-Bromo-2'-deoxyuridine (BrdU) (B5002-5G)	Sigma Aldrich
Ethylene glycol, EMSURE®	Merck
Fluoromount aqueous mounting media	Sigma Aldrich
Glycerol	Sigma Aldrich
mGM-CSF (SHD-200-15-1MG) (short treatment 5-month-old mice)	Shenandoah Biotechnology/Biozol
mGM-CSF (415-ML-010/CF), carrier free (short treatment 14-month-old mice and long treatment)	R&D Systems
Hoechst 33342	Thermo Fisher Scientific
Microscope glass slides (cut frosted)	Thermo Fisher Scientific
Microscope cover glasses (24 x 60 mm)	Thermo Fisher Scientific
Normal goat serum	Sigma Aldrich
Optimal Cutting Temperature (O.C.T.) compound (Tissue-Tek embedding medium)	Sakura

Paraformaldehyde (PFA)	Merck
PBS 1x, pH 7 (sterile, for mouse GM-CSF injections)	Gibco
Relief paste	Marabu
Saline isotonic solution (NaCl 0.9%), Braun Ecofl	B. Braun Melsungen
Sodium chloride (NaCl)	Roth
Sodium citrate tribasic dihydrate (C <sub>6</sub> H <sub>5</sub> Na <sub>3</sub> O <sub>7</sub> × 2H <sub>2</sub> O)	Merck
Sodium phosphate dibasic dihydrate (Na <sub>2</sub> HPO <sub>4</sub> × 2H <sub>2</sub> O)	Merck
Sodium phosphate monobasic monohydrate (NaH <sub>2</sub> PO <sub>4</sub> × H <sub>2</sub> O)	Merck
Thiazine red	Sigma Aldrich
Triton X-100	Merck

Table 14. Reagents used for mouse procedures

## 1.7.3.2. Primary antibodies

Name (antigen)	Host Specie	Source or reference	Identifiers	Dilution (notes)
APOE (HJ6.3)	mouse monoclonal	(Kim <i>et al</i> , 2012b)		1:100 (biotinylated)
APP (Y188)	rabbit monoclonal	Abcam	Cat#: 1565-1 RRID: <a href="#">AB 562042</a>	1:2000
Aβ (3552)	rabbit polyclonal	(Yamasaki <i>et al</i> , 2006)		1:5000
Aβ (NAB228)	mouse monoclonal	Santa Cruz	Cat#: sc-32277 RRID: <a href="#">AB 626670</a>	1:2000
BrdU	rat monoclonal	Abcam	Cat#: ab6326 RRID: <a href="#">AB 305426</a>	1:200
CD68	rat monoclonal	Bio-Rad	Cat#: MCA1957G RRID: <a href="#">AB 324217</a>	1:500 (IF) 1:1000 (org. slices)
CLEC7a	rat monoclonal	Invivogen	Cat#: mabg-mdect RRID: <a href="#">AB 2753143</a>	1:50
IBA1	rabbit polyclonal	Wako	Cat#: 019-19741 RRID: <a href="#">AB 839504</a>	1:500
IBA1	goat polyclonal	Abcam	Cat#: ab5076 RRID: <a href="#">AB 2224402</a>	1:500
pE3-Aβ (J8)	mouse monoclonal	(Hartlage-Rubsamen <i>et al</i> , 2018)		1:500 (antigen retrieval)
TMEM119	rabbit monoclonal	Abcam	Cat#: ab209064 RRID: <a href="#">AB 2800343</a>	1:200
TREM2	sheep polyclonal	R&D Systems	Cat#: AF1729 RRID: <a href="#">AB 354956</a>	1:50

Table 15. List of primary antibodies used for immunofluorescence

IF: Immunofluorescence; org. slices: organotypic brain slices

### 1.7.3.3. Secondary antibodies

Fluorescently conjugated (H+L) Alexa Fluor 488, 555 and 647, or streptavidin conjugated Alexa Fluor 488 secondary antibodies raised in goat or donkey were used at 1:500 dilution (normal 30  $\mu$ m brain slices) or 1:250 dilution (organotypic brain slices). All antibodies were purchased from Life Technologies.

### 1.7.3.4. Solutions

Solution	Composition
Anti-freezing solution (for storage of brain slices after cryosectioning)	25% Glycerol 25% Ethylene glycol in 0.1M PBS
Citrate buffer (10 mM) (for antigen retrieval)	10mM C <sub>6</sub> H <sub>5</sub> Na <sub>3</sub> O <sub>7</sub> x 2H <sub>2</sub> O in dH <sub>2</sub> O, pH 6
Blocking solution	5% Goat/donkey serum in PBS-T
BrdU drinking solution (for <i>in vivo</i> study) (light sensitive!)	1mg/mL BrdU 1% sucrose desalted H <sub>2</sub> O
Cryoprotectant solution (for brains freezing)	30% sucrose in 1x PBS
Fixation solution (organotypic brain slices)	4% PFA 4% Sucrose in dH <sub>2</sub> O, pH 7.4
GM-CSF injection solution (short treatment 5-month-old mice)	200 $\mu$ g/Kg weight in saline (NaCl, 0.9% sterile)
GM-CSF injection solution (short treatment 14-month-old mice and long treatment)	200 $\mu$ g/Kg weight in sterile PBS (Gibco)
Hoechst (for nuclei staining)	1:2000 dilution in blocking solution
Ketamine-Xylazine anesthetic (for perfusion, euthanasia)	60% Ketamine (400 mg/kg) 20% Xylazine (27 mg/kg) 20% NaCl
Perfusion/brain post-fixation solution	4% PFA in 1x PBS
Permeabilization/washing solution (PBS-T)	0.5% Triton X-100 in PBS (1x)
Phosphate buffer solution (PBS) 1x (0.1M) (for perfusion and histology)	154 mM NaCl 19 mM NaH <sub>2</sub> PO <sub>4</sub> x H <sub>2</sub> O 81 mM Na <sub>2</sub> HPO <sub>4</sub> x 2H <sub>2</sub> O in dH <sub>2</sub> O, pH 7.4
Thiazine red solution	2 $\mu$ M Thiazine red in PBS

**Table 16. Solutions utilized for mouse procedures including histology**

## 1.7.4. Biochemistry: Western blotting

### 1.7.4.1. Reagents and key consumables

Reagent	Company
Acrylamide/Bis solution 37.5:1	Serva
Ammonium persulfate (APS)	Roche
BCA (Bicinchoninic acid) protein assay kit	Interchim
Bromophenol blue	Fluka
Diethylamine	Sigma Aldrich
ECL™ Prime Western Blotting System	GE Healthcare
Ethylenediaminetetraacetic Acid (EDTA) 0.5M, UltraPure™, pH 8.0	Thermo Fisher Scientific
Formic acid	Sigma Aldrich
Glycerol	Sigma Aldrich
IGEPAL® CA-630	Sigma Aldrich
Isopropanol	Roth
Milk (skim) powder	Sigma Aldrich
NaCl	Roth
Nitrocellulose membrane, 0.1 µm	GE Healthcare
Phosphatase Inhibitor Cocktail (PhosSTOP)	Sigma Aldrich
Precellys homogenization tubes (2 mL)	Bertin Corp.
Precision Plus Protein™ Dual Color Standards (protein Standard)	Bio-Rad
Precision Plus Protein™ Dual Xtra Prestained (protein Standard)	Bio-Rad
Protease Inhibitor Cocktail cOmplete™, EDTA-free	Sigma Aldrich
Protein Assay Dye Reagent Concentrate (for Bradford assay)	Bio-Rad
PVDF membranes, Immobilon-P	Millipore
Running Buffer (10X) Novex® Tricine SDS (for Tricine gels)	Thermo Fisher scientific
Sodium dodecyl sulfate (SDS)	Sigma Aldrich
Sodium Deoxycholate	Sigma Aldrich
Sodium pyrophosphate	Sigma Aldrich
Tetramethylethylenediamin (TEMED) (99%)	Roth
10-20% Tricine Protein Gels, 1.0 mm, 12-well Novex™ (for XCell SureLock Mini-Cell electrophoresis system)	Thermo Fisher scientific
Tris	AppliChem
Tris/Glycine Buffer (10x)	Bio-Rad
Tween-20	Merck
Western HRP substrate Immobilon	Merck
β-Mercaptoethanol	Roth

**Table 17. Reagents used for Western blotting**

### 1.7.4.2. Primary antibodies

Name (antigen)	Host Specie	Source or reference	Identifiers	Dilution	Notes*
A $\beta$ (3552)	rabbit polyclonal	(Yamasaki <i>et al.</i> , 2006)	-	1:2000	Reducing, Ag retrieval
A $\beta$ (2D8)	rat monoclonal	(Shirotani <i>et al.</i> , 2007)	-	1:50	Reducing, Ag retrieval
APOE	goat polyclonal	Millipore	Cat#: AB947 RRID: <a href="#">AB_2258475</a>	1:1000	Reducing, Ag retrieval
CD68	rat monoclonal	Bio-Rad	Cat#: MCA1957G RRID: <a href="#">AB_324217</a>	1:1000	Non-reducing
CSF1R	goat polyclonal	Cell Signaling	Cat#: 3152 RRID: <a href="#">AB_2085233</a>	1:1000	Reducing
FABP5	goat polyclonal	R&D Systems	Cat#: AF1476 RRID: <a href="#">AB_2293656</a>	1:400	Reducing
GAPDH	mouse monoclonal	Abcam	Cat#: ab8245 RRID: <a href="#">AB_2107448</a>	1:2000	Reducing
SYK	rabbit polyclonal	Cell Signaling	Cat#: 2712 RRID: <a href="#">AB_2197223</a>	1:1000	Reducing
p-SYK (Tyr525/526)	rabbit polyclonal	Cell Signaling	Cat#: 2711 RRID: <a href="#">AB_2197215</a>	1:1000	Reducing
TREM2 (5F4)	rat monoclonal	(Xiang <i>et al.</i> , 2016)		1:10	Reducing

**Table 18.** List of primary antibodies used for protein detection by Western blotting

- Non-Reducing conditions: proteins do not receive any pre-treatment (no denaturation of proteins required) before protein electrophoresis.
- Reducing conditions: denaturation of proteins with reducing agent such as  $\beta$ -mercaptoethanol before protein electrophoresis.
- Ag retrieval: After protein transfer, membrane is boiled to unmask protein epitope and this way facilitate antibody binding.

### 1.7.4.3. Secondary antibodies

Horse radish peroxidase (HRP) coupled secondary antibodies raised in goat or donkey against different species (rabbit, rat, mouse or goat) were used at a 1:4000 dilution and purchased from Promega and Santa Cruz Biotechnology.

## 1.7.4.4. Solutions

Solution	Composition
Antibody solution	0.4% BSA (1mL 5% BSA solution) in TBS-T (12 mL)
Blocking solution (total proteins)	5% skim milk in TBS-T solution
Blocking solution (phosphorylated proteins)	5% BSA in TBS-T solution
BSA solution	5% BSA in dH <sub>2</sub> O
DEA buffer	0,2% Diethylamine 1x protease inhibitor (add freshly) 1x phosphatase inhibitor (add freshly) 50 mM NaCl, in dH <sub>2</sub> O, pH 10
Formic acid (FA) solution	70% FA in dH <sub>2</sub> O
Laemmli buffer (4x) (loading buffer)	8% SDS 40% Glycerol 125 mM Tris pH 6.8 0.025% Bromophenol blue 10% β-Mercaptoethanol (without it for non-reducing conditions) in dH <sub>2</sub> O
RIPA buffer (5x stock solution)	100 mM Tris pH 7,4 750 mM NaCl 5% IGEPAL 12.5 mM Sodium pyrophosphate 5% Sodium-deoxycholate in dH <sub>2</sub> O
RIPA buffer (1x) (lysis buffer)	1x RIPA buffer (from stock 5x) 1mM EDTA 1x protease inhibitor (add freshly) 1x phosphatase inhibitor (add freshly) 0.1% SDS in dH <sub>2</sub> O
Running buffer (for Tricine gels)	1x Novex® Tricine SDS Running buffer in dH <sub>2</sub> O (from 10x stock)

Running buffer (for bis-tris acrylamide gels)	1x Tris/Glycine Buffer in dH <sub>2</sub> O (from 10x stock) 0.1% SDS
Running/separating gel buffer (4x) (for separating acrylamide gel)	1.5 M Tris 0.4% SDS in dH <sub>2</sub> O, pH 8.8
Stacking gel buffer (4x) (for stacking acrylamide gel)	0.5% Tris 0.4% SDS in dH <sub>2</sub> O, pH 6.8
STET buffer 1x (lysis buffer)	50 mM Tris 2 mM EDTA 150 mM NaCl 1% Triton X-100 1x Protease inhibitor (add freshly) 1x Phosphatase inhibitor (add freshly) in dH <sub>2</sub> O, pH 7.5
TBS (10x) buffer	200 mM Tris base 1.5 M NaCl in dH <sub>2</sub> O
TBS-T solution	1x TBS 0.1% Tween-20
Transfer buffer	1x Tris/Glycine Buffer (from 10x stock) in dH <sub>2</sub> O

Table 19. Solutions used for sample lysis and western blotting

## 1.8. Software

Name	Source
Adobe Illustrator	Adobe Systems, Inc, USA
DAVID version 6.8	<a href="https://david.ncifcrf.gov/">https://david.ncifcrf.gov/</a>
GraphPad Prism 8	<a href="https://www.graphpad.com/scientific-software/prism/">https://www.graphpad.com/scientific-software/prism/</a>
ImageJ-FIJI	NIH ( <a href="https://imagej.nih.gov/ij/">https://imagej.nih.gov/ij/</a> )
Maxquant	<a href="https://www.maxquant.org/">https://www.maxquant.org/</a> , Max-Planck Institute Munich
Spectronaut (version 12.0.20491.11)	Biognosys
FlowJo	Tree Star

Table 20. Software tools used in this study

## 2. Methods

### 2.1. Genotyping of transgenic mouse lines

To extract the genomic DNA from mouse biopsies (ear or tail piece), alkaline lysis was performed using 100  $\mu\text{L}$  of 50mM NaOH solution per sample and incubating at 95°C for 45 min on a heating block. Every 15 min samples were briefly vortexed in order to ease the tissue lysis. Then, samples were neutralized with 10 $\mu\text{L}$  of 1.5M Tris buffer (pH 8.8) and centrifuged at maximum speed (at 4°C) in a tabletop centrifuge. The supernatant containing mice genomic DNA was used for the polymerase chain reaction (PCR).

For the PCR, a master mix was prepared for all samples (final volume of 20  $\mu\text{L}$  per sample), as follows:

Reagent	Amount (1 sample)
5x Buffer GoTaq	4 $\mu\text{L}$
dNTPs (10 mM)	0.5 $\mu\text{L}$
Fw-Primer (10 pmol/ $\mu\text{L}$ )	1 $\mu\text{L}$
Rev-Primer (10 pmol/ $\mu\text{L}$ )	1 $\mu\text{L}$
Taq-Polymerase (5 U/ $\mu\text{L}$ )	0.2 $\mu\text{L}$
dH <sub>2</sub> O	12.3 $\mu\text{L}$
*DNA (was added to each sample tube as last step)	1 $\mu\text{L}$

Table 21. PCR master mix recipe

#### 2.1.1. PCR program for APPPS1 genotyping

For genotyping of the APPPS1 line, two separate PCRs were performed, one to detect the human *APP* transgene and the second one to detect the *PS1* transgene (corresponding primers were listed in section 1.7.1.1). The thermocycler program was the same for both PCRs, defined as follows:

Step	Temperature	Duration	Cycles
Initial denaturation	95°C	10 min	1x
Denaturation	95°C	30 sec	30x
Annealing	63°C	30 sec	
Extension	72°C	30 sec	
Final extension	72°C	5 min	1x
Holding	4°C	hold	

Table 22. PCR program used to genotype the APPPS1 line

PCR products were separated by electrophoresis on a 1% agarose gel prepared in TAE buffer supplemented with 1:20000 GelRed (for DNA bands visualization). The gel electrophoresis was run in TAE buffer at 100 V for approximately 30 min depending on desired band separation. PCR

amplification products were visualized under UV light uncovering specific bands for each transgene: APP: ~250 bp and PS1: ~250 bp.

### 2.1.2. PCR program for APP<sup>NL-G-F</sup> genotyping

For determining the genotype of the APP<sup>NL-G-F</sup> line, I also used two separate PCRs, one to detect the knock-in (KI) human mutated A $\beta$  sequence within the mouse *App* gene (between exons 16 and 17) and the second one to detect the mouse WT A $\beta$  sequence using the corresponding primers (section 1.7.1.1). The same thermocycler program was used for both PCRs and defined as follows:

Step	Temperature	Duration	Cycles
Initial denaturation	95°C	3 min	1x
Denaturation	94°C	30 sec	35x
Annealing	49°C	30 sec	
Extension	72°C	30 sec	
Final extension	72°C	5 min	1x
Holding	4°C	hold	

**Table 23. PCR program used to genotype the APP<sup>NL-G-F</sup> line**

The PCR products were separated using a 1.5% agarose-TAE gel using the same conditions as described for the APPPS1 line. PCR product bands were ~700 bp (WT band) and ~400 bp (KI band).

## 2.2. Microglia isolation, *in vitro* and *ex vivo* assays

### 2.2.1. Microglia isolation

Isolation of CD11b-positive microglia from APPPS1 and APP-KI mice was performed using the magnetic-activated cell sorting (MACS) technology. Briefly, mice were euthanized by CO<sub>2</sub> inhalation and subsequent cervical dislocation. From isolated brains, the cerebellum, brain stem and olfactory bulb were removed and the remaining brain tissue (cerebrum) was freed from meninges and subsequently chopped into small pieces. Tissue pieces were then dissociated by enzymatic digestion using the Neural Tissue Dissociation Kit (P) and further homogenized by mechanical dissociation using three glass Pasteur pipettes of decreasing diameter. Next, the brain homogenate was incubated with CD11b-coupled magnetic microbeads and loaded into MACS magnetic LS columns for separating the CD11b-labelled microglia fraction (CD11b-enriched fraction) and the CD11b-depleted fraction (flow-through containing the rest of brain cells). A detailed step-by-step protocol is outlined in appendix section 2.

For mass spectrometry-based proteomic analysis and western blotting, microglia pellets were washed twice with HBSS buffer in order to remove the BSA of the MACS buffer and then snap frozen in liquid nitrogen and stored at -80°C until the analysis.

### **2.2.2. Microglial phagocytosis of labelled-*E.coli* particles**

Analysis of microglial phagocytic uptake was performed similarly as previously described (Kleinberger *et al.*, 2014). Briefly, MACS-isolated microglia from 3- and 6-month-old APPPS1, APP-KI and WT mice were cultured in a 24 well plate at a density of  $2 \times 10^5$  cells/well in microglia media in a humidified incubator at 37°C and 5% CO<sub>2</sub>. One day after plating, media was exchanged in order to remove un-attached dead cells from the culture. After 5 days in culture, microglia were incubated with 50 µL of *E.coli*-pHrodo suspension for 60 min. As negative control, CytoD (10 µM) was used as phagocytosis inhibitor and was applied 30 min before the addition of *E.coli* particles. After 60 min of microglial incubation with bacteria particles, all further steps were done on ice (or at 4°C). Non-phagocytosed *E.coli* particles were carefully washed 4 times with PBS and microglia attached to the plate were incubated with CD11b-APC-Cy7 antibody (1:200) in fluorescence activated cell sorting (FACS) buffer (section 1.7.2.2) for 30 min. Finally, microglia were washed two times with PBS and scraped off in 500 µL of FACS buffer and transferred to FACS tubes for flow cytometry analysis. Per experiment, a minimum of three replicates per genotype and age were used. A total of three (3-month-old group) and 2 (6-month-old group) independent experiments were performed.

*E.coli*-pHrodo suspension was prepared according to manufacturer instructions by reconstituting the lyophilized product with 2 mL of PBS at a concentration of 1mg/mL. In order facilitate the homogenization of the suspension, few minutes before adding the bacterial solution to microglia in culture, it was sonicated (in a water bath sonicator) for 5 min. Bacterial suspension was reused for a maximum of 5 days after reconstitution and stored at 4°C protected from the light.

### **2.2.3. FACS analysis**

For the analysis of MACS-isolated microglia purity, around 12000 cells from freshly isolated CD11b-enriched (microglia) and CD11b-depleted (flow-through) fractions were incubated with CD11b-APC-Cy7 antibody (1:200) in FACS buffer for 30 min at 4°C. Then, cells were washed with PBS, resuspended in 300 µL of FACS buffer and transferred to FACS tubes. Prior analysis by flow cytometry, 10 µL of PI solution was added per sample and after few minutes of incubation analysis was performed.

For microglia isolation quality control and phagocytosis assay, unstained and single stained samples, including *E.coli*-pHrodo suspension, were used for the gating strategy in a FACSverse flow cytometer (BD Biosciences). For the detection of the CD11b positive population and *E.coli*-pHrodo, a 635 nm and a 488 nm lasers were used, respectively. A forward scatter height (FSC-H) versus forward scatter area (FSC-A) dot plot allowed the selection of single cells (excluding doublets). PI staining was used to discriminate living (PI negative) from dead (PI positive) for the quality control assessment. FACS data processing was performed using the FlowJo software (Treestar) by Dr. Stefan Roth from Prof. Arthur Liesz lab (ISD institute, Munich) (Sebastian Monasor *et al*, 2020). The mean fluorescence intensity (MFI) of the intracellular *E.coli*-pHrodo was calculated out of the CD11b positive population and represented as the geometric mean according to the FITC fluorochrome.

#### **2.2.4. Preparation of organotypic brain slices and GM-CSF treatments**

Organotypic brain slices from 5-month-old APP-KI mice were prepared similarly to previously described (Daria *et al.*, 2017). Briefly, mice were euthanized by CO<sub>2</sub> inhalation followed by cervical dislocation. Then brains were carefully isolated and placed in 6 cm dish containing 3 mL of pre-cooled dissection media (section 1.7.2.3). Under a dissection microscope, the two brain hemispheres were gently separated using a large (wide rounded) spatula and olfactory bulb, midbrain, brain stem and cerebellum were removed leaving the neocortex and hippocampus intact. Using a thin spatula each hemisphere was placed on the cutting surface and gently flattened with the hippocampus facing up in a perpendicular position to the tissue chopper blade. 350 µm thick sections were cut using the tissue chopper and by using the small spatula, collected into a new 6 cm dish containing 5 mL of fresh dissection media on ice. Under the dissection microscope, cut slices were dissected using fine forceps and undamaged tissue sections of similar size were selected and transferred into a new dish containing 5 mL of fresh dissection media. Brain slices were incubated for 30 min at 4°C in order to stabilize the tissue after the cut. Two slices per dish were plated onto membrane inserts in 3.5 mL dishes filled with 1 mL of pre-warmed and CO<sub>2</sub> equilibrated slice culture media (section 1.7.2.3) and incubated in a humidified incubator at 37°C, 5% CO<sub>2</sub>. 24 hours after plating, media was exchanged and then every 3-4 days. GM-CSF treatments were done in every media exchange for two weeks (4 treatments in total). A solution of 5 ng/mL of GM-CSF (from 1 µg/mL GM-CSF stock solution stored at -20°C) was freshly prepared in pre-warmed and CO<sub>2</sub> equilibrated slice culture media before added to the 3.5 cm dishes (1 mL per dish) 0.1% BSA-PBS (solvent for GM-CSF) was used as a control vehicle.

## 2.3. Mouse procedures

### 2.3.1. GM-CSF treatments of APP-KI mice

GM-CSF injection solution was prepared according to the manufacturer instructions. GM-CSF from Shenandoah/Biozol (used for the short treatment in 5-month-old mice) was dissolved in saline isotonic solution, while GM-CSF from R&D systems (used for the short treatment in 14-month-old mice and for the long treatment) was dissolved in PBS. GM-CSF solution was always prepared sterile before the start of the experiment, aliquoted and stored at -20°C. For every injection, a freshly thawed aliquot was used. The GM-CSF solvent (saline/PBS) was used as a vehicle for the control group. The weight of mice was measured at the beginning of the experiment and an average weight was calculated for females and males in order to keep an injection volume constant per sex group based on the drug dose. Mice health conditions were monitored at the day of the treatment (short treatment) and one day after the treatment (long treatment) using an approved scoring protocol.

BrdU is a synthetic thymidine analog that was used to trace proliferating cells by antibody-mediated detection. BrdU water was freshly prepared one day before administration to the mice (only to Cohort 2, Figure 7 and Figure 8) at a concentration of 1mg/mL and supplemented with 1% sucrose (to mask the bitterness of the BrdU compound). Mice drinking bottles were covered with aluminum foil to protect the solution from the light. BrdU water was provided for a maximum of 2 weeks (Figure 7 and Figure 8).

*In vivo* GM-CSF application were performed following two different experimental paradigms: a short (Figure 7) and a long (Figure 8) treatments.

The short-term application was carried out in 5- and 14-month old APP-KI mice in two mouse cohorts per age group (cohort 1 and 2, Figure 7), following the previously published experimental conditions (Boyd *et al.*, 2010). The mouse cohort 1 was treated with daily GM-CSF (200µg/kg) or vehicle subcutaneous (s.c.) injections for 7 days and the mouse cohort 2 for 21 days, as outlined in Figure 7.

The long-term application was performed in 4-month-old APP-KI mice using again two mouse cohorts (cohort 1 and 2, Figure 8). Mice were treated with weekly GM-CSF (200 µg/kg) or vehicle intraperitoneal (i.p.) injections for a period of 3 months as depicted in Figure 8.

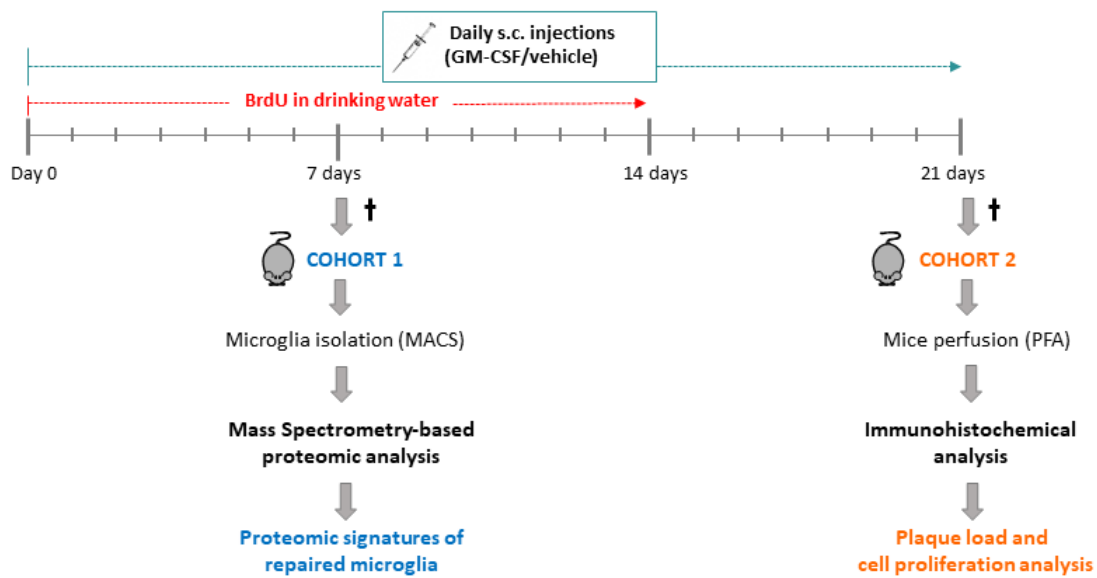


**Figure 7. Experimental paradigm of short-term GM-CSF application.**

Scheme illustrating the experimental setup for GM-CSF short treatment in two different APP-KI mice cohorts. Mouse cohort 1 is treated for 7 days with daily s.c. injections of GM-CSF/vehicle and then brains processed for microglia isolation followed by mass spectrometry-based proteomic analysis. Mouse cohort 2 was treated for 21 days with daily injections of GM-CSF/vehicle and provided during the first 14 days with BrdU in the drinking water. One day after the last injection, mice were perfused, and brains processed for immunohistochemical analysis.

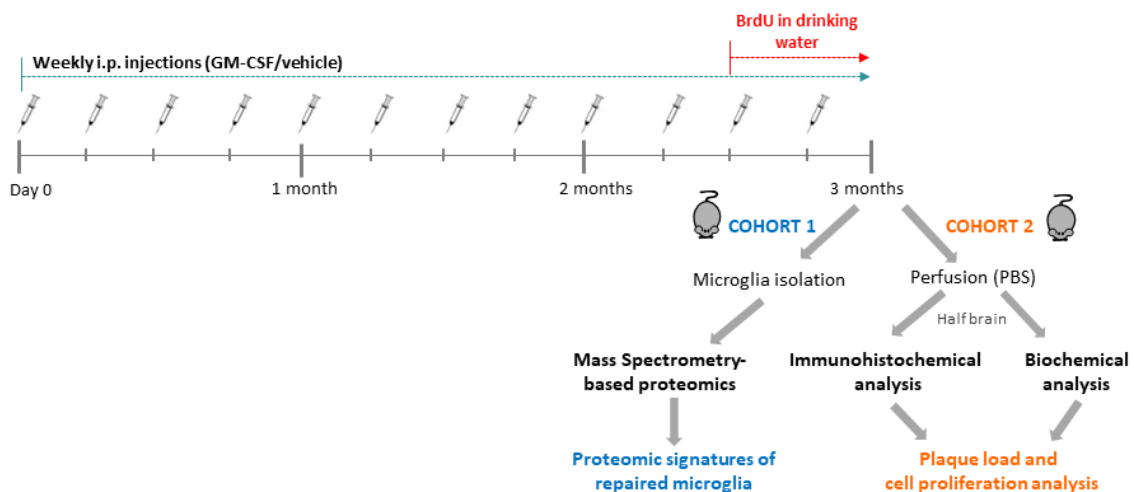


**Figure 8. Experimental paradigm of long-term GM-CSF application.**

Scheme illustrating the experimental setup for GM-CSF longer treatment in two different APP-KI mice cohorts. Mouse cohorts 1 and 2 were treated with i.p. injections of GM-CSF/vehicle for 3 months. One week after the last injection, mice brains from mouse cohort 1 were processed for microglia isolation followed by mass spectrometry-based proteomic analysis. Mice from cohort 2 were provided with BrdU in the drinking water during the last 2 weeks of the treatment. One week after the last injection, mice were perfused with PBS and half brain processed for immunohistochemical analysis and the other half for biochemical analysis.

The information about the mice used in this *in vivo* study is outlined in the following table:

GM-CSF application	Mice age	Cohort	Mice number (N)	Mice sex
Short-term	5 months	1	5	Control (2 ♂ + 3 ♀) Treated (2 ♂ + 3 ♀)
		2	3	Control (3 ♀) Treated (1 ♂ + 2 ♀)
	14 months	1	6	Control (3 ♂ + 3 ♀) Treated (3 ♂ + 3 ♀)
		2	4	Control (3 ♂ + 1 ♀) Treated (2 ♂ + 2 ♀)
Long-term	4 months	1	5	Control (4 ♂ + 1 ♀) Treated (3 ♂ + 2 ♀)
		2	6	Control (2 ♂ + 4 ♀) Treated (3 ♂ + 3 ♀)

**Table 24. Information about mice used for *in vivo* GM-CSF application study**

## 2.3.2. Histology

### 2.3.2.1. Transcardial perfusion

Mice were anesthetized by injecting (i.p.) a mixture of Ketamine and Xylazine solution (section 1.7.3.4). When sensory reflex was absent upon pinching the mouse paws, mice were fixed to a polystyrene surface by the limbs using small pins. At the level of the sternum, a transversal cut in the skin and subjacent muscular layer was made and by cutting longitudinally the thoracic cavity (without damaging internal organs), the heart was exposed. Gently, the tip of a 15-gauge needle (or butterfly needle) attached to the peristaltic pump was introduced in the left ventricle (heart tissue looks lighter) and the needle was fixed in such position to the polystyrene surface (in order to prevent the needle from moving) with the help of a bended needle. Subsequently, the peristaltic pump connected with a cold PBS solution was started and immediately after, a second cut was made in the mouse right atrium in order for the solution to get out of the mouse body. The flow rate was set to 5 mL/min. After 5 minutes of perfusion with PBS, the pump was briefly stopped, and the solution was exchanged by the cold fixation solution (4% PFA, section 1.7.3.4) that was perfused for further 10-15 minutes. The mouse was then decapitated and the brain isolated (color should be whitish if perfusion worked properly) by carefully opening the skull. Brain was post-fixed (4% PFA) for 20 minutes. If one brain hemisphere had to be dedicated to biochemical analysis (like for the long GM-CSF treatment paradigm), mice were perfused only with PBS and one brain hemisphere was post-fixed for 6 hours. Fixed brains were then transferred

to a cryoprotectant solution (30% sucrose) until they sunk to the bottom of the tube (typically within 2 days) and then embedded in O.C.T compound using embedding plastic molds and frozen on dry ice. Embedded frozen brains were stored at -80°C until sectioning.

### **2.3.2.2. Mouse brain cryosectioning**

Whole brains were cut using a cryostat in 30 µm thick coronal sections. Serial sections were collected in two 6-well plates filled with PBS (each cut slice was placed into a new well until the 12<sup>th</sup> well and the process was repeated with the rest of the tissue). When only one hemisphere was embedded, sectioning was done sagittally following the abovementioned procedure. After sectioning, brain slices were briefly washed from O.C.T compound on a shaker and kept on PBS at 4°C up to a maximum of three weeks. After that, brain sections were placed in anti-freezing storing solution maintaining the serial sampling and kept at -20°C until use.

### **2.3.2.3. Immunofluorescence staining of brain sections**

A detailed step-by-step immunohistochemistry protocol was included in our recent publication (“Immunohistological analysis of free floating brain sections”: <https://bio-protocol.org/prep421>) (Sebastian Monasor *et al.*, 2020). Briefly, staining of 30 µm thick brain sections was performed using free-floating conditions. Sections stored in anti-freezing solution were washed in PBS for 10 min and permeabilized in PBS-T (section 1.7.3.4) for 30 minutes in a 12 or 24 well plate. All steps involving incubation or washes were done on a shaker to facilitate a homogeneous tissue staining. If antigen retrieval was required (e.g. for staining of BrdU and pE3-Aβ), citrate buffer (10 mM) was prewarmed in 2 mL tubes for 20 min at 95°C in a heating block and then brain sections were introduced in the buffer and incubated for 25 min at 95°C and low speed shaking (to prevent brain sections from sticking together). Sections were subsequently washed with PBS and cooled down to proceed with staining. To avoid unspecific antibody binding, sections were blocked for 1 hour in blocking solution (5% goat or donkey serum in PBS-T, according to secondary antibodies species). Until here, all steps were performed at RT. Subsequently, brain sections were incubated with corresponding primary antibodies (section 1.7.3.2) in blocking solution overnight at 4°C. The next day, sections were washed 3 times with PBS-T for 10 min and incubated with secondary antibody solution (containing corresponding secondary antibodies-section 1.7.3.3-, and Hoechst stain in blocking solution) for 2 hours at RT. As secondary antibodies are light sensitive, plates were covered with aluminum foil during the incubation. After that, sections were washed 3 times with PBS-T (10 min). If Thiazine red (ThR) staining was performed, after secondary antibody incubation, sections were incubated with ThR solution (2 µM ThR in PBS) for 20 min at RT. Subsequently, sections were washed 3 times with PBS-T and mounted onto

glass slides with the help of a small painting brush. Sections were dried for at least 1 hour and finally covered with mounting media and a coverslip for microscopic analysis. Slides were left to dry at R. in a dark place overnight and then stored at 4°C until microscopic examination.

#### **2.3.2.4. Immunofluorescence staining of organotypic brain slices.**

Fixation of organotypic brain slices was performed with a fixation solution containing 4% PFA/sucrose (section 1.7.3.4) for 15 min at room temperature (RT), followed by 3 washes with PBS within the 3.5 cm dishes used for culturing. Fixed organotypic brain slices attached to membrane inserts were permeabilized with PBS-T for 30 minutes within the same culture dishes. All staining steps were done at RT, including primary and secondary antibody incubations. The membrane where the brain slices were attached was cut out of the insert with a scalpel and placed on a piece of parafilm within a wet metallic chamber to avoid evaporation. Staining was done on a drop of solution covering the membrane that was exchanged using a vacuum pump system. Blocking was performed in the corresponding blocking solution (5% goat or donkey serum) for 1 hour followed by incubation with primary antibodies (in blocking solution) overnight. Brain slices were then washed 3 times with PBS-T and incubated with secondary antibodies (in blocking solution) for 3 hours. After 3 additional washes, the membrane containing the brain slices was mounted onto a glass slide by removing the excess of liquid and covered with few drops of mounting media. Before placing the coverslip, the membrane was surrounded with relief paste to seal the slices and avoid tissue drying.

#### **2.4. Immunofluorescence analyses: image acquisition and quantifications**

Immunofluorescence analyses were performed on microscopy images acquired on a confocal (TCS SP5, Leica Microsystems) or epifluorescence (AxioImager A2, Zeiss) microscopes. Confocal microscope was equipped with an automatic tile-scan system. In order to enable a comparative analysis, microscopy settings were always kept constant during image acquisition for the analyzed experimental groups. For imaging dedicated to quantifications, the scanning speed was set to 600 Hz and for representative pictures to 400 Hz. The pinhole was always kept at 1 AU. Images format was set to 1024 x 1024 pixels.

The specifications for each representative image used in this study are described in figure legends. Images acquired by confocal microscopy are shown as maximum intensity projections from z-stack images.

### 2.4.1. Analysis of plaque load and proliferation upon GM-CSF treatments *in vivo* and *ex vivo*

For the quantification of plaque load (A $\beta$  signal, 3552 antibody) from GM-CSF/PBS-treated organotypic brain slices, 9 pictures (from 3 individual culture dishes) per experiment and condition were taken using a 20x dry objective of a confocal microscope (Leica) for a total of 3 independent experiments. The area covered by A $\beta$  plaques (% A $\beta$  coverage from the total image area) was measured using the “Threshold” and “Analyze particles” functions from ImageJ software. The average from the three independent experiments was calculated.

For immunohistological analysis of plaque load (A $\beta$  signal, 3552 or NAB228 antibodies) and proliferation (BrdU positive cells) from the *in vivo* GM-CSF-treatments, a similar analysis was performed for each experimental group. In the following table, experimental details of each individual analysis including number of images acquired and instrument used, are described:

Mouse cohort	Total A $\beta$	Fibrillar A $\beta$	BrdU+ cells
5-month-old mice (short treatment, pilot study) N=3	8 cortical images from 2 coronal brain sections (10x objective, epifluorescence microscope)	12 cortical images from 3 coronal brain sections (10x objective epifluorescence microscope)	8 cortical images from 2 coronal brain sections (10x objective epifluorescence microscope)
14-month-old mice (short treatment) N=4	18 cortical and 8 hippocampal z-stack images from 3 coronal brain sections (20x dry objective plus 1.5 optical zoom, confocal microscope)	18 cortical and 6 hippocampal images from 3 coronal brain sections (10x objective, epifluorescence microscope)	18 cortical and 8 hippocampal z-stack images from 3 coronal brain sections (20x dry objective plus 1.5 optical zoom, confocal microscope)
	Whole section image analysis (z-stacks) using 3 coronal sections (10x dry objective, confocal microscope with tile-scanning function)	Whole section image analysis (z-stacks) using 3 coronal sections (10x dry objective, confocal microscope with tile-scanning function)	---
4-month-old mice (long treatment) N=6	20 cortical and 5 hippocampal z-stack images from 5 sagittal brain sections (20x dry objective, confocal microscope)	20 cortical and 5 hippocampal z-stack images from 5 sagittal brain sections (20x dry objective, confocal microscope)	20 cortical and 5 hippocampal z-stack images from 5 sagittal brain sections (20x dry objective, confocal microscope)

**Table 25. Details of immunohistological analysis of *in vivo* GM-CSF treatments**

For the quantitative analysis of BrdU positive cells and plaque load, ImageJ software was used. From confocal z-stack images the maximum intensity projection was generated. BrdU positive cells were manually quantified by using the cell counter function. Total and fibrillar A $\beta$  areas (%)

A $\beta$  coverage) were quantified using a self-programmed ImageJ macro (see example in appendix section 3).

#### **2.4.2. Analysis of microglia recruitment, plaque size, dystrophic neurites and CD68 coverage area in APPPS1 and APP-KI mice**

3-month-old APPPS1 and APP-KI mice were used for these analyses. 30 z-stack images (from 3-6 coronal brain sections per mouse) of randomly selected single plaques from similar areas of the neocortex, were taken using a 63X immersion water objective (with 2x digital zoom) of a confocal microscope. For the analysis of these immunofluorescence images, ImageJ software was used. A region of interest (ROI) was manually drawn around every single A $\beta$  plaque area (NAB228 antibody signal). Microglia recruited to the plaque were manually counted throughout the z-stack within the defined ROI using the cell counter function. Then, the maximum intensity projection from each z-stack image was generated and the areas (in  $\mu\text{m}^2$ ) covered by A $\beta$  plaques, dystrophic neurites (APP-Y188 antibody signal) and CD68 were quantified within the ROI using the "Threshold" and "Analyze particles" functions. Number of microglia recruited to A $\beta$  plaques or associated to dystrophic neurites, was normalized to the plaque or dystrophic neurite area, respectively. Similarly, CD68 coverage was normalized to the plaque area or to the number of microglia recruited to amyloid plaques. For dystrophic neurites and A $\beta$  plaques size the absolute values (in  $\mu\text{m}^2$ ) were represented. The number of mice used for each experiment is indicated in figure legends.

#### **2.4.3. Analysis of A $\beta$ and pE3-A $\beta$ coverage area in APPPS1 and APP-KI mice**

3- and 12-month-old APPPS1 and APP-KI mice (N=4 per genotype and age group) were used for the analysis of total A $\beta$  (3552 antibody) coverage and pE3-A $\beta$  coverage, respectively. For each analysis, 18 images in similar neocortical regions from 3 brain sections were taken with a 20x dry objective of a confocal microscope. Quantification of areas covered by total A $\beta$  and pE3-A $\beta$  were performed using a self-programmed macro in ImageJ as depicted in the macro example in Appendix section 3 (for total A $\beta$  quantification) and specifically, in our published manuscript (<https://cdn.elifesciences.org/articles/54083/elifesciences-54083-suppl6-v1.docx>) (Sebastian Monasor *et al.*, 2020).

## 2.5. Biochemistry

### 2.5.1. Western blotting analysis for microglial proteome validation

For the validation of proteomic data, MACS-isolated microglial pellets (frozen) from WT, APPPS1 and APP-KI mice, were used for western blotting. For the validation of APOE, TREM2, CD68, FABP5 and CSF1R, microglia from 12-month old mice were used (N=2 per genotype). For the validation of SYK and p-SYK, microglia from 14-15-month old mice were used (N=2 per genotype). Briefly, microglial pellets were lysed in 100  $\mu$ L STET buffer (section 1.7.4.4) supplemented with 1x proteases and phosphatases inhibitors and incubated on ice for 20 min. To enhance cell lysis, the lysate was sonicated for 4 cycles of 30 sec in a water bath sonicator. Finally, microglial lysates were centrifuged at 9600 x g in a tabletop centrifuge for 5 min at 4°C and pellet was discarded. Protein concentration from microglial samples was measured from 1-5  $\mu$ L of microglia lysates using the Bradford assay (Bio-Rad) according to manufacturer instructions. Samples were mixed with 1x Laemmli buffer (section 1.7.4.4) with or without  $\beta$ -mercaptoethanol (according to reducing or non-reducing conditions, respectively). Samples that required reducing conditions were incubated at 95°C for 5 min before loading into acrylamide gels. 10  $\mu$ g of microglial lysates from two different mice per genotype and 8  $\mu$ L of protein standard were loaded into a bis-tris acrylamide gel (8% or 12%) and separated in a protein electrophoresis system (Mini-protean) in 1x Tris/Glycine running buffer (section 1.7.4.4) at constant voltage (started at 80 V until dye front line went out of the stacking gel into the separating gel, then voltage was increased to 120 V). Proteins were transferred onto PVDF membrane or a nitrocellulose membrane (if antigen retrieval was required) using a sandwich system (wet transfer) in transfer buffer (section 1.7.4.4) for 65 min at constant current (400 mA). After transfer, membranes were blocked in blocking solution (or 5% BSA-TBS-T solution for p-SYK) (section 1.7.4.4). If antigen retrieval was necessary (e.g. for APOE), prior the blocking step, nitrocellulose membrane was boiled (100°C) for 5 min in PBS and then cooled down for few minutes in PBS at RT. After blocking, membranes were briefly washed with PBS and incubated overnight at 4° with corresponding antibodies (section 1.7.4.2) in antibody solution at constant shaking. The next day, membranes were washed 3 times with TBS-T for 10 min and incubated with corresponding HRP-coupled secondary antibodies in antibody solution for 1 hour at RT. Finally, membranes were washed 3 times with TBS-T (10 min) and incubated with HRP chemiluminescent reagent (Western HRP substrate Immobilon or ECL Prime) for antibody band detection with a luminescent image analyzer. GAPDH protein was used as a loading control.

### 2.5.2. Western blotting using mouse tissue for A $\beta$ quantification

For biochemical analysis of A $\beta$  load upon GM-CSF long-term treatment, a fractionation protocol that is based on protein solubility in different lysis buffers (DEA, RIPA and FA) was used. The DEA and RIPA fractions will contain soluble proteins and the FA fraction the more insoluble proteins. A detailed step-by-step protocol can be found in our manuscript ("Biochemical characterization of mouse brain homogenates": <https://bio-protocol.org/prep421>). Briefly, frozen brain hemispheres from N=6 mice (per treatment and control group) were homogenized in 1 mL DEA buffer (1x) using a Precellys homogenizer (6500 rpm, 30sec, 8°C) and homogenates centrifuged (10 min, 5000 x g). The supernatant was then ultracentrifuged (100 000 x g, 30 min, 4°C) and the pellet resuspended in 1 mL RIPA and used further for RIPA protein extraction. From the fraction that was ultracentrifuged, the supernatant (DEA fraction) was collected and neutralized with 10% of 0,5 M Tris, pH 6,8 and stored at -80°C until use. The pellet left after ultracentrifugation was resuspended in 0.1 mL RIPA buffer and used afterwards. The 1mL RIPA lysate from the step before was further homogenized with the Precellys homogenizer (5000 rpm, 12 sec, 8°C) and then centrifuged (5000 x g, 10 min). The pellet was resuspended in 0.5 mL 70% formic acid (FA) and further processed FA extraction and the supernatant was mixed with the 0.1 mL RIPA lysate from the step before and after an ultracentrifugation (100 000 x g, 60 min, 4°C), the supernatant was collected (pellet discarded) as RIPA fraction and stored at -80°C until use. The FA lysate (0.5 mL) was sonicated for 7 min at 4°C and after centrifugation (20 000 x g, 30 min, 4°C), the supernatant was collected (pellet discarded) and neutralized by diluting it 1:20 in 1M Tris buffer pH 9.5 and stored at -80°C until use.

Protein quantification from the DEA and RIPA fractions was performed using the BCA assay according to manufacturer instructions. As protein quantification from the FA fraction is not possible due to incompatibility of FA buffer with protein quantification assays, the volume of lysate used from this fraction for western blot analysis was calculated according to the protein concentration from the DEA fraction for each sample. 40  $\mu$ g and 28  $\mu$ g of tissue lysate (mixed with loading buffer) per line were loaded from the DEA and RIPA fractions, respectively, into 10-20 % Tricin-Protein-Gels (Novex) and separated by protein electrophoresis (XCell SureLock Mini-Cell) in 1x Tricin SDS-Running buffer according to manufacturer instructions. After protein transfer into a nitrocellulose membrane (wet transfer), antigen retrieval was performed by boiling the membrane in PBS for 5 min. The following steps involving antibody-based protein detection were performed as described for the western blot from microglial lysates. For the detection of A $\beta$  from the GM-CSF/vehicle-treated mice, the 2D8 anti-A $\beta$  antibody was used (section 1.7.4.2).

GAPDH and ACTIN were used as loading controls. A $\beta$  quantifications from western blot analysis were performed using ImageJ software, using loading controls as normalization factor.

Western blotting of fibrillar A $\beta$  (FA fraction) from 3, 6 and 12-month-old APPPS1 and APP-KI mice brains was done by Michael Willem and Heike Hampel from Prof. Christian Haass laboratory (DZNE, Munich) following the above described protocol (Sebastian Monasor *et al.*, 2020). For the detection of A $\beta$  the 3552 anti-A $\beta$  antibody was used (section 1.7.4.2).

## 2.6. Proteomic analysis

Frozen pellets of MACS-isolated microglia ( $2 \times 10^6$  cells in average) from 1-, 3-, 6- and 12-month-old APPPS1, APP-KI and corresponding age-matched WT (C57BL/6J) mice (N=3 per genotype and age) were used for mass spectrometry-based proteomic analysis. APPPS1/WT and APP-KI/WT microglial samples were analyzed independently. Similarly, microglia pellets from APP-KI mice treated with GM-CSF/vehicle (from three independent experiments: 5-month old mice, short treatment: N=5 mice; 14-month-old mice, short-treatment: N=6 mice; 4-month-old mice, long treatment: N=5 mice), were processed for mass spectrometry analysis. Sample processing and mass spectrometry analysis, were performed by Dr. Stephan Müller from Prof. Stefan Lichtenthaler lab (DZNE, Munich) (Sebastian Monasor *et al.*, 2020).

### 2.6.1. Sample processing

Briefly, microglial pellets were lysed in STET lysis buffer (section 1.7.4.4) and after protein quantification (Pierce 660 nm protein assay, Thermo Fisher Scientific), 15  $\mu$ g of protein per sample were processed for protein tryptic digestion following the filter aided sample preparation protocol (FASP) (Wisniewski *et al.*, 2009) using Vivacon spin filters (30 kDa cut-off, Sartorius).

### 2.6.2. Mass spectrometry analysis

For label-free quantification (LFQ) of proteins, peptides were analyzed using a LC-MS/MS set up, equipped with an EASY-nLC 1000/1200 UHPLC system (Thermo Fisher Scientific), a NanoFlex ion source (Thermo Fisher Scientific) with a PRSO-V1 column oven (Sonation) and a Q-Exactive HF Hybrid Quadrupol-Orbitrap mass (Thermo Fisher Scientific). 1.3  $\mu$ g of peptides were separated using a binary gradient (180 min) of water and acetonitrile with 0.1% formic acid on home-made C-18 columns (30 cm x 75  $\mu$ m) at 50°C.

For the generation of the spectral library, the APPPS1/WT samples were analyzed applying the Data Dependent Acquisition (DDA) using a full MS scan (m/z range: 300-1400; resolution: 120000,

followed by 15 MS/MS scans of the most intense peptide ions (normalized collision energy (NCE): 26%). A dynamic exclusion of 120s was applied for peptide fragmentation.

Proteomic data from APPPS1, APP-KI and WT microglia and APP-KI microglia from GM-CSF/vehicle-treated mice, was acquired using Data Independent Acquisition (DIA), which included a full MS scan (m/z range: 300–1400; resolution: 120000) and 25 MS/MS scans (m/z range: 300–1400 with consecutive m/z windows, resolution: 30000). A stepped NCE of  $26 \pm 2.6\%$  was used for peptide fragmentation.

### 2.6.3. Data analysis

DDA data was analyzed with the Maxquant software. The UniProt canonical fasta database of *Mus musculus* (downloaded on 01.11.2017), was used as a reference library for the analysis, in addition to the sequence of human *APP* with the Swedish mutation and the iRT peptides. Trypsin was defined as the protease and two missed cleavages were permitted for the database search. Only unique peptides were considered for the quantification. LFQ intensities normalization was performed independently for each age group. The False Discovery Rate (FDR) was set to 1% for both peptides and proteins. With the Maxquant results of the APPPS1 dataset, a spectral library was generated using the Spectronaut software (version 12.0.20491.11, Biognosys) applying the default settings, and the DIA datasets from both mouse models were analyzed with this spectral library. LFQ of proteins (on peptide fragment ions) was set to at least one quantified peptide per protein. Protein quantification was based on maximum three peptides per protein group.

Using the Perseus software, protein LFQ intensities were log<sub>2</sub> transformed and log<sub>2</sub> fold changes were calculated between transgenic and WT samples, or from GM-CSF-treated and control samples, for each age group and mouse model. Only the proteins showing a consistent quantification in all samples of an age group were used for statistical testing. A two-sided Student's t-test was used to analyze the statistical significance of changed proteins (log<sub>2</sub> fold change of the transgenic *versus* the WT, or GM-CSF-treated *versus* control) for each age group. In addition, a permutation-based FDR estimation (FDR threshold= 5%, s<sub>0</sub>= 0.1) was applied for multiple hypothesis correction. The significance of changed proteins was defined as the log<sub>2</sub> fold change larger than 0.5, or smaller than -0.5, with p-value lower than 0.05 and significant regulation after FDR. The same criteria were used for the comparative analysis with transcriptomics data.

Gene ontology (GO) enrichment analysis was performed using the web-software DAVID. Up- and down-regulated early, middle and advanced MARPs were analyzed independently for cellular component, biological process and molecular function using all consistently quantified proteins in APPPS1 and APP-KI microglia, as database background with a medium stringency. An enrichment score of 1.3 was considered as threshold for the GO analysis.

Mass spectrometry raw data analysis from APPPS1 and APP-KI microglia can be found at the ProteomeXchange Consortium through the PRIDE partner repository (Perez-Riverol *et al.*, 2019) with the identifier: PXD016075. The full list of early-, middle- and advanced-MARPS can be found as Figure 2-source data 1 in our manuscript: <https://cdn.elifesciences.org/articles/54083/elifesciences-54083-fig2-data1-v1.xlsx>; (Sebastian Monasor *et al.*, 2020). The list of significantly regulated proteins (by p value) from microglial proteomic analysis of GM-CSF-treated APP-KI mice can be found in the appendix section 1.

## 2.7. Statistical analysis

Statistical analyses for all experiments (excluding mass spectrometry analysis) were performed in GraphPad Prism using the appropriate test according to each experimental design. The statistical test used for each analysis including the number of biological replicates (N) is indicated in the figure legends. Analyzed data are expressed as the mean  $\pm$  standard deviation (SD) from at least 3 independent experiments, except for the results from the phagocytosis assay from 6-month-old mice, where only two independent experiments were performed. P-value statistical significance was defined as  $p < 0.05$  (\*  $p < 0.05$ , \*\*  $p < 0.01$ , \*\*\*  $p < 0.001$  and \*\*\*\*  $p < 0.0001$ , n.s: not significant).

## Results

### 1. Characterization of microglial proteome dynamics along AD progression

The first aim of my study was to examine microglial proteomic changes in response to amyloid accumulation along AD progression. To address that, I took advantage of two different amyloidosis mouse models, the APPPS1 and the APP<sup>NL-G-F</sup> knock-in (APP-KI) mouse model (Radde *et al.*, 2006; Saito *et al.*, 2014). APPPS1 mice overexpress the human mutated *APP* (Swedish- K670N/M671L) and *PS1* (L166P) genes under the neuronal mouse Thy-1 promoter (Radde *et al.*, 2006). In turn, the APP-KI mice, express the humanized A $\beta$  sequence with three familial AD mutations (Swedish (K670N/M671L), Arctic (E693G) and Iberian (I716F)) under the control of the endogenous mouse promoter (Saito *et al.*, 2014). Although these mouse models differ in regard to APP expression (overexpression *versus* physiological), both manifest a robust A $\beta$  plaque pathology starting at 6-8 weeks, (Radde *et al.*, 2006; Saito *et al.*, 2014). The majority of the data presented within the results section 1 was recently published (Sebastian Monasor *et al.*, 2020).

#### 1.1. Amyloid plaque burden in APPPS1 and APP-KI mouse models: definition of pathological stages

Since I was interested in analyzing microglial proteomic changes during AD progression, I first defined the pathological stages to be investigated based on the A $\beta$  burden. As already indicated, plaque deposition starts between 6-8 weeks in both mouse models, therefore, 1 month of age represented a pre-deposition stage and 3, 6 and 12 months of age were defined as early, middle and advanced stages of A $\beta$  pathology, respectively. Immunohistochemical analysis of A $\beta$  coverage revealed a comparable plaque load between both mouse models at the three pathological stages (Figure 9).

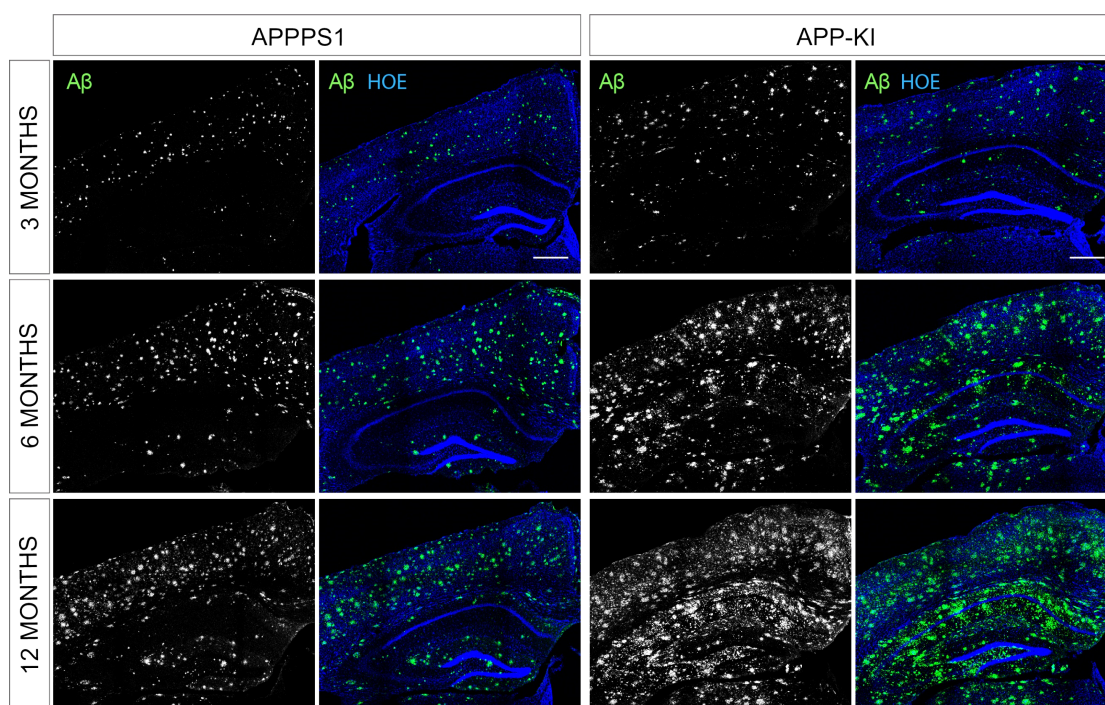


**Figure 9. Immunohistological analysis of A $\beta$  burden in APPS1 and APP-KI mice.**

Representative images of A $\beta$  pathology in 3, 6 and 12-month-old APPS1 and APP-KI mice in comparable cortico-hippocampal regions. NAB228 antibody was used for A $\beta$  detection (green) and Hoechst (HOE, blue) for nuclear staining. Images were acquired with a 10x dry objective with a tile-scanning system. Scale bar: 400  $\mu$ m. Retrieved from (Sebastian Monasor *et al.*, 2020).

## 1.2. MACS microglial isolation enables proteomic analysis of AD microglia

In contrast to transcriptomic analyses, which do not require a large number of cells (~1000 cells) (Krasemann *et al.*, 2017), mass spectrometry-based proteomics demands a significantly larger amount of cells (500.000-1.000.000 cells) for the analysis. In order to achieve high microglial yields without pooling different biological samples, I used MACS technology as method for microglial isolation. For that, the mice cerebrum, that is the most affected region by A $\beta$  pathology (Radde *et al.*, 2006; Saito *et al.*, 2014), was used for the isolation procedure, resulting in a CD11b-enriched fraction (microglia) and a CD11b-depleted fraction (rest of brain cells). An average of  $2 \times 10^6$  CD11b positive microglia were obtained per mouse brain, which enabled proteomic analysis of single mice. The purity of isolated microglia was controlled by FACS, which revealed a 97% of CD11b positive microglia in the CD11b-enriched fraction (Figure 10A). Remarkably, only 0.49% of CD11b positive cells were detected in the CD11b-depleted fraction (Figure 10B), indicating a high purity and efficiency of the isolation procedure.

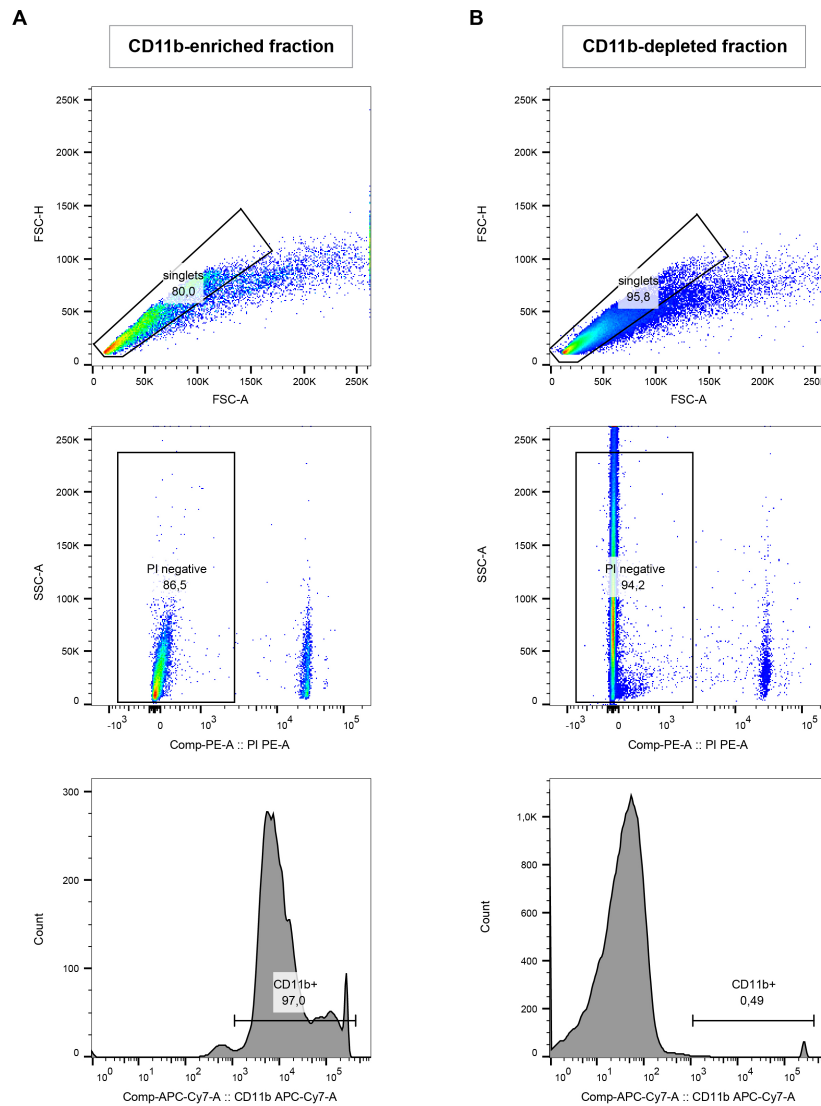


**Figure 10. Microglia isolation quality control by FACS.**

FACS analysis of MACS isolated microglia from CD11-enriched fraction (A) and CD11b-depleted fraction (B). For every cellular fraction, FACS analysis was performed from upper (single cell selection) to lower panels (CD11b positive or negative population). Propidium Iodide (PI) was used for cell viability assessment (PI negative fraction represents the viable population). Numbers within the plots indicate percentages of the population selected in the upper plot. Retrieved from (Sebastian Monasor et al., 2020).

### 1.3. Microglial proteome changes appear earlier in APPPS1 than in APP-KI mice

To investigate how the microglial proteome changes in response to A $\beta$  accumulation, MACS-isolated microglia from APPPS1 and APP-KI mice at 1 month (pre-deposition stage) and 3, 6 and 12 months (early, middle and advanced disease stages, respectively) and their corresponding aged-matched WT controls, were subjected to mass spectrometry-based proteomics. This analysis

revealed a consistent relative protein quantification of over 5000 proteins across the different disease stages in both mouse models (Table 26 and Table 27).

	APPPS1 vs. WT			
	1M	3M	6M	12M
Total quantified	5491	5789	5848	5669
Regulated	98	1010	679	1409
Up-regulated	76	332	365	776
Down-regulated	22	678	314	633
Up-regulated FDR corrected	0	332	309	776
Down-regulated FDR corrected	0	678	261	633

**Table 26. Proteomic data analysis from APPPS1 microglia.**

Modified from (Sebastian Monasor et al., 2020).

	APP-KI vs. WT			
	1M	3M	6M	12M
Total quantified	5713	5711	5653	5715
Regulated	41	700	559	1337
Up-regulated	19	22	245	704
Down-regulated	54	109	267	666
Up-regulated FDR corrected	0	1	140	704
Down-regulated FDR corrected	0	0	151	666

**Table 27. Proteomic data analysis from APP-KI microglia.**

Modified from (Sebastian Monasor et al., 2020).

Since each mouse model was independently analyzed by mass spectrometry, as quality control, we examined how many proteins were consistently quantified in each individual analysis. We detected an overlap of 93.5% (5500 proteins) quantified proteins between the APPPS1 and APP-KI at the 12 months stage (Figure 11), that indicated a robust and consistent data acquisition from both mouse models and excluded differences linked to a model-dependent analysis.

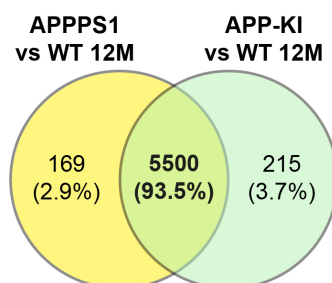


**Figure 11. Consistent protein quantification by mass spectrometry-based proteomic analysis in APPPS1 and APP-KI microglia at 12 months.**

Ven diagram showing the overlap in relative protein quantification in both mouse models. Percentages indicate the amount of proteins identified in both mouse models relative to the total amount of quantified proteins in the respective mice. Modified from (Sebastian Monasor et al., 2020).

To assess proteomic alterations in AD microglia compared to WT at the different pathological stages, significant changes were defined according to the following criteria: a log<sub>2</sub> fold change (transgenic *versus* WT) larger than 0.5 or smaller than -0.5, with a significant p-value (p<0.05) and in addition, significance after FDR correction. FDR correction provides another level of control to avoid false positive changes.

Proteomic analysis results represented by volcano plots revealed no changes in any of the two transgenic mice at 1 month of age (Figure 12A and B, and Table 26 and Table 27), indicating that microglia shows no response prior amyloid deposition. However, at the early pathological stage (3 months), prominent changes (both up and down-regulated) were already observed in APPPS1 microglia (Figure 12C and Table 26). In contrast, the proteome of APP-KI microglia remained mostly unchanged at this early stage (Figure 12D and Table 27). These differences in microglial response at the age of 3 months were surprising, as both mouse models showed a comparable plaque burden (Figure 9). At 6 months of age, APPPS1 microglia continued to show progressive proteomic changes (Figure 12E and Table 26). The first proteomic alterations were now also observed in APP-KI microglia (Figure 12F and Table 27). At 12 months of age, when both mouse models presented an extensive A $\beta$  pathology (Figure 9), a substantial number of microglial proteomic changes could be observed in both models (Figure 12G and H and Table 26 and Table 27).

Taken together, this study revealed a dataset of microglial proteomic alterations along the progression of A $\beta$  pathology. In addition, I discovered that microglial response to A $\beta$ , occurs earlier in the APPPS1 mouse model compared to the APP-KI, while both models show similar responses at advanced pathological stages.

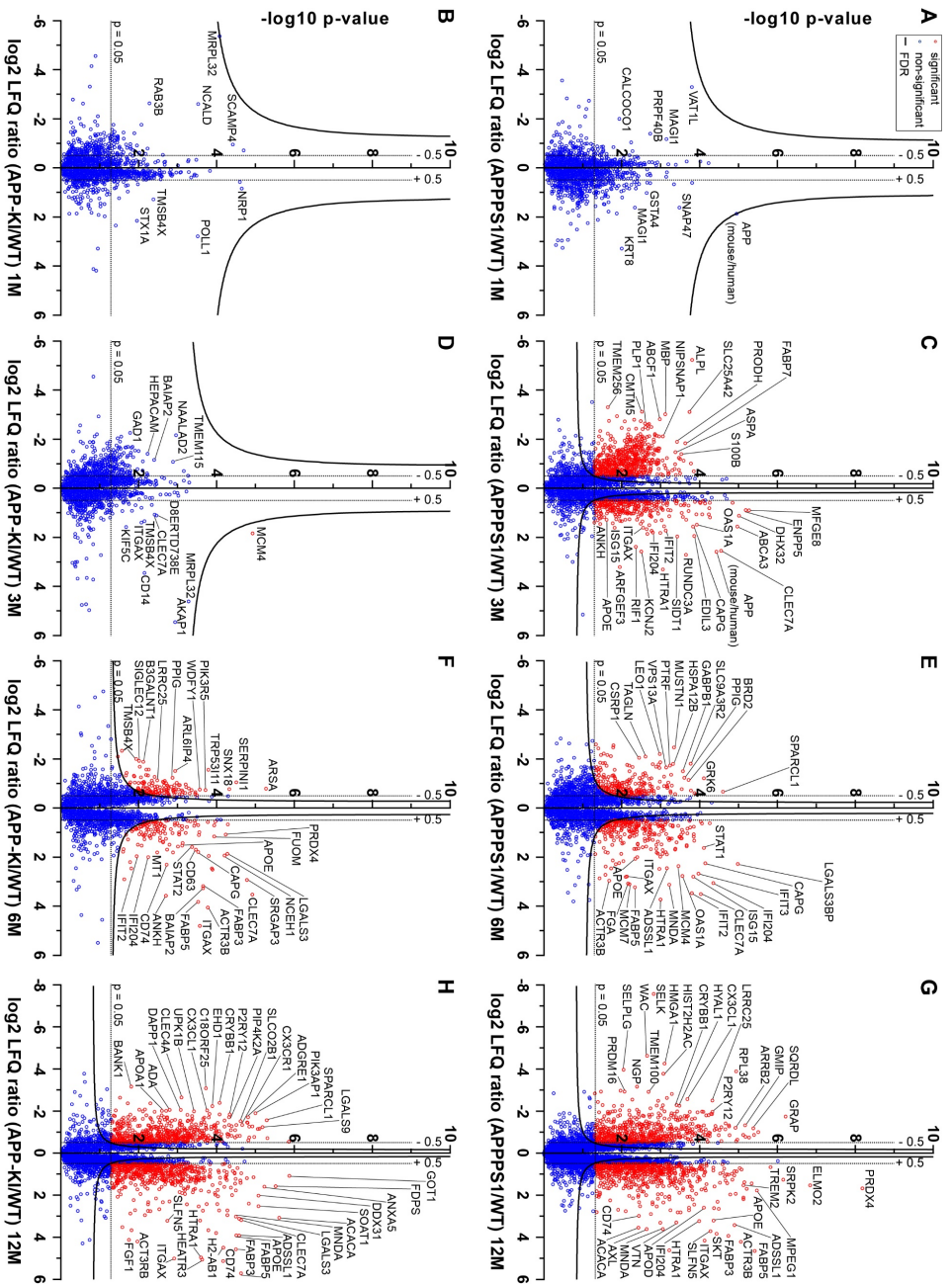


**Figure 12. Proteomic analysis of APPS1 and APP-KI microglia during AD progression.**

Volcano plots representing the  $-\log_{10}$  transformed p-value against the  $\log_2$  transformed LfQ ratios ( $\log_2$  fold changes) of APPS1 and APP-KI *versus* WT microglia at 1 (A and B), 3 (C and D), 6 (E and F) and 12 (G and H) months of age. Hyperbolic curves show the FDR estimation. Proteins with  $\log_2$  fold change lower than -0.5 or higher than +0.5 with a p-value less than 0.05 which passed the FDR correction (FDR = 0.05,  $s_0 = 0.1$ ) are indicated in red. Non-significantly changed proteins are indicated in blue. Selected proteins are labelled using their gene names. Retrieved from (Sebastian Monasor *et al.*, 2020).

#### 1.4. Identification of Microglial A $\beta$ Response Proteins (MARPs)

Microglial proteomic analysis revealed a substantial amount of proteins that were progressively up- or down-regulated following the kinetics of amyloid accumulation. This pattern was found in both mouse models, even if changes were detected earlier in APPPS1 mice (Figure 13A). Therefore, these proteins were classified as **Microglial A $\beta$  Response Proteins (MARPs)**. MARP signatures underscore microglial response to A $\beta$  at the different disease stages, revealing distinct microglial-response phases. As the APPPS1 microglial proteome showed a clear distinction of changes at early, middle and advanced pathological stages, this model was taken as a reference to define the time-resolved MARPs. Thus, early-MARPs included proteins that first appeared to be regulated (up or down) at the early pathological stage (3 months) but remained changed (in the same direction) at 6 and 12 months. In turn, middle- and advanced-MARPs included proteins regulated at 6 and 12 months or only at 12 months, respectively. As I aimed at identifying a robust and model-independent dataset of MARP signatures, early-, middle- and advanced-MARPs only included proteins that were also regulated in the APP-KI microglia (at 6 and 12 months or only at 12 months). This classification resulted in 90 early-MARPs, 176 middle-MARPs and 435 advanced-MARPs (Figure 13B). Of note, all MARPs showed a good correlation between the two mouse models at 12 months of age, which illustrates a similar microglial response to A $\beta$  in both models at advanced pathological stages (Figure 13C).

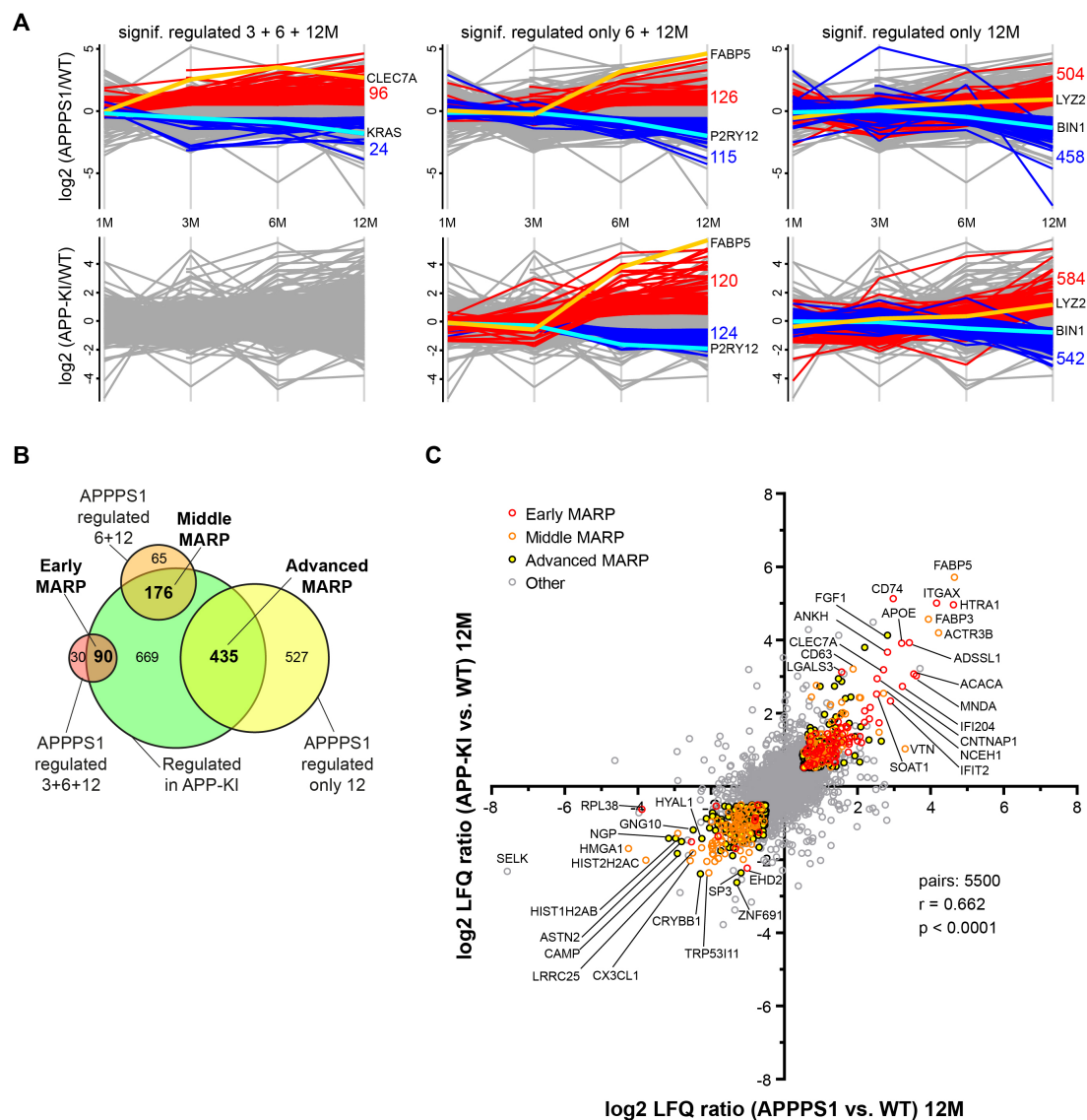


**Figure 13. Classification of MARPs and their dynamics in APPS1 and APP-KI microglia.**

**A.** Profile plot representing proteomic fold changes ( $\log_2$ ) of APPS1 and APP-KI versus WT microglia at 1, 3, 6, and 12 months. Lines connect each protein fold change at the different disease stages. Regulated proteins were plotted according to 3 profiles: significantly up- or down-regulated ( $\log_2$  fold change  $> 0.5$  or  $< -0.5$ ;  $p < 0.05$ ; FDR significant) at 3, 6, and 12 months, or at 6 and 12, or only at 12 months. Up-regulated proteins are indicated in red and down-regulated in blue. Examples of up- or down-regulated proteins are colored in orange and cyan, respectively. **B.** Venn diagram showing the classification of APPS1 and APP-KI regulated microglial proteins into early, middle and advanced MARPs. **C.** Plot showing the correlation between microglial protein fold changes ( $\log_2$ ) from 12-month-old APPS1 and APP-KI versus WT microglia. Early, middle, and advanced MARPs are colored in red, orange, and black, respectively. Selected proteins are labeled with their respective gene names. A significant ( $p < 0.0001$ ) positive ( $r = 0.662$ ) correlation of proteomic changes is observed between both mouse models at 12 months. Modified from (Sebastian Monasor et al., 2020).

The whole list of identified MARPs (Source data) can be accessed under: <https://cdn.elifesciences.org/articles/54083/elifesciences-54083-fig2-data1-v1.xlsx> (Sebastian Monasor et al., 2020). Early-MARPs may represent the first molecular changes in response to A $\beta$  that progress

as pathology evolves and included 80 up-regulated and 10 down-regulated proteins. Some of the up-regulated proteins, were previously identified at transcriptomic level as DAM markers (Keren-Shaul *et al.*, 2017) and included APOE, CLEC7a, ITGAX (CD11c) and LGALS3 (Galectin 3) (Figure 14A, Source data). Among up-regulated early-MARPs, I also found proteins involved in antigen presentation, such as CD74, ITGAX, H2-D1, H2-K1, TAP2 and TAPBP, but also a substantial number of proteins that belong to the interferon (IFN) response like MNDA, IFIT2, IFIT3, OAS1A, ISG15, GVIN1 and STAT1, and in addition, several lysosomal proteins such as cathepsins (CTS2 and CTSH), CD68 and NPC2 (Figure 14A, Source data).

Middle-MARPs included 86 up-regulated and 90 down-regulated proteins, which reflect microglial response to a fully established A $\beta$  pathology. Among the up-regulated proteins, I identified lipid binding proteins such as FABP3, FABP5 and APOD, proteins that play a role in signal transduction such as TREM2, or cell to cell signaling like the exosome marker CD63 or the pro-inflammatory cytokine MIF (Figure 14B, Source data). Notably, middle MARPs revealed the downregulation of microglial homeostatic markers such as TMEM119, P2RY12 and CX3CR1 (Figure 14B, Source data). In addition, I identified down-regulated proteins involved in cell motility and migration like CX3CL1, SYK, BIN2 and FER (Figure 14B, Source data), suggesting the loss of microglial physiological signatures and function throughout AD progression.

Advanced-MARPs represent the response of microglia to an extensive A $\beta$  pathology. This classification included 197 up-regulated and 238 down-regulated proteins. Among the up-regulated, I identified proteins involved in energy metabolism such as TIGAR, GPI, PGM, ACSS2 and FASN, but also in calcium binding like MYO5A, NCAN, HPCAL4, GCA and TTYH1 (Figure 14C, Source data). Down-regulated advanced-MARPs included proteins that belong to the endo-lysosomal system such as TFEB, TFE3 and BIN1, and the actin cytoskeleton machinery like ABI3, RAC2, VAV2, CFL1 and ACTN4, but also, several Histone proteins such as HIST1H2A, HIST1H2B and H3F3, and proteins involved in G protein-coupled receptor signaling like GNG2, GNG5 and GNG10 (Figure 14C, Source data).

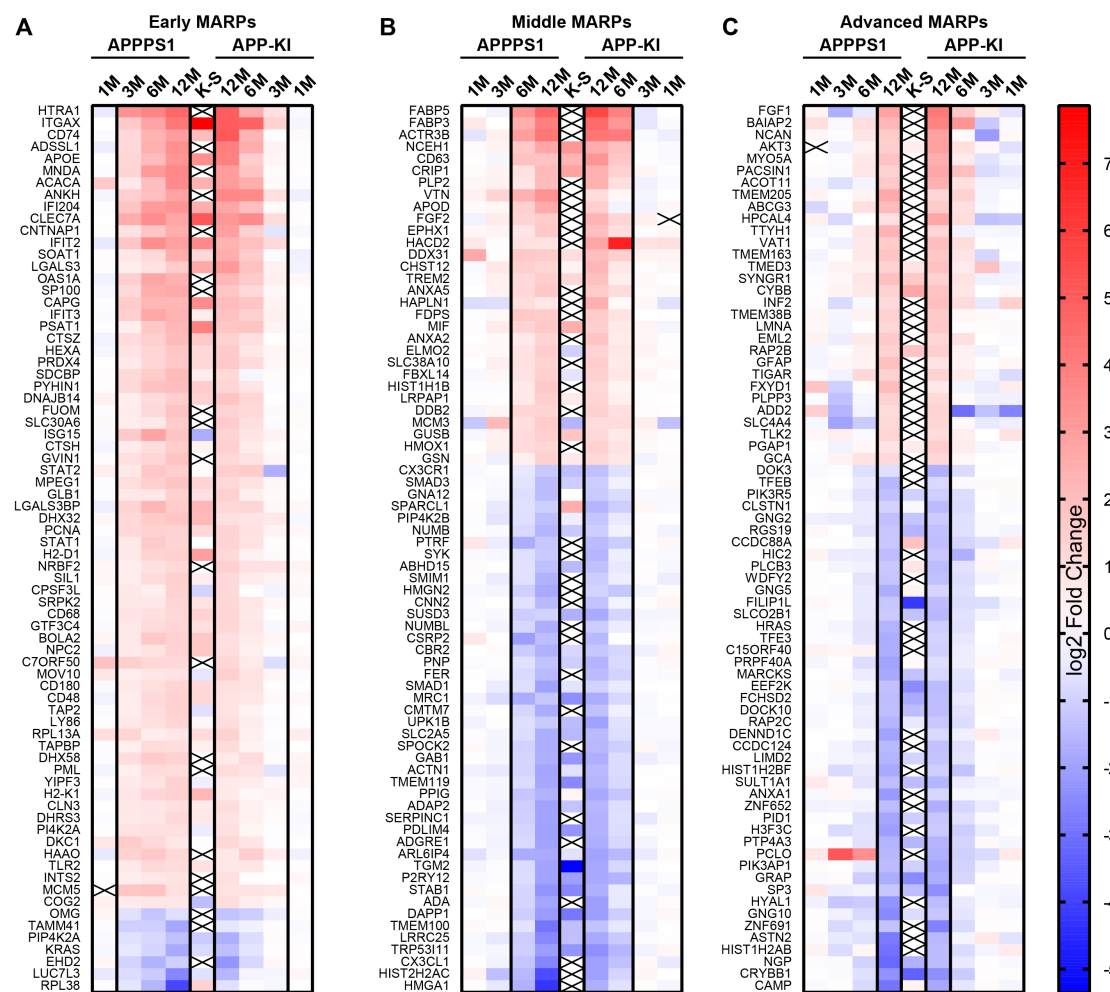


**Figure 14. Early, middle and advanced-MARPs and comparative analysis with the transcriptome.**

Heatmaps display the fold changes ( $\log_2$ , APPS1/APP-KI *vs.* WT) of the top 74 up- or down-regulated proteins for early- (A), middle- (B) and advanced- (C) MARPs and are compared to the fold changes ( $\log_2$ , DAM *vs.* homeostatic) reported from the single cell transcriptome study (Keren-Shaul *et al.*, 2017), depicted as K-S. Crosses indicate non-detected genes in the transcriptome dataset. Modified from (Sebastian Monasor *et al.*, 2020).

## 1.5. Microglial proteomic and transcriptomic changes in response to A $\beta$ only partially overlap

I was also interested in elucidating to which extent microglial proteome and transcriptome overlap in response to A $\beta$ . For that, we compared our proteome dataset with the reported single-cell transcriptome study (Keren-Shaul *et al.*, 2017). When comparing the number of total relatively quantified proteins common in APPS1 and APP-KI microglia at 12 months (only detected proteins, not regulated), with the single-cell microglial transcripts quantified from 5XFAD mice (Keren-Shaul *et al.*, 2017), we detected 3348 matching protein/transcripts (Figure 15) accounting to 57.2% of all quantified proteins, while 2152 and 2841 were only identified at protein and transcriptome level respectively.

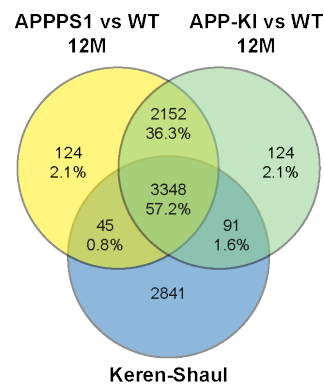


**Figure 15. Comparison of quantified proteins from APPPS1 and APP-KI microglia with identified single-cell microglial transcripts.**

Venn diagram showing overlapping proteins and transcripts quantified by proteomics in APPPS1 (yellow) and APP-KI (green) *vs.* WT microglia at 12 months and by single-cell transcriptomics from 5XFAD microglia (blue) in Keren-Shaul study (Keren-Shaul *et al.*, 2017). Percentages are relative to the total number of quantified proteins in APPPS1 and APP-KI microglia (100%). Modified from (Sebastian Monasor *et al.*, 2020)

However, when comparing the number of commonly regulated proteins (APPPS1/APP-KI *versus* WT at 12 months) and transcripts (DAM *versus* homeostatic) (Keren-Shaul *et al.*, 2017), we detected an overlap of 227 protein/transcripts that represented only 9.5% of all identified regulated proteins (Figure 16A). Moreover, this comparison revealed higher overlap of the transcriptome with early-MARPs (Figure 16B and Figure 14A), rather than with middle- and advanced-MARPs (Figure 16B and Figure 14B and C). Of note, proteins with an opposite regulation compared to the transcriptome were also identified. This was the case for the early-MARPs ISG15, TAP2, COG2 and RPL38 (Figure 14A), the middle-MARPs SPARCL1 and MCM3 (Figure 14B) or the advanced-MARPs CCDC88A and PLCB3 (Figure 14C).

Taken together, microglial proteome and transcriptome in the context of amyloidosis seem to overlap only partially, suggesting that also post-translational mechanisms are involved in the regulation of microglial response to A $\beta$  pathology.

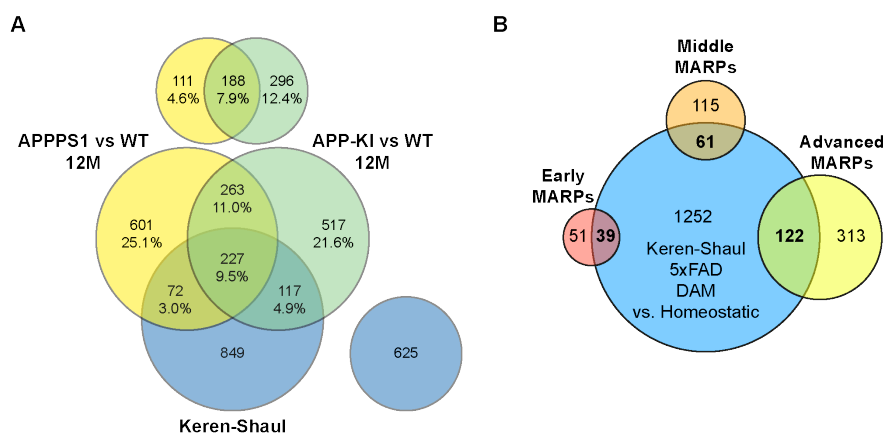


**Figure 16. Comparison of total regulated proteins in APPPS1 and APP-KI microglia and identified MARP signatures with regulated single-cell transcripts.**

**A.** Venn diagram showing the overlap between significantly regulated proteins identified in APPPS1 (yellow) and APP-KI (green) *versus* WT microglia and the regulated transcripts detected in the single-cell transcriptomic study using microglia from 5XFAD mice (blue) (Keren-Shaul *et al.*, 2017). Specific proteins and transcripts identified exclusively by proteomics or transcriptomics are displayed on the top or bottom-right respectively. Indicated percentages are expressed relative to the total number of regulated proteins in APPPS1 and APP-KI. **B.** Venn diagram showing the overlap (bold numbers) between early-(red), middle-(orange) and advanced-MARPs (yellow) and the regulated transcripts identified by single-cell transcriptomics (blue) (Keren-Shaul *et al.*, 2017). Modified from (Sebastian Monasor *et al.*, 2020)

## 1.6. Gene ontology analysis of MARP signatures

To investigate the biological processes and molecular mechanisms regulated by MARPs, GO analysis of early-, middle- and advanced-MARPs was performed (Figure 17 and Figure 18). Results from this analysis revealed that early-MARPs mainly involved up-regulated pathways related to immune responses, such as viral, interferon-beta and cytokine-mediated responses, and antigen processing and presentation mechanisms (Figure 17A). Moreover, early-MARPs, were enriched in cellular compartments like lysosomes, endosomes, Golgi and endoplasmic reticulum (Figure 18A).

In turn, GO analysis of middle-MARPs showed an upregulation of biological processes involved in energy metabolism (metabolism of hexoses, carbohydrates and pyridine nucleotides), but also, in tissue regeneration and wound healing (Figure 17B). Moreover, these MARPs displayed an enrichment in cellular compartments like endoplasmic reticulum and exosomes, in addition to molecular processes like glycosaminoglycan binding (Figure 18B and E). Interestingly, middle-MARPs also revealed a prominent downregulation of important microglial physiological processes such as cell proliferation, motility, migration and chemotaxis, along with a reduction of signaling transduction mechanisms (Figure 17B and Figure 18B and E).

Finally, GO analysis of advanced-MARPs showed an enrichment in carbohydrate metabolism as observed in middle-MARPs, but also displayed an up-regulation of proteins involved in protein glycosylation, regulation of pH and cation and lipid metabolism (Figure 17C). Moreover, up-regulated advanced-MARPs were found to be enriched in endoplasmic reticulum, Golgi apparatus, lysosomes, endosomes and exosomes along with different cellular mechanisms like glycosyltransferase activity, carbohydrate binding, active and passive transmembrane transport and ATPase, oxidoreductase, aldehyde dehydrogenase and ion channel activity (Figure 18C and F). In turn, down-regulated advanced-MARPs included biological processes such as cell motility, migration, proliferation and chemotaxis, as found in middle-MARPs, but also, phosphorylation and signal transduction, GTPase activity, TLR response and actin cytoskeleton organization among others (Figure 17C and Figure 18F). In addition, we also identified down-regulated proteins enriched in exosomes, vacuoles, endosomes and lysosomes, even though proteins involved in some of these cellular compartments were also found up-regulated among advanced-MARPs (Figure 18C), possibly indicating feed-back regulatory mechanisms.

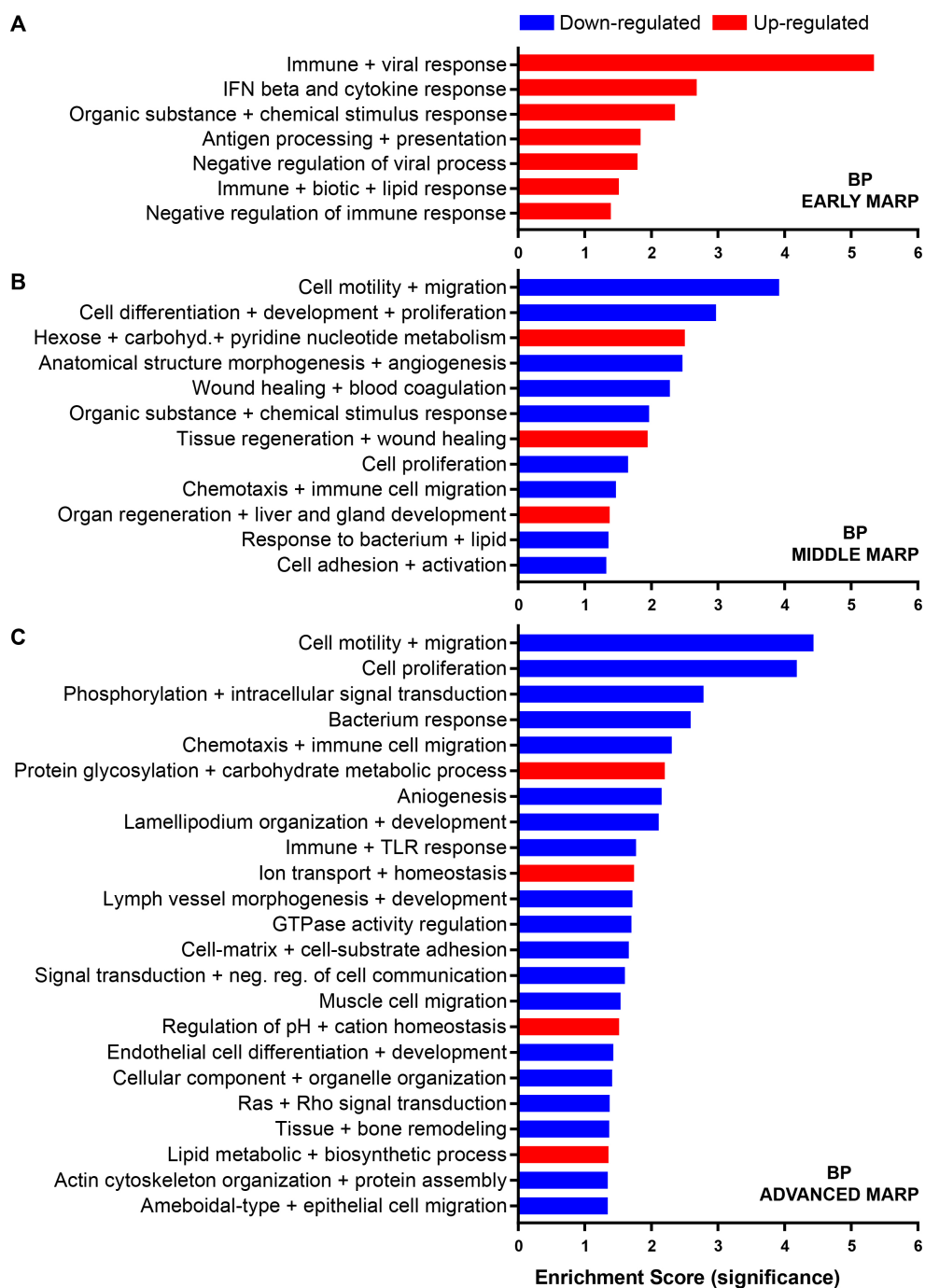


**Figure 17. Gene ontology enrichment analysis of MARPs according to biological processes.**

Bar plots show enrichment of early-MARPs (A), middle-MARPs (B) and advanced MARPs (C) for biological processes (BP). Significantly enriched categories (enrichment score > 1.301) for up-and down-regulated proteins are depicted in red and blue, respectively. Retrieved from (Sebastian Monasor *et al.*, 2020).

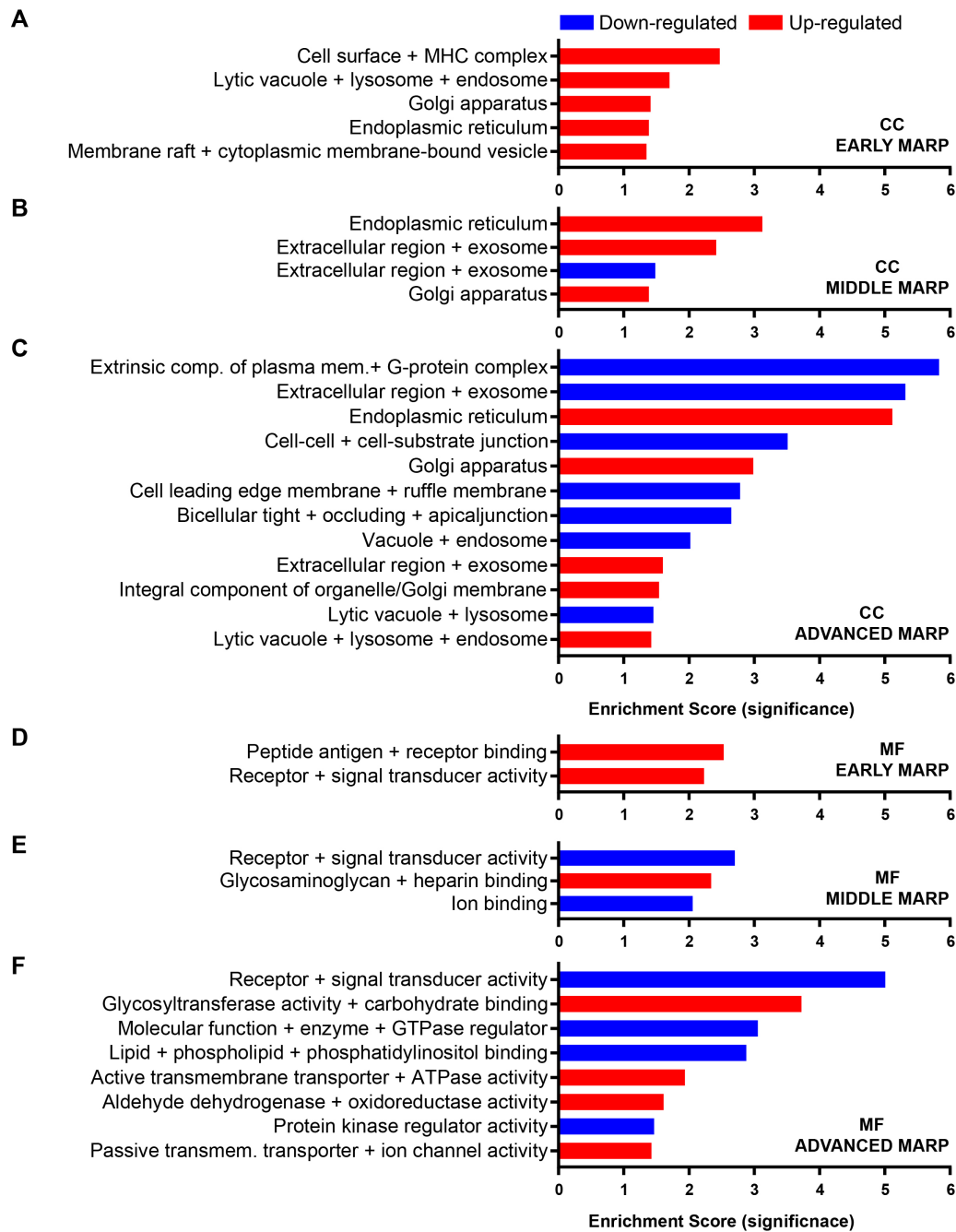


**Figure 18. Gene ontology enrichment analysis of MARPs according to cellular compartment and molecular function.**

Bar plots show enrichment of early-MARPs (A, D), middle-MARPs (B, E) and advanced-MARPs (C, F) for cellular compartment (CC) and molecular function (MF). Significantly enriched categories (enrichment score > 1.301) for up- and down-regulated proteins are depicted in red and blue, respectively. Retrieved from (Sebastian Monasor *et al.*, 2020).

## 1.7. Microglial AD risk genes are altered in APPS1 and APP-KI proteomes

As discussed earlier, numerous AD risk genes have been linked with microglial function. Thus, I examined if the proteins encoded by AD risk genes were found altered in the APPS1 and APP-

KI microglial proteomes throughout disease progression. Indeed, several AD risk markers such as APOE, TREM2 and INPP5D were significantly increased at protein level in both mouse models, especially at 6 and 12 months (Table 28). APPPS1 microglia also showed an up-regulation of the risk marker CLU at 12 months (Table 28). Moreover, I detected ABI3 and BIN1 being down-regulated in both models at 12 months (Table 28). In addition, the risk marker PLCG2 displayed lower abundance in APP-KI microglia at 12 months of age (Table 28).

Taken together, this dataset revealed alterations of AD risk genes at protein level in both mouse models, and these changes progressively followed A $\beta$  pathology development.

Gene/Protein Name	Fold change APPPS1 vs. WT				Fold change APP-KI vs. WT			
	1 M	3 M	6 M	12 M	1 M	3 M	6 M	12 M
APOE	1.01	2.44	4.20	9.25	1.06	1.22	2.88	15.03
TREM2	0.94	1.40	2.20	2.88	0.99	1.12	1.44	3.85
CLU	1.15	0.97	1.07	1.87	0.84	1.10	0.76	0.72
INPP5D	1.10	1.38	1.80	1.71	0.94	1.08	1.26	1.34
PLCG2	0.99	1.05	0.99	0.86	0.97	0.99	0.74	0.66
ABI3	1.00	1.05	0.90	0.52	0.95	0.95	0.67	0.53
BIN1	0.95	1.03	0.74	0.40	0.99	0.97	0.72	0.59

**Table 28. AD risk genes are found altered in APPPS1 and APP-KI microglial proteome.**

Significantly regulated protein fold changes are colored in blue ( $p < 0.05$ ). Modified from (Sebastian Monasor *et al.*, 2020).

## 1.8. MARPs are detected in microglia recruited at amyloid plaques

To validate the identified MARP signatures, I analyzed selected proteins by western blotting using microglia isolated from 12-15-month-old WT, APPPS1 and APP-KI mice. This analysis confirmed the increase of all analyzed proteins, including the early-MARPs APOE and CD68, the middle-MARPs TREM2 and FABP5, as well as a decrease in the advanced-MARP CSF1R, in both amyloidosis mouse models compared to WT (Figure 19A). Moreover, I could also validate the reduction of the Tyrosine Kinase SYK, that is required for TREM2 downstream signaling, as well as a reduction of its active form, p-SYK (Figure 19B).

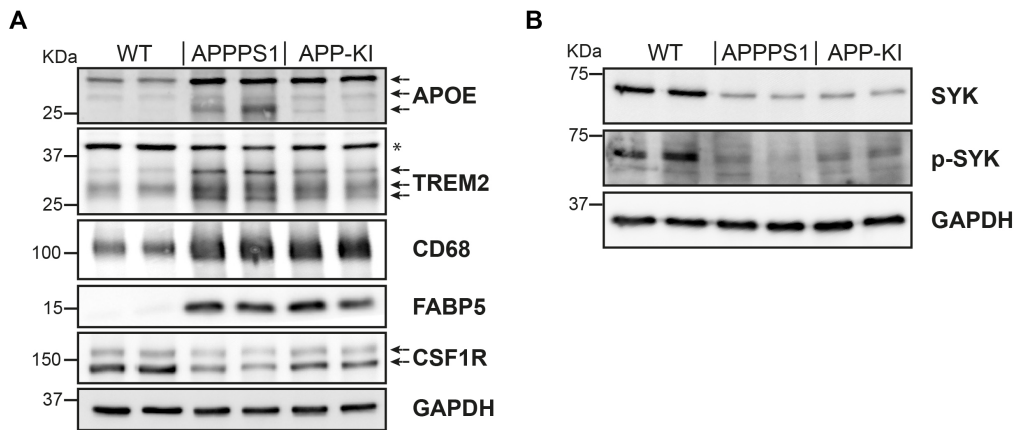


**Figure 19. Selected MARPs were validated by western blot analysis.**

Microglia lysates from 12-month-old (A) and 14-15-month-old (B) WT, APPPS1 and APP-KI mice were used for western blot analysis. For every protein, the lysates from two mice per genotype were analyzed. GAPDH was used as a loading control. Arrows indicate specific bands and asterisk unspecific bands. Results shown in A were modified from (Sebastian Monasor et al., 2020).

Next, I also validated some selected MARPs by immunohistochemistry, in order to determine their cellular localization and spatial distribution in APPPS1 and APP-KI compared to WT mice. Immunohistochemical analysis of 3-month-old mice confirmed increased levels of the early-MARP CLEC7a in APPPS1 compared to WT mice, but the increase was also observed, to a lesser extent, in APP-KI mice (Figure 20). Interestingly, CLEC7a reactivity was detected specifically colocalizing with IBA positive microglia recruited at amyloid plaques, but not detected in microglia away from plaques (Figure 20).

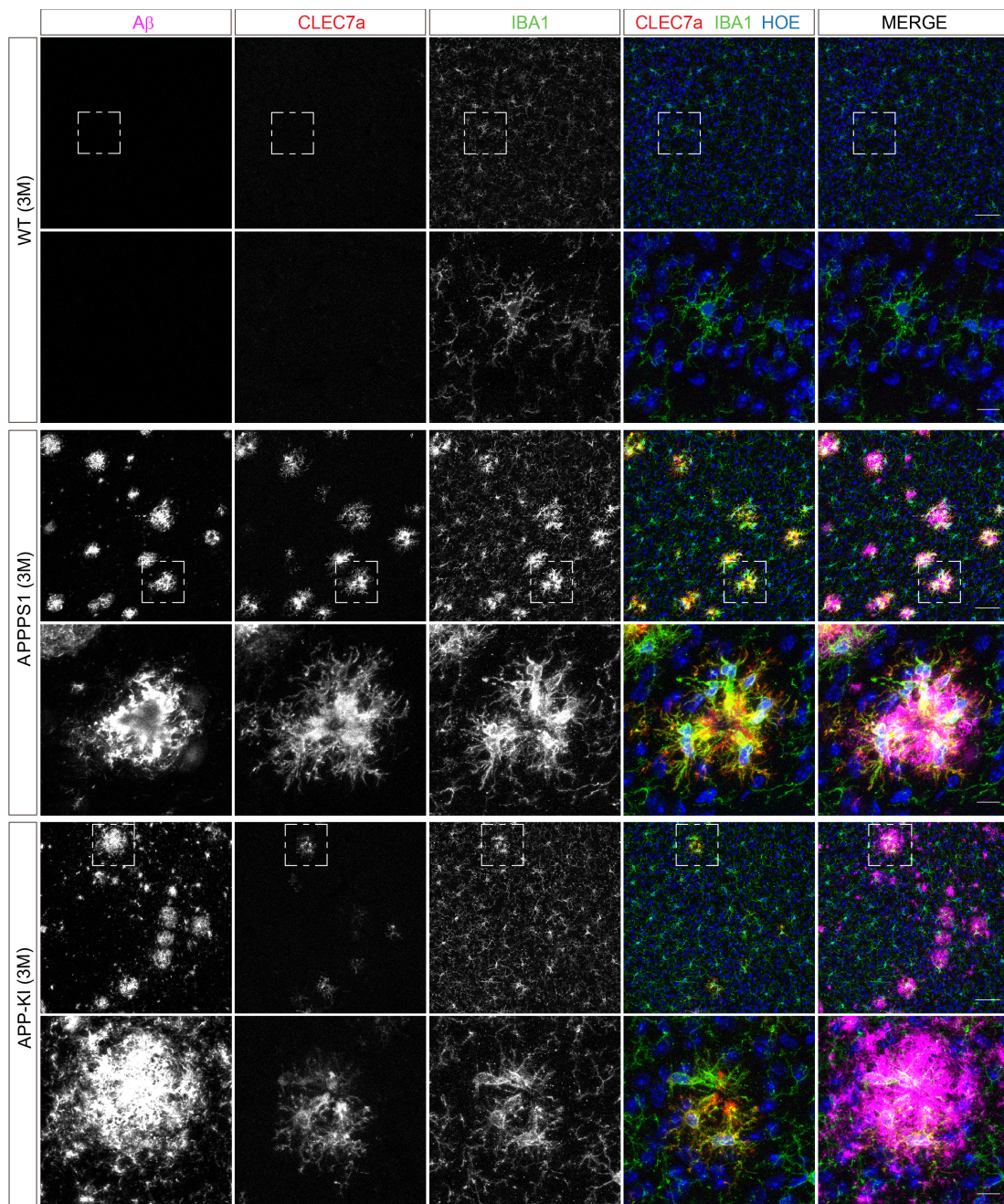


**Figure 20. CLEC7a shows a greater increase in 3-month-old plaque-associated APPS1 microglia.**

Immunohistochemical analysis of CLEC7a (red) in 3-month-old mice shows a prominent increase of this early MARP in APPS1 IBA1 positive microglia (green) clustered at amyloid plaques (magenta) in comparison to WT microglia, where this protein was barely detected. Plaque-associated APP-KI microglia showed a less pronounced increase in CLEC7a signal. Hoechst (HOE, blue) was used to visualize cells nuclei. Upper panel images were acquired with a 20x dry objective; scale bar: 50  $\mu\text{m}$ . Selected boxed areas in upper panels, are depicted with a higher magnification in lower panels, acquired with a 63X water immersion objective (3x digital zoom); scale bar: 10  $\mu\text{m}$ . Retrieved from (Sebastian Monasor *et al.*, 2020).

Similarly, I analyzed the middle-MARP TREM2 in 3-month-old mice, to test whether differences could already be detected at this early stage by immunohistochemistry. As shown in Table 28, TREM2 was already slightly but significantly up-regulated (by p value) at 3 months of age in

APPPS1 microglia, however, it was not classified as early-MARP since it did not pass the FDR correction criteria. Immunohistological analysis revealed a prominent TREM2 reactivity in APPPS1 compared to WT mice, which was less pronounced in APP-KI mice (Figure 21). This increase in TREM2 signal was again specific to IBA1 positive microglia clustering around A $\beta$  plaques, although low basal TREM2 levels were, as expected, also observed in microglia away from plaques and in WT microglia (Figure 21).

In addition, I analyzed the early-MARP APOE by immunohistochemistry in 3-month-old mice. As discussed above, APOE is one of the main AD risk genes, which even if it is not microglia-specific, has been linked to microglial function in the context of AD and found up-regulated in microglia (Parhizkar *et al.*, 2019). Immunohistochemical analysis revealed, as previously reported, APOE reactivity in the core of A $\beta$  plaques and in astrocytes (Figure 22). However, I could also confirm the increased APOE levels observed in our proteomic dataset in APPPS1 microglia recruited at plaques compared to WT (Figure 22). A less prominent increase in APP-KI plaque-associated microglia was also detected (Figure 22).

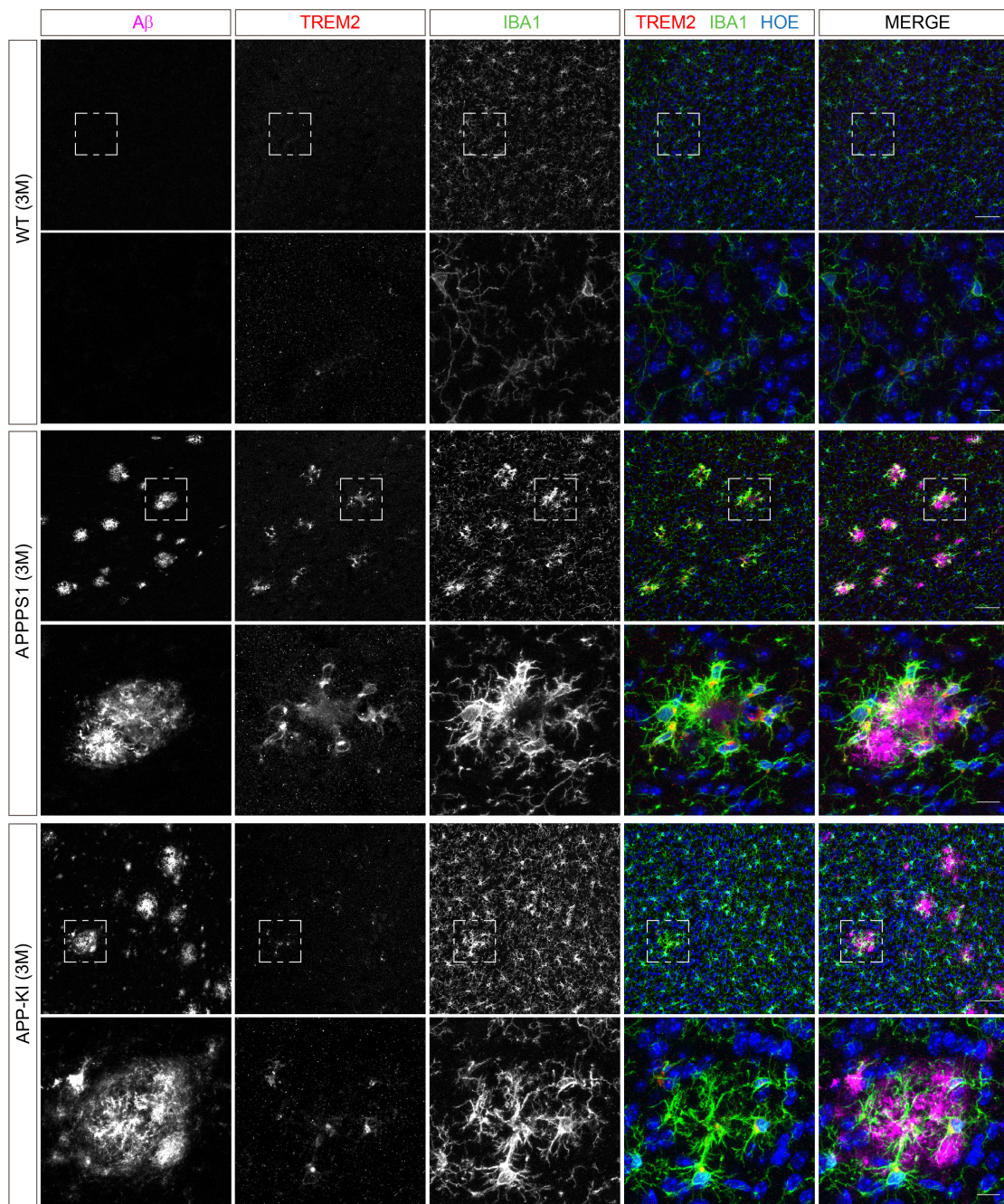


**Figure 21. TREM2 is markedly upregulated in 3-month-old plaque-associated APPPS1 microglia.**

Immunohistochemical analysis in 3-month-old mice shows a prominent increase of TREM2 (red) specifically in IBA1 positive microglia (green) recruited at amyloid plaques (magenta) in APPPS1 mice compared to WT. TREM2 was also upregulated in APP-KI plaque-associated microglia, but to a lesser extent. Hoechst (HOE, blue) was used to visualize cells nuclei. Upper panel images were acquired with a 20x dry objective; scale bar: 50  $\mu$ m. Selected boxed areas in upper panels, are depicted with a higher magnification in lower panels, acquired with a 63X water immersion objective (3x digital zoom); scale bar: 10  $\mu$ m. Retrieved from (Sebastian Monasor *et al.*, 2020).

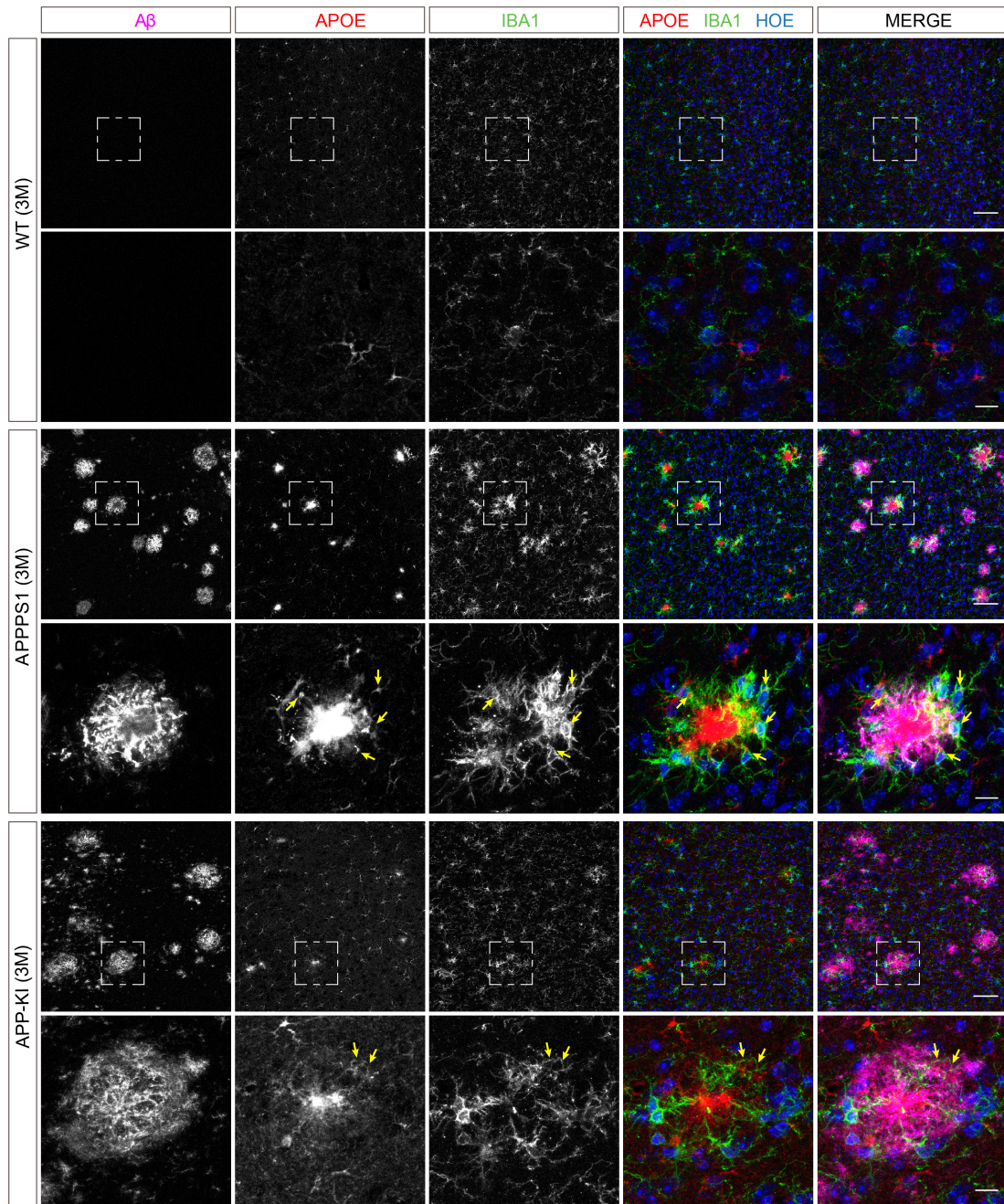


**Figure 22. APOE shows a higher upregulation in 3-month-old plaque-associated APPS1 microglia.**

Immunohistochemical analysis of 3-month-old mice shows an upregulation of APOE (red, yellow arrows) in IBA1 positive microglia (green) from APPS1 mice compared to WT, which is less pronounced in APP-KI mice. This increase is observed in microglia recruited at plaques (magenta), but also in the plaque core. In WT mice, only astrocytic APOE is observed. Hoechst (HOE, blue) was used to visualize cells nuclei. Upper panel images were acquired with a 20x dry objective; scale bar: 50  $\mu$ m. Selected boxed areas in upper panels, are depicted with a higher magnification in lower panels, acquired with a 63X water immersion objective (3x digital zoom); scale bar: 10  $\mu$ m. Retrieved from (Sebastian Monasor *et al.*, 2020).

Finally, I examined the levels and spatial pattern of MARPs also at the advanced disease stage. Thus, I performed immunohistological analysis of the early-MARP CLEC7a and the middle-MARP TMEM119 in 12-month-old mice. Results from these analyses were in agreement with the proteomic data, revealing an increase in CLEC7a (Figure 23) and a decrease in TMEM119 (Figure 24) in both AD mouse models compared to WT. As seen at the early stage (3 months), changes in CLEC7a and TMEM119 were also restricted to microglia associated to A $\beta$  plaques (Figure 23 and Figure 24).

In sum, I validated selected MARPs by biochemical and immunohistochemical approaches. Moreover, I could verify the kinetic differences in the appearance of A $\beta$ -associated proteome alterations between APPPS1 and APP-KI microglia. As changes in MARPs seem to be specifically associated to microglia clustering around A $\beta$  plaques, it appears likely that microglial proteomic alterations are indeed triggered as a response to A $\beta$ .

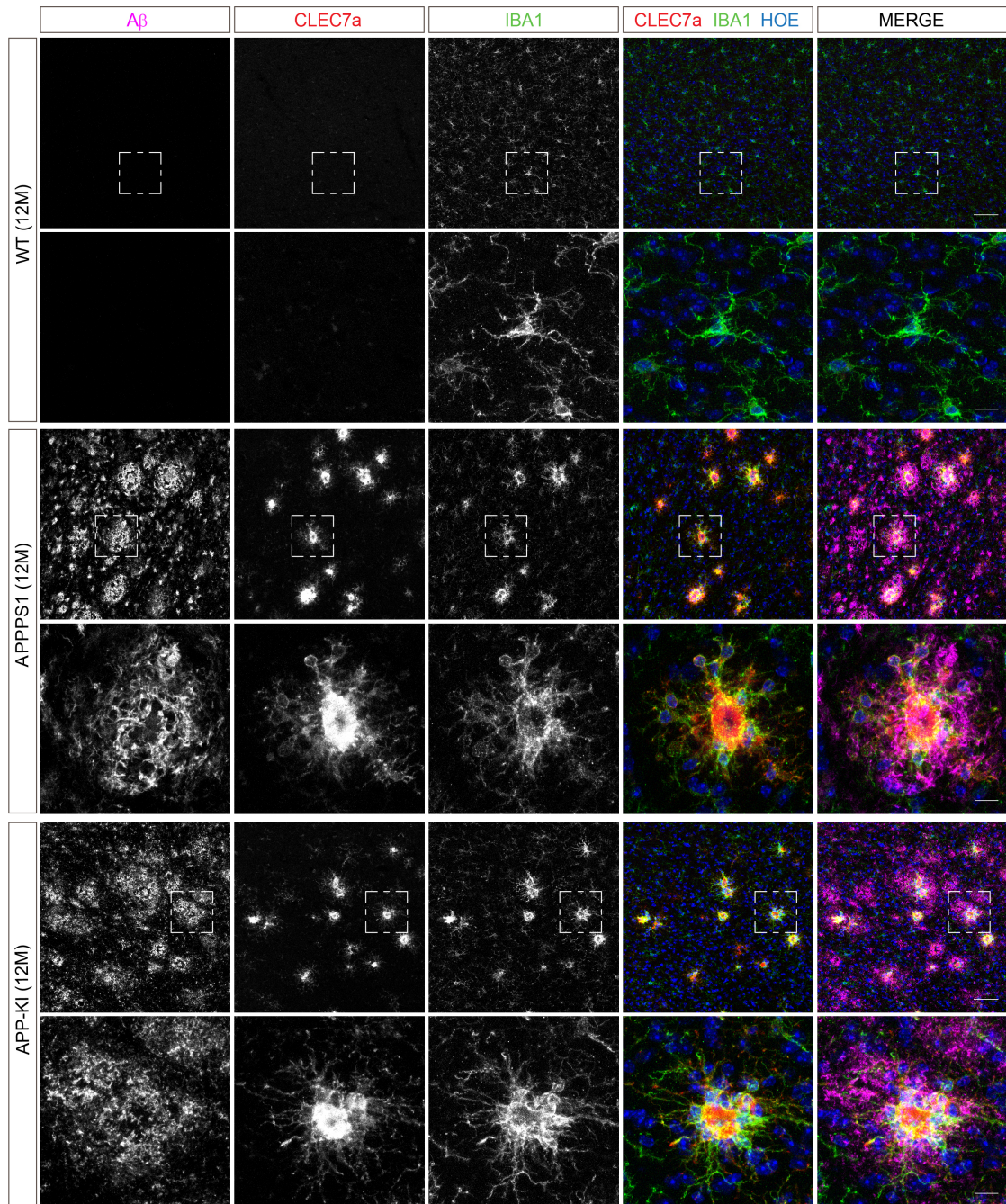


**Figure 23. CLEC7a shows a similar upregulation in 12-month-old APPS1 and APP-KI plaque-associated microglia.**

Immunohistological analysis in 12-month-old mice reveals a comparable CLEC7a (red) microglial upregulation in APPS1 and APP-KI mice, compared to WT. The signal is specific to IBA1 positive microglia (green) clustered at plaques (magenta). Hoechst (HOE, blue) was used to visualize cells nuclei. Upper panel images were acquired with a 20x dry objective; scale bar: 50  $\mu$ m. Selected boxed areas in upper panels, are depicted with a higher magnification in lower panels, acquired with a 63X water immersion objective (3x digital zoom); scale bar: 10  $\mu$ m. Retrieved from (Sebastian Monasor *et al.*, 2020).

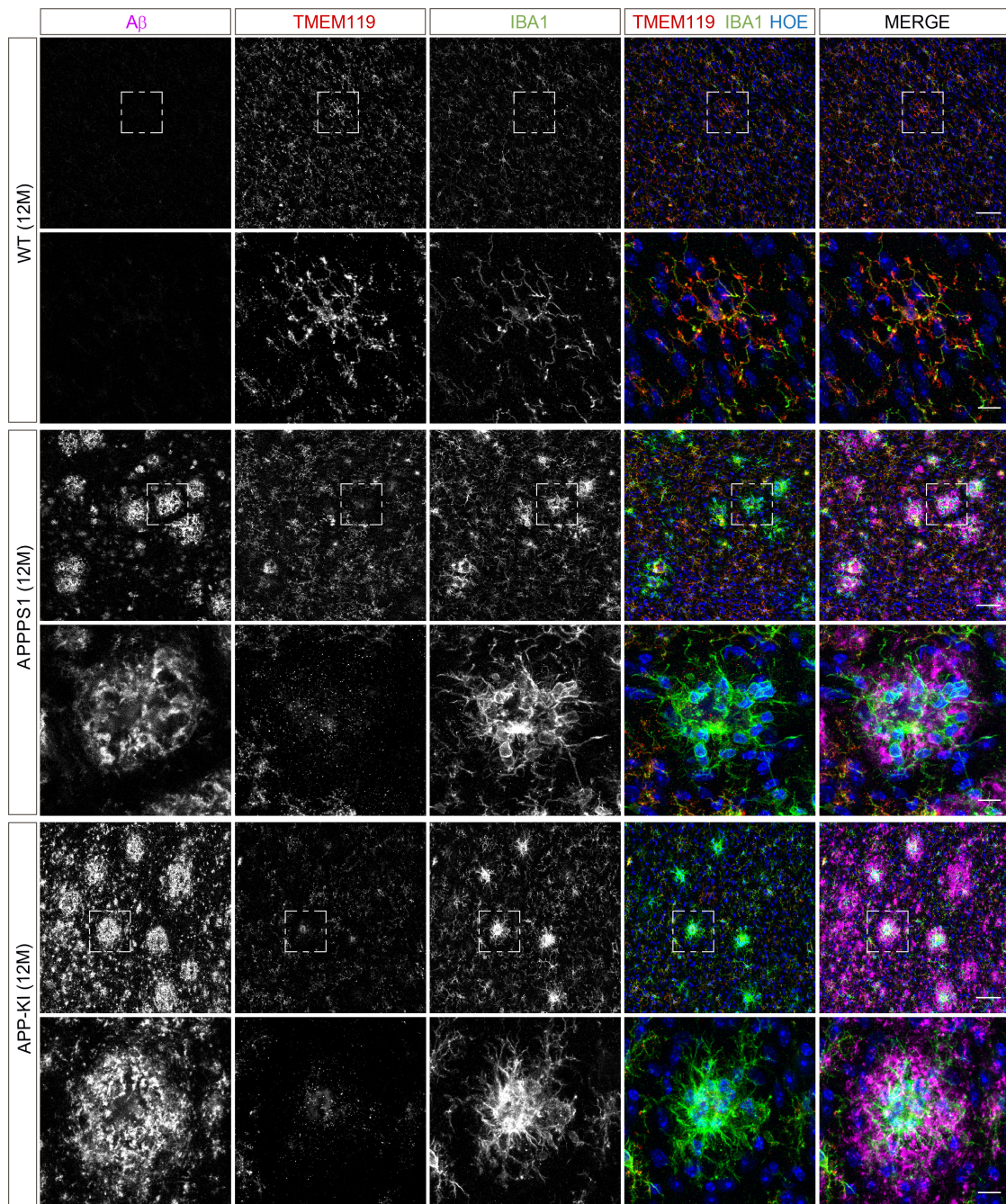


**Figure 24. TMEM119 shows a similar downregulation in 12-month-old APPS1 and APP-KI plaque-associated microglia.**

Immunohistological analysis in 12-month-old mice reveals a comparable TMEM119 (red) microglial downregulation in APPS1 and APP-KI mice, compared to WT. The decrease is specifically observed in IBA1 positive microglia (green) clustered at plaques (magenta), while the WT shows a homogeneous TMEM119 signal that colocalizes with all IBA1 positive cells. Hoechst (HOE, blue) was used to visualize cells nuclei. Upper panel images were acquired with a 20x dry objective; scale bar: 50  $\mu$ m. Selected boxed areas in upper panels, are depicted with a higher magnification in lower panels, acquired with a 63X water immersion objective (3x digital zoom); scale bar: 10  $\mu$ m. Retrieved from (Sebastian Monasor *et al.*, 2020).

## 1.9. APPPS1 and APP-KI plaques show different structural properties

As shown above, proteomic analysis revealed a microglial response that followed the kinetics of amyloid accumulation and disease progression in both mouse models. However, proteomic changes appeared earlier in APPPS1 than in APP-KI, even though plaque load seemed comparable between models (Figure 9). Interestingly, plaque coverage analysis revealed a higher plaque burden in APP-KI mice at the early disease stage (Figure 25), making the early response of APPPS1 microglia even more intriguing.

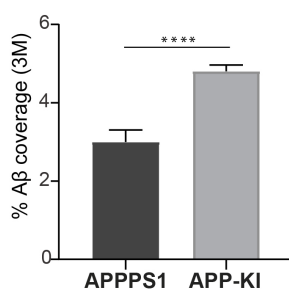


**Figure 25. APP-KI mice show higher Aβ coverage at 3 months compared to APPPS1.**

Analysis of Aβ coverage in the neocortex of 3-month-old APPPS1 and APP-KI mice. Values represent the percentage of the brain area covered by Aβ and were calculated as the mean ( $\pm$  SD) from N=4 mice (\*\*\*\* $p < 0.0001$ , unpaired two-tailed Student's T-test). Modified from (Sebastian Monasor et al., 2020).

Thus, I hypothesized that plaque properties could be different between APPPS1 and APP-KI mice, which in turn, would trigger a distinct microglial response in each mouse model. In order to prove this hypothesis, I analyzed amyloid plaques from 3, 6 and 12-month-old APPPS1 and APP-KI mice by immunohistochemistry. I used the anti-Aβ antibody (NAB228) to visualize whole Aβ plaques and Thiazine-red (ThR) to detect the levels of fibrillar Aβ, normally found in the core of amyloid plaques. Results from this analysis revealed prominent ThR positive fibrillar plaque cores already in 3-month-old APPPS1 mice (Figure 26A), as previously described (Radde *et al.*, 2006). Surprisingly, APP-KI mice at 3 months showed almost undetectable fibrillar plaque cores. At 6 and 12 months, the amounts of ThR fibrillar cores increased in APP-KI mice, but still remained lower in comparison to APPPS1 mice (Figure 26A). Biochemical analysis of the insoluble fraction from APPPS1 and APP-KI brains, confirmed lower levels of fibrillar Aβ in APP-KI mice, especially at 3 months of age, where once again, no fibrillar Aβ material was detected (Figure 26B), excluding possible detection limitations of the immunohistochemical method.

Taken together, I revealed differences in the fibrillarization properties of amyloid plaques between APPPS1 and APP-KI mice, which were especially prominent at 3 months of age.

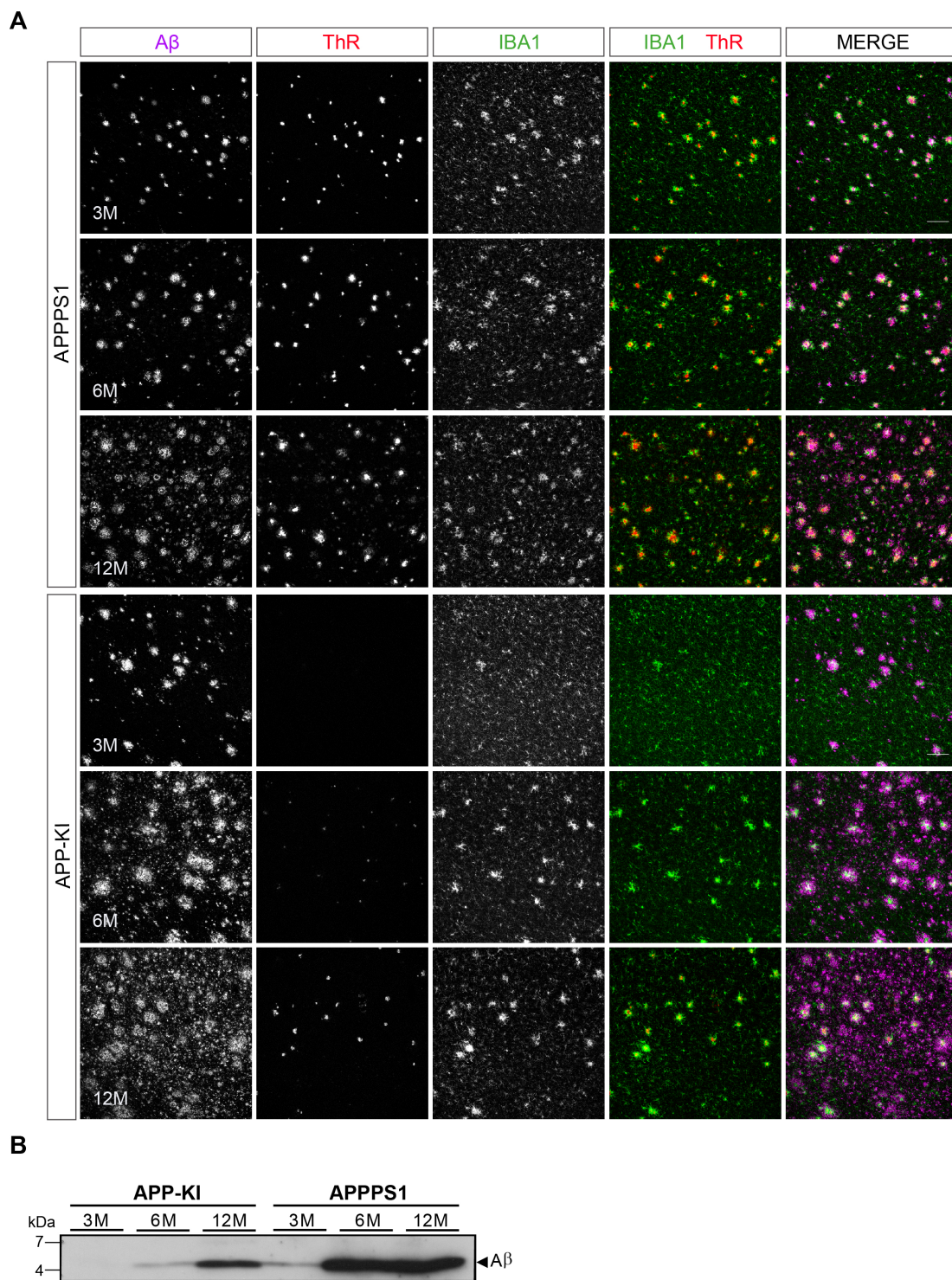


**Figure 26. APPPS1 mice show higher levels of fibrillar A $\beta$  compared to APP-KI mice.**

**A.** Immunohistological analysis of A $\beta$  plaques from 3, 6 and 12-month-old APPPS1 and APP-KI mice showing A $\beta$  plaques (magenta), fibrillar A $\beta$  plaque cores (ThR, red) and microglia (IBA1, green). Images from comparable cortical regions were acquired with a 20x dry objective; scale bar: 100  $\mu$ m. **B.** Western blot analysis of A $\beta$  from insoluble brain fraction from 3, 6 and 12-month-old APPPS1 and APP-KI mice. 2 mice samples were used per age group and genotype. The 3552 antibody was used for A $\beta$  detection. Modified from (Sebastian Monasor et al., 2020).

### 1.10. Microglial recruitment is triggered by fibrillar A $\beta$

The striking differences found in the content of fibrillar A $\beta$  between APPPS1 and APP-KI mice at the early disease stage, could explain the delayed response of APP-KI microglia to amyloid plaques observed by proteomics. To assess microglial response to fibrillar A $\beta$  plaques, I quantified microglial recruitment to amyloid plaques in 3-month-old APPPS1 and APP-KI mice. Immunohistological analysis showed APPPS1 microglia, clustered around and in close contact with the very prominent ThR positive fibrillar cores (Figure 27A). This observation was even more striking in APP-KI mice, where microglia appeared polarized towards the small fibrillar cores forming in the center of the plaques, but not to the surrounding non-fibrillar plaque material (Figure 27A). This suggested a higher ability of fibrillar compared to non-fibrillar A $\beta$  to trigger microglia recruitment. Quantification of microglia recruited to amyloid plaques showed an increase in the number of IBA1 positive microglia clustering around APPPS1 A $\beta$  plaques compared to APP-KI mice (Figure 27A and B). The average size of whole A $\beta$  plaques was, however, significantly larger in APP-KI mice (Figure 27A and C) and thus, does not correlate the reduced number of microglia recruited to plaques. Coverage analysis of the microglial lysosomal marker CD68, showed an increase in CD68 signal per plaque area in APPPS1 compared to APP-KI mice (Figure 27D and E), correlating with the higher number of plaque-recruited microglia. Interestingly, CD68 signal per microglial cell at plaques was similar in the two mouse models (Figure 27F). This indicated that microglial activation state, indirectly inferred by their lysosomal activity, was comparable in microglia recruited at plaques in both mouse models. Therefore, the main difference I detected between the two mouse models, was the number of microglia recruited to A $\beta$  plaques, which correlated well with the fibrillar A $\beta$ -content of their specific plaques.

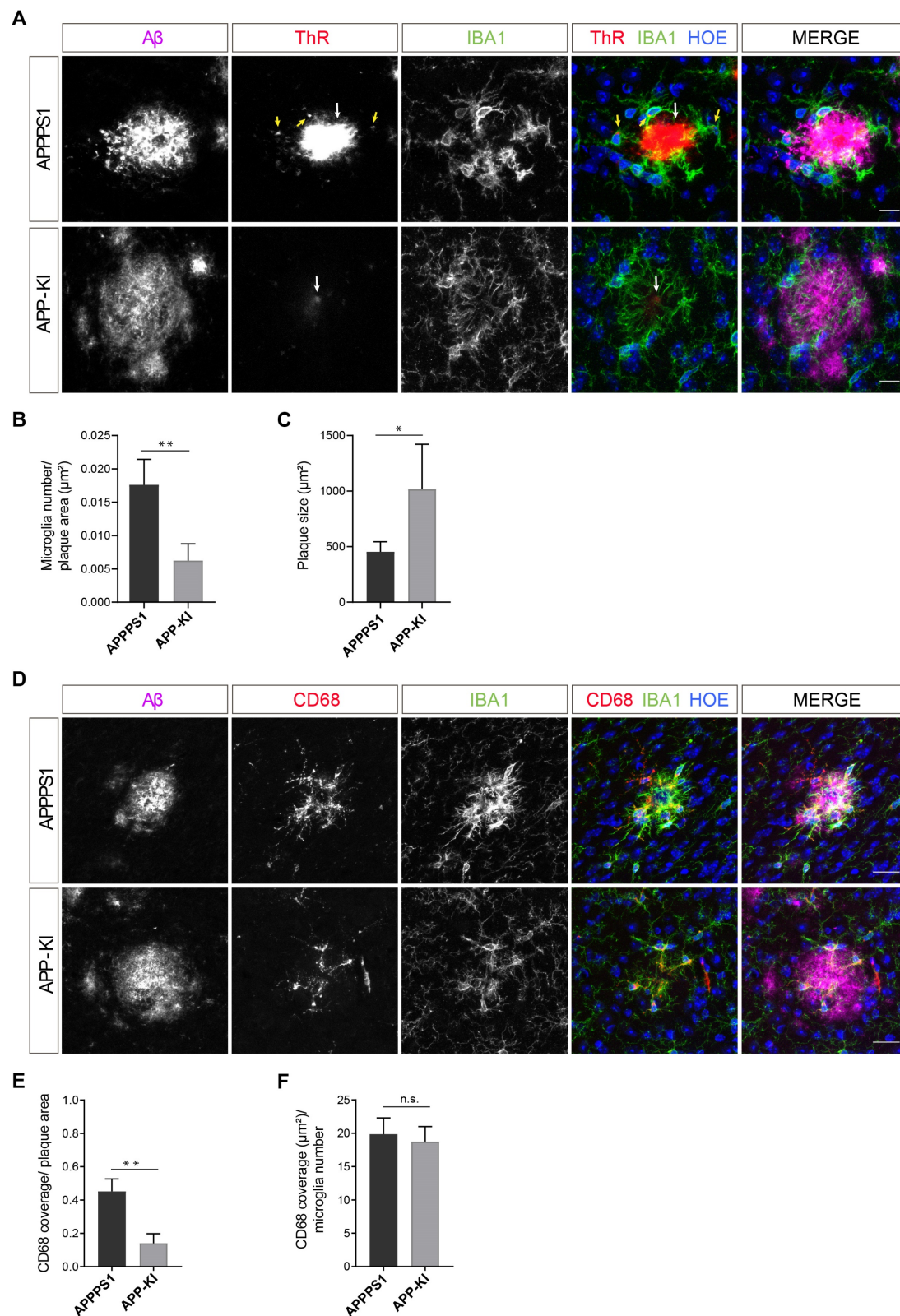


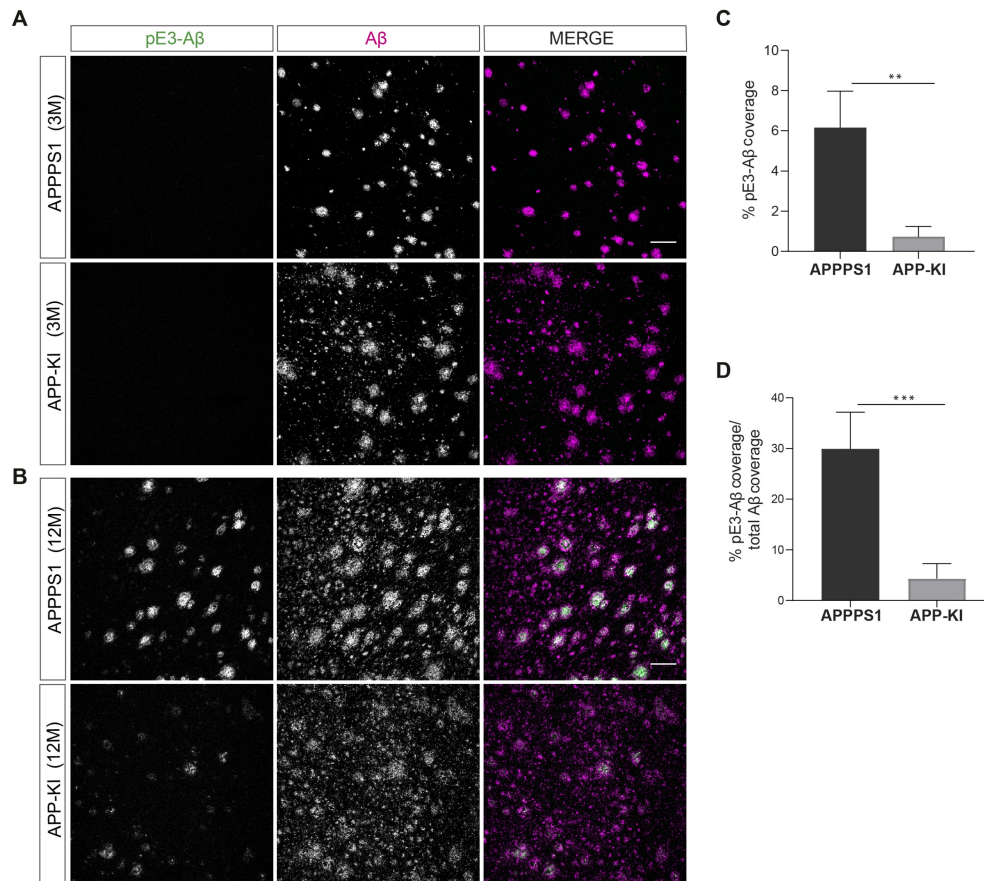
**Figure 27. Microglial recruitment is higher in 3-month-old APPPS1 mice and triggered by fibrillar A $\beta$ .**

**A.** Immunohistochemical analysis of 3-month-old APPPS1 and APP-KI mice showing IBA1 positive microglia (green) polarized towards ThR fibrillar cores (white arrows, red), but not to the plaque halo (magenta). Intracellular fibrillar A $\beta$  is indicated with yellow arrows. Hoechst (HOE, blue) was used to visualize cells nuclei. Representative images were acquired with a 63x water immersion objective (3x digital zoom); scale bar: 10  $\mu\text{m}$ . **B.**

## Results

Quantification of microglia recruited to A $\beta$  plaques relative to the plaque size. **C.** Quantification of plaque size. **D.** Immunohistological analysis of CD68 (red) positive microglia (IBA1, green) recruited to A $\beta$  plaques (magenta), in 3-month-old APPPS1 and APP-KI mice. Hoechst (HOE, blue) was used to visualize cells nuclei. Representative images were acquired with a 63x water immersion objective (2x digital zoom); scale bar: 20  $\mu$ m. **E.** Quantification of CD68 coverage relative to the single plaque area. **F.** Quantification of CD68 coverage relative to the number of recruited microglia per single plaque. Values in B, C are expressed as the mean of N=5 (APPPS1) and N=4 (APP-KI) mice  $\pm$  SD and in E and F as the mean of N=3 mice per genotype  $\pm$  SD (\*p < 0.05; \*\*p < 0.01, unpaired two-tailed Student's T-test; n.s: not significant). Modified from (Sebastian Monasor et al., 2020).

As fibrillar A $\beta$  was found to correlate with microglial recruitment to A $\beta$  plaques and the appearance of proteomic changes, I questioned whether A $\beta$  modifications that favor fibrillarity, such as pyroglutamate (pE3-A $\beta$ ), could be responsible for microglial recruitment. To assess this hypothesis, I analyzed pE3-A $\beta$  signal by immunohistochemistry in 3 and 12-month-old APPPS1 and APP-KI mice, using an antibody that has been previously validated (Hartlage-Rubsamen et al., 2018). Results from this analysis showed pE3-A $\beta$  signal detected only in 12-month-old mice, which was higher in APPPS1 than in APP-KI mice (Figure 28A-D). This result was in agreement with the differences in fibrillar A $\beta$  found between the models (Figure 26). As I did not detect any pE3-A $\beta$  signal in 3-month-old APPPS1 mice (Figure 28A), where microglial proteome changes were already observed, it is not likely that pE3-A $\beta$  is the main trigger for microglial recruitment.

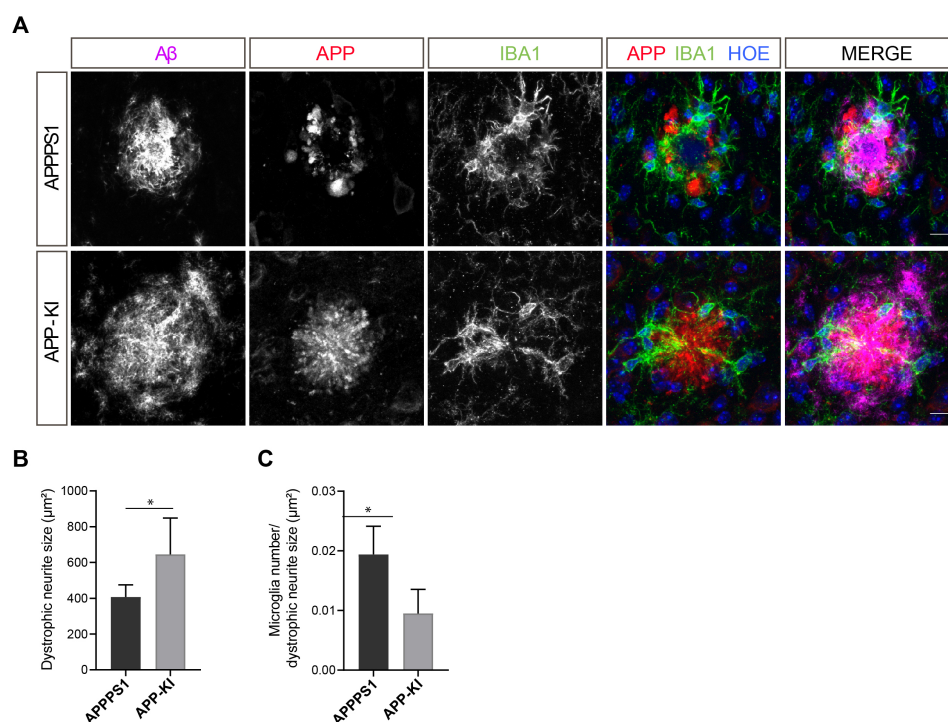


**Figure 28. (previous page) pE3-A $\beta$  is not responsible for microglial recruitment.**

Immunohistochemical analysis of pE3-A $\beta$  (green) in 3 (A) and 12-month-old (B) APPPS1 and APP-KI mice. Total A $\beta$  (magenta) was used as a reference for A $\beta$  pathology. Representative images in A and B were acquired with a 20x dry confocal microscope objective; scale bar: 100  $\mu$ m. Quantification of pE3-A $\beta$  coverage signal in 12-month-old APPPS1 and APP-KI mice is represented as percentage from the total analyzed area (C) and as percentage of the total A $\beta$  coverage (D). Quantification values in C and D are represent the mean  $\pm$  SD from N=4 mice (\*\*p < 0.01, \*\*\*p < 0.001, unpaired two-tailed Student's T-test). Modified from (Sebastian Monasor *et al.*, 2020).

In addition to A $\beta$ , neuronal damage has been reported to trigger microglial response and recruitment (Krasemann *et al.*, 2017). To assess if neuritic damage could trigger microglial recruitment and proteomic changes in the early disease stage, I analyzed dystrophic neurites in 3-month-old APPPS1 and APP-KI mice. Interestingly, immunohistological analysis of dystrophic neurites revealed larger dystrophies in APP-KI compared to APPPS1 mice (Figure 29A and B), which correlated with the bigger plaques observed in the first model (Figure 27A and C), but not to the number of recruited microglia (Figure 29C). Thus, dystrophic neurites do not seem to be the main cause for the observed earlier recruitment of APPPS1 microglia to A $\beta$  plaques and appearance of proteomic changes.

Taken together, I could show that fibrillar A $\beta$  seems to be the main trigger for microglial recruitment to amyloid plaques, that translates into the acquisition of MARP signatures.

**Figure 29. Dystrophic neurites do not correlate with microglial recruitment and proteomic changes.**

A. Immunohistochemical analysis of dystrophic neurites (APP, red) and associated microglia (IBA1, green). A $\beta$  plaques are visualized in magenta (A $\beta$ ) and cells nuclei with Hoechst (HOE, blue). Representative images were

acquired with a 63x water immersion objective (3x digital zoom); scale bar: 10  $\mu\text{m}$ . Quantification of dystrophic neurites area (B) and microglia recruited to dystrophic neurites (C) in 3-month-old APPPS1 and APP-KI mice. Values are expressed as the mean of N=5 (APPPS1) and N=4 (APP-KI) mice  $\pm$  SD (\* $p < 0.05$ , unpaired two-tailed Student's T-test). Modified from (Sebastian Monasor *et al.*, 2020).

### 1.11. Phagocytic deficiency correlates with the presence of fibrillar A $\beta$ and acquisition of MARP signatures

Finally, I investigated how the acquisition of MARP signatures translated into microglial function. To that end, I tested the phagocytic capacity of microglia from 3 and 6-month-old APPPS1 and APP-KI mice compared to WT. As phagocytic substrate, I used the *E.coli*-pHrodo particles and analyzed the differences in microglial phagocytosis by FACS. This assay revealed a significant decrease in the levels of intracellular *E.coli* particles detected in APPPS1 microglia already at 3 months of age (Figure 30A), as well as a reduction in number of microglial cells that were able to uptake bacterial particles compared to WT microglia (Figure 30B). Interestingly, microglia from 3-month-old APP-KI mice, showed no difference in the phagocytic capacity compared to WT microglia (Figure 30A and B), indicating a preserved microglial function at 3 months of age. At 6 months of age, microglia from APPPS1 mice showed a comparable phagocytic deficiency as at 3 months, in regard to both, the number of microglia able to uptake *E.coli* particles, as well as the amount of intracellular phagocytosed material (Figure 30A and B). Strikingly, at 6 months of age, microglia from APP-KI mice, showed a similar phagocytic impairment as the one displayed by the APPPS1 microglia (Figure 30A and B).

Overall, this data suggests, that the acquisition of MARP signatures by microglia that was observed at 3 and 6 months of age in APPPS1 and APP-KI mice, correspondingly, correlates with a decline in microglial phagocytic function, which in turn, could be associated to the presence of fibrillar A $\beta$ .

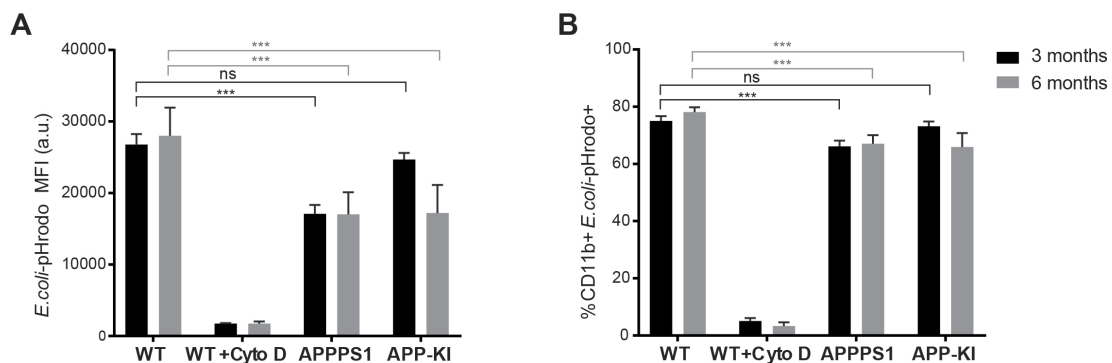


Figure 30. Phagocytosis deficiency correlates with the acquisition of MARP signatures.

**A.** Mean Fluorescence Intensity (MFI) of phagocytosed *E.coli*-pHrodo particles within CD11b positive microglia from 3 and 6 month old WT, APPPS1 and APP-KI mice analyzed by FACS. CytoD was used as an inhibitor of phagocytosis, as negative control. **B.** Percentage of CD11b and *E.coli*-pHrodo double positive microglia out of the whole CD11b positive microglial population used in the assay. Values in A and B represent the mean of N=3 mice (3-month time point) per genotype  $\pm$  SD and N=2 mice (6-month time point) per genotype  $\pm$  SD (\*\* $p < 0.001$ , Two-way ANOVA, Dunnett's multiple comparison test; n.s: not significant). Modified from (Sebastian Monasor et al., 2020).

## 2. Testing the potential of GM-CSF for microglial repair

As shown and discussed in previous sections, microglia display a deficiency in phagocytosis that likely contributes to amyloid accumulation and AD progression. Thus, the second aim of my PhD study, was to use GM-CSF as immunomodulatory factor to repair microglial function *in vivo* and reveal the proteomic signatures of functionally repaired microglia. To that end, I chose the APP-KI mouse model for the GM-CSF therapeutic study, as it avoids possible artifacts of A $\beta$  overexpression mouse models. I used two different experimental paradigms, one short (21 days, Figure 7), following previously published experimental conditions (Boyd *et al.*, 2010) and one longer treatment paradigm (3 months, Figure 8). The age groups used for the therapeutic study were selected based on microglial proteomic changes of the APP-KI mice (proteomic study, section 1), defining a preventive (4-5- month-old mice) and a repair (14-month-old mice) strategies.

### 2.1. GM-CSF induces A $\beta$ plaque clearance in APP-KI organotypic brain slices

GM-CSF was demonstrated to have an effect on inducing plaque clearance in organotypic brain slices from APPPS1 mice (Daria *et al.*, 2017). Therefore, I first tested the effect of GM-CSF in organotypic brain slices from 5-month-old APP-KI mice. Brain slices were treated for two weeks with GM-CSF or PBS, as vehicle, and analyzed for A $\beta$  plaque coverage. Immunohistological analysis showed a 70% reduction in A $\beta$  burden upon GM-CSF treatment, compared to the control condition (Figure 31A and B). This pronounced A $\beta$  clearance effect was accompanied with a massive proliferation of microglia indicated by the increase in CD68 positive cells (Figure 31A), as already observed in the APPPS1 mouse model (Daria *et al.*, 2017). In addition, I detected intracellular A $\beta$  material within CD68 positive lysosomal structures of microglia upon GM-CSF treatment (Figure 31A), strongly supporting the efficacy of GM-CSF in inducing microglial phagocytic clearance of A $\beta$ .

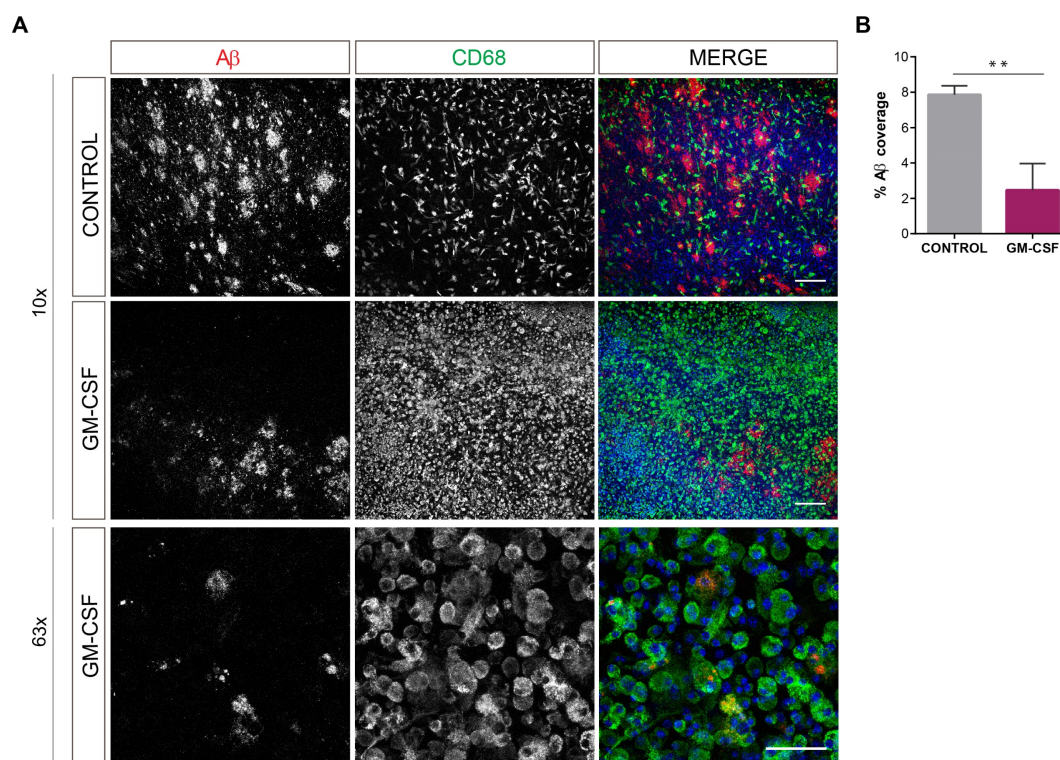


**Figure 31. GM-CSF induces A $\beta$  plaque clearance and microglia proliferation in an APP-KI *ex vivo* model.**

**A.** Immunohistological analysis of A $\beta$  plaques (red) and microglia (CD68, green) in organotypic brain slices from 5-month-old APP-KI mice treated for two weeks with 5ng/mL GM-CSF or PBS (control). The first two panels show the control and the GM-CSF-treated conditions. Representative images were acquired with a 10x dry objective; scale bar: 200 $\mu$ m. The third panel shows a zoom-in detail of microglia containing internalized A $\beta$  within the CD68-positive lysosomal compartments from the GM-CSF treatment condition. Images were acquired with a 63x water immersion objective; scale bar: 50 $\mu$ m. **B.** Quantification of A $\beta$  coverage in GM-CSF-treated organotypic brain slices *versus* control slices. Values are expressed as percentage of A $\beta$  signal and represent the mean of N=3 mice  $\pm$  SD (\*\*p < 0.005, unpaired two-tailed Student's T-test).

## 2.2. Short-term GM-CSF treatment does not modulate microglial A $\beta$ clearance *in vivo*

To test the capacity of GM-CSF to trigger microglial proteomic changes and A $\beta$  plaque clearance *in vivo*, I treated 5- and 14-month-old APP-KI mice following a short-term treatment paradigm (Figure 7).

Treatment of 5-month-old mice aimed to assess GM-CSF potential to preserve microglial phagocytic function (preventive strategy). Microglial proteomic analysis from 5-month-old mice treated with GM-CSF/vehicle (Cohort 1, Figure 7), resulted in mild significant proteomic alterations. However, none of the significant protein changes (by p value) passed the FDR correction criteria. Yet, small alterations could reflect important biological processes that occur in a restricted microglial population. Among the significantly upregulated proteins (p<0.05), I found the Activity-Dependent Neuroprotector Homeobox Protein (ADNP) (Figure 32, Table 29), which suggests a microglial neuroprotective response. Moreover, I detected several up-regulated

proteins related to the actin-cytoskeleton machinery (TBCE and EZR), but also proteins involved in cell cycle (JPT1 and S100a4) and DNA replication and repair (TREX1) (Figure 32 and Table 29). Among the down-regulated proteins, CEND1 and ATL1 were detected, which have a role in the differentiation and development of neurons (Figure 32 and Table 29), indicating a suppression in neuronal maturation. Thus, proteomic changes observed in microglia upon GM-CSF treatment in 5-month-old mice were mild, and pointed towards neuronal survival, cell proliferation and DNA repair pathways.

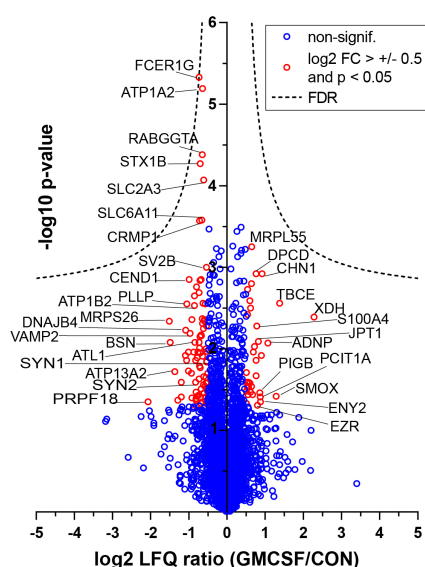


**Figure 32. Proteomic changes upon short GM-CSF treatment in 5-month-old mice suggest induction of neuroprotective mechanism.**

Volcano plots representing the  $-\log_{10}$  transformed p-value against the  $\log_2$  transformed LFQ ratios ( $\log_2$  fold changes) of GM-CSF-treated *versus* control microglia. Proteins with a  $\log_2$  fold change bigger than 0.5 or smaller than -0.5 with a significant p value ( $p < 0.05$ ) are marked in red. Non significantly regulated proteins are indicated in blue. Some selected regulated proteins are labelled with their gene names. Isolated microglia from N=5 APP-KI mice were used for this analysis.

Immunohistochemical analysis of 5-month-old APP-KI mice treated with GM-CSF/vehicle (Cohort 2, Figure 7), showed no change in A $\beta$  plaque load (for both, total and fibrillar A $\beta$ ) in the treated group compared to control mice (Figure 33A-C). Consistently, assessment of cell proliferation by quantification of BrdU positive cells, did not result in significant differences between the two groups (Figure 33A and D). Thus, GM-CSF did not show efficacy in preventing microglial phagocytic decline or enhancing A $\beta$  clearance in 5-month-old mice following this short treatment paradigm.

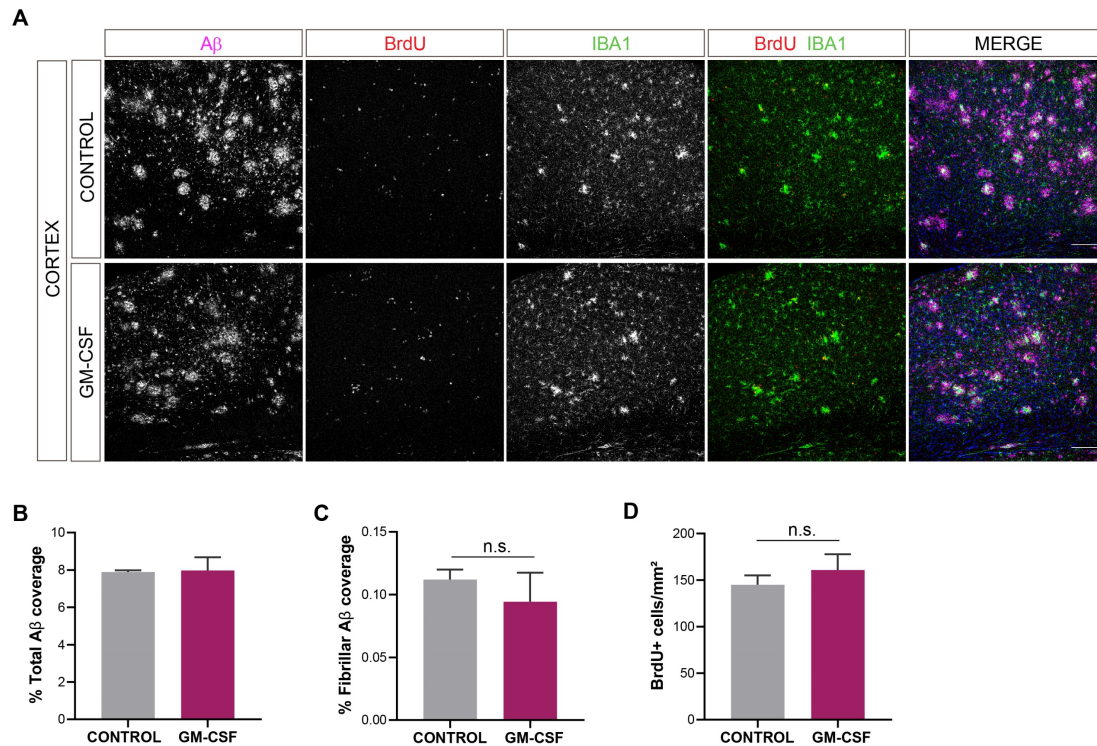


**Figure 33. Short GM-CSF treatment of 5-month-old APP-KI mice did not induce changes in plaque load or proliferation.**

**A.** Representative image of immunohistological analysis of A $\beta$  load (magenta) and proliferation (BrdU, red) in the cortex. Microglia are visualized with IBA1 (green) and cells nuclei with Hoechst (blue). Images were acquired with a 20x dry objective; scale bar: 100  $\mu$ m. Quantification of total A $\beta$  (**B**) and fibrillar A $\beta$  (**C**) signal coverage expressed as percentage of the cortical area analyzed in the control and the treatment group. **D.** Quantification of BrdU positive cells in the cortex of the control and GM-CSF-treated group. Values in **B**, **C** and **D** represent the mean of N=3 mice  $\pm$  SD (n.s.: not significant, unpaired two-tailed Student's T-test)

The lack of effect obtained from the study in 5-month-old mice led us hypothesize, that perhaps microglia was required to be in a dysfunctional state for GM-CSF to induce a “repair” mechanism on them. Thus, to test GM-CSF rejuvenation potential (repair strategy) on aged and dysfunctional microglia, 14-month-old APP-KI mice were treated following the same short-treatment paradigm (Figure 7).

Microglial proteomic analysis from 14-month-old-treated mice (cohort 1, Figure 7), also revealed mild GM-CSF-triggered alterations compared to control mice (Figure 34). Similar to the 5-month-old treatment group, none of the significant proteomic alterations passed the FDR correction. Significantly regulated changes included several histone proteins (HIS1H4A, H3F3/C, H2AF and HIST1H2B), the histone deacetylase SAP18 and the DNA methyltransferase DNMT3A (Figure 34 and Table 30), which suggest induction of DNA-reorganization mechanisms. Besides histones, I found proteins with increased abundance related to the maintenance of nuclear integrity (CDAN1), cell cycle regulation (CDK17 and NUCKS1) and actin cytoskeleton (CARMIL1), that

might indicate an induction of cell division (Figure 34 and Table 30). As downregulated proteins, I observed several ribosomal proteins (RPS23, MRPL14 and RPS29) and proteins involved in lipid metabolism (ACACA and PEX3) (Figure 34 and Table 30).

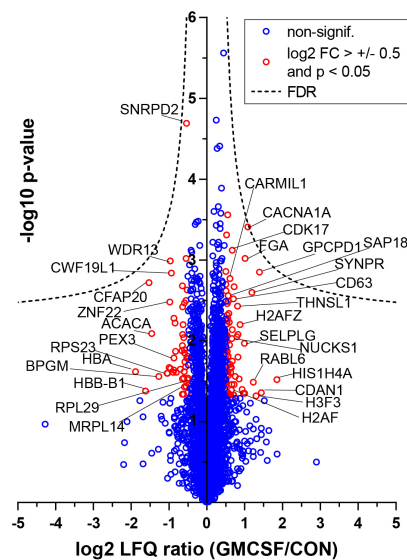


**Figure 34. Proteomic changes upon short GM-CSF treatment in 14-month-old mice indicate an induction of DNA reorganization and cell cycle.**

Volcano plots representing the  $-\log_{10}$  transformed p-value against the  $\log_2$  transformed LFQ ratios ( $\log_2$  fold changes) of GM-CSF-treated *versus* control microglia. Proteins with a  $\log_2$  fold change bigger than 0.5 or smaller than -0.5 with a significant p value ( $p < 0.05$ ) are marked in red. Non significantly regulated proteins are indicated in blue. Some selected regulated proteins are labelled with their gene names. Isolated microglia from N=6 APP-KI mice per group were used for this analysis.

Immunohistochemical analysis of 14-month-old mice (cohort 2, Figure 7), did not show significant changes in A $\beta$  burden (total and fibrillar A $\beta$ ) between GM-CSF-treated and control mice, for any of the regions analyzed (Figure 35A-B and D-G). Along the same lines, quantification of BrdU positive cells revealed no differences in proliferation upon GM-CSF treatment (Figure 35A and C). Therefore, GM-CSF was not proven more effective on inducing plaque clearance in older animals.

Taken together, short-GM-CSF treatment resulted in mild microglial proteomic changes that were age-dependent. However, I did not detect prominent changes in microglial homeostatic or DAM signatures.

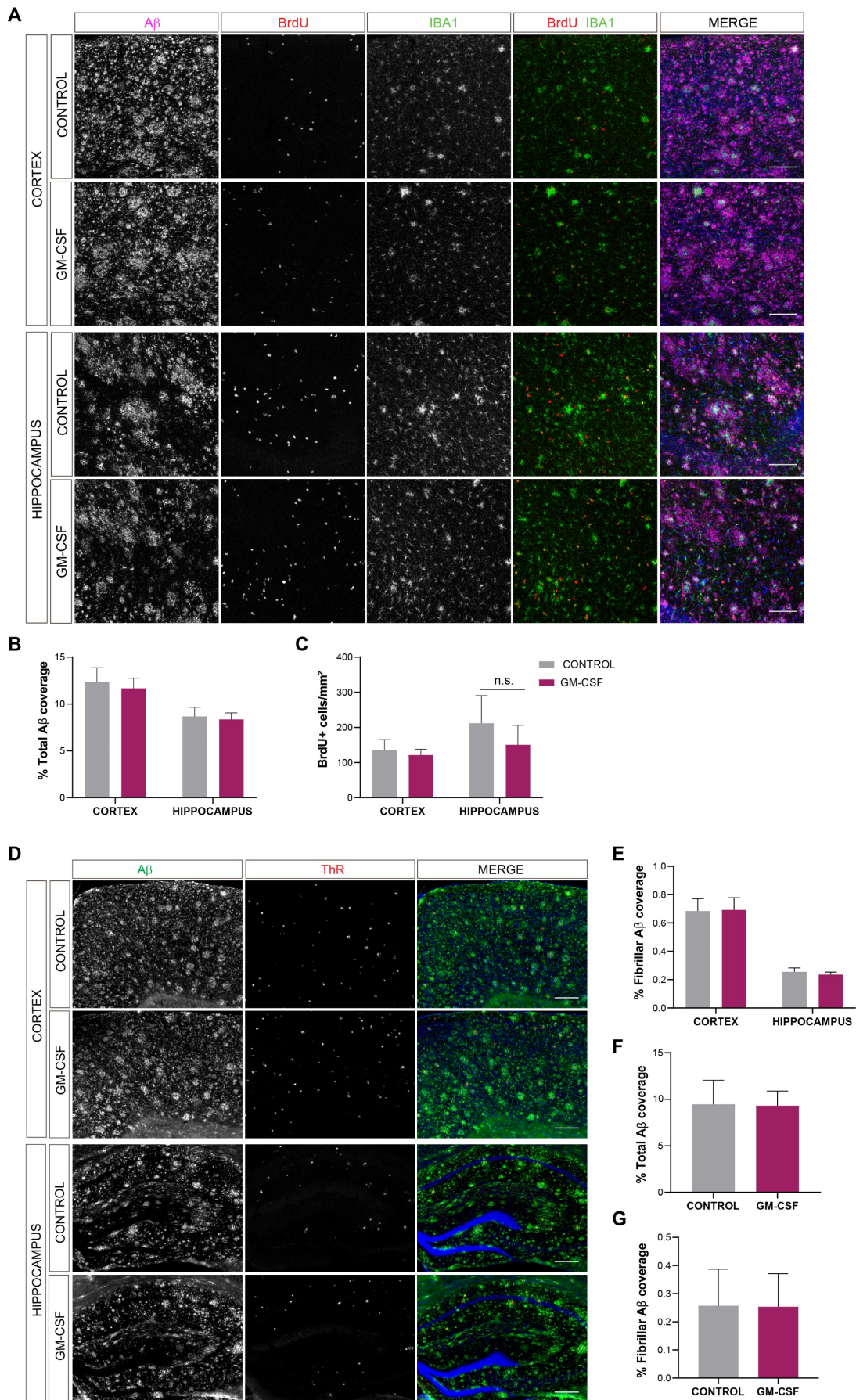


**Figure 35. (previous page). Short GM-CSF treatment did not change A $\beta$  burden nor induced proliferation in 14-month-old mice.**

A. Representative image of immunohistological analysis of A $\beta$  load (NAB228, magenta) and proliferation (BrdU, red) in the cortex (upper panels) and in the hippocampus (lower panels). Microglia are visualized with IBA1 (green) and cells nuclei with Hoechst (blue). Images were acquired with a 20x dry objective (1.5 optical zoom); scale bar: 100  $\mu$ m. B. Quantification of total A $\beta$  coverage in the cortex and hippocampus expressed as percentage of the area analyzed. C. Quantification of BrdU positive cells in the cortex and hippocampus. D. Representative image of the immunohistoological analysis of fibrillar A $\beta$  (ThR, red) in the cortex (upper panels) and hippocampus (lower panels). Total A $\beta$  is visualized in green and cells nuclei with Hoechst (blue). Images were acquired with a 10x dry objective; scale bar: 200  $\mu$ m E. Quantification analysis of fibrillar A $\beta$  coverage in cortex and hippocampus. Quantification of total A $\beta$  (F) and fibrillar A $\beta$  (G) coverage in whole coronal sections. Values in B, C, E, F and G represent the mean of N=4 mice  $\pm$  SD (n.s.: not significant, unpaired two-tailed Student's T-test)

### 2.3. Long-term GM-CSF treatment is not sufficient to enhance microglial A $\beta$ clearance *in vivo*

As short GM-CSF treatment did not lead to increased A $\beta$  clearance and only induced few proteomic changes in microglia, I examined a longer GM-CSF experimental paradigm (3 months, Figure 8). Mice were 4 months old at the beginning of the study with the aim of preventing microglia from getting into a disease state and to promote A $\beta$  clearance when the pathology is still not too extensive.

Microglial proteomic analysis (cohort 1, Figure 8), resulted in very mild significant changes upon GM-CSF treatment that did not pass the FDR correction. Among the significantly altered proteins with increased abundance, I detected proteins involved in the endo-lysosomal system (AP4E1, PPT2 and CHMP2A), in autophagy (ATG16L1) and the proteasome (PSMB9) (Figure 36 and Table 31), suggesting an induction of substrate degradation systems in microglia. Among the proteins that presented a significantly lower abundance in microglia from the GM-CSF-treated compared to control, I found very few proteins such as the E3 ubiquitin-protein ligase LTN1, the translation initiation factor EIF4E3 and the Z-DNA binding protein ZBP1 (Figure 36 and Table 31).

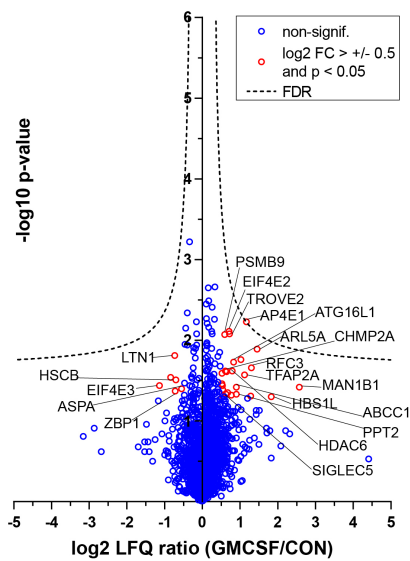


**Figure 36. Chronic GM-CSF treatment in 4-month-old mice induced only mild microglial proteomic changes related to substrate degradation systems.**

Volcano plots representing the  $-\log_{10}$  transformed p-value against the  $\log_2$  transformed LFK ratios ( $\log_2$  fold changes) of GM-CSF-treated *versus* control microglia. Proteins with a  $\log_2$  fold change bigger than 0.5 or smaller than -0.5 with a significant p value ( $p < 0.05$ ) are marked in red. Non significantly regulated proteins are indicated in blue. Some selected regulated proteins are labelled with their gene names. Isolated microglia from N=5 APP-KI mice per group were used for this analysis.

Immunohistochemical analysis of treated mice (cohort 2, Figure 8), did not reveal significant changes in the amount of total and fibrillar  $A\beta$  burden when comparing the treatment to the control group (Figure 37A, B and C). I also did not observe differences in the number of BrdU positive cells upon GM-CSF treatment, in any of the brain regions analyzed (Figure 37D), which was in agreement with the lack of effect on  $A\beta$  clearance.

Western blot analysis confirmed the absence of  $A\beta$  reduction in three different biochemical fractions: DEA-fraction, containing soluble  $A\beta$ , (Figure 38A-B), RIPA-fraction, containing the triton-soluble  $A\beta$ , (Figure 38A and C) and the formic acid (FA)-fraction that contains insoluble  $A\beta$  (Figure 38A and D) in GM-CSF-treated mice compared to control mice.

Overall, chronic GM-CSF treatment for 3 months did not lead to  $A\beta$  burden changes or major microglial proteomic rearrangements in APP-KI mice.

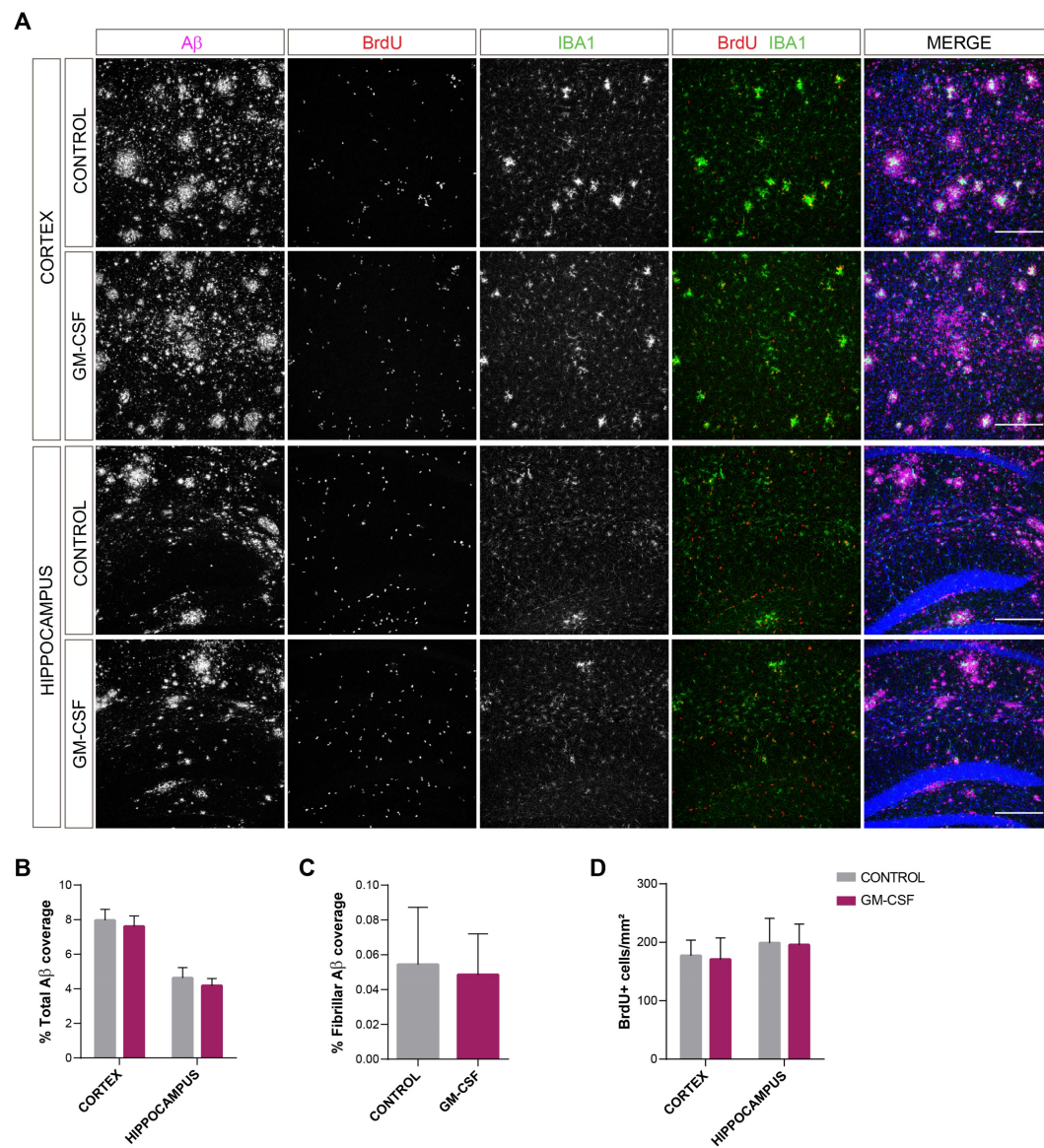


**Figure 37. Long-term GM-CSF treatment does not induce A $\beta$  clearance or proliferation in 4-month-old APP-KI mice.**

**A.** Representative image of immunohistological analysis of A $\beta$  load (magenta) and proliferation (BrdU, red) in the cortex (upper panels) and in the hippocampus (lower panels). Microglia are visualized with IBA1 (green) and cells nuclei with Hoechst (blue). Images were acquired with a 20x dry objective, scale bar: 100  $\mu$ m. **B.** Quantification of total A $\beta$  coverage in the cortex and hippocampus expressed as percentage of the area analyzed. **C.** Quantification analysis of fibrillar A $\beta$  coverage in the cortex expressed as percentage of the area analyzed. **D.** Quantification of BrdU positive cells in the cortex and hippocampus. Values in B, C and D represent the mean of N=6 mice  $\pm$  SD.

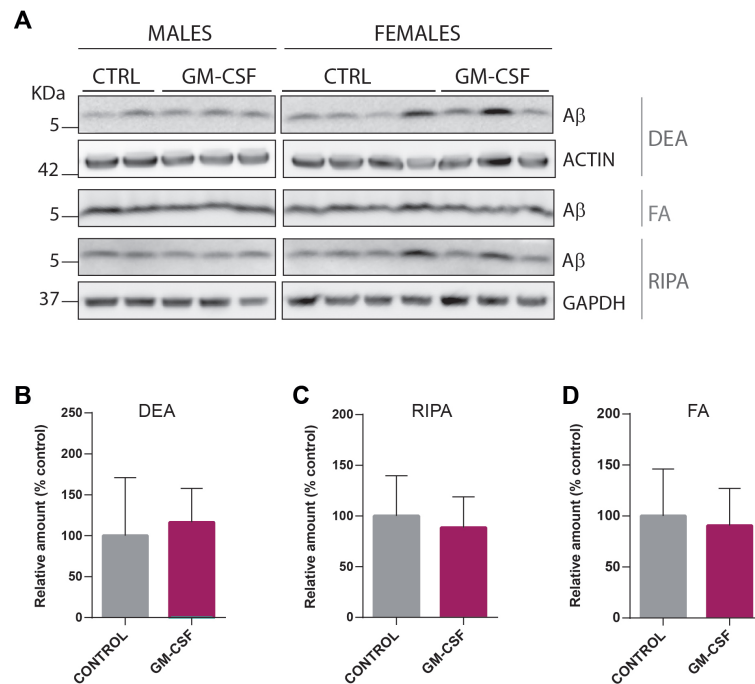


**Figure 38. Biochemical analysis of A $\beta$  load confirms the lack of amyloid reduction upon GM-CSF long treatment.**

**A.** Western blot analysis of A $\beta$  levels from GM-CSF-treated and control mice brains using sequential extraction protocol with different lysis buffers: DEA (enrichment in soluble A $\beta$ ), RIPA (enrichment in A $\beta$  soluble 1% triton) and FA (enrichment in insoluble A $\beta$ ). The 2D8 antibody was used to detect A $\beta$ . Quantification of western blot analysis is shown for the DEA fraction (**B**), RIPA fraction (**C**) and FA fraction (**D**). Quantifications from DEA and RIPA fractions were normalized to their loading controls (ACTIN and GAPDH), respectively, and for the FA fraction to the loading control of DEA fraction (ACTIN). Values in B, C and D represent the mean of N=6 mice  $\pm$  SD.

Taken together, GM-CSF was not proven to be an effective microglial modulator in terms of enhancing microglial A $\beta$  clearance *in vivo*. Even though some GM-CSF-triggered microglial changes were linked to the endo-lysosomal system, they did not efficiently translate into A $\beta$  burden reduction. Therefore, future studies are needed to design optimal microglial modulation strategies that lead to A $\beta$  clearance and to discover the molecular signatures of repaired microglia.

## Discussion

In the present study, I performed an in-depth molecular characterization of microglia by mass spectrometry-based proteomics using two different amyloidosis mouse models at different stages of A $\beta$  pathology. Furthermore, after identifying the signatures of AD microglia, I explored the potential of the hematopoietic cytokine GM-CSF, to reverse microglial disease signatures and restore their phagocytic function. For both studies, I used the MACS technology to achieve a high microglial yield (in average  $2 \times 10^6$  cells), necessary to perform mass spectrometry analysis of microglia from individual mice. With this methodology, I also attained a fairly pure population of microglia/macrophages (97%), with a minimal proportion of microglia (0.5%) remaining in the microglia-depleted fraction. Thus, I improved previously published microglial isolation protocols that reported an average yield of  $2 \times 10^5$  cells per mouse and therefore, required sample pooling to perform proteomic analysis (Rangaraju *et al.*, 2018). Although this study also utilized the MACS technology, the reduced microglial yield might be linked to the use of Percoll gradient, which has been shown to decrease the isolation yield of different cell types (Lee & Tansey, 2013; Rangaraju *et al.*, 2018; Horner *et al.*, 2019). Moreover, our proteomic analysis revealed many transmembrane proteins, such as the characteristic homeostatic microglial proteins TMEM119 and P2RY12, that were not detected by Rangaraju and colleagues, which they ascribe to the cell isolation procedure (Rangaraju *et al.*, 2018). Overall, I improved the cell isolation procedure that enabled reliable microglial proteomic analyses for the different purposes of my PhD project.

### **1. MARP signatures characterize microglial response to A $\beta$ along AD progression**

Proteomic analysis of microglia at different stages of amyloid pathology (3, 6 and 12 months) revealed a panel MARP signatures that progressively changed following the kinetics of amyloid accumulation along disease progression. Although the appearance of proteomic changes was detected earlier in APPPS1 (3 months) than in APP-KI microglia (6 months), MARP signatures were found in both mouse models, indicating the robustness of proteomic changes in response to A $\beta$  accumulation. Strikingly, at the pre-plaque deposition stage (1 month), no proteomic changes were displayed by microglia from any of the two mouse models, confirming that microglial response is specific to extracellular A $\beta$  deposits, as postulated by the amyloid-cascade hypothesis (Hardy & Higgins, 1992; Selkoe & Hardy, 2016). In addition, as also shown by transcriptomic studies (DAMs and MGnD), MARPs were detected altered in plaque-associated microglia

(Keren-Shaul *et al.*, 2017; Krasemann *et al.*, 2017), further supporting A $\beta$  pathology as the main trigger for microglial molecular changes.

As earlier discussed, it has been suggested that microglia might have a beneficial effect in early disease stages by clearing amyloid plaques from the brain parenchyma but become deficient in this function, and even detrimental as disease progresses by promoting uncontrolled inflammation and clearance of neuronal structures (Hansen *et al.*, 2018). Therefore, a time-resolved analysis of microglial proteomic changes was required to decipher these beneficial and detrimental mechanisms at the molecular level.

### **1.1. Early-MARPs reflect a protective but frustrated microglial response to A $\beta$**

Early MARPs represent the first molecular changes occurring in microglia as a response to newly formed plaques. Interestingly, in most cases, early-MARPs progressively increased (or decreased) as disease evolved, which indicates that these molecular changes are not just switched on upon initial microglial activation, but persistently follow the development of A $\beta$  pathology. This pattern suggests that early-MARPs might have an initial protective role on A $\beta$  clearance that is augmented as more plaques are forming and pathology is not resolved, trying to compensate for the clearance failure. However, antagonizing mechanisms could also be involved in this early response, which may account for the inefficient resolution of the pathological insult.

#### **1.1.1. Increase of immune-response mechanisms**

##### **1.1.1.1. Antigen presentation**

Among early-MARPs, mainly up-regulated proteins were found, involved in pathways related to microglial activation and immune-response such as antigen processing and presentation. Enriched in this pathway I found proteins like the typical dendritic cell marker CD11C (ITGAX), Major Histocompatibility Complex class-I (MHC-I)-related proteins like H2-D1, H2-K1, TAP2 and TAPBP and the MHC-II component CD74. Specifically, CD11C and CD74 were detected among the most up-regulated early-MARPs. The role of microglia as antigen presenting cells is still debated. Intracerebral injection of A $\beta$ -specific Th1-cells in a model of AD (5XFAD) resulted in an increase of MHC-II-positive microglia that led to reduced A $\beta$  load by increasing the phagocytic capacity of microglia. On the contrary, knocking out MHC-II in these mice exacerbated amyloid pathology and inflammation (Mittal *et al.*, 2019). An increase in both MHC-I and MHC-II-positive microglia has been reported in postmortem AD brains (McGeer *et al.*, 1987; Tooyama *et al.*, 1990; Parachikova *et al.*, 2007; Hopperton *et al.*, 2018) and AD mouse models (Keren-Shaul *et al.*, 2017; Mathys *et al.*, 2017). However, a recent study showed that although the number

of MHC-II-positive microglia increased over the disease course in a model of AD, the amount of surface MHC-II molecules per microglial cell decreased accordingly, and this inhibition was mediated by oligomeric A $\beta$ 42 in an in vitro system (Gericke *et al*, 2020). Therefore, although the initial upregulation of antigen presenting molecules could point to protective mechanisms, the levels of these molecules might decrease per microglia over time, making this process less effective as disease progresses. CD11C-positive cells have also been found at amyloid plaques as a subset of recruited activated microglia in AD human brains and mouse models (Kamphuis *et al*, 2016; Keren-Shaul *et al.*, 2017; Hopperton *et al.*, 2018). Analysis of their transcriptome showed an increment in immune, metabolic and lysosomal-related genes, but also in anti-inflammatory and T-cell tolerogenic transcripts (Kamphuis *et al.*, 2016). Interestingly, CD11c-positive microglia have been suggested as a subgroup of microglia with protective functions during development, aging and pathological conditions (Benmamar-Badel *et al*, 2020).

#### 1.1.1.2. Interferon-response

The anti-viral IFN signaling was one of the most enriched pathways among early-MARPs which includes proteins such as MNDA, IFIT2, IFIT3, IFI204, OAS1A, GVIN1, STAT1, STAT2 and ISG15, specially belonging to the type-I IFN signaling. Regulation of this pathway by microglia in neurodegenerative conditions has also been shown by others (Mathys *et al.*, 2017; Sala Frigerio *et al.*, 2019). Interestingly, type-I IFN signaling has been recently reported to be triggered by nucleic acids within amyloid plaques, which induced indiscriminate synapse engulfment by microglia (Roy *et al*, 2020). Moreover, deletion of the same signaling pathway was also recently shown to increase microglial A $\beta$  clearance (Moore *et al*, 2020), suggesting that IFN signaling inhibits microglial phagocytosis contributing to A $\beta$  accumulation and AD progression.

#### 1.1.2. Stimulation of the endo-lysosomal system

Among early MARPs we also find many up-regulated proteins involved in the endo-lysosomal system such as CD68, CTSD, CTSH, CTSZ, HEXA, GLB1, CLN3 and NPC2, which may indicate an increase in lysosomal function and therefore in the degradation of extracellular substrates like A $\beta$ . Interestingly, NPC2 together with the other member of the family, NPC1, regulate cholesterol egress from the lysosomes for its recycling, and their dysfunction cause a lysosomal storage disorder called Niemann-Pick type C (Wang *et al*, 2010a). Thus, an increase of NPC2 could point to an accumulation of cholesterol within the lysosomes. Interestingly, an study reported that the reduction of microglial cholesterol levels by APOE resulted in an enhancement of A $\beta$  trafficking to lysosomes and degradation, without the direct interaction between APOE and A $\beta$  (Lee *et al*,

2012). In fact, APOE was also found among up-regulated early-MARPs. This early-MARP has been shown to enhance soluble A $\beta$  degradation by proteinases both in microglia and extracellularly (Jiang *et al.*, 2008), and might mediate microglial response to amyloid plaques (Ulrich *et al.*, 2018).

Apart from APOE, different proteins involved in A $\beta$  phagocytosis or clearance were found up-regulated among early-MARPs. This is the case of the A $\beta$  receptor TLR2, which has been shown to promote A $\beta$  phagocytosis in cultured microglia but also neuroinflammation in an AD mouse model (Liu *et al.*, 2012). Moreover, mice lacking this receptor failed to phagocytose fibrillar A $\beta$  (Reed-Geaghan *et al.*, 2009). Among early-MARPs I also detected a high up-regulation of the C-type lectin CLEC7a (Dectin-1), one of the key markers attributed to the DAM, MGnD and CD11C-specific microglial transcriptomic signatures, (Kamphuis *et al.*, 2016; Keren-Shaul *et al.*, 2017; Krasemann *et al.*, 2017). Interestingly, although the levels of CLEC7a were increased throughout all disease stages compared to the WT, they peaked at the middle and showed a reduction at the advanced disease stage in both mouse models. This might indicate a compensatory increase that was followed by a functional decline. However, the exact contribution of CLEC7a to microglial function in AD remains to be further investigated. In addition, we also found an up-regulation of other lectins like Galectin-3 (LGALS3) and its ligand LGALS3BP. Of note, LGALS3 was recently reported to be upregulated in microglia in response to fibrillar A $\beta$  and promotes a detrimental effect on amyloid clearance by induction of pro-inflammatory signaling and increase amyloid aggregation (Boza-Serrano *et al.*, 2019). On the contrary, the serine protease HTRA1, which showed a very prominent up-regulation at early disease stage has been implicated in fibrillar A $\beta$  disintegration facilitating its degradation (Poepsel *et al.*, 2015).

Finally, we also detected several early-MARPs with higher abundance implicated in cell cycle, such as PCNA, CDK6 and MCM5, which is consistent with the increase in microglial proliferation upon activation and response to different insults, including A $\beta$  (Kreutzberg, 1996; Hansen *et al.*, 2018).

Overall, early-MARPs included proteins implicated in microglial activation, immune response and an enhanced phagocytic activity, which suggest a protective role of microglia in A $\beta$  detection and clearance. However, these beneficial effects might be insufficient when exposed to a chronic insult and even counteracted by other signaling pathways with antagonizing and detrimental effects such as interferon signaling. Therefore, an increase in immune and phagocytic pathways may just reflect an attempt for enhanced clearance that does not translate in improved function. In addition, both protective and detrimental mechanisms might coexist, depending to the specific

microenvironment that microglia are exposed to, or due to microglial heterogeneous functions. Interestingly, early-MARPs showed a high overlap with transcriptomic changes reported by Keren-Shaul and colleagues (2017), who attributed a beneficial function to the DAM signatures (Keren-Shaul *et al.*, 2017). However, similar microglial signatures were interpreted to be neurotoxic (MGnD) in the same context (Krasemann *et al.*, 2017). Yet, none of these interpretations was based on functional studies and thus, this kind of categorizations might be misleading. Thus, functional studies are required to link specific microglial signatures with their functional outcome in AD.

## **1.2. Middle-MARPs show a metabolic switch and loss of microglial homeostatic functions**

Protein changes that belong to middle-MARPs appear when amyloid pathology is fully established. Among these MARPs, both up-regulated and down-regulated protein changes were found, which might reflect on the one hand, a stronger microglial activation due to the overt pathology and on the other hand, obvious signs of dysfunction or senescence.

### **1.2.1. Increase of lipid and glucose metabolism**

Middle-MARPs included the up-regulation of the AD risk marker TREM2, which function has been shown to be pivotal for microglial recruitment to amyloid plaques and phagocytosis (Wang *et al.*, 2015; Xiang *et al.*, 2016; Parhizkar *et al.*, 2019). In addition, we found several lipid binding proteins like FABP3, FABP5 and APOD, proteins involved in fatty acid metabolism such as AACS, ACOX3, EPHX1, HACD2, HSD17B12 and NCEH1, or in fatty acid transport like ABCD2. Interestingly, TREM2 has been reported to sense damage-associated lipid patterns from neuronal membranes that associate to fibrillar A $\beta$ , triggering microglial response to A $\beta$  deposits (Wang *et al.*, 2015). Moreover, TREM2 can bind to APOE and other apolipoproteins like APOJ/CLU, which form A $\beta$ -apolipoprotein complexes and facilitate A $\beta$  engulfment by microglia in a TREM2 dependent manner (Yeh *et al.*, 2016). Therefore, other lipid binding proteins could have similar functions in microglia. Increased levels of FABP3 are in accordance with studies reporting higher levels of FABP3 in the CSF of AD patients and supports its value as biomarker candidate for AD (Guo *et al.*, 2013; Chiasserini *et al.*, 2017). In addition, validation of FABP5 increase by western blot revealed the specific presence of this marker in AD but not in healthy microglia, which also points to this fatty acid binding protein as potential AD biomarker candidate. Furthermore, altered lipid metabolism has been linked to AD pathogenesis in regard to APP processing, A $\beta$  aggregation, neuronal and synaptic activity (Haughey *et al.*, 2010). An up-regulation in genes related to lipid

metabolism has also been described by others in AD microglia (Keren-Shaul *et al.*, 2017). Interestingly, increased microglial lipid metabolism is suggested as a source of energy to promote protective mechanisms like phagocytosis (Loving & Bruce, 2020). Therefore, an increment in the use of lipids as energy source might indicate the activation of mechanisms to bust A $\beta$  clearance. Proteins involved in glycolysis/gluconeogenesis such as ALDOA, PKM, PGK1, PFKL PGAM2 and TPI1 were also found up-regulated among middle-MARPs. Strikingly, ALDOA, PKM and PGK1 have also been found elevated in the CSF of AD patients compared to healthy individuals (Bader *et al*, 2020). Interestingly, microglia seem to go through a metabolic switch from oxidative phosphorylation in a steady state to glycolysis when acutely exposed to A $\beta$ . On the contrary, chronic exposure leads to reduced glucose consumption and metabolic defects (Baik *et al*, 2019). Moreover, iPSC-derived microglia bearing loss of function-TREM2 variants revealed an impaired ability of performing this metabolic switch, which translates in functional defects like phagocytic impairment (Piers *et al*, 2020). However, the switch from oxidative phosphorylation to glycolysis has also been linked to the induction of pro-inflammatory signaling in microglia and correspondingly, pro-inflammatory signaling increases microglial glucose consumption (Gimeno-Bayon *et al*, 2014; Huang *et al*, 2019; Devanney *et al*, 2020; Lauro & Limatola, 2020). This data suggests that microglial activation state and metabolic changes are strongly associated in AD.

### **1.2.2. Increment of exosome biogenesis and pro-inflammatory signaling**

The exosome was the cellular compartment that showed one of the highest enrichments in middle-MARPs according to our GO analysis. Exosomes are a type of extracellular vesicles (less than 150 nm in diameter) of endocytic origin that are released to the extracellular space by the fusion of a multivesicular body vesicle with the plasma membrane and are involved in important processes such as elimination of cellular waste or cell-to cell communications (Hessvik & Llorente, 2018). In fact CD63 was found among up-regulated MARPs and it is considered a common marker for exosomes (Paolicelli *et al*, 2019). Microglia can release exosomes but also be the recipient for exosomes secreted from other cell types (Paolicelli *et al.*, 2019). Since this marker has also been shown to be up-regulated at transcriptome level in AD (Keren-Shaul *et al.*, 2017), it is more likely that the increase in CD63 protein is due to an increment in microglial exocytosis machinery. Microglia has been shown to participate in extracellular clearance of A $\beta$  by the release exosomes containing the A $\beta$ -degrading enzyme IDE, when stimulated with lipid lowering drugs (Tamboli *et al*, 2010). On the contrary, extracellular vesicles bearing neurotoxic A $\beta$  species were

found in high levels in the CSF of AD patients and might contribute to A $\beta$  pathology spreading (Joshi *et al.*, 2014). Moreover, microglia can regulate inflammation by the release of exosomes containing pro- or anti-inflammatory factors (Paolicelli *et al.*, 2019).

MIF was also among up-regulated middle-MARPs. This pro-inflammatory cytokine has been shown to be elevated in the brain of AD patients and AD mouse models and in the CSF of individuals with AD (Bacher *et al.*, 2010; Zhang *et al.*, 2019). However, conflicting results were reported in terms of the role of MIF in AD. Although MIF expression has been associated to microglia recruited to A $\beta$  plaques and A $\beta$  deposits themselves, in one study MIF had a neuroprotective function (Zhang *et al.*, 2019), and in another study led to neurotoxic effects (Bacher *et al.*, 2010). Therefore, the role of MIF in AD requires further investigation.

### **1.2.3. Progressive loss of microglial homeostatic functions**

#### **1.2.3.1. Inhibition of key microglial homeostatic signatures**

Interestingly, among middle-MARPs we found a decrease of known microglial homeostatic proteins such as CX3CR1 and its ligand CX3CL1, P2RY12 and TMEM119 (Butovsky *et al.*, 2014). The downregulation of these homeostatic markers in AD microglia has also been demonstrated at the transcriptome level (Keren-Shaul *et al.*, 2017; Krasemann *et al.*, 2017; Sala Frigerio *et al.*, 2019), indicating the transcriptional regulation of these homeostatic genes in AD. The CX3CR1-CX3CL1 axis plays an important role in microglia-neuron communication (Szepesi *et al.*, 2018). During development and adult neurogenesis, CX3CR1 has been shown to be pivotal for correct synapse pruning (Zhan *et al.*, 2014; Reshef *et al.*, 2017). However, in the context of AD, both beneficial and deleterious functions have been associated to CX3CR1. Microglial CX3CR1 deletion has been demonstrated to increase Tau pathology, neurotoxicity and cognitive decline due to enhanced production of pro-inflammatory factors (Bhaskar *et al.*, 2010; Cho *et al.*, 2011). In another study, CX3CR1-deficient mice showed reduced amyloid load due to increased microglial phagocytosis (Lee *et al.*, 2010; Liu *et al.*, 2010), which also protected from A $\beta$ -associated neurotoxicity and memory impairments (Wu *et al.*, 2013; Dworzak *et al.*, 2015). Therefore, the downregulation of the CX3CR1-CX3CL1 axis might be beneficial due to the stimulation of A $\beta$  clearance, but detrimental as it promotes inflammation-associated neurotoxicity. The purinergic receptor P2RY12 has been shown to be involved in microglial migration to injury sites in response to extracellular ATP/ADP (Haynes *et al.*, 2006). Interestingly, microglia secrete ATP and UTP when exposed to A $\beta$  oligomers and fibrils in order to attract more microglia to amyloid plaques through the activation of P2RY12, also promoting A $\beta$  uptake (Kim *et al.*, 2012a). An increase in

microglial P2RY12 was observed in patients that received A $\beta$  immunotherapy, which was associated to increased microglial motility (Franco-Bocanegra *et al*, 2019a). Therefore, a decrease in P2RY12 might indicate the loss of microglial ability to migrate towards an insult like A $\beta$  and detect chemotactic signals. Moreover, the expression of the middle-MARP TMEM119 was found in both mouse and human microglia, however its role in microglia is still unknown and largely understudied in the context of AD (Bennett *et al*, 2016). Although the repression of homeostatic signatures might represent the loss of key microglial functions, increased microglial homeostatic and reduced DAM markers were observed after treatment of 2 AD mouse models with a small synthetic molecule, DAPPD. Moreover, this effect, was associated to increased phagocytic function, reduction in A $\beta$  load and improved cognition (Park *et al*, 2019). However, locking microglia in a homeostatic state, like has been reported in *Trem2*-deficient mice, seems to be detrimental for AD pathology as microglia lose their capacity of responding to A $\beta$  plaques and injury conditions (Wang *et al.*, 2015; Jay *et al*, 2017; Keren-Shaul *et al.*, 2017; Mazaheri *et al*, 2017; Gotzl *et al*, 2019). Interestingly, contrary to AD mouse microglia, human AD microglia express higher levels of homeostatic markers such as *P2RY12*, *TMEM119* and *CX3CR1* compared to healthy controls (Zhou *et al.*, 2020). Therefore, whether the suppression of specific microglial homeostatic signatures is beneficial or detrimental for microglial function in AD is not fully understood and deserves further investigation.

#### **1.2.3.2. Decay of cell motility, phagocytosis and proliferation**

An important physiological machinery for microglial normal function is the actin cytoskeleton, which is necessary for key microglial processes like motility and phagocytosis (Franco-Bocanegra *et al*, 2019b). In fact, actin cytoskeleton and motility were some of the most downregulated signaling pathways according to our GO analysis of middle-MARPs. Involved in this pathway we found reduced levels of *ACTN1*, *BIN2*, *CDC42BPB*, *CNN2*, *FER*, *FSCN1*, *PDLIM4* and *PDLIM5*, among others. This is in accordance with reduced microglial motility and phagocytosis observed in AD models (Krabbe *et al*, 2013). However, among middle-MARPs some actin cytoskeleton proteins such as *ACTR3B* and *TRIOBP* were detected at higher levels. Particularly, *ACTR3B* showed an 18-fold up-regulation at 12 months in both mouse models and already a 7- and 16-fold increase by 6 months in APPPS1 and APP-KI respectively. This protein was found to be enriched in neurons under healthy conditions, and is a component of Arp2/3 complex (Jay *et al*, 2000), which is involved in directed motility (Franco-Bocanegra *et al.*, 2019b). Alterations in this marker were, however, not detected at the transcriptome level (Keren-Shaul *et al.*, 2017) and

its role in microglia is unknown. Thus, the function of this protein in AD deserves further investigation.

Two proteins implicated in phagocytosis such as SYK and TLR9, were also detected at reduced levels among middle-MARPs. Stimulation of TLR9 was found to significantly reduce cortical and vascular amyloid load in an AD mouse model (Scholtzova *et al.*, 2009), therefore its downregulation suggests a reduction in microglial phagocytic capacity. In turn, SYK is a known downstream molecule of TREM2 signaling pathway (Konishi & Kiyama, 2018). Although alterations in this marker were not detected at transcriptome level (Keren-Shaul *et al.*, 2017), we could validate proteomic results by western blot analysis, confirming that both SYK and its active phosphorylated form (p-SYK), are indeed decreased in AD microglia. This result was surprising since, as mentioned earlier, TREM2 was found upregulated among middle-MARPs suggesting its active signaling. As SYK is a common downstream effector of different signaling pathways such as CSF1 or Fc receptors (Lowell, 2011; Konishi & Kiyama, 2018), the reduction of this protein might be the result of the cross talk with other pathways with inhibitory functions. Importantly, this result reveals the malfunction of the TREM2 signaling in AD microglia, which might have been overlooked due to the consistently reported increased levels of the receptor by several studies (Keren-Shaul *et al.*, 2017; Krasemann *et al.*, 2017; Sala Frigerio *et al.*, 2019).

As discussed earlier, another important function of microglia is proliferation, necessary for microglial activation in AD in response to A $\beta$  pathology (Kamphuis *et al.*, 2012). However, we found this pathway to be one the most significantly down-regulated ones in our GO analysis, which suggests the loss of microglial ability to respond to A $\beta$  at this middle pathological stage.

Overall, middle-MARPs reflect a metabolic switch towards increased glycolysis and lipid metabolism, which might indicate an attempt to enhance their activation status and clearance mechanisms, also reflected by the increased exosome activity and pro-inflammatory signaling. However, middle-MARPs also represent the progressive loss of important microglial functional mechanisms like motility, proliferation, chemotaxis and phagocytosis that might contribute to microglial dysfunction in AD.

### **1.3. Advanced-MARPs reflect an aged and dysfunctional microglial phenotype**

Proteins classified as advanced-MARPs might be the result of microglial response to chronic A $\beta$  exposure and aging.

### 1.3.1. Continued increase in glucose and lipid metabolism

As observed with middle-MARPs, glycolysis/gluconeogenesis was also one of the up-regulated pathways represented by advanced-MARPs according to GO analysis. Among the proteins involved in this pathway I detected GPI, GYS1, PGM1, ENO1, TIGAR and PGAM1, among other. Moreover, I found an enrichment of proteins involved in protein glycosylation. Although altered glycosylation has been linked to AD in the context of APP processing, A $\beta$  generation and neuronal function (Schedin-Weiss *et al*, 2014; Regan *et al*, 2019), not much is known about the role of protein glycosylation in AD microglia. Similarly, I also observed an increase in lipid metabolism. Specifically I found an increase in ECHS1, which participates in fatty acid catabolism through beta oxidation, but also, in ACSBG1, ACSS2, ELOVL1 and FASN, which are involved in lipid biosynthesis, indicating both the catabolism of lipids for their use as a source of energy and their synthesis for different cellular functions. These microglial changes in energy metabolism might be in line with the prominent relationship between metabolic diseases like type 2 diabetes mellitus or obesity and AD (Ott *et al*, 1999; Cai *et al*, 2012)

### 1.3.2. Alterations in endo-lysosomal system and oxidative stress

Among advanced-MARPs, I found a significant amount of up-regulated proteins that are part of the lysosomal V-ATPases proton channel such as ATP6V0A1, ATP6V1A, ATP6V1B2, ATP6V1C1, ATP6V1D, ATP6V1E1 and ATP6V1H. These proteins participate in the acidification of endocytic vacuoles by pumping protons into the lumen of these vacuoles in an ATP-dependent fashion (Forgac, 2007; Maxson & Grinstein, 2014). Therefore, this data suggests an increase in lysosomal acidification, perhaps as a compensatory mechanism due to the accumulation of undigested A $\beta$  within lysosomal vesicles. Of note, the acidification of microglial lysosomes has been reported to be insufficient to degrade fibrillar A $\beta$ , but activation with M-CSF was able to induce proper acidification and fibrillar A $\beta$  degradation (Majumdar *et al.*, 2007; Majumdar *et al.*, 2011). In addition, we found a significant down-regulation (~50-60% reduction) of important transcription factors involved in the regulation of lysosomal function like TFEB and TFE3. Interestingly, TFEB overexpression in microglia led to increased phagocytic ability to degrade fibrillar A $\beta$  by increasing lysosomal biogenesis, which was even more enhanced when TFEB was deacetylated (Bao *et al.*, 2016). It has been shown that TFEB and TFE3 are influenced by metabolic changes, cellular stress and immune-related factors (Raben & Puertollano, 2016), therefore multiple mechanisms underlying AD pathogenesis might be responsible for the reduction of these transcription factors in microglia, and these changes may contribute to microglial phagocytic impairment in AD.

Furthermore, I detected a substantial downregulation of advanced-MARPs involved in actin cytoskeleton regulation and phagocytosis/endocytosis such as the AD risk markers BIN1 and ABI3, but also other proteins like LYN, MARCKS, RAC2, VAV2, CFL1, PIK3R5, MRAS, NRAS, HRAS and PXN, among others. Of note, a regulator of actin dynamics, Cofilin 1 (CFL1), has been shown to be important for microglial phagocytosis and migration since CFL1-deficient microglia showed reduced LPS-induced activation, phagocytic activity and migration rates (Alhadidi & Shah, 2018). Strikingly, LYN is a SRC kinase that can phosphorylate SYK, for its activation and transduction of the downstream signaling cascade that involves other down-regulated advanced-MARPs such as VAV2 (Konishi & Kiyama, 2018). As mentioned above, SYK was detected among the down-regulated middle-MARPs. Both SYK and LYN have been identified as AD risk genes by GWAS studies but below the significance threshold and have been shown to upregulate their expression upon exposure to A $\beta$  pathology (Sierksma *et al.*, 2020). Therefore, this data further supports the finding that even though TREM2 itself is up-regulated, its downstream signaling might be inhibited and thus, could contribute to the defective clearance function of microglia.

In addition, we found an increase of the NADPH oxidase CYBB (NOX2), which is linked to a pro-inflammatory phenotype in microglia due to its involvement in the production of reactive oxygen species (ROS) (Wilkinson & Landreth, 2006). Moreover, NOX2 has been shown to get up-regulated when exposed to A $\beta$ , especially in aged mice, leading to ROS production, microgliosis and increase of pro-inflammatory cytokines like IL-1 $\beta$ . In addition, NOX2-deficient old mice showed decreased amyloid load correlating with decreased microgliosis (Geng *et al.*, 2020). Therefore, NOX2 increase might contribute to microglial phagocytic dysfunction, oxidative damage and neuroinflammation in AD.

### 1.3.3. Enhanced reduction of homeostatic signatures

Similar to what we observed with middle-MARPs, advanced-MARPs reflected a further decay of microglial functions. Cell division was one of the most significantly down-regulated pathways found among advanced-MARPs, indicating again the progressive loss of microglial function to react to A $\beta$  pathology.

I also detected important microglial homeostatic markers such as TGFBR1 and CSF1R being prominently downregulated among advanced-MARPs. TGF- $\beta$  signaling is considered a master regulator of microglial homeostatic signature and it is down-regulated upon microglia activation and acquisition of AD-signatures (Butovsky *et al.*, 2014; Keren-Shaul *et al.*, 2017; Krasemann *et al.*, 2017). Interestingly, we already observed a prominent down-regulation of TGF- $\beta$  downstream

signaling proteins SMAD1 and SMAD3 among middle-MARPs and also SMAD2 among advanced-MARPs. TGF- $\beta$ 1 signaling regulates microglia reactive phenotype by decreasing the secretion of pro-inflammatory cytokines and ROS (von Bernhardt *et al*, 2015). Overexpression of TGF- $\beta$ 1 in an AD mouse model resulted in reduced A $\beta$  load, which correlated with microglial activation. Moreover, TGF- $\beta$  induced microglial A $\beta$  clearance *in vitro* (Wyss-Coray *et al*, 2001). In addition, although the levels of TGF- $\beta$  have been reported to increase with aging (Tichauer *et al*, 2014; Fessel, 2019), the downstream signaling pathway seems to be impaired, which may lead to microglial cytotoxic effects due to increased secretion of neuroinflammatory factors (Tichauer *et al*, 2014). Therefore, aging might be an important factor that predisposes to reduced protective TGF- $\beta$  signaling in microglia that could get enhanced in AD. In turn, CSF1R signaling, which as discussed earlier, can be activated by two ligands, CSF1 (M-CSF) and IL-34, is essential for microglia/macrophages survival, proliferation and differentiation in physiological conditions (Erblich *et al*, 2011; Elmore *et al*, 2014). CSF1 has been shown to reduce microglial neuroinflammatory effects in different brain diseases (Wylot *et al*, 2019; Hu *et al*, 2020). Interestingly, human microglia treated with CSF1 showed increased proliferation and phagocytosis of A $\beta$  *in vitro* (Smith *et al*, 2013). Moreover, treatment of an AD mouse model with CSF1 resulted in higher number of microglia and reduction of A $\beta$  load due to enhanced microglial phagocytosis, that was accompanied by amelioration of cognitive decline (Boissonneault *et al*, 2009). Thus, CSF1R reduction might be detrimental for microglial proliferation and survival, but also for its ability to phagocytose A $\beta$ , which could account for the observed reduction in cell cycle-related proteins and diminished phagocytic ability.

#### **1.3.4. DNA destabilization and senescence**

Among advanced-MARPs I also detected several members of core histone complexes such as H3.3, H2A and H2B to be downregulated. Reduction of canonical histones has been linked to genetic instability and senescence (Prado *et al*, 2017). In addition, the Histone PARylation factor 1 (HPF1), which is expressed in response to DNA damage (Gibbs-Seymour *et al*, 2016), was detected up-regulated among advanced MARPs. In fact, microglia senescence has been described in normal aged individuals which present dystrophic morphology (Streit *et al*, 2004), but this phenotype seems to be even more prominent in AD patients due to exposure to A $\beta$  (Flanary *et al*, 2007). Moreover, DNA damage has been reported in aged microglia, especially in the mitochondria (Hayashi *et al*, 2008; von Bernhardt *et al*, 2015).

Taken together, advanced-MARPs reflect an enhanced microglial dysfunctional phenotype already observed at middle pathological stage, probably due to chronic exposure to A $\beta$  pathology, which might be aggravated by aging.

#### **1.4. MARP signatures reflect a continuum of microglial changes along AD pathology**

Overall, MARP signatures identified in this study, reflect a mixture of signaling pathways at every disease stage, some suggesting an attempt to clear A $\beta$ , but some others indicating a suppression of microglial function or detrimental pro-inflammatory signaling. This might be the result of the inherent two-faced function of microglia (Gomes-Leal, 2012; Ferreira & Bernardino, 2015). On one hand microglia aim to clear potential toxic insults from the brain parenchyma, by which they often need to bust immune response by release of inflammatory factors; but on the other hand, they also have the function of supporting and protecting the neuronal network. However, as the clearing function might compromise the neuroprotective one, microglial response must be well titrated in order to avoid neurotoxic effects. Thus, a deeper understanding on single molecular mechanisms combined with functional assays will help to identify specific pathways that can be targeted at right time window without compromising the neuronal architecture.

Taken together, MARP signatures represent a valuable dataset of microglial proteomic changes along AD progression, by revealing mechanistic insights into microglial response to A $\beta$  pathology and novel molecular targets for microglial repair in AD.

## **2. A $\beta$ conformation determines microglial recruitment and acquisition of MARP signatures**

What triggers microglial activation and recruitment in AD is still not fully understood. In the present study, I demonstrated that the appearance of microglial proteomic changes depends on the presence of fibrillar A $\beta$  in the plaque core, which correlates with microglial recruitment to amyloid plaques. The APP-KI mouse model showed bigger and more diffuse plaques at early-stage pathology than the APPPS1, that displayed smaller and compacted fibrillar plaques. However, despite having bigger plaques, APP-KI mice showed substantially less microglia recruitment compared to APPPS1 mice, which was in line with the very low levels of fibrillar A $\beta$  in the plaque core of these mice. Therefore, I hypothesized that the structural conformation of A $\beta$  within the plaques seems to be pivotal for microglial reactivity. In fact, this finding is in line with previous reports of other mouse models or Down-syndrome and AD brains, where dense-core fibrillar plaques were found to be associated with higher microglial reactivity compared to

diffuse plaques, that were mostly devoid of microglia (Motte & Williams, 1989; Stalder *et al*, 1999; D'Andrea *et al*, 2004).

As microglial activation has also been reported to be triggered upon neuronal damage (Krasemann *et al.*, 2017), we examined if higher microglial recruitment could be associated with the size of dystrophic neurites. However, we found that the extent of neuronal damage did not correlate with the number of recruited microglia to dystrophic neurites, but rather, with the size of amyloid plaques and their structural conformation. Interestingly, the same finding was reported in *Trem2*- and *ApoE*-deficient mice which display bigger and more diffuse plaques associated to less recruited microglia but larger dystrophic neurites areas (Ulrich *et al.*, 2018; Meilandt *et al*, 2020). These results are in line with the idea that microglia form a protective barrier around amyloid plaques by participating in plaques compaction and thereby, prevent the plaque-associated damage from extending (Condello *et al*, 2015; Yuan *et al*, 2016; Zhao *et al*, 2017). Notably, non-demented individuals have been reported to present a high load of diffuse amyloid plaques, but these plaques were not associated with dystrophic neurites or reactive microglia (Perez-Nievas *et al*, 2013). Thus, it might be possible that specific A $\beta$  species and/or A $\beta$  structural conformations trigger neuronal damage, while others do not. Hence, a deeper understanding into these neurotoxic plaques and their discrimination with non-invasive techniques such as PET imaging using conformation specific A $\beta$  ligands, would serve as a powerful diagnostic tool for AD.

Fibrillar deposits have shown to cause spine loss and permanent damage of neuronal connections (Tsai *et al*, 2004). However, A $\beta$  in a soluble form such as A $\beta$  oligomers, were suggested as the most neurotoxic species (Walsh *et al*, 2002; Haass & Selkoe, 2007; Brouillette *et al*, 2012; Choi *et al*, 2013) and contribute to plaques build up (Finder & Glockshuber, 2007). Thus, therapeutic strategies aiming at targeting soluble A $\beta$  or promoting A $\beta$  aggregation in order to induce early microglial recruitment that leads to efficient clearance before soluble species or big fibrillar deposits induce neuronal damage, might represent promising therapeutic options for reducing AD progression.

### **3. Fibrillar A $\beta$ is associated to acquisition of MARP signatures and phagocytic impairment**

The ability of microglia to clear A $\beta$  plaques is known to be either deficient or insufficient in AD, which contributes to amyloid accumulation and disease progression (Hickman *et al.*, 2008; Lee & Landreth, 2010; Hellwig *et al.*, 2015; Anwar & Rivest, 2020). Moreover, this impairment has been associated to aging and inflammatory milieu (Hickman *et al.*, 2008; Floden & Combs, 2011). In the

present study I demonstrated that the decay in microglial phagocytosis using the *E.coli* pH-rodo uptake assay correlates with the presence of fibrillar A $\beta$  plaques and the acquisition of MARP signatures already upon early pathology in APPPS1 mice. Similarly, Krabbe and colleagues reported that microglial phagocytosis impairment was associated to the appearance of amyloid pathology and restored upon reduction of amyloid load by anti-A $\beta$  antibody therapy (Krabbe *et al.*, 2013). Fibrillar A $\beta$  can be efficiently engulfed by microglia but difficult to degrade intracellularly, showing only a partial degradation over the first days after uptake (Paresce *et al.*, 1997; Chung *et al.*, 1999). This impairment to degrade fibrillar A $\beta$  might be due to insufficient lysosomal acidification reported in microglia (Majumdar *et al.*, 2007). Therefore, it seems likely that microglia get recruited to fibrillar plaque cores and their early-MARPs program is switched on, which induces the phagocytic and immune machinery to clear the insult. However, accumulation of undigestible fibrillar material within the lysosomes could saturate these organelles for further phagocytosis and clearance. Moreover, pro-inflammatory factors derived from microglial activation such as early-MARP IFN signaling or LGALS3 might contribute to dampen phagocytosis (Koenigsnecht-Talboo & Landreth, 2005; Moore *et al.*, 2020). In APPPS1, as A $\beta$  is overproduced and rapidly aggregated due to high levels of A $\beta$ 42 (Radde *et al.*, 2006), microglial lysosomes may get quickly saturated with fibrillar A $\beta$ , already at an early disease stage, leading to phagocytic dysfunction. This is consistent with the lack of change in plaque load observed in APPPS1 mice upon microglia depletion at early AD pathology (Grathwohl *et al.*, 2009). Along these lines, the delay in phagocytic impairment observed in APP-KI microglia could be due to the lower amounts of fibrillar A $\beta$  initially present in this mouse model, which triggered less microglial activation, recruitment and phagocytic uptake. However, even though the acquisition of early-MARPs correlates with microglial phagocytic impairment, we cannot claim that early MARPs are causal for deficient microglial clearance. As early MARPs include the upregulation of many lysosomal proteins, this signature might also represent the unsuccessful attempt of microglia to clear A $\beta$ . Further research using functional assays with physiological microglial substrates such as A $\beta$ , myelin or synapses is required to shed light into the specific signaling pathways that promote microglial phagocytic clearance and the ones that reflect an impairment in microglial function that contributes to AD. The time-resolved proteome dataset generated in this study is a valuable resource for the identification pathways that are causal for microglial dysfunction and when manipulated can contribute to microglial functional repair.

#### 4. The challenge of microglial immunomodulation in AD

Microglial modulation is considered a promising therapeutic option for restoring microglial function in AD. However, it also represents a challenge due to the difficulty to fine tune microglial activation to achieve A $\beta$  clearance without causing neuronal damage (Anwar & Rivest, 2020). Different approaches have been used to modulate microglia in AD, from passive and active immunization therapies (Schenk *et al.*, 1999; Bard *et al.*, 2000; Bacskai *et al.*, 2002; Wilcock *et al.*, 2004), to anti-inflammatory (Koenigsknecht-Talboo & Landreth, 2005; Zelcer *et al.*, 2007; Shie *et al.*, 2009; Park *et al.*, 2019), pro-inflammatory (Shaftel *et al.*, 2007; Boissonneault *et al.*, 2009; Chakrabarty *et al.*, 2010; Rivera-Escalera *et al.*, 2019) and agonistic (Cheng *et al.*, 2018; Schlepckow *et al.*, 2020) strategies. Despite the success of some of these studies in modulating microglial function and reducing plaque load, we still lack the signatures of repaired microglia at the molecular level. This information will be tremendously useful to understand the molecular mechanisms behind improved microglial function in AD and will help to design more effective therapies to tackle AD or to monitor treatment efficacy.

The hematopoietic growth factor GM-CSF, was proven effective in inducing A $\beta$  plaque clearance and ameliorating cognitive decline in an AD mouse model (Boyd *et al.*, 2010) and had a potent effect on reducing A $\beta$  plaque burden in organotypic brain slices from old APPPS1 mice, which was associated to an increase in microglial proliferation (Daria *et al.*, 2017). In the present study, I confirmed amyloid plaque clearance property of GM-CSF in APP-KI mice *ex vivo*. However, following the same experimental paradigm used by Boyd and colleagues (2010), I was not able to recapitulate the plaque reduction effect *in vivo*, even when a longer treatment paradigm was performed. Compared to their study, which used 12-month-old mice that overexpress the human APP Swedish mutation (Boyd *et al.*, 2010), I used 4-, 5- and 14-month-old APP-KI mice, that express the human Swedish, Iberian and Arctic APP mutations under the endogenous *App* mouse promoter. Therefore, differences in mouse models pathology (overexpression *versus* physiological APP expression) could contribute to the different outcomes of the treatment. In line with my results, no reduction in A $\beta$  plaque load upon GM-CSF treatment was reported by Kiyota and colleagues, who also used a different mouse model presenting the APP-Swedish and PS1 mutations (Kiyota *et al.*, 2018). In this case, they only observed a reduction of oligomeric A $\beta$  species in the brain parenchyma and an increase in A $\beta$ 40 drainage to the blood circulation, which was also accompanied by an improvement in cognitive function (Kiyota *et al.*, 2018). Drug reachability to the target cells in sufficient concentration might have been a limiting factor in our study. GM-CSF was reported to cross the BBB when injected into the jugular vein (McLay *et al.*,

1997). However, GM-CSF injected subcutaneously or intraperitoneally may be less successfully delivered to the brain. Of note, the distribution and elimination half-life of injected GM-CSF in serum were reported to be 0.9 min and 12 min in average, respectively, representing a pretty short-term availability of these molecules to reach the target (Daro *et al.*, 2000). Moreover, as hematopoietic factor GM-CSF can also find its targets in the bloodstream, such as monocytes or granulocytes (Ruef & Coleman, 1990), which may also decrease its availability to reach the brain in sufficient amounts. However, activation of the peripheral immune system by GM-CSF could also contribute to reduce amyloid pathology, as reported by Kiyota and colleagues (Kiyota *et al.*, 2018). Thus, possible variations in drug administration that could affect protein availability and reachability, summed onto differences in mice amyloid pathology and age, might be behind the lack of GM-CSF effect on plaque clearance in my study.

Proteomic analysis of microglia from GM-CSF-injected mice only showed mild changes that were mainly age and treatment-dependent. Microglial proteomic analysis from 4-month-old APP-KI mice that received the long GM-CSF treatment showed very few significant changes, that mainly involved the increase of proteins implicated in the endo-lysosomal system. As no changes in amyloid clearance were observed, it is possible that weekly injections were not enough to trigger a sustained response in microglia, or a higher dose was necessary for a proper stimulation. Interestingly, microglial proteome from 5-month-old mice treated for 1 week showed an increase in ADNP. This protein seems to be implicated in neuronal survival and was reported to be upregulated in response to injury (Gozes *et al.*, 2005). In fact, several studies have reported a neuroprotective effect of GM-CSF in different disease conditions such as brain or spinal cord trauma (Ha *et al.*, 2005; Shultz *et al.*, 2014; Kelso *et al.*, 2015), Parkinson's disease (Kim *et al.*, 2009b) and AD (Boyd *et al.*, 2010; Kiyota *et al.*, 2018). This effect of GM-CSF is not surprising as neurons also present GM-CSFR $\alpha$  and has been shown to act as a neurotrophic factor and play an important role for neuronal plasticity and memory (Schabitz *et al.*, 2008; Krieger *et al.*, 2012). Therefore, GM-CSF-induced neuroprotective effect should be examined in further detail. Moreover, I detected an increase in proteins involved in actin cytoskeleton and cell cycle in 5-month-old treated mice, indicating a role of GM-CSF in promoting microglial proliferation. However, BrdU quantification analysis did not support this finding. Finally, GM-CSF treatment of 14-month-old mice induced the upregulation of different histone and DNA-associated proteins in microglial proteome but also, as seen for the 5-month-old treated mice, of proteins involved in cell cycle and actin cytoskeleton. This finding is very intriguing, as I detected a prominent reduction of those histone proteins among middle- and advanced-MARPs and cell cycle mechanisms were also

downregulated at advanced disease stage. This might indicate that GM-CSF is inducing survival and rejuvenating mechanisms in microglia that are however, not sufficient to translate into reduced A $\beta$  load (Lee *et al.*, 1994; Daria *et al.*, 2017). The differences in microglial proteomic changes observed in every experimental condition, might be explained by the pleiotropic functions ascribed to GM-CSF depending to the pathophysiological state of the target cells, including age, activation state and surrounding environmental conditions (Zhan *et al.*, 2019).

Overall, GM-CSF did not demonstrate efficacy in repairing microglial phagocytic function and reducing A $\beta$  load *in vivo*. Thus, more robust approaches are needed to discover the molecular fingerprints of repaired microglia. As GM-CSF neuroprotective effect seems to be a common denominator in different disease settings, a combinatorial treatment of GM-CSF with other immunomodulatory approaches such as anti-A $\beta$  therapies, might hold promise for targeting the two main pathological insults in AD, amyloid plaques and neurodegeneration.

## 5. Conclusions

In this study I revealed a panel of MARP signatures that reflect microglial response to A $\beta$  at different pathological stages along disease progression. Interestingly, I found that fibrillar A $\beta$  from the plaque core seems to be responsible for triggering microglial proteomic changes that underscore their activation and recruitment to amyloid plaques but also, their phagocytic dysfunction. Time-resolved MARP signatures represent a valuable resource of protein changes for the identification of novel targets for microglial repair in AD.

Treatment with GM-CSF *in vivo* was not sufficient to trigger microglial functional and molecular repair. Therefore, further efforts are necessary to elucidate the mechanisms of microglial immunomodulation and repair *in vivo*. The here identified microglial proteomic signatures, provide the basis to design and monitor microglial immunomodulatory and repair strategies, and will facilitate the discovery of microglial repair signatures.

## Appendix

### 1. Microglial proteomic analysis from GM-CSF-treated APP-KI mice (raw data)

Gene name	Protein Accessions	Protein Description	Ratio (GMCSF /CTRL)	log2 (GMCSF /CTRL)	-log10 p	p-value
Xdh	Q00519	Xanthine	4.86	2.28	2.39	4.06E-03
Tbce	Q8CIV8	Tubulin-specific chaperone E	2.60	1.38	2.56	2.76E-03
Smox	Q99K82	Spermine oxidase	2.45	1.29	1.42	3.83E-02
Adnp	Q9Z103	Activity-dependent neuroprotector homeobox protein	2.09	1.07	2.07	8.48E-03
Chn1	Q91V57	N-chimaerin	1.89	0.92	2.92	1.21E-03
Acot2	Q9QYR9	Acyl-coenzyme A thioesterase 2, mitochondrial	1.86	0.90	1.92	1.21E-02
Eny2	Q9JIX0	Transcription and mRNA export factor ENY2	1.84	0.88	1.35	4.50E-02
Pcyt1a	P49586	Choline-phosphate cytidyltransferase A	1.82	0.87	1.41	3.85E-02
Pigb	Q9JJQ0	GPI mannosyltransferase 3	1.81	0.86	1.46	3.50E-02
Jpt1	P97825	Jupiter microtubule associated homolog 1	1.77	0.82	2.09	8.17E-03
Ezr	P26040	Ezrin	1.74	0.80	1.31	4.84E-02
S100a4	P07091	Protein S100-A4	1.72	0.78	2.28	5.28E-03
Calml3	Q9D6P8	Calmodulin-like protein 3	1.70	0.76	1.86	1.40E-02
Dpcd	Q8BPA8	Protein DPCD	1.69	0.76	2.92	1.19E-03
Trex1	Q91XB0	Three-prime repair exonuclease 1	1.69	0.76	1.67	2.13E-02
Trmt10c	Q3UFY8	tRNA methyltransferase 10 homolog C	1.64	0.72	2.03	9.25E-03
Srsf10	Q9R0U0	Serine/arginine-rich splicing factor 10	1.61	0.69	1.96	1.11E-02
Dnmt3a	O88508	DNA (cytosine-5)-methyltransferase 3A	1.59	0.67	1.44	3.63E-02
Mrpl55	Q9CZ83	39S ribosomal protein L55, mitochondrial	1.56	0.65	3.25	5.57E-04
Pts	Q9R1Z7	6-pyruvoyl tetrahydrobiopterin synthase	1.56	0.64	2.80	1.59E-03
Pnn	O35691	Pinin	1.55	0.64	1.54	2.87E-02
Lig3	P97386	DNA ligase 3	1.53	0.62	1.47	3.37E-02
Mocs3	A2BDX3	Adenylyltransferase and sulfurtransferase MOCS3	1.53	0.62	2.50	3.19E-03
Stim2	P83093	Stromal interaction molecule 2	1.52	0.60	2.59	2.58E-03
Ppif	Q99KR7	Peptidyl-prolyl cis-trans isomerase F, mitochondrial	1.51	0.60	1.58	2.62E-02
Ugt8	Q64676	2-hydroxyacylsphingosine 1-beta-galactosyltransferase	1.48	0.56	1.53	2.97E-02

Appendix

Fip1l1	Q9D824	Pre-mRNA 3'-end-processing factor FIP1	1.47	0.56	1.59	2.56E-02
Gipc2	Q9Z2H7	PDZ domain-containing protein GIPC2	1.47	0.55	1.44	3.61E-02
Supt4h1a ;Supt4h1b	P63271;Q9Z199	Transcription elongation factor SPT4-A;Transcription elongation factor SPT4-B	1.46	0.54	1.53	2.93E-02
Srsf9	Q9D0B0	Serine/arginine-rich splicing factor 9	1.46	0.54	2.42	3.78E-03
Ralgps2	Q9ERD6	Ras-specific guanine nucleotide-releasing factor RalGPS2	1.45	0.54	2.73	1.85E-03
Akr1c13	Q8VC28	Aldo-keto reductase family 1 member C13	1.45	0.53	1.54	2.91E-02
Pctp	P53808	Phosphatidylcholine transfer protein	1.43	0.52	1.59	2.55E-02
Mrpl50	Q8VDT9	39S ribosomal protein L50, mitochondrial	1.43	0.51	1.71	1.94E-02
Dab2	P98078	Disabled homolog 2	1.42	0.51	1.33	4.73E-02
Zbtb8os	Q505B7	Protein archease	1.42	0.51	1.48	3.28E-02
Hnrnpc	Q9Z204	Heterogeneous nuclear ribonucleoproteins C1/C2	1.41	0.50	2.40	4.01E-03
Slc1a3	P56564	Excitatory amino acid transporter 1	0.71	-0.50	2.56	2.73E-03
Cox7a2l	Q61387	Cytochrome c oxidase subunit 7A-related protein, mitochondrial	0.71	-0.50	1.36	4.32E-02
Ttyh1	Q9D3A9	Protein tweety homolog 1	0.71	-0.50	1.38	4.16E-02
Mbp	P04370	Myelin basic protein	0.71	-0.50	1.33	4.66E-02
Cnp	P16330	2',3'-cyclic-nucleotide 3'-phosphodiesterase	0.71	-0.50	1.70	2.01E-02
Speg	Q62407	Striated muscle-specific serine/threonine-protein kinase	0.70	-0.52	1.58	2.64E-02
Elov1l	Q9JLJ5	Elongation of very long chain fatty acids protein 1	0.70	-0.52	1.37	4.28E-02
Mrpl10	Q3TBW2	39S ribosomal protein L10, mitochondrial	0.70	-0.52	1.49	3.26E-02
Flcn	Q8QZS3	Folliculin	0.69	-0.53	1.35	4.51E-02
Lnpk	Q7TQ95	Endoplasmic reticulum junction formation protein lunapark	0.69	-0.53	1.84	1.43E-02
Adk	P55264	Adenosine kinase	0.69	-0.53	1.97	1.07E-02
Syn1	O88935	Synapsin-1	0.69	-0.53	1.85	1.40E-02
Pex3	Q9QXY9	Peroxisomal biogenesis factor 3	0.69	-0.54	1.52	3.01E-02
Vamp5	Q9Z2P8	Vesicle-associated membrane protein 5	0.69	-0.54	2.28	5.21E-03
Sv2b	Q8BG39	Synaptic vesicle glycoprotein 2B	0.69	-0.54	3.00	9.94E-04

Tomm5	B1AXP6	Mitochondrial import receptor subunit TOM5 homolog	0.68	-0.55	1.58	2.64E-02
Crym	O54983	Ketimine reductase mu-crystallin	0.68	-0.55	2.00	1.00E-02
Aplp2	Q06335	Amyloid-like protein 2	0.68	-0.55	1.65	2.24E-02
Apoh	Q01339	Beta-2-glycoprotein 1	0.68	-0.55	1.33	4.65E-02
Cd200	O54901	OX-2 membrane glycoprotein	0.68	-0.56	1.41	3.92E-02
Stxbp1	O08599	Syntaxin-binding protein 1	0.67	-0.57	2.55	2.82E-03
Fam162a	Q9D6U8	Protein FAM162A	0.67	-0.58	1.54	2.85E-02
Atp1a3	Q6PIC6	Sodium/potassium-transporting ATPase subunit alpha-3	0.67	-0.59	2.34	4.56E-03
Slc25a22	Q9D6M3	Mitochondrial glutamate carrier 1	0.66	-0.59	2.36	4.33E-03
Cyfp2	Q5SQX6	Cytoplasmic FMR1-interacting protein 2	0.66	-0.60	1.46	3.47E-02
Rab5b	P61021	Ras-related protein Rab-5B	0.66	-0.61	1.66	2.21E-02
Slc2a3	P32037	Solute carrier family 2, facilitated glucose transporter member 3	0.66	-0.61	4.07	8.53E-05
Surf2	P09926	Surfeit locus protein 2	0.65	-0.62	1.56	2.78E-02
Ca2	P00920	Carbonic anhydrase 2	0.65	-0.62	2.25	5.67E-03
Slc6a1	P31648	Sodium- and chloride-dependent GABA transporter 1	0.65	-0.63	2.56	2.74E-03
Gnao1	P18872	Guanine nucleotide-binding protein G(o) subunit alpha	0.64	-0.63	1.90	1.26E-02
Atp1a2	Q6PIE5	Sodium/potassium-transporting ATPase subunit alpha-2	0.64	-0.64	5.19	6.41E-06
Gad2	P48320	Glutamate decarboxylase 2	0.64	-0.64	2.31	4.93E-03
Rars2	Q3U186	Probable arginine--tRNA ligase, mitochondrial	0.64	-0.64	1.35	4.52E-02
Kpna1	Q60960	Importin subunit alpha-5	0.64	-0.64	1.91	1.24E-02
Rabggta	Q9JHK4	Geranylgeranyl transferase type-2 subunit alpha	0.64	-0.65	4.38	4.13E-05
Rab3a	P63011	Ras-related protein Rab-3A	0.64	-0.65	2.37	4.28E-03
Slc6a11	P31650	Sodium- and chloride-dependent GABA transporter 3	0.63	-0.66	3.58	2.65E-04
Arf5	P84084	ADP-ribosylation factor 5	0.63	-0.67	2.16	6.91E-03
Slc4a4	O88343	Electrogenic sodium bicarbonate cotransporter 1	0.63	-0.68	2.85	1.40E-03
Jagn1	Q5XKN4	Protein jagunal homolog 1	0.63	-0.68	1.51	3.08E-02
Tomm20	Q9DCC8	Mitochondrial import receptor subunit TOM20 homolog	0.62	-0.68	1.33	4.65E-02
Eef1a2	P62631	Elongation factor 1-alpha 2	0.62	-0.68	2.17	6.80E-03
Poll	Q9QXE2	DNA polymerase lambda	0.62	-0.69	1.40	3.94E-02
Calb1	P12658	Calbindin	0.62	-0.69	2.14	7.18E-03

Appendix

Plp1	P60202	Myelin proteolipid protein	0.62	-0.70	1.95	1.13E-02
Shc1	P98083	SHC-transforming protein 1	0.61	-0.70	1.77	1.69E-02
Stx1b	P61264	Syntaxin-1B	0.61	-0.70	4.27	5.35E-05
Gnpat	P98192	Dihydroxyacetone phosphate acyltransferase	0.61	-0.71	2.84	1.45E-03
Thy-1	P01831	Thy-1 membrane glycoprotein	0.61	-0.71	2.15	7.13E-03
Tmbim6	Q9D2C7	Bax inhibitor 1	0.61	-0.72	1.79	1.61E-02
Crmp1	P97427	Dihydropyrimidinase-related protein 1	0.61	-0.72	3.57	2.67E-04
H2afy	Q9QZQ8	Core histone macro-H2A.1	0.61	-0.72	2.01	9.80E-03
Usp11	Q99K46	Ubiquitin carboxyl-terminal hydrolase 11	0.60	-0.73	1.63	2.36E-02
Nrgn	P60761	Neurogranin	0.60	-0.73	2.69	2.04E-03
Hist1h2bm;Hist1h2bh;Hist2h2bb;Hist1h2bc	P10854	Histone H2B type 1-M;Histone H2B type 1-H;Histone H2B type 2-B;Histone H2B type 1-C/E/G	0.60	-0.73	2.08	8.23E-03
Fcgr1g	P20491	High affinity immunoglobulin epsilon receptor subunit gamma	0.60	-0.73	5.33	4.71E-06
Map6	Q7TSJ2	Microtubule-associated protein 6	0.59	-0.75	1.43	3.69E-02
Sec61b	Q9CQS8	Protein transport protein Sec61 subunit beta	0.59	-0.76	1.96	1.10E-02
Ppfbp2	O35711	Liprin-beta-2	0.59	-0.77	1.41	3.92E-02
	Q922R1	UPF0183 protein C16orf70 homolog	0.58	-0.78	1.89	1.29E-02
Mapkapk3	Q3UMW7	MAP kinase-activated protein kinase 3	0.58	-0.78	1.42	3.79E-02
Them4	Q3UUI3	Acyl-coenzyme A thioesterase THEM4	0.58	-0.80	2.76	1.73E-03
Cadm1	Q8R5M8	Cell adhesion molecule 1	0.57	-0.81	1.39	4.10E-02
Mtco1	P00397	Cytochrome c oxidase subunit 1	0.57	-0.81	1.30	4.97E-02
Abcf1	Q6P542	ATP-binding cassette sub-family F member 1	0.57	-0.81	1.47	3.35E-02
Abcg1	Q64343	ATP-binding cassette sub-family G member 1	0.57	-0.81	1.37	4.24E-02
	Q3UE31	Uncharacterized protein KIAA0930 homolog	0.57	-0.82	1.86	1.39E-02
Syn2	Q64332	Synapsin-2	0.57	-0.82	1.59	2.58E-02
At1l	Q8BH66	Atlastin-1	0.56	-0.84	2.08	8.34E-03
Plxdc1	Q91ZV7	Plexin domain-containing protein 1	0.56	-0.85	2.65	2.26E-03
Atp1b2	P14231	Sodium/potassium-transporting ATPase subunit beta-2	0.55	-0.85	2.53	2.93E-03
Dnajc28	Q8VCE1	DnaJ homolog subfamily C member 28	0.55	-0.87	1.96	1.09E-02
Stum	Q0VBF8	Protein stum homolog	0.53	-0.92	2.36	4.41E-03

Slc43a2	Q8CGA3	Large neutral amino acids transporter small subunit 4	0.53	-0.92	1.40	3.96E-02
Bri3bp	Q8BXV2	BRI3-binding protein	0.52	-0.93	1.70	2.01E-02
Vamp2	P63044	Vesicle-associated membrane protein 2	0.51	-0.97	2.19	6.53E-03
Cend1	Q9JKC6	Cell cycle exit and neuronal differentiation protein 1	0.50	-0.99	2.85	1.42E-03
Ca4	Q64444	Carbonic anhydrase 4	0.50	-1.01	1.96	1.11E-02
Ap4e1	Q80V94	AP-4 complex subunit epsilon-1	0.50	-1.01	1.73	1.86E-02
Plip	Q9DCU2	Plasmolipin	0.48	-1.05	2.55	2.83E-03
Pum3	Q8BKS9	Pumilio homolog 3	0.48	-1.06	1.86	1.38E-02
Dnajb4	Q9D832	Dnaj homolog subfamily B member 4	0.47	-1.08	2.23	5.90E-03
Mark3	Q03141	MAP/microtubule affinity-regulating kinase 3	0.47	-1.09	1.92	1.19E-02
Tmlhe	Q91ZE0	Trimethyllysine dioxygenase, mitochondrial	0.44	-1.20	1.59	2.59E-02
Fam20b	Q8VCS3	Glycosaminoglycan xylosylkinase	0.44	-1.20	1.41	3.86E-02
Lgi3	Q8K406	Leucine-rich repeat LGI family member 3	0.41	-1.29	1.37	4.29E-02
Atp13a2	Q9CTG6	Cation-transporting ATPase 13A2	0.39	-1.37	1.72	1.91E-02
Bsn	O88737	Protein bassoon	0.36	-1.49	2.08	8.37E-03
Mrps26	Q80ZS3	28S ribosomal protein S26, mitochondrial	0.35	-1.51	2.34	4.53E-03
Prpf18	Q8BM39	Pre-mRNA-splicing factor 18	0.24	-2.07	1.35	4.48E-02

**Table 29. Significantly regulated microglial proteins upon short-GM-CSF treatment in 5-month-old APP-KI mice.**

Only significantly regulated proteins ( $p < 0.05$ ) and a  $\log_2$  fold change (treatment *vs.* control) bigger than 0.5 (highlighted in red) or smaller than -0.5 (highlighted in blue) are shown.

Gene name	Protein Accessions	Protein Description	Ratio (GMCSF /CTRL)	$\log_2$ (GMCSF /CTRL)	$-\log_{10} p$	p-value
Hist1h4a	P62806	Histone H4	3.61	1.85	1.52	2.99E-02
Cdan1	Q8CC12	Codanin-1	2.72	1.44	1.36	4.40E-02
Gpcpd1	Q8C0L9	Glycerophosphocholine phosphodiesterase GPCPD1	2.61	1.39	2.85	1.43E-03
H3f3c;H3f3a	P02301;P84244	Histone H3.3C;Histone H3.3	2.47	1.30	1.32	4.74E-02
Rabl6	Q5U3K5	Rab-like protein 6	2.35	1.23	1.49	3.23E-02
Synpr	Q8BGN8	Synaptoporin	2.29	1.19	2.60	2.52E-03
Cacna1a	P97445	Voltage-dependent P/Q-type calcium channel subunit	2.12	1.08	3.41	3.89E-04
Fga	E9PV24	Fibrinogen alpha chain	2.02	1.01	3.02	9.57E-04

Appendix

Hist1h2bm;Hist1h2bh;Hist2h2bb;Hist1h2bc	P10854;Q64478;Q64525;Q6ZWY9	Histone H2B type 1-M;Histone H2B type 1-H;Histone H2B type 2-B;Histone H2B type 1-C/E/G	2.00	1.00	1.35	4.51E-02
Selplg	Q62170	P-selectin glycoprotein ligand 1	1.98	0.99	1.97	1.07E-02
Minos1	Q7TNS2	MICOS complex subunit Mic10	1.96	0.97	1.35	4.46E-02
Fbxo2	Q80UW2	F-box only protein 2	1.90	0.93	1.40	3.95E-02
H2afz;H2afv	P0C0S6;Q3THW5	Histone H2A.Z;Histone H2A.V	1.84	0.88	2.20	6.30E-03
Ptk2	P34152	Focal adhesion kinase 1	1.80	0.85	1.53	2.93E-02
Nudt13	Q8JZU0	Nucleoside diphosphate-linked moiety X motif 13	1.77	0.82	2.08	8.32E-03
Fam114a	Q9D281	Protein Noxp20	1.76	0.82	1.80	1.57E-02
Thns1	Q8BH55	Threonine synthase-like 1	1.75	0.81	2.43	3.71E-03
Sft2d2	Q8VD57	Vesicle transport protein SFT2B	1.73	0.79	2.05	8.96E-03
Ecsit	Q9QZH6	Evolutionarily conserved signaling intermediate in Toll	1.68	0.75	1.56	2.76E-02
Fgg	Q8VCM7	Fibrinogen gamma chain	1.65	0.72	2.67	2.14E-03
Kdelr1	Q99JH8	ER lumen protein-retaining receptor 1	1.65	0.72	1.46	3.48E-02
Romo1	P60603	Reactive oxygen species modulator 1	1.63	0.71	1.33	4.69E-02
Cd63	P41731	CD63 antigen	1.63	0.70	2.52	3.01E-03
Ap1p1	Q03157	Amyloid-like protein 1	1.62	0.70	1.33	4.69E-02
Gad1	P48318	Glutamate decarboxylase 1	1.59	0.67	2.14	7.25E-03
Arfgef3	Q3UGY8	Brefeldin A-inhibited guanine nucleotide-exchange protein	1.59	0.67	1.75	1.77E-02
Cdk17	Q8K0D0	Cyclin-dependent kinase 17	1.59	0.67	3.12	7.56E-04
Nucks1	Q80XU3	Nuclear ubiquitous casein and cyclin-dependent kinase substrate 1	1.59	0.66	2.03	9.30E-03
Pxmp2	P42925	Peroxisomal membrane protein 2	1.58	0.66	1.46	3.48E-02
Ernm	Q5EBJ4	Ermin	1.57	0.65	1.67	2.14E-02
H2afy	Q9QZQ8	Core histone macro-H2A.1	1.57	0.65	1.39	4.08E-02
Minpp1	Q9Z2L6	Multiple inositol polyphosphate phosphatase 1	1.55	0.63	1.33	4.69E-02
Nup85	Q8R480	Nuclear pore complex protein Nup85	1.55	0.63	1.61	2.45E-02
Tbc1d1	Q60949	TBC1 domain family member 1	1.54	0.63	1.68	2.08E-02
Akr1b7	P21300	Aldose reductase-related protein 1	1.53	0.62	1.71	1.97E-02
Carmil1	Q6EDY6	F-actin-uncapping protein LRRC16A	1.53	0.61	2.77	1.71E-03
	Q8BGX2	Uncharacterized protein C19orf52 homolog	1.52	0.60	1.34	4.61E-02

Mrpl18	Q9CQL5	39S ribosomal protein L18, mitochondrial	1.51	0.60	1.95	1.12E-02
Pqlc3	Q8C6U2	PQ-loop repeat-containing protein 3	1.50	0.59	2.23	5.85E-03
Rbm5	Q91YE7	RNA-binding protein 5	1.49	0.58	2.34	4.61E-03
Sf3a2	Q62203	Splicing factor 3A subunit 2	1.48	0.57	1.34	4.56E-02
Atp1b2	P14231	Sodium/potassium-transporting ATPase subunit	1.48	0.57	1.70	1.98E-02
Utp14a	Q640M1	U3 small nucleolar RNA-associated protein 14	1.48	0.57	1.57	2.68E-02
Sap18	O55128	Histone deacetylase complex subunit SAP18	1.48	0.56	2.56	2.74E-03
Fam134b	Q8VE91	Reticulophagy receptor Fam134b	1.48	0.56	2.49	3.22E-03
Mpp2	Q9WV34	MAGUK p55 subfamily member 2	1.47	0.56	1.81	1.56E-02
Ltn1	Q6A009	E3 ubiquitin-protein ligase listerin	1.47	0.56	1.62	2.40E-02
Cplx2	P84086	Complexin-2	1.47	0.55	2.28	5.21E-03
Eef1b	O70251	Elongation factor 1-beta	1.46	0.55	3.56	2.76E-04
Sv2c	Q69ZS6	Synaptic vesicle glycoprotein 2C	1.46	0.55	1.36	4.32E-02
Gabra1	P62812	Gamma-aminobutyric acid receptor subunit alpha-1	1.45	0.54	1.87	1.34E-02
S100a11	P50543	Protein S100-A11	1.45	0.54	1.59	2.55E-02
Aph1a	Q8BVF7	Gamma-secretase subunit APH-1A	1.45	0.54	2.32	4.81E-03
Srpk2	O54781	SRSF protein kinase 2	1.45	0.54	2.25	5.67E-03
Pnkd	Q69ZP3	Probable hydrolase PNKD	1.45	0.54	2.46	3.48E-03
Plp1	P60202	Myelin proteolipid protein	1.44	0.53	2.21	6.21E-03
Txlng	Q8BHN1	Gamma-taxilin	1.44	0.53	1.32	4.84E-02
Slc17a7	Q3TXX4	Vesicular glutamate transporter 1	1.44	0.53	2.07	8.46E-03
Dnmt3a	O88508	DNA (cytosine-5)-methyltransferase 3A	1.44	0.53	2.05	8.84E-03
Stk25	Q9Z2W1	Serine/threonine-protein kinase 25	1.44	0.53	1.87	1.34E-02
Cyth2	P63034	Cytohesin-2	1.43	0.52	1.62	2.40E-02
Cox15	Q8BJ03	Cytochrome c oxidase assembly protein COX15	1.43	0.52	1.76	1.74E-02
Dpgt1	P42867	UDP-N-acetylglucosamine--dolichyl-phosphate N-	1.43	0.52	1.83	1.47E-02
Ifitm3	Q9CQW9	Interferon-induced transmembrane protein 3	1.43	0.52	1.99	1.02E-02
Scai	Q8C8N2	Protein SCAI	1.43	0.52	3.31	4.93E-04
Slc14a1	Q8VHL0	Urea transporter 1	1.43	0.51	1.49	3.21E-02
Pnpla8	Q8K1N1	Calcium-independent phospholipase A2-gamma	1.42	0.51	2.62	2.41E-03
Wapl	Q65Z40	Wings apart-like protein homolog	1.42	0.51	1.90	1.26E-02
Mlc1	Q8VHK5	Membrane protein MLC1	1.42	0.51	1.34	4.56E-02

Appendix

Cldn5	O54942	Claudin-5	1.42	0.51	1.50	3.15E-02
Nell2	Q61220	Protein kinase C-binding protein NELL2	1.42	0.50	1.53	2.98E-02
Scn1b	P97952	Sodium channel subunit beta-1	1.42	0.50	1.48	3.33E-02
Epb4111	Q9Z2H5	Band 4.1-like protein 1	1.42	0.50	2.86	1.38E-03
Rtn1	Q8K0T0	Reticulon-1	1.42	0.50	1.91	1.23E-02
Hkdc1	Q91W97	Putative hexokinase HKDC1	1.42	0.50	1.45	3.56E-02
Fut8	Q9WTS2	Alpha-(1,6)-fucosyltransferase	1.42	0.50	2.70	2.00E-03
Srfbp1	Q9CZ91	Serum response factor-binding protein 1	0.71	-0.50	1.54	2.86E-02
Prorsd1	Q9D820	Prolyl-tRNA synthetase associated domain-containing	0.70	-0.51	1.78	1.67E-02
Rpl7l1	Q9D8M4	60S ribosomal protein L7-like 1	0.70	-0.51	1.81	1.57E-02
Nfs1	Q9Z1J3	Cysteine desulfurase, mitochondrial	0.70	-0.51	1.52	3.00E-02
Nosip	Q9D6T0	Nitric oxide synthase-interacting protein	0.70	-0.51	1.36	4.41E-02
Btd	Q8CIF4	Biotinidase	0.70	-0.52	2.63	2.32E-03
Znf830	Q8R1N0	Zinc finger protein 830	0.69	-0.53	1.79	1.61E-02
Rps29	P62274	40S ribosomal protein S29	0.69	-0.53	1.48	3.32E-02
Snrpd2	P62317	Small nuclear ribonucleoprotein Sm D2	0.69	-0.54	4.69	2.06E-05
Pdlim4	P70271	PDZ and LIM domain protein 4	0.68	-0.55	2.50	3.19E-03
Fam3a	Q9D8T0	Protein FAM3A	0.68	-0.55	3.02	9.57E-04
Mrpl14	Q9D1I6	39S ribosomal protein L14, mitochondrial	0.68	-0.55	1.44	3.63E-02
Lonp2	Q9DBN5	Lon protease homolog 2, peroxisomal	0.68	-0.56	1.68	2.10E-02
	Q3UJP5	Protein C8orf37 homolog	0.67	-0.58	1.74	1.81E-02
Trmt6	Q8CE96	tRNA (adenine(58)-N(1))-methyltransferase non-catalytic subunit TRM6	0.67	-0.59	1.43	3.69E-02
Xrcc1	Q60596	DNA repair protein XRCC1	0.67	-0.59	2.47	3.39E-03
Pfdn6	Q03958	Prefoldin subunit 6	0.66	-0.59	1.89	1.28E-02
	Q3UTZ3	Uncharacterized protein C7orf43 homolog	0.66	-0.59	1.85	1.40E-02
Ift22	Q9DAI2	Intraflagellar transport protein 22 homolog	0.66	-0.60	1.62	2.42E-02
Fbf1	A2A870	Fas-binding factor 1	0.66	-0.61	1.54	2.86E-02
Poll	Q9QXE2	DNA polymerase lambda	0.65	-0.61	2.04	9.11E-03
Srsf10	Q9R0U0	Serine/arginine-rich splicing factor 10	0.65	-0.62	1.34	4.58E-02
Suox	Q8R086	Sulfite oxidase, mitochondrial	0.65	-0.63	2.20	6.32E-03
Nubp1	Q9R060	Cytosolic Fe-S cluster assembly factor NUBP1	0.64	-0.64	2.42	3.78E-03
Exosc1	Q9DAA6	Exosome complex component CSL4	0.64	-0.64	2.08	8.35E-03

Taf8	Q9EQH4	Transcription initiation factor TFIID subunit 8	0.64	-0.65	1.94	1.15E-02
Slc25a15	Q9WVD5	Mitochondrial ornithine transporter 1	0.64	-0.65	1.34	4.54E-02
Wasf1	Q8R5H6	Wiskott-Aldrich syndrome protein family member 1	0.64	-0.65	2.68	2.09E-03
P33monox	Q9DBN4	Putative monooxygenase p33MONOX	0.64	-0.65	1.53	2.95E-02
Sephs2	P97364	Selenide, water dikinase 2	0.63	-0.66	1.88	1.32E-02
Churc1	Q6DG52	Protein Churchill	0.62	-0.70	1.65	2.23E-02
Rpl36a	P83882	60S ribosomal protein L36a	0.57	-0.81	1.61	2.43E-02
Eml5	Q8BQM8	Echinoderm microtubule-associated protein-like 5	0.56	-0.83	1.87	1.36E-02
Ubn1	Q4G0F8	Ubinuclein-1	0.56	-0.84	2.22	6.03E-03
Hdhd3	Q9CYW4	Haloacid dehalogenase-like hydrolase domain-containing	0.55	-0.87	1.64	2.28E-02
Znf787	Q8BIF9	Zinc finger protein 787	0.55	-0.87	2.28	5.28E-03
Pex3	Q9QXY9	Peroxisomal biogenesis factor 3	0.55	-0.87	1.79	1.61E-02
Ftl1	P29391	Ferritin light chain 1	0.54	-0.89	1.61	2.44E-02
Cwf1911	Q8CI33	CWF19-like protein 1	0.52	-0.94	2.84	1.45E-03
Plxdc1	Q91ZV7	Plexin domain-containing protein 1	0.51	-0.96	1.66	2.18E-02
Wdr13	Q91V09	WD repeat-containing protein 13	0.51	-0.97	2.99	1.03E-03
Znf22	Q9ERU3	Zinc finger protein 22	0.51	-0.98	2.48	3.35E-03
Atp5o	Q9DB20	ATP synthase subunit O, mitochondrial	0.50	-1.00	1.67	2.16E-02
Psmf1	Q8BHL8	Proteasome inhibitor PI31 subunit	0.49	-1.04	1.60	2.51E-02
Rps23	P62267	40S ribosomal protein S23	0.48	-1.05	1.60	2.50E-02
Bpgm	P15327	Bisphosphoglycerate mutase	0.42	-1.27	1.56	2.77E-02
Acaca	Q5SWU9	Acetyl-CoA carboxylase 1	0.36	-1.46	2.09	8.15E-03
Cfap20	Q8BTU1	Cilia- and flagella-associated protein 20	0.35	-1.53	2.72	1.92E-03
Hbb-b1	P02088	Hemoglobin subunit beta-1	0.33	-1.62	1.38	4.18E-02
Hba	P01942	Hemoglobin subunit alpha	0.27	-1.89	1.62	2.39E-02

**Table 30. Significantly regulated microglial proteins upon short-GM-CSF treatment in 14-month-old APP-K1 mice.**

Only significantly regulated proteins ( $p < 0.05$ ) and a  $\log_2$  fold change (treatment *vs.* control) bigger than 0.5 (highlighted in red) or smaller than -0.5 (highlighted in blue) are shown.

Gene name	Protein Accessions	Protein Description	Ratio (GMCSF /CTRL)	$\log_2$ (GMCSF /CTRL)	$-\log_{10} p$	p-value
Man1b1	A2AJ15	Endoplasmic reticulum mannosyl-oligosaccharide 1,2-alpha-mannosidase	5.95	2.57	1.42	3.80E-02
Hbs1l	Q69ZS7	HBS1-like protein	3.55	1.83	1.30	4.97E-02
Arl5a	Q80ZU0	ADP-ribosylation factor-like protein 5A	2.73	1.45	1.89	1.28E-02

Appendix

Rfc3	Q8R323	Replication factor C subunit 3	2.47	1.30	1.66	2.17E-02
Arhgef10 l	A2AWP8	Rho guanine nucleotide exchange factor 10-like	2.43	1.28	1.31	4.88E-02
Ap4e1	Q80V94	AP-4 complex subunit epsilon-1	2.24	1.17	2.23	5.92E-03
Tfap2a	P34056	Transcription factor AP-2-alpha	2.18	1.12	1.57	2.72E-02
Serpinc1	P32261	Antithrombin-III	2.02	1.02	1.76	1.73E-02
Ppt2	O35448	Lysosomal thioesterase PPT2	1.87	0.90	1.33	4.68E-02
Abcc1	O35379	Multidrug resistance-associated protein 1	1.86	0.90	1.42	3.83E-02
Atg16l1	Q8C0J2	Autophagy-related protein 16-1	1.78	0.83	1.73	1.85E-02
Hdac6	Q9Z2V5	Histone deacetylase 6	1.73	0.79	1.62	2.42E-02
Gopc	Q8BH60	Golgi-associated PDZ and coiled-coil motif-containing	1.71	0.77	1.32	4.83E-02
Trove2	O08848	60 kDa SS-A/Ro ribonucleoprotein	1.65	0.72	2.08	8.32E-03
Eif4e2	Q8BMB3	Eukaryotic translation initiation factor 4E type 2	1.63	0.71	2.11	7.72E-03
Lace1	Q3V384	Lactation elevated protein 1	1.59	0.67	1.35	4.45E-02
Chmp2a	Q9DB34	Charged multivesicular body protein 2a	1.56	0.64	1.61	2.46E-02
Pnn	O35691	Pinin	1.55	0.63	1.33	4.71E-02
Phkg2	Q9DB30	Phosphorylase b kinase gamma catalytic chain,	1.52	0.61	1.62	2.39E-02
Psbm9	P28076	Proteasome subunit beta type-9	1.50	0.59	2.07	8.52E-03
Jup	Q02257	Junction plakoglobin	1.46	0.54	1.39	4.10E-02
Siglec5	Q920G3	Sialic acid-binding Ig-like lectin 5	1.45	0.54	1.31	4.95E-02
Bop1	P97452	Ribosome biogenesis protein BOP1	1.44	0.53	1.44	3.66E-02
Cox17	P56394	Cytochrome c oxidase copper chaperone	1.44	0.52	1.59	2.56E-02
Calhm2	Q8VEC4	Calcium homeostasis modulator protein 2	1.43	0.52	1.46	3.50E-02
Aspa	Q8R3P0	Aspartoacylase	0.68	-0.55	1.40	3.94E-02
Hscb	Q8K3A0	Iron-sulfur cluster co-chaperone protein HscB,	0.61	-0.70	1.51	3.13E-02
Zbp1	Q9QY24	Z-DNA-binding protein 1	0.61	-0.72	1.37	4.24E-02
Ltn1	Q6A009	E3 ubiquitin-protein ligase listerin	0.60	-0.73	1.81	1.56E-02
	Q8VE95	UPF0598 protein C8orf82 homolog	0.56	-0.84	1.54	2.86E-02
Eif4e3	Q9DBB5	Eukaryotic translation initiation factor 4E type 3	0.45	-1.14	1.44	3.62E-02

**Table 31. Significantly regulated microglial proteins upon long-GM-CSF treatment in 4-month-old APP-KI mice.**

Only significantly regulated proteins ( $p < 0.05$ ) and a  $\log_2$  fold change (treatment *vs.* control) bigger than 0.5 (highlighted in red) or smaller than -0.5 (highlighted in blue) are shown.

## 2. Step-by-step mouse microglia isolation protocol

In order to facilitate experimental reproducibility, a detailed protocol on mouse microglial isolation, which was a key method in this study, is described as follows:

➤ Solutions and instruments required for the preparation:

- HBSS buffer (supplemented with 7 mM HEPES)
- MACS Buffer: 0.5% BSA, 2 mM EDTA in PBS (1x)
- 4% BSA in H<sub>2</sub>O (for coating Pasteur pipettes)
- Microglia Media (pre-equilibrated in incubator at least 3hrs before plating): DMEM-F12 +10% FCS +1% Pen-Strep
- CD11b (microglia) magnetic Microbeads (Miltenyi)
- LS magnetic columns (Miltenyi)
- QuadroMACS separator
- 50 mL and 15mL tubes (centrifuge clear and normal)
- Cell strainer (40µm)
- Sterile Pasteur pipettes with cotton (3/animal)
- Sterile surgical instruments (Dumont #5, straight fine forceps)
- 6 cm dishes
- Water bath at 37°C
- Neural tissue dissociation kit-P (Miltenyi): Enzyme Mix 1 and Enzyme Mix 2 (freshly prepared before starting)
  - Enzyme Mix 1 (2 mL tube/sample): 50µl Enzyme P (-20°C) + 1900µL Buffer X (+4°C) --> mix and pre-warm in water bath until use (37°C, in order to activate Papain enzyme)
  - Enzyme Mix 2 (0.5 mL tube/sample): 20µl Buffer Y (+4°C) + 10µl Enzyme A (-20°C) -> mix and keep at RT until use)

➤ Procedure:

1. Fire-polish three glass Pasteur pipettes with decreasing tip diameters (first is wide open and the following two roughly half the diameter as the previous) and coat them with 4% BSA by pipetting up and down several times.
2. Prepare 2x 6cm dishes per sample (one to isolate the brain and clean it from meninges: 3mL HBSS, and the second: 5mL HBSS for the cleaned hemispheres)
3. Isolate the mouse brain and determine the weight (should not be more than 400mg per sample/isolation column later on)
4. Dissect out the cerebellum, brain stem and olfactory bulb and separate the two hemispheres. Clean the brain from meninges using the fine forceps, especially in the area ("pocket") where the midbrain covers the hippocampus and transfer the clean brain tissue (free from meninges) to the second clean dish. Cut the brain into small pieces using the forceps.

5. Transfer the pieces with a 10mL pipette into a clear 15ml tube (let the pieces precipitate and use the supernatant to wash and take the left pieces in the dish and add them to the tube). Let the pieces sink again or spin down briefly (300 x g)
6. Remove the supernatant with the 10mL pipette carefully.
7. Add 1950µL of preheated Enzyme Mix 1, mix gently by tap shaking, do not vortex!
8. Incubate for 15min at 37°C in the water bath, shake the tube from time to time
9. Add 30µL of Enzyme Mix2 to the sample and mix gently, do not vortex!
10. Dissociate tissue mechanically using the wide-tipped, fire-polished Pasteur pipette and pipetting up and down around 10 times, avoid making air bubbles.
11. Incubate at 37°C for 10min and shake the tube from time to time.
12. Dissociate tissue mechanically using again the wide-tipped pipette and then the other two fire-polished pipettes in decreasing diameter. Pipette slowly up and down 10 times with each pipette, or as long as tissue pieces are still observable, avoid formation of air bubbles
13. Incubate at 37°C for 10min and shake the tube from time to time.
14. Add 5mL of HBSS through a 40µm cell strainer, placed on a 50mL tube (for conditioning the cell strainer)
15. Add the cell suspension through the cell strainer
16. Wash the cell strainer with extra 5mL HBSS.
17. Discard cell strainer and centrifuge at 300 x g for 10min at RT. Remove supernatant completely with the 10mL pipette.
18. Resuspend cells in 10mL HBSS buffer and determine cell number (dilute 1:2 with Trypan Blue: 10uL Trypan Blue+ 10uL cell suspension)  
 Counting (cell counting using disposable chamber):  $X \text{ cell number from average of 4 big squares} \times 2 \text{ (Trypan Blue dilution)} \times 10.000 = X \text{ cells/mL} \times 10\text{mL} = X \text{ total cells before the isolation}$
19. [While cell counting]: Centrifuge cell suspension at 300 x g for 10min at RT. Aspirate supernatant completely (count the cells during the centrifugation)
20. When working with mouse cells, resuspend cell pellet in 90µl of MACS buffer per  $10^7$  total cells (always consider you have around  $5 \times 10^6$  cells more when calculating the buffer and beads volume)
21. When working with mouse cells, add 10µL of CD11b (Microglia) MicroBeads per  $10^7$  total cells (mix up-down with the 200uL pipette)
22. Mix well, do not vortex and incubate for 15 min at 4°C and mix (by tap-shaking) from time to time (every 5 min or so)
23. Wash cells by adding 3 mL of MACS buffer and centrifuge at 300 x g for 10min at RT. [During this time place the magnetic columns in the magnet and the 15mL normal tubes that will collect the flow-through under the columns in a rack]
24. Remove the supernatant completely using a 10mL pipette and resuspend cell pellet in 1mL MACS buffer
25. Condition the columns by adding 3mL of MACS buffer
26. Apply cell suspension onto the column (1 column per sample)

27. Perform washing steps by adding MACS buffer 3x 1mL (do not add the following 1mL until the first did not stop dropping out of the column)
28. After the last wash, quickly, remove column from the separator and place it on a fresh 15ml collection tube (clear tubes). Add 2.5 mL MACS buffer onto the column and flush out the cells by firmly pushing the plunger into the column (one sample at a time).
29. To enhance microglia isolation purity: Repeat the whole process one more time (from step 25) by applying the collected CD11b positive cell fraction from step 28 into a new column.
30. Determine cell number (dilute 1:2 with Trypan Blue)  
Counting (cell counting using disposable chamber):  $X$  cell number from average of 4 big squares  $\times 2$  (Trypan Blue dilution)  $\times 10.000 = X$  cells/mL  $\times 2.5$  mL =  $X$  total cells after the isolation
31. Centrifuge at 300 x g for 5 min at RT. and remove the supernatant carefully (with 1mL pipette).
32. For microglia culture: resuspend the cell pellet in microglia media and plate in desired format.
33. For mass spectrometry or biochemical analysis: it is necessary to remove as much BSA from the MACS buffer as possible: wash 2 times with HBSS (add 1mL and shortly resuspend, then centrifugate for 5 min, 300 x g). At the end remove as much HBSS as possible from the supernatant and snap freeze the pellet in liquid nitrogen and store at -80°C.

### 3. Self-programmed ImageJ macro for analysis of A $\beta$ load

This is an example of a self-programmed macro using ImageJ software for the quantification of total and fibrillar A $\beta$ . Comments about the macro functions are shown in green (after //). Every picture (raw data from the microscope) to be quantified is run through this macro and data is collected and analyzed afterwards. Automatic macros allow a non-bias analysis of the data.

```
n=getDirectory("Choose a Directory to save");
imageCount = nImages
for (image = 1; image <= imageCount; image++) {
    name=getTitle(); //print(imageName);
run("Z Project...", "projection=[Max Intensity]"); //Creates a maximum intensity projection from the z-
stack images
run("Split Channels"); //separates the 4 image channels
green = "C2-MAX_" + name;
blue = "C1-MAX_" + name;
red = "C3-MAX_" + name;
magenta = "C4-MAX_" + name;
selectWindow(red); //For fibrillar A $\beta$  quantification (Thiazine red staining)
run("8-bit");
run("Subtract Background...", "rolling=50"); //Removes staining background
run("Auto Threshold", "method=MaxEntropy white"); //Threshold filter used to identify the true
staining signal to be quantified based on the signal to noise ratio, several filters can be used and have
to be tested before using them in this macro
setOption("BlackBackground", true);
run("Convert to Mask");
run("Analyze Particles...", "size=2-Infinity show=Outlines display summarize"); //Quantifies the signal
"particles" excluding the ones that are smaller than 2  $\mu\text{m}^2$ 
saveAs("Results",n+name+"ThR"+" .csv"); //Saves this data in a file format that can be opened with excel
run("Clear Results");
maskcount= "Drawing of " + red;
saveAs("PNG", n+maskcount+ "ThR"+ ".png"); //Saves the picture of particles that were quantified to
be able to see if the real signal was quantified correctly

close();
close();
selectWindow(green); //For total A $\beta$  quantification (repeats the process for this quantification)
run("8-bit");
run("Subtract Background...", "rolling=50");
```

---

```
run("Auto Threshold", "method=Otsu white"); //Threshold filter used for detecting the signal from
total A $\beta$ 
setOption("BlackBackground", true);
run("Convert to Mask");
run("Analyze Particles...", "size=2-Infinity show=Outlines display summarize");
saveAs("Results", n+name+"abeta"+" .csv");
run("Clear Results");
maskcount= "Drawing of " + green;
saveAs("PNG", n+maskcount+"Abeta"+" .png");
selectWindow("Summary");
saveAs("Results", n+name + "Abtea-ThR"+"Summary.csv"); //Saves a summary of the data collected
from the fibrillar and total A $\beta$  quantifications including the sum of all particles (area covered by these
two types of A $\beta$ ) per picture.
close();
close();
close();
close();
close();
```

## References

- Ahmed M, Davis J, Aucoin D, Sato T, Ahuja S, Aimoto S, Elliott JL, Van Nostrand WE, Smith SO (2010) Structural conversion of neurotoxic amyloid-beta(1-42) oligomers to fibrils. *Nat Struct Mol Biol* 17: 561-567
- Ajami B, Bennett JL, Krieger C, Tetzlaff W, Rossi FM (2007) Local self-renewal can sustain CNS microglia maintenance and function throughout adult life. *Nat Neurosci* 10: 1538-1543
- Akiyama H, Barger S, Barnum S, Bradt B, Bauer J, Cole GM, Cooper NR, Eikelenboom P, Emmerling M, Fiebich BL *et al* (2000) Inflammation and Alzheimer's disease. *Neurobiol Aging* 21: 383-421
- Alhadidi Q, Shah ZA (2018) Cofilin Mediates LPS-Induced Microglial Cell Activation and Associated Neurotoxicity Through Activation of NF-kappaB and JAK-STAT Pathway. *Mol Neurobiol* 55: 1676-1691
- Alzheimer A (1907) Über einen eigenartigen schweren Erkrankungsprozess der Hirnrinde. *Allgemeine Zeitschrift für Psychiatrie und Psychisch-Gerichtliche Medizin* 64: 146-148
- Alzheimer A, Stelzmann RA, Schnitzlein HN, Murtagh FR (1995) An English translation of Alzheimer's 1907 paper, "Über eine eigenartige Erkankung der Hirnrinde". *Clin Anat* 8: 429-431
- Anwar S, Rivest S (2020) Alzheimer's disease: microglia targets and their modulation to promote amyloid phagocytosis and mitigate neuroinflammation. *Expert Opin Ther Targets* 24: 331-344
- Asai H, Ikezu S, Tsunoda S, Medalla M, Luebke J, Haydar T, Wolozin B, Butovsky O, Kugler S, Ikezu T (2015) Depletion of microglia and inhibition of exosome synthesis halt tau propagation. *Nat Neurosci* 18: 1584-1593
- Askew K, Li K, Olmos-Alonso A, Garcia-Moreno F, Liang Y, Richardson P, Tipton T, Chapman MA, Riecken K, Beccari S *et al* (2017) Coupled Proliferation and Apoptosis Maintain the Rapid Turnover of Microglia in the Adult Brain. *Cell Rep* 18: 391-405
- Association As (2020) 2020 Alzheimer's disease facts and figures. *Alzheimers Dement* 16: 391– 460
- Bacher M, Deuster O, Aljabari B, Egensperger R, Neff F, Jessen F, Popp J, Noelker C, Reese JP, Al-Abed Y *et al* (2010) The role of macrophage migration inhibitory factor in Alzheimer's disease. *Mol Med* 16: 116-121
- Bacskaï BJ, Kajdasz ST, McLellan ME, Games D, Seubert P, Schenk D, Hyman BT (2002) Non-Fc-mediated mechanisms are involved in clearance of amyloid-beta in vivo by immunotherapy. *J Neurosci* 22: 7873-7878
- Bader JM, Geyer PE, Muller JB, Strauss MT, Koch M, Leyboldt F, Koertvelyessy P, Bittner D, Schipke CG, Incesoy EI *et al* (2020) Proteome profiling in cerebrospinal fluid reveals novel biomarkers of Alzheimer's disease. *Mol Syst Biol* 16: e9356
- Baik SH, Kang S, Lee W, Choi H, Chung S, Kim JI, Mook-Jung I (2019) A Breakdown in Metabolic Reprogramming Causes Microglia Dysfunction in Alzheimer's Disease. *Cell Metab* 30: 493-507 e496
- Bao J, Zheng L, Zhang Q, Li X, Zhang X, Li Z, Bai X, Zhang Z, Huo W, Zhao X *et al* (2016) Deacetylation of TFEB promotes fibrillar Aβ degradation by upregulating lysosomal biogenesis in microglia. *Protein Cell* 7: 417-433
- Bard F, Cannon C, Barbour R, Burke RL, Games D, Grajeda H, Guido T, Hu K, Huang J, Johnson-Wood K *et al* (2000) Peripherally administered antibodies against amyloid beta-peptide enter the central nervous system and reduce pathology in a mouse model of Alzheimer disease. *Nat Med* 6: 916-919

- Bateman RJ, Aisen PS, De Strooper B, Fox NC, Lemere CA, Ringman JM, Salloway S, Sperling RA, Windisch M, Xiong C (2011) Autosomal-dominant Alzheimer's disease: a review and proposal for the prevention of Alzheimer's disease. *Alzheimers Res Ther* 3: 1
- Bekris LM, Yu CE, Bird TD, Tsuang DW (2010) Genetics of Alzheimer disease. *J Geriatr Psychiatry Neurol* 23: 213-227
- Benmamar-Badel A, Owens T, Wlodarczyk A (2020) Protective Microglial Subset in Development, Aging, and Disease: Lessons From Transcriptomic Studies. *Front Immunol* 11: 430
- Bennett ML, Bennett FC, Liddel SA, Ajami B, Zamanian JL, Fernhoff NB, Mulinyawe SB, Bohlen CJ, Adil A, Tucker A *et al* (2016) New tools for studying microglia in the mouse and human CNS. *Proc Natl Acad Sci U S A* 113: E1738-1746
- Benzing WC, Mufson EJ, Armstrong DM (1993) Alzheimer's disease-like dystrophic neurites characteristically associated with senile plaques are not found within other neurodegenerative diseases unless amyloid beta-protein deposition is present. *Brain Res* 606: 10-18
- Benzing WC, Wujek JR, Ward EK, Shaffer D, Ashe KH, Younkin SG, Brunden KR (1999) Evidence for glial-mediated inflammation in aged APP(SW) transgenic mice. *Neurobiol Aging* 20: 581-589
- Bertram L, Lange C, Mullin K, Parkinson M, Hsiao M, Hogan MF, Schjeide BM, Hooli B, Divito J, Ionita I *et al* (2008) Genome-wide association analysis reveals putative Alzheimer's disease susceptibility loci in addition to APOE. *Am J Hum Genet* 83: 623-632
- Beutner C, Linnartz-Gerlach B, Schmidt SV, Beyer M, Mallmann MR, Staratschek-Jox A, Schultze JL, Neumann H (2013) Unique transcriptome signature of mouse microglia. *Glia* 61: 1429-1442
- Bhaskar K, Konerth M, Kokiko-Cochran ON, Cardona A, Ransohoff RM, Lamb BT (2010) Regulation of tau pathology by the microglial fractalkine receptor. *Neuron* 68: 19-31
- Bitan G, Kirkitadze MD, Lomakin A, Vollers SS, Benedek GB, Teplow DB (2003) Amyloid beta -protein (A $\beta$ ) assembly: A $\beta$ 40 and A $\beta$ 42 oligomerize through distinct pathways. *Proc Natl Acad Sci U S A* 100: 330-335
- Boissonneault V, Filali M, Lessard M, Relton J, Wong G, Rivest S (2009) Powerful beneficial effects of macrophage colony-stimulating factor on beta-amyloid deposition and cognitive impairment in Alzheimer's disease. *Brain* 132: 1078-1092
- Bolmont T, Haiss F, Eicke D, Radde R, Mathis CA, Klunk WE, Kohsaka S, Jucker M, Calhoun ME (2008) Dynamics of the microglial/amyloid interaction indicate a role in plaque maintenance. *J Neurosci* 28: 4283-4292
- Boyd TD, Bennett SP, Mori T, Governatori N, Runfeldt M, Norden M, Padmanabhan J, Neame P, Wefes I, Sanchez-Ramos J *et al* (2010) GM-CSF upregulated in rheumatoid arthritis reverses cognitive impairment and amyloidosis in Alzheimer mice. *J Alzheimers Dis* 21: 507-518
- Boza-Serrano A, Ruiz R, Sanchez-Varo R, Garcia-Revilla J, Yang Y, Jimenez-Ferrer I, Paulus A, Wennstrom M, Vilalta A, Allendorf D *et al* (2019) Galectin-3, a novel endogenous TREM2 ligand, detrimentally regulates inflammatory response in Alzheimer's disease. *Acta Neuropathol* 138: 251-273
- Braak H, Braak E (1997) Frequency of stages of Alzheimer-related lesions in different age categories. *Neurobiol Aging* 18: 351-357
- Brothers HM, Gosztyla ML, Robinson SR (2018) The Physiological Roles of Amyloid-beta Peptide Hint at New Ways to Treat Alzheimer's Disease. *Front Aging Neurosci* 10: 118

## References

---

- Brouillette J, Caillierez R, Zommer N, Alves-Pires C, Benilova I, Blum D, De Strooper B, Buee L (2012) Neurotoxicity and memory deficits induced by soluble low-molecular-weight amyloid-beta1-42 oligomers are revealed in vivo by using a novel animal model. *J Neurosci* 32: 7852-7861
- Buchsel PC, Forgey A, Grape FB, Hamann SS (2002) Granulocyte macrophage colony-stimulating factor: current practice and novel approaches. *Clin J Oncol Nurs* 6: 198-205
- Butovsky O, Jedrychowski MP, Moore CS, Cialic R, Lanser AJ, Gabriely G, Koeglsperger T, Dake B, Wu PM, Doykan CE *et al* (2014) Identification of a unique TGF-beta-dependent molecular and functional signature in microglia. *Nat Neurosci* 17: 131-143
- Butovsky O, Weiner HL (2018) Microglial signatures and their role in health and disease. *Nat Rev Neurosci* 19: 622-635
- Cacabelos R (2020) How plausible is an Alzheimer's disease vaccine? *Expert Opin Drug Discov* 15: 1-6
- Cai H, Cong WN, Ji S, Rothman S, Maudsley S, Martin B (2012) Metabolic dysfunction in Alzheimer's disease and related neurodegenerative disorders. *Curr Alzheimer Res* 9: 5-17
- Cao X, Sudhof TC (2001) A transcriptionally [correction of transcriptively] active complex of APP with Fe65 and histone acetyltransferase Tip60. *Science* 293: 115-120
- Chakrabarty P, Jansen-West K, Beccard A, Ceballos-Diaz C, Levites Y, Verbeeck C, Zubair AC, Dickson D, Golde TE, Das P (2010) Massive gliosis induced by interleukin-6 suppresses Abeta deposition in vivo: evidence against inflammation as a driving force for amyloid deposition. *FASEB J* 24: 548-559
- Cheng Q, Danao J, Talreja S, Wen P, Yin J, Sun N, Li CM, Chui D, Tran D, Koirala S *et al* (2018) TREM2-activating antibodies abrogate the negative pleiotropic effects of the Alzheimer's disease variant Trem2(R47H) on murine myeloid cell function. *J Biol Chem* 293: 12620-12633
- Chiasserini D, Biscetti L, Eusebi P, Salvadori N, Frattini G, Simoni S, De Roeck N, Tambasco N, Stoops E, Vanderstichele H *et al* (2017) Differential role of CSF fatty acid binding protein 3, alpha-synuclein, and Alzheimer's disease core biomarkers in Lewy body disorders and Alzheimer's dementia. *Alzheimers Res Ther* 9: 52
- Chiu IM, Morimoto ET, Goodarzi H, Liao JT, O'Keeffe S, Phatnani HP, Muratet M, Carroll MC, Levy S, Tavazoie S *et al* (2013) A neurodegeneration-specific gene-expression signature of acutely isolated microglia from an amyotrophic lateral sclerosis mouse model. *Cell Rep* 4: 385-401
- Cho SH, Sun B, Zhou Y, Kauppinen TM, Halabisky B, Wes P, Ransohoff RM, Gan L (2011) CX3CR1 protein signaling modulates microglial activation and protects against plaque-independent cognitive deficits in a mouse model of Alzheimer disease. *J Biol Chem* 286: 32713-32722
- Choi YJ, Chae S, Kim JH, Barald KF, Park JY, Lee SH (2013) Neurotoxic amyloid beta oligomeric assemblies recreated in microfluidic platform with interstitial level of slow flow. *Sci Rep* 3: 1921
- Chung H, Brazil MI, Soe TT, Maxfield FR (1999) Uptake, degradation, and release of fibrillar and soluble forms of Alzheimer's amyloid beta-peptide by microglial cells. *J Biol Chem* 274: 32301-32308
- Cline EN, Bicca MA, Viola KL, Klein WL (2018) The Amyloid-beta Oligomer Hypothesis: Beginning of the Third Decade. *J Alzheimers Dis* 64: S567-S610
- Colonna M, Butovsky O (2017) Microglia Function in the Central Nervous System During Health and Neurodegeneration. *Annu Rev Immunol* 35: 441-468

- Condello C, Yuan P, Schain A, Grutzendler J (2015) Microglia constitute a barrier that prevents neurotoxic protofibrillar Abeta42 hotspots around plaques. *Nat Commun* 6: 6176
- Corder EH, Saunders AM, Strittmatter WJ, Schmechel DE, Gaskell PC, Small GW, Roses AD, Haines JL, Pericak-Vance MA (1993) Gene dose of apolipoprotein E type 4 allele and the risk of Alzheimer's disease in late onset families. *Science* 261: 921-923
- Crotti A, Ransohoff RM (2016) Microglial Physiology and Pathophysiology: Insights from Genome-wide Transcriptional Profiling. *Immunity* 44: 505-515
- D'Andrea MR, Cole GM, Ard MD (2004) The microglial phagocytic role with specific plaque types in the Alzheimer disease brain. *Neurobiol Aging* 25: 675-683
- Dai XM, Ryan GR, Hapel AJ, Dominguez MG, Russell RG, Kapp S, Sylvestre V, Stanley ER (2002) Targeted disruption of the mouse colony-stimulating factor 1 receptor gene results in osteopetrosis, mononuclear phagocyte deficiency, increased primitive progenitor cell frequencies, and reproductive defects. *Blood* 99: 111-120
- Daria A, Colombo A, Llovera G, Hampel H, Willem M, Liesz A, Haass C, Tahirovic S (2017) Young microglia restore amyloid plaque clearance of aged microglia. *EMBO J* 36: 583-603
- Daro E, Pulendran B, Brasel K, Teepe M, Pettit D, Lynch DH, Vremec D, Robb L, Shortman K, McKenna HJ *et al* (2000) Polyethylene glycol-modified GM-CSF expands CD11b(high)CD11c(high) but not CD11b(low)CD11c(high) murine dendritic cells in vivo: a comparative analysis with Flt3 ligand. *J Immunol* 165: 49-58
- Das BC, Dasgupta S, Ray SK (2019) Potential therapeutic roles of retinoids for prevention of neuroinflammation and neurodegeneration in Alzheimer's disease. *Neural Regen Res* 14: 1880-1892
- Das P, Howard V, Loosbrock N, Dickson D, Murphy MP, Golde TE (2003) Amyloid-beta immunization effectively reduces amyloid deposition in FcRgamma<sup>-/-</sup> knock-out mice. *J Neurosci* 23: 8532-8538
- Dawkins E, Small DH (2014) Insights into the physiological function of the beta-amyloid precursor protein: beyond Alzheimer's disease. *J Neurochem* 129: 756-769
- De Strooper B, Umans L, Van Leuven F, Van Den Berghe H (1993) Study of the synthesis and secretion of normal and artificial mutants of murine amyloid precursor protein (APP): cleavage of APP occurs in a late compartment of the default secretion pathway. *J Cell Biol* 121: 295-304
- Deane R, Bell RD, Sagare A, Zlokovic BV (2009) Clearance of amyloid-beta peptide across the blood-brain barrier: implication for therapies in Alzheimer's disease. *CNS Neurol Disord Drug Targets* 8: 16-30
- DeTure MA, Dickson DW (2019) The neuropathological diagnosis of Alzheimer's disease. *Mol Neurodegener* 14: 32
- Devanney NA, Stewart AN, Gensel JC (2020) Microglia and macrophage metabolism in CNS injury and disease: The role of immunometabolism in neurodegeneration and neurotrauma. *Exp Neurol* 329: 113310
- Drummond E, Wisniewski T (2017) Alzheimer's disease: experimental models and reality. *Acta Neuropathol* 133: 155-175
- Dworzak J, Renvoise B, Habchi J, Yates EV, Combadiere C, Knowles TP, Dobson CM, Blackstone C, Paulsen O, Murphy PM (2015) Neuronal Cx3cr1 Deficiency Protects against Amyloid beta-Induced Neurotoxicity. *PLoS One* 10: e0127730

## References

---

- Edbauer D, Winkler E, Regula JT, Pesold B, Steiner H, Haass C (2003) Reconstitution of gamma-secretase activity. *Nat Cell Biol* 5: 486-488
- Efthymiou AG, Goate AM (2017) Late onset Alzheimer's disease genetics implicates microglial pathways in disease risk. *Mol Neurodegener* 12: 43
- Elmore MR, Najafi AR, Koike MA, Dagher NN, Spangenberg EE, Rice RA, Kitazawa M, Matusow B, Nguyen H, West BL *et al* (2014) Colony-stimulating factor 1 receptor signaling is necessary for microglia viability, unmasking a microglia progenitor cell in the adult brain. *Neuron* 82: 380-397
- Erblich B, Zhu L, Etgen AM, Dobrenis K, Pollard JW (2011) Absence of colony stimulation factor-1 receptor results in loss of microglia, disrupted brain development and olfactory deficits. *PLoS One* 6: e26317
- Fakhoury M (2018) Microglia and Astrocytes in Alzheimer's Disease: Implications for Therapy. *Curr Neuropharmacol* 16: 508-518
- Ferreira R, Bernardino L (2015) Dual role of microglia in health and disease: pushing the balance toward repair. *Front Cell Neurosci* 9: 51
- Fessel J (2019) Ineffective levels of transforming growth factors and their receptor account for old age being a risk factor for Alzheimer's disease. *Alzheimers Dement (N Y)* 5: 899-905
- Finder VH, Glockshuber R (2007) Amyloid-beta aggregation. *Neurodegener Dis* 4: 13-27
- Flanary BE, Sammons NW, Nguyen C, Walker D, Streit WJ (2007) Evidence that aging and amyloid promote microglial cell senescence. *Rejuvenation Res* 10: 61-74
- Floden AM, Combs CK (2011) Microglia demonstrate age-dependent interaction with amyloid-beta fibrils. *J Alzheimers Dis* 25: 279-293
- Forgac M (2007) Vacuolar ATPases: rotary proton pumps in physiology and pathophysiology. *Nat Rev Mol Cell Biol* 8: 917-929
- Franco-Bocanegra DK, George B, Lau LC, Holmes C, Nicoll JAR, Boche D (2019a) Microglial motility in Alzheimer's disease and after Abeta42 immunotherapy: a human post-mortem study. *Acta Neuropathol Commun* 7: 174
- Franco-Bocanegra DK, McAuley C, Nicoll JAR, Boche D (2019b) Molecular Mechanisms of Microglial Motility: Changes in Ageing and Alzheimer's Disease. *Cells* 8
- Friedrich RP, Tepper K, Ronicke R, Soom M, Westermann M, Reymann K, Kaether C, Fandrich M (2010) Mechanism of amyloid plaque formation suggests an intracellular basis of Abeta pathogenicity. *Proc Natl Acad Sci U S A* 107: 1942-1947
- Frost JL, Le KX, Cynis H, Ekpo E, Kleinschmidt M, Palmour RM, Ervin FR, Snigdha S, Cotman CW, Saido TC *et al* (2013) Pyroglutamate-3 amyloid-beta deposition in the brains of humans, non-human primates, canines, and Alzheimer disease-like transgenic mouse models. *Am J Pathol* 183: 369-381
- Frost JL, Schafer DP (2016) Microglia: Architects of the Developing Nervous System. *Trends Cell Biol* 26: 587-597
- Fuger P, Hefendehl JK, Veeraraghavalu K, Wendeln AC, Schlosser C, Obermuller U, Wegenast-Braun BM, Neher JJ, Martus P, Kohsaka S *et al* (2017) Microglia turnover with aging and in an Alzheimer's model via long-term in vivo single-cell imaging. *Nat Neurosci* 20: 1371-1376

- Galatro TF, Holtman IR, Lerario AM, Vainchtein ID, Brouwer N, Sola PR, Veras MM, Pereira TF, Leite REP, Moller T *et al* (2017) Transcriptomic analysis of purified human cortical microglia reveals age-associated changes. *Nat Neurosci* 20: 1162-1171
- Games D, Adams D, Alessandrini R, Barbour R, Berthelette P, Blackwell C, Carr T, Clemens J, Donaldson T, Gillespie F *et al* (1995) Alzheimer-type neuropathology in transgenic mice overexpressing V717F beta-amyloid precursor protein. *Nature* 373: 523-527
- Gautier EL, Shay T, Miller J, Greter M, Jakubzick C, Ivanov S, Helft J, Chow A, Elpek KG, Gordonov S *et al* (2012) Gene-expression profiles and transcriptional regulatory pathways that underlie the identity and diversity of mouse tissue macrophages. *Nat Immunol* 13: 1118-1128
- Geng L, Fan LM, Liu F, Smith C, Li J (2020) Nox2 dependent redox-regulation of microglial response to amyloid-beta stimulation and microgliosis in aging. *Sci Rep* 10: 1582
- Gericke C, Mallone A, Engelhardt B, Nitsch RM, Ferretti MT (2020) Oligomeric Forms of Human Amyloid-Beta(1-42) Inhibit Antigen Presentation. *Front Immunol* 11: 1029
- Geula C, Wu CK, Saroff D, Lorenzo A, Yuan M, Yankner BA (1998) Aging renders the brain vulnerable to amyloid beta-protein neurotoxicity. *Nat Med* 4: 827-831
- Gibbs-Seymour I, Fontana P, Rack JGM, Ahel I (2016) HPF1/C4orf27 Is a PARP-1-Interacting Protein that Regulates PARP-1 ADP-Ribosylation Activity. *Mol Cell* 62: 432-442
- Gilman S, Koller M, Black RS, Jenkins L, Griffith SG, Fox NC, Eisner L, Kirby L, Rovira MB, Forette F *et al* (2005) Clinical effects of Abeta immunization (AN1792) in patients with AD in an interrupted trial. *Neurology* 64: 1553-1562
- Gimeno-Bayon J, Lopez-Lopez A, Rodriguez MJ, Mahy N (2014) Glucose pathways adaptation supports acquisition of activated microglia phenotype. *J Neurosci Res* 92: 723-731
- Ginhoux F, Greter M, Leboeuf M, Nandi S, See P, Gokhan S, Mehler MF, Conway SJ, Ng LG, Stanley ER *et al* (2010) Fate mapping analysis reveals that adult microglia derive from primitive macrophages. *Science* 330: 841-845
- Ginhoux F, Lim S, Hoeffel G, Low D, Huber T (2013) Origin and differentiation of microglia. *Front Cell Neurosci* 7: 45
- Ginhoux F, Prinz M (2015) Origin of microglia: current concepts and past controversies. *Cold Spring Harb Perspect Biol* 7: a020537
- Giulian D, Ingeman JE (1988) Colony-stimulating factors as promoters of amoeboid microglia. *J Neurosci* 8: 4707-4717
- Glenner GG (1989) Amyloid beta protein and the basis for Alzheimer's disease. *Prog Clin Biol Res* 317: 857-868
- Gomes-Leal W (2012) Microglial physiopathology: how to explain the dual role of microglia after acute neural disorders? *Brain Behav* 2: 345-356
- Gosselin D, Link VM, Romanoski CE, Fonseca GJ, Eichenfield DZ, Spann NJ, Stender JD, Chun HB, Garner H, Geissmann F *et al* (2014) Environment drives selection and function of enhancers controlling tissue-specific macrophage identities. *Cell* 159: 1327-1340

## References

---

- Gotzl JK, Brendel M, Werner G, Parhizkar S, Sebastian Monasor L, Kleinberger G, Colombo AV, Deussing M, Wagner M, Winkelmann J *et al* (2019) Opposite microglial activation stages upon loss of PGRN or TREM2 result in reduced cerebral glucose metabolism. *EMBO Mol Med* 11
- Gozes I, Zaltzman R, Hauser J, Brenneman DE, Shohami E, Hill JM (2005) The expression of activity-dependent neuroprotective protein (ADNP) is regulated by brain damage and treatment of mice with the ADNP derived peptide, NAP, reduces the severity of traumatic head injury. *Curr Alzheimer Res* 2: 149-153
- Grathwohl SA, Kalin RE, Bolmont T, Prokop S, Winkelmann G, Kaeser SA, Odenthal J, Radde R, Eldh T, Gandy S *et al* (2009) Formation and maintenance of Alzheimer's disease beta-amyloid plaques in the absence of microglia. *Nat Neurosci* 12: 1361-1363
- Griciuc A, Serrano-Pozo A, Parrado AR, Lesinski AN, Asselin CN, Mullin K, Hooli B, Choi SH, Hyman BT, Tanzi RE (2013) Alzheimer's disease risk gene CD33 inhibits microglial uptake of amyloid beta. *Neuron* 78: 631-643
- Grundke-Iqbal I, Iqbal K, Tung YC, Quinlan M, Wisniewski HM, Binder LI (1986) Abnormal phosphorylation of the microtubule-associated protein tau (tau) in Alzheimer cytoskeletal pathology. *Proc Natl Acad Sci U S A* 83: 4913-4917
- Guerreiro R, Bras J (2015) The age factor in Alzheimer's disease. *Genome Med* 7: 106
- Guerreiro R, Wojtas A, Bras J, Carrasquillo M, Rogaeva E, Majounie E, Cruchaga C, Sassi C, Kauwe JS, Younkin S *et al* (2013) TREM2 variants in Alzheimer's disease. *N Engl J Med* 368: 117-127
- Guo LH, Alexopoulos P, Pernecky R (2013) Heart-type fatty acid binding protein and vascular endothelial growth factor: cerebrospinal fluid biomarker candidates for Alzheimer's disease. *Eur Arch Psychiatry Clin Neurosci* 263: 553-560
- Ha Y, Park HS, Park CW, Yoon SH, Park SR, Hyun DK, Kim EY, Park HC (2005) Synthes Award for Resident Research on Spinal Cord and Spinal Column Injury: granulocyte macrophage colony stimulating factor (GM-CSF) prevents apoptosis and improves functional outcome in experimental spinal cord contusion injury. *Clin Neurosurg* 52: 341-347
- Haass C (2004) Take five--BACE and the gamma-secretase quartet conduct Alzheimer's amyloid beta-peptide generation. *EMBO J* 23: 483-488
- Haass C, Hung AY, Schlossmacher MG, Teplow DB, Selkoe DJ (1993) beta-Amyloid peptide and a 3-kDa fragment are derived by distinct cellular mechanisms. *J Biol Chem* 268: 3021-3024
- Haass C, Selkoe DJ (1993) Cellular processing of beta-amyloid precursor protein and the genesis of amyloid beta-peptide. *Cell* 75: 1039-1042
- Haass C, Selkoe DJ (2007) Soluble protein oligomers in neurodegeneration: lessons from the Alzheimer's amyloid beta-peptide. *Nat Rev Mol Cell Biol* 8: 101-112
- Hagemeyer N, Hanft KM, Akriditou MA, Unger N, Park ES, Stanley ER, Staszewski O, Dimou L, Prinz M (2017) Microglia contribute to normal myelinogenesis and to oligodendrocyte progenitor maintenance during adulthood. *Acta Neuropathol* 134: 441-458
- Hall AM, Roberson ED (2012) Mouse models of Alzheimer's disease. *Brain Res Bull* 88: 3-12
- Hanisch UK, Kettenmann H (2007) Microglia: active sensor and versatile effector cells in the normal and pathologic brain. *Nat Neurosci* 10: 1387-1394
- Hansen DV, Hanson JE, Sheng M (2018) Microglia in Alzheimer's disease. *J Cell Biol* 217: 459-472

- Hansen G, Hercus TR, McClure BJ, Stomski FC, Dottore M, Powell J, Ramshaw H, Woodcock JM, Xu Y, Guthridge M *et al* (2008) The structure of the GM-CSF receptor complex reveals a distinct mode of cytokine receptor activation. *Cell* 134: 496-507
- Hardy JA, Higgins GA (1992) Alzheimer's disease: the amyloid cascade hypothesis. *Science* 256: 184-185
- Harold D, Abraham R, Hollingworth P, Sims R, Gerrish A, Hamshere ML, Pahwa JS, Moskvina V, Dowzell K, Williams A *et al* (2009) Genome-wide association study identifies variants at CLU and PICALM associated with Alzheimer's disease. *Nat Genet* 41: 1088-1093
- Hartlage-Rubsamen M, Bluhm A, Piechotta A, Linnert M, Rahfeld JU, Demuth HU, Lues I, Kuhn PH, Lichtenthaler SF, Rossner S *et al* (2018) Immunohistochemical Evidence from APP-Transgenic Mice for Glutaminyl Cyclase as Drug Target to Diminish pE-Abeta Formation. *Molecules* 23
- Haughey NJ, Bandaru VV, Bae M, Mattson MP (2010) Roles for dysfunctional sphingolipid metabolism in Alzheimer's disease neuropathogenesis. *Biochim Biophys Acta* 1801: 878-886
- Hayashi Y, Yoshida M, Yamato M, Ide T, Wu Z, Ochi-Shindou M, Kanki T, Kang D, Sunagawa K, Tsutsui H *et al* (2008) Reverse of age-dependent memory impairment and mitochondrial DNA damage in microglia by an overexpression of human mitochondrial transcription factor a in mice. *J Neurosci* 28: 8624-8634
- Haynes SE, Hollopeter G, Yang G, Kurpius D, Dailey ME, Gan WB, Julius D (2006) The P2Y12 receptor regulates microglial activation by extracellular nucleotides. *Nat Neurosci* 9: 1512-1519
- Hellwig S, Masuch A, Nestel S, Katzmarski N, Meyer-Luehmann M, Biber K (2015) Forebrain microglia from wild-type but not adult 5xFAD mice prevent amyloid-beta plaque formation in organotypic hippocampal slice cultures. *Sci Rep* 5: 14624
- Hessvik NP, Llorente A (2018) Current knowledge on exosome biogenesis and release. *Cell Mol Life Sci* 75: 193-208
- Hickman S, Izzy S, Sen P, Morsett L, El Khoury J (2018) Microglia in neurodegeneration. *Nat Neurosci* 21: 1359-1369
- Hickman SE, Allison EK, El Khoury J (2008) Microglial dysfunction and defective beta-amyloid clearance pathways in aging Alzheimer's disease mice. *J Neurosci* 28: 8354-8360
- Hickman SE, Kingery ND, Ohsumi TK, Borowsky ML, Wang LC, Means TK, El Khoury J (2013) The microglial sensome revealed by direct RNA sequencing. *Nat Neurosci* 16: 1896-1905
- Hoeffel G, Chen J, Lavin Y, Low D, Almeida FF, See P, Beaudin AE, Lum J, Low I, Forsberg EC *et al* (2015) C-Myb(+) erythro-myeloid progenitor-derived fetal monocytes give rise to adult tissue-resident macrophages. *Immunity* 42: 665-678
- Holcomb L, Gordon MN, McGowan E, Yu X, Benkovic S, Jantzen P, Wright K, Saad I, Mueller R, Morgan D *et al* (1998) Accelerated Alzheimer-type phenotype in transgenic mice carrying both mutant amyloid precursor protein and presenilin 1 transgenes. *Nat Med* 4: 97-100
- Hollingworth P, Harold D, Sims R, Gerrish A, Lambert JC, Carrasquillo MM, Abraham R, Hamshere ML, Pahwa JS, Moskvina V *et al* (2011) Common variants at ABCA7, MS4A6A/MS4A4E, EPHA1, CD33 and CD2AP are associated with Alzheimer's disease. *Nat Genet* 43: 429-435
- Holmes C, Boche D, Wilkinson D, Yadegarfar G, Hopkins V, Bayer A, Jones RW, Bullock R, Love S, Neal JW *et al* (2008) Long-term effects of Abeta42 immunisation in Alzheimer's disease: follow-up of a randomised, placebo-controlled phase I trial. *Lancet* 372: 216-223

## References

---

- Holtzman DM, Morris JC, Goate AM (2011) Alzheimer's disease: the challenge of the second century. *Sci Transl Med* 3: 77sr71
- Hopperton KE, Mohammad D, Trepanier MO, Giuliano V, Bazinet RP (2018) Markers of microglia in post-mortem brain samples from patients with Alzheimer's disease: a systematic review. *Mol Psychiatry* 23: 177-198
- Horner R, Gassner J, Kluge M, Tang P, Lippert S, Hillebrandt KH, Moosburner S, Reutzel-Selke A, Pratschke J, Sauer IM *et al* (2019) Impact of Percoll purification on isolation of primary human hepatocytes. *Sci Rep* 9: 6542
- Hsiao K, Chapman P, Nilsen S, Eckman C, Harigaya Y, Younkin S, Yang F, Cole G (1996) Correlative memory deficits, A $\beta$  elevation, and amyloid plaques in transgenic mice. *Science* 274: 99-102
- Hu X, Li S, Doycheva DM, Huang L, Lenahan C, Liu R, Huang J, Xie S, Tang J, Zuo G *et al* (2020) Rh-CSF1 attenuates neuroinflammation via the CSF1R/PLCG2/PKCepsilon pathway in a rat model of neonatal HIE. *J Neuroinflammation* 17: 182
- Huang LK, Chao SP, Hu CJ (2020) Clinical trials of new drugs for Alzheimer disease. *J Biomed Sci* 27: 18
- Huang Y, Liao Z, Lin X, Wu X, Chen X, Bai X, Zhuang Y, Yang Y, Zhang J (2019) Overexpression of miR-146a Might Regulate Polarization Transitions of BV-2 Cells Induced by High Glucose and Glucose Fluctuations. *Front Endocrinol (Lausanne)* 10: 719
- Iqbal K, Alonso Adel C, Chen S, Chohan MO, El-Akkad E, Gong CX, Khatoon S, Li B, Liu F, Rahman A *et al* (2005) Tau pathology in Alzheimer disease and other tauopathies. *Biochim Biophys Acta* 1739: 198-210
- Iqbal K, Liu F, Gong CX, Grundke-Iqbal I (2010) Tau in Alzheimer disease and related tauopathies. *Curr Alzheimer Res* 7: 656-664
- Iwatsubo T, Odaka A, Suzuki N, Mizusawa H, Nukina N, Ihara Y (1994) Visualization of A $\beta$  42(43) and A $\beta$  40 in senile plaques with end-specific A $\beta$  monoclonals: evidence that an initially deposited species is A $\beta$  42(43). *Neuron* 13: 45-53
- Jankowsky JL, Zheng H (2017) Practical considerations for choosing a mouse model of Alzheimer's disease. *Mol Neurodegener* 12: 89
- Jay P, Berge-Lefranc JL, Massacrier A, Roessler E, Wallis D, Muenke M, Gastaldi M, Taviaux S, Cau P, Berta P (2000) ARP3beta, the gene encoding a new human actin-related protein, is alternatively spliced and predominantly expressed in brain neuronal cells. *Eur J Biochem* 267: 2921-2928
- Jay TR, Hirsch AM, Broihier ML, Miller CM, Neilson LE, Ransohoff RM, Lamb BT, Landreth GE (2017) Disease Progression-Dependent Effects of TREM2 Deficiency in a Mouse Model of Alzheimer's Disease. *J Neurosci* 37: 637-647
- Jiang Q, Lee CY, Mandrekar S, Wilkinson B, Cramer P, Zelcer N, Mann K, Lamb B, Willson TM, Collins JL *et al* (2008) ApoE promotes the proteolytic degradation of A $\beta$ . *Neuron* 58: 681-693
- Jiang T, Tan L, Zhu XC, Zhang QQ, Cao L, Tan MS, Gu LZ, Wang HF, Ding ZZ, Zhang YD *et al* (2014) Upregulation of TREM2 ameliorates neuropathology and rescues spatial cognitive impairment in a transgenic mouse model of Alzheimer's disease. *Neuropsychopharmacology* 39: 2949-2962
- Jonsson T, Atwal JK, Steinberg S, Snaedal J, Jonsson PV, Bjornsson S, Stefansson H, Sulem P, Gudbjartsson D, Maloney J *et al* (2012) A mutation in APP protects against Alzheimer's disease and age-related cognitive decline. *Nature* 488: 96-99

- Jonsson T, Stefansson H, Steinberg S, Jonsdottir I, Jonsson PV, Snaedal J, Bjornsson S, Huttenlocher J, Levey AI, Lah JJ *et al* (2013) Variant of TREM2 associated with the risk of Alzheimer's disease. *N Engl J Med* 368: 107-116
- Joshi P, Turola E, Ruiz A, Bergami A, Libera DD, Benussi L, Giussani P, Magnani G, Comi G, Legname G *et al* (2014) Microglia convert aggregated amyloid-beta into neurotoxic forms through the shedding of microvesicles. *Cell Death Differ* 21: 582-593
- Kamphuis W, Kooijman L, Schettters S, Orre M, Hol EM (2016) Transcriptional profiling of CD11c-positive microglia accumulating around amyloid plaques in a mouse model for Alzheimer's disease. *Biochim Biophys Acta* 1862: 1847-1860
- Kamphuis W, Orre M, Kooijman L, Dahmen M, Hol EM (2012) Differential cell proliferation in the cortex of the APP<sup>swe</sup>PS1<sup>dE9</sup> Alzheimer's disease mouse model. *Glia* 60: 615-629
- Karch CM, Goate AM (2015) Alzheimer's disease risk genes and mechanisms of disease pathogenesis. *Biol Psychiatry* 77: 43-51
- Kaur D, Sharma V, Deshmukh R (2019) Activation of microglia and astrocytes: a roadway to neuroinflammation and Alzheimer's disease. *Inflammopharmacology* 27: 663-677
- Kelso ML, Elliott BR, Haverland NA, Mosley RL, Gendelman HE (2015) Granulocyte-macrophage colony stimulating factor exerts protective and immunomodulatory effects in cortical trauma. *J Neuroimmunol* 278: 162-173
- Keren-Shaul H, Spinrad A, Weiner A, Matcovitch-Natan O, Dvir-Szternfeld R, Ulland TK, David E, Baruch K, Lara-Astaiso D, Toth B *et al* (2017) A Unique Microglia Type Associated with Restricting Development of Alzheimer's Disease. *Cell* 169: 1276-1290 e1217
- Kierdorf K, Erny D, Goldmann T, Sander V, Schulz C, Perdiguero EG, Wieghofer P, Heinrich A, Riemke P, Holscher C *et al* (2013) Microglia emerge from erythromyeloid precursors via Pu.1- and Irf8-dependent pathways. *Nat Neurosci* 16: 273-280
- Kim HJ, Ajit D, Peterson TS, Wang Y, Camden JM, Gibson Wood W, Sun GY, Erb L, Petris M, Weisman GA (2012a) Nucleotides released from Abeta(1)(-)(4)(2) -treated microglial cells increase cell migration and Abeta(1)(-)(4)(2) uptake through P2Y(2) receptor activation. *J Neurochem* 121: 228-238
- Kim J, Basak JM, Holtzman DM (2009a) The role of apolipoprotein E in Alzheimer's disease. *Neuron* 63: 287-303
- Kim J, Eltorai AE, Jiang H, Liao F, Verghese PB, Kim J, Stewart FR, Basak JM, Holtzman DM (2012b) Anti-apoE immunotherapy inhibits amyloid accumulation in a transgenic mouse model of Abeta amyloidosis. *J Exp Med* 209: 2149-2156
- Kim NK, Choi BH, Huang X, Snyder BJ, Bukhari S, Kong TH, Park H, Park HC, Park SR, Ha Y (2009b) Granulocyte-macrophage colony-stimulating factor promotes survival of dopaminergic neurons in the 1-methyl-4-phenyl-1,2,3,6-tetrahydropyridine-induced murine Parkinson's disease model. *Eur J Neurosci* 29: 891-900
- King A (2018) The search for better animal models of Alzheimer's disease. *Nature* 559: S13-S15
- Kiyota T, Machhi J, Lu Y, Dyavarshetty B, Nemati M, Yokoyama I, Mosley RL, Gendelman HE (2018) Granulocyte-macrophage colony-stimulating factor neuroprotective activities in Alzheimer's disease mice. *J Neuroimmunol* 319: 80-92

## References

---

- Kleinberger G, Yamanishi Y, Suarez-Calvet M, Czirr E, Lohmann E, Cuyvers E, Struyfs H, Pettkus N, Wenninger-Weinzierl A, Mazaheri F *et al* (2014) TREM2 mutations implicated in neurodegeneration impair cell surface transport and phagocytosis. *Sci Transl Med* 6: 243ra286
- Koellhoffer EC, McCullough LD, Ritzel RM (2017) Old Maids: Aging and Its Impact on Microglia Function. *Int J Mol Sci* 18
- Koenigsknecht-Talboo J, Landreth GE (2005) Microglial phagocytosis induced by fibrillar beta-amyloid and IgGs are differentially regulated by proinflammatory cytokines. *J Neurosci* 25: 8240-8249
- Koffie RM, Meyer-Luehmann M, Hashimoto T, Adams KW, Mielke ML, Garcia-Alloza M, Micheva KD, Smith SJ, Kim ML, Lee VM *et al* (2009) Oligomeric amyloid beta associates with postsynaptic densities and correlates with excitatory synapse loss near senile plaques. *Proc Natl Acad Sci U S A* 106: 4012-4017
- Kojro E, Fahrenholz F (2005) The non-amyloidogenic pathway: structure and function of alpha-secretases. *Subcell Biochem* 38: 105-127
- Konishi H, Kiyama H (2018) Microglial TREM2/DAP12 Signaling: A Double-Edged Sword in Neural Diseases. *Front Cell Neurosci* 12: 206
- Krabbe G, Halle A, Matyash V, Rinnenthal JL, Eom GD, Bernhardt U, Miller KR, Prokop S, Kettenmann H, Heppner FL (2013) Functional impairment of microglia coincides with Beta-amyloid deposition in mice with Alzheimer-like pathology. *PLoS One* 8: e60921
- Krasemann S, Madore C, Cialic R, Baufeld C, Calcagno N, El Fatimy R, Beckers L, O'Loughlin E, Xu Y, Fanek Z *et al* (2017) The TREM2-APOE Pathway Drives the Transcriptional Phenotype of Dysfunctional Microglia in Neurodegenerative Diseases. *Immunity* 47: 566-581 e569
- Kreutzberg GW (1996) Microglia: a sensor for pathological events in the CNS. *Trends Neurosci* 19: 312-318
- Krieger M, Both M, Kranig SA, Pitzer C, Klugmann M, Vogt G, Draguhn A, Schneider A (2012) The hematopoietic cytokine granulocyte-macrophage colony stimulating factor is important for cognitive functions. *Sci Rep* 2: 697
- Lambert JC, Ibrahim-Verbaas CA, Harold D, Naj AC, Sims R, Bellenguez C, DeStafano AL, Bis JC, Beecham GW, Grenier-Boley B *et al* (2013) Meta-analysis of 74,046 individuals identifies 11 new susceptibility loci for Alzheimer's disease. *Nat Genet* 45: 1452-1458
- Lambert MP, Barlow AK, Chromy BA, Edwards C, Freed R, Liosatos M, Morgan TE, Rozovsky I, Trommer B, Viola KL *et al* (1998) Diffusible, nonfibrillar ligands derived from Abeta1-42 are potent central nervous system neurotoxins. *Proc Natl Acad Sci U S A* 95: 6448-6453
- Lane CA, Hardy J, Schott JM (2018) Alzheimer's disease. *Eur J Neurol* 25: 59-70
- Lauro C, Limatola C (2020) Metabolic Reprogramming of Microglia in the Regulation of the Innate Inflammatory Response. *Front Immunol* 11: 493
- Lawson LJ, Perry VH, Dri P, Gordon S (1990) Heterogeneity in the distribution and morphology of microglia in the normal adult mouse brain. *Neuroscience* 39: 151-170
- Lee CY, Landreth GE (2010) The role of microglia in amyloid clearance from the AD brain. *J Neural Transm (Vienna)* 117: 949-960
- Lee CY, Tse W, Smith JD, Landreth GE (2012) Apolipoprotein E promotes beta-amyloid trafficking and degradation by modulating microglial cholesterol levels. *J Biol Chem* 287: 2032-2044

- Lee JK, Tansey MG (2013) Microglia isolation from adult mouse brain. *Methods Mol Biol* 1041: 17-23
- Lee S, Varvel NH, Konerth ME, Xu G, Cardona AE, Ransohoff RM, Lamb BT (2010) CX3CR1 deficiency alters microglial activation and reduces beta-amyloid deposition in two Alzheimer's disease mouse models. *Am J Pathol* 177: 2549-2562
- Lee SC, Liu W, Brosnan CF, Dickson DW (1994) GM-CSF promotes proliferation of human fetal and adult microglia in primary cultures. *Glia* 12: 309-318
- Lenz KM, Nelson LH (2018) Microglia and Beyond: Innate Immune Cells As Regulators of Brain Development and Behavioral Function. *Front Immunol* 9: 698
- Li T, Braunstein KE, Zhang J, Lau A, Sibener L, Deeble C, Wong PC (2016) The neuritic plaque facilitates pathological conversion of tau in an Alzheimer's disease mouse model. *Nat Commun* 7: 12082
- Liddel SA, Guttenplan KA, Clarke LE, Bennett FC, Bohlen CJ, Schirmer L, Bennett ML, Munch AE, Chung WS, Peterson TC *et al* (2017) Neurotoxic reactive astrocytes are induced by activated microglia. *Nature* 541: 481-487
- Lin H, Lee E, Hestir K, Leo C, Huang M, Bosch E, Halenbeck R, Wu G, Zhou A, Behrens D *et al* (2008) Discovery of a cytokine and its receptor by functional screening of the extracellular proteome. *Science* 320: 807-811
- Liu S, Liu Y, Hao W, Wolf L, Kiliaan AJ, Penke B, Rube CE, Walter J, Heneka MT, Hartmann T *et al* (2012) TLR2 is a primary receptor for Alzheimer's amyloid beta peptide to trigger neuroinflammatory activation. *J Immunol* 188: 1098-1107
- Liu Z, Condello C, Schain A, Harb R, Grutzendler J (2010) CX3CR1 in microglia regulates brain amyloid deposition through selective protofibrillar amyloid-beta phagocytosis. *J Neurosci* 30: 17091-17101
- Loving BA, Bruce KD (2020) Lipid and Lipoprotein Metabolism in Microglia. *Front Physiol* 11: 393
- Lowell CA (2011) Src-family and Syk kinases in activating and inhibitory pathways in innate immune cells: signaling cross talk. *Cold Spring Harb Perspect Biol* 3
- Ma X, Lin WY, Chen Y, Stawicki S, Mukhyala K, Wu Y, Martin F, Bazan JF, Starovasnik MA (2012) Structural basis for the dual recognition of helical cytokines IL-34 and CSF-1 by CSF-1R. *Structure* 20: 676-687
- Majumdar A, Capetillo-Zarate E, Cruz D, Gouras GK, Maxfield FR (2011) Degradation of Alzheimer's amyloid fibrils by microglia requires delivery of CIC-7 to lysosomes. *Mol Biol Cell* 22: 1664-1676
- Majumdar A, Cruz D, Asamoah N, Buxbaum A, Sohar I, Lobel P, Maxfield FR (2007) Activation of microglia acidifies lysosomes and leads to degradation of Alzheimer amyloid fibrils. *Mol Biol Cell* 18: 1490-1496
- Makin S (2018) The amyloid hypothesis on trial. *Nature* 559: S4-S7
- Mandrekar S, Jiang Q, Lee CY, Koenigsnecht-Talboo J, Holtzman DM, Landreth GE (2009) Microglia mediate the clearance of soluble A $\beta$  through fluid phase macropinocytosis. *J Neurosci* 29: 4252-4262
- Maphis N, Xu G, Kokiko-Cochran ON, Jiang S, Cardona A, Ransohoff RM, Lamb BT, Bhaskar K (2015) Reactive microglia drive tau pathology and contribute to the spreading of pathological tau in the brain. *Brain* 138: 1738-1755
- Marin-Teva JL, Dusart I, Colin C, Gervais A, van Rooijen N, Mallat M (2004) Microglia promote the death of developing Purkinje cells. *Neuron* 41: 535-547

## References

---

- Masters CL, Bateman R, Blennow K, Rowe CC, Sperling RA, Cummings JL (2015) Alzheimer's disease. *Nat Rev Dis Primers* 1: 15056
- Masters CL, Simms G, Weinman NA, Multhaup G, McDonald BL, Beyreuther K (1985) Amyloid plaque core protein in Alzheimer disease and Down syndrome. *Proc Natl Acad Sci U S A* 82: 4245-4249
- Matcovitch-Natan O, Winter DR, Giladi A, Vargas Aguilar S, Spinrad A, Sarrazin S, Ben-Yehuda H, David E, Zelada Gonzalez F, Perrin P *et al* (2016) Microglia development follows a stepwise program to regulate brain homeostasis. *Science* 353: aad8670
- Mathys H, Adaikkan C, Gao F, Young JZ, Manet E, Hemberg M, De Jager PL, Ransohoff RM, Regev A, Tsai LH (2017) Temporal Tracking of Microglia Activation in Neurodegeneration at Single-Cell Resolution. *Cell Rep* 21: 366-380
- Mathys H, Davila-Velderrain J, Peng Z, Gao F, Mohammadi S, Young JZ, Menon M, He L, Abdurrob F, Jiang X *et al* (2019) Single-cell transcriptomic analysis of Alzheimer's disease. *Nature* 570: 332-337
- Mawuenyega KG, Sigurdson W, Ovod V, Munsell L, Kasten T, Morris JC, Yarasheski KE, Bateman RJ (2010) Decreased clearance of CNS beta-amyloid in Alzheimer's disease. *Science* 330: 1774
- Maxson ME, Grinstein S (2014) The vacuolar-type H(+)-ATPase at a glance - more than a proton pump. *J Cell Sci* 127: 4987-4993
- Mazaheri F, Snaidero N, Kleinberger G, Madore C, Daria A, Werner G, Krasemann S, Capell A, Trumbach D, Wurst W *et al* (2017) TREM2 deficiency impairs chemotaxis and microglial responses to neuronal injury. *EMBO Rep* 18: 1186-1198
- McGeer PL, Itagaki S, Tago H, McGeer EG (1987) Reactive microglia in patients with senile dementia of the Alzheimer type are positive for the histocompatibility glycoprotein HLA-DR. *Neurosci Lett* 79: 195-200
- McLay RN, Kimura M, Banks WA, Kastin AJ (1997) Granulocyte-macrophage colony-stimulating factor crosses the blood-brain and blood-spinal cord barriers. *Brain* 120 ( Pt 11): 2083-2091
- McQuade A, Blurton-Jones M (2019) Microglia in Alzheimer's Disease: Exploring How Genetics and Phenotype Influence Risk. *J Mol Biol* 431: 1805-1817
- Meilandt WJ, Ngu H, Gogineni A, Lalehzadeh G, Lee SH, Srinivasan K, Imperio J, Wu T, Weber M, Kruse AJ *et al* (2020) Trem2 Deletion Reduces Late-Stage Amyloid Plaque Accumulation, Elevates the Aβ42:Aβ40 Ratio, and Exacerbates Axonal Dystrophy and Dendritic Spine Loss in the PS2APP Alzheimer's Mouse Model. *J Neurosci* 40: 1956-1974
- Metcalf MJ, Figueiredo-Pereira ME (2010) Relationship between tau pathology and neuroinflammation in Alzheimer's disease. *Mt Sinai J Med* 77: 50-58
- Mittal K, Eremenko E, Berner O, Elyahu Y, Strominger I, Apelblat D, Nemirovsky A, Spiegel I, Monsonego A (2019) CD4 T Cells Induce A Subset of MHCII-Expressing Microglia that Attenuates Alzheimer Pathology. *iScience* 16: 298-311
- Mohamed A, Posse de Chaves E (2011) Aβ internalization by neurons and glia. *Int J Alzheimers Dis* 2011: 127984
- Monier A, Evrard P, Gressens P, Verney C (2006) Distribution and differentiation of microglia in the human encephalon during the first two trimesters of gestation. *J Comp Neurol* 499: 565-582
- Moore Z, Mobilio F, Walker FR, Taylor JM, Crack PJ (2020) Abrogation of type-I interferon signalling alters the microglial response to Aβ1-42. *Sci Rep* 10: 3153

- Morley JE, Farr SA (2012) Hormesis and amyloid-beta protein: physiology or pathology? *J Alzheimers Dis* 29: 487-492
- Morley JE, Farr SA, Banks WA, Johnson SN, Yamada KA, Xu L (2010) A physiological role for amyloid-beta protein: enhancement of learning and memory. *J Alzheimers Dis* 19: 441-449
- Morley JE, Farr SA, Nguyen AD, Xu F (2019) Editorial: What is the Physiological Function of Amyloid-Beta Protein? *J Nutr Health Aging* 23: 225-226
- Motta M, Imbesi R, Di Rosa M, Stivala F, Malaguarnera L (2007) Altered plasma cytokine levels in Alzheimer's disease: correlation with the disease progression. *Immunol Lett* 114: 46-51
- Motte J, Williams RS (1989) Age-related changes in the density and morphology of plaques and neurofibrillary tangles in Down syndrome brain. *Acta Neuropathol* 77: 535-546
- Mucke L, Masliah E, Yu GQ, Mallory M, Rockenstein EM, Tatsuno G, Hu K, Kholodenko D, Johnson-Wood K, McConlogue L (2000) High-level neuronal expression of abeta 1-42 in wild-type human amyloid protein precursor transgenic mice: synaptotoxicity without plaque formation. *J Neurosci* 20: 4050-4058
- Muller UC, Deller T, Korte M (2017) Not just amyloid: physiological functions of the amyloid precursor protein family. *Nat Rev Neurosci* 18: 281-298
- Muller UC, Zheng H (2012) Physiological functions of APP family proteins. *Cold Spring Harb Perspect Med* 2: a006288
- Murphy MP, LeVine H, 3rd (2010) Alzheimer's disease and the amyloid-beta peptide. *J Alzheimers Dis* 19: 311-323
- Naj AC, Jun G, Beecham GW, Wang LS, Vardarajan BN, Buross J, Gallins PJ, Buxbaum JD, Jarvik GP, Crane PK *et al* (2011) Common variants at MS4A4/MS4A6E, CD2AP, CD33 and EPHA1 are associated with late-onset Alzheimer's disease. *Nat Genet* 43: 436-441
- Nimmerjahn A, Kirchhoff F, Helmchen F (2005) Resting microglial cells are highly dynamic surveillants of brain parenchyma in vivo. *Science* 308: 1314-1318
- Oakley H, Cole SL, Logan S, Maus E, Shao P, Craft J, Guillozet-Bongaarts A, Ohno M, Disterhoft J, Van Eldik L *et al* (2006) Intraneuronal beta-amyloid aggregates, neurodegeneration, and neuron loss in transgenic mice with five familial Alzheimer's disease mutations: potential factors in amyloid plaque formation. *J Neurosci* 26: 10129-10140
- Oddo S, Caccamo A, Shepherd JD, Murphy MP, Golde TE, Kaye R, Metherate R, Mattson MP, Akbari Y, LaFerla FM (2003) Triple-transgenic model of Alzheimer's disease with plaques and tangles: intracellular Abeta and synaptic dysfunction. *Neuron* 39: 409-421
- Olah M, Patrick E, Villani AC, Xu J, White CC, Ryan KJ, Piehowski P, Kapasi A, Nejad P, Cimpean M *et al* (2018) A transcriptomic atlas of aged human microglia. *Nat Commun* 9: 539
- Ott A, Stolk RP, van Harskamp F, Pols HA, Hofman A, Breteler MM (1999) Diabetes mellitus and the risk of dementia: The Rotterdam Study. *Neurology* 53: 1937-1942
- Paolicelli RC, Bergamini G, Rajendran L (2019) Cell-to-cell Communication by Extracellular Vesicles: Focus on Microglia. *Neuroscience* 405: 148-157
- Parachikova A, Agadjanyan MG, Cribbs DH, Blurton-Jones M, Perreau V, Rogers J, Beach TG, Cotman CW (2007) Inflammatory changes parallel the early stages of Alzheimer disease. *Neurobiol Aging* 28: 1821-1833

## References

---

- Paresce DM, Chung H, Maxfield FR (1997) Slow degradation of aggregates of the Alzheimer's disease amyloid beta-protein by microglial cells. *J Biol Chem* 272: 29390-29397
- Parhizkar S, Arzberger T, Brendel M, Kleinberger G, Deussing M, Focke C, Nuscher B, Xiong M, Ghasemigharagoz A, Katzmarski N *et al* (2019) Loss of TREM2 function increases amyloid seeding but reduces plaque-associated ApoE. *Nat Neurosci* 22: 191-204
- Park MH, Lee M, Nam G, Kim M, Kang J, Choi BJ, Jeong MS, Park KH, Han WH, Tak E *et al* (2019) N,N'-Diacetyl-p-phenylenediamine restores microglial phagocytosis and improves cognitive defects in Alzheimer's disease transgenic mice. *Proc Natl Acad Sci U S A* 116: 23426-23436
- Parkhurst CN, Yang G, Ninan I, Savas JN, Yates JR, 3rd, Lafaille JJ, Hempstead BL, Littman DR, Gan WB (2013) Microglia promote learning-dependent synapse formation through brain-derived neurotrophic factor. *Cell* 155: 1596-1609
- Pearson HA, Peers C (2006) Physiological roles for amyloid beta peptides. *J Physiol* 575: 5-10
- Perez-Nievas BG, Stein TD, Tai HC, Dols-Icardo O, Scotton TC, Barroeta-Espar I, Fernandez-Carballo L, de Munain EL, Perez J, Marquie M *et al* (2013) Dissecting phenotypic traits linked to human resilience to Alzheimer's pathology. *Brain* 136: 2510-2526
- Perez-Riverol Y, Csordas A, Bai J, Bernal-Llinares M, Hewapathirana S, Kundu DJ, Inuganti A, Griss J, Mayer G, Eisenacher M *et al* (2019) The PRIDE database and related tools and resources in 2019: improving support for quantification data. *Nucleic Acids Res* 47: D442-D450
- Piers TM, Cosker K, Mallach A, Johnson GT, Guerreiro R, Hardy J, Pocock JM (2020) A locked immunometabolic switch underlies TREM2 R47H loss of function in human iPSC-derived microglia. *FASEB J* 34: 2436-2450
- Poepsel S, Sprengel A, Sacca B, Kaschani F, Kaiser M, Gatsogiannis C, Raunser S, Clausen T, Ehrmann M (2015) Determinants of amyloid fibril degradation by the PDZ protease HTRA1. *Nat Chem Biol* 11: 862-869
- Pomilio C, Gorjod RM, Riudavets M, Vinuesa A, Presa J, Gregosa A, Bentivegna M, Alaimo A, Alcon SP, Sevlever G *et al* (2020) Microglial autophagy is impaired by prolonged exposure to beta-amyloid peptides: evidence from experimental models and Alzheimer's disease patients. *Geroscience* 42: 613-632
- Prado F, Jimeno-Gonzalez S, Reyes JC (2017) Histone availability as a strategy to control gene expression. *RNA Biol* 14: 281-286
- Prinz M, Jung S, Priller J (2019) Microglia Biology: One Century of Evolving Concepts. *Cell* 179: 292-311
- Puzzo D, Privitera L, Fa M, Staniszewski A, Hashimoto G, Aziz F, Sakurai M, Ribe EM, Troy CM, Mercken M *et al* (2011) Endogenous amyloid-beta is necessary for hippocampal synaptic plasticity and memory. *Ann Neurol* 69: 819-830
- Raben N, Puertollano R (2016) TFEB and TFE3: Linking Lysosomes to Cellular Adaptation to Stress. *Annu Rev Cell Dev Biol* 32: 255-278
- Radde R, Bolmont T, Kaeser SA, Coomaraswamy J, Lindau D, Stoltze L, Calhoun ME, Jaggi F, Wolburg H, Gengler S *et al* (2006) Abeta42-driven cerebral amyloidosis in transgenic mice reveals early and robust pathology. *EMBO Rep* 7: 940-946
- Ramsden M, Kotilinek L, Forster C, Paulson J, McGowan E, SantaCruz K, Guimaraes A, Yue M, Lewis J, Carlson G *et al* (2005) Age-dependent neurofibrillary tangle formation, neuron loss, and memory impairment in a mouse model of human tauopathy (P301L). *J Neurosci* 25: 10637-10647

- Rangaraju S, Dammer EB, Raza SA, Gao T, Xiao H, Betarbet R, Duong DM, Webster JA, Hales CM, Lah JJ *et al* (2018) Quantitative proteomics of acutely-isolated mouse microglia identifies novel immune Alzheimer's disease-related proteins. *Mol Neurodegener* 13: 34
- Reed-Geaghan EG, Savage JC, Hise AG, Landreth GE (2009) CD14 and toll-like receptors 2 and 4 are required for fibrillar A $\beta$ -stimulated microglial activation. *J Neurosci* 29: 11982-11992
- Regan P, McClean PL, Smyth T, Doherty M (2019) Early Stage Glycosylation Biomarkers in Alzheimer's Disease. *Medicines (Basel)* 6
- Reshef R, Kudryavitskaya E, Shani-Narkiss H, Isaacson B, Rimmerman N, Mizrahi A, Yirmiya R (2017) The role of microglia and their CX3CR1 signaling in adult neurogenesis in the olfactory bulb. *Elife* 6
- Reu P, Khosravi A, Bernard S, Mold JE, Salehpour M, Alkass K, Perl S, Tisdale J, Possnert G, Druid H *et al* (2017) The Lifespan and Turnover of Microglia in the Human Brain. *Cell Rep* 20: 779-784
- Ricciarelli R, Fedele E (2017) The Amyloid Cascade Hypothesis in Alzheimer's Disease: It's Time to Change Our Mind. *Curr Neuropharmacol* 15: 926-935
- Ridwan S, Bauer H, Frauenknecht K, von Pein H, Sommer CJ (2012) Distribution of granulocyte-monocyte colony-stimulating factor and its receptor alpha-subunit in the adult human brain with specific reference to Alzheimer's disease. *J Neural Transm (Vienna)* 119: 1389-1406
- Ries M, Sastre M (2016) Mechanisms of A $\beta$  Clearance and Degradation by Glial Cells. *Front Aging Neurosci* 8: 160
- Río-Hortega Pd (1919a) El "Tercer Elemento de los Centros Nerviosos". II. Intervención de la Microglía en los Procesos Patológicos (Células en Bastoncito y Cuerpos Gránuloadiposos). *Boletín de la Sociedad Española de Biología VIII*: 91-103 (in Spanish)
- Río-Hortega Pd (1919b) El "Tercer Elemento de los Centros Nerviosos". IV. Poder Fagocitario y Movilidad de la Microglía. *Boletín de la Sociedad Española de Biología VIII*: 154-171 (in Spanish)
- Río-Hortega Pd (1919c) El "Tercer Elemento" de los Centros Nerviosos. I. La Microglía en Estado Normal. *Boletín de la Sociedad Española de Biología VIII*: 67-82 (in Spanish)
- Río-Hortega Pd (1919d) El "Tercer Elemento" de los Centros Nerviosos. III. Naturaleza Probable de la Microglía. *Boletín de la Sociedad Española de Biología VIII*: 108-121 (in Spanish)
- Rivera-Escalera F, Pinney JJ, Owlett L, Ahmed H, Thakar J, Olschowka JA, Elliott MR, O'Banion MK (2019) IL-1 $\beta$ -driven amyloid plaque clearance is associated with an expansion of transcriptionally reprogrammed microglia. *J Neuroinflammation* 16: 261
- Rogers JT, Morganti JM, Bachstetter AD, Hudson CE, Peters MM, Grimmig BA, Weeber EJ, Bickford PC, Gemma C (2011) CX3CR1 deficiency leads to impairment of hippocampal cognitive function and synaptic plasticity. *J Neurosci* 31: 16241-16250
- Roy ER, Wang B, Wan YW, Chiu G, Cole A, Yin Z, Propson NE, Xu Y, Jankowsky JL, Liu Z *et al* (2020) Type I interferon response drives neuroinflammation and synapse loss in Alzheimer disease. *J Clin Invest* 130: 1912-1930
- Ruef C, Coleman DL (1990) Granulocyte-macrophage colony-stimulating factor: pleiotropic cytokine with potential clinical usefulness. *Rev Infect Dis* 12: 41-62

## References

---

- Sadleir KR, Kandalepas PC, Buggia-Prevot V, Nicholson DA, Thinakaran G, Vassar R (2016) Presynaptic dystrophic neurites surrounding amyloid plaques are sites of microtubule disruption, BACE1 elevation, and increased A $\beta$  generation in Alzheimer's disease. *Acta Neuropathol* 132: 235-256
- Saido T, Leissring MA (2012) Proteolytic degradation of amyloid beta-protein. *Cold Spring Harb Perspect Med* 2: a006379
- Saido TC, Iwatsubo T, Mann DM, Shimada H, Ihara Y, Kawashima S (1995) Dominant and differential deposition of distinct beta-amyloid peptide species, A $\beta$  N3(pE), in senile plaques. *Neuron* 14: 457-466
- Saito T, Matsuba Y, Mihira N, Takano J, Nilsson P, Itohara S, Iwata N, Saido TC (2014) Single App knock-in mouse models of Alzheimer's disease. *Nat Neurosci* 17: 661-663
- Saito T, Saido TC (2018) Neuroinflammation in mouse models of Alzheimer's disease. *Clin Exp Neuroimmunol* 9: 211-218
- Sala Frigerio C, Wolfs L, Fattorelli N, Thrupp N, Voytyuk I, Schmidt I, Mancuso R, Chen WT, Woodbury ME, Srivastava G *et al* (2019) The Major Risk Factors for Alzheimer's Disease: Age, Sex, and Genes Modulate the Microglia Response to A $\beta$  Plaques. *Cell Rep* 27: 1293-1306 e1296
- Salloway S, Sperling R, Fox NC, Blennow K, Klunk W, Raskind M, Sabbagh M, Honig LS, Porsteinsson AP, Ferris S *et al* (2014) Two phase 3 trials of bapineuzumab in mild-to-moderate Alzheimer's disease. *N Engl J Med* 370: 322-333
- Santacruz K, Lewis J, Spire T, Paulson J, Kotilinek L, Ingelsson M, Guimaraes A, DeTure M, Ramsden M, McGowan E *et al* (2005) Tau suppression in a neurodegenerative mouse model improves memory function. *Science* 309: 476-481
- Sarlus H, Heneka MT (2017) Microglia in Alzheimer's disease. *J Clin Invest* 127: 3240-3249
- Sasaki Y, Ohsawa K, Kanazawa H, Kohsaka S, Imai Y (2001) Iba1 is an actin-cross-linking protein in macrophages/microglia. *Biochem Biophys Res Commun* 286: 292-297
- Schabitz WR, Kruger C, Pitzer C, Weber D, Laage R, Gassler N, Aronowski J, Mier W, Kirsch F, Dittgen T *et al* (2008) A neuroprotective function for the hematopoietic protein granulocyte-macrophage colony stimulating factor (GM-CSF). *J Cereb Blood Flow Metab* 28: 29-43
- Schedin-Weiss S, Winblad B, Tjernberg LO (2014) The role of protein glycosylation in Alzheimer disease. *FEBS J* 281: 46-62
- Schenk D, Barbour R, Dunn W, Gordon G, Grajeda H, Guido T, Hu K, Huang J, Johnson-Wood K, Khan K *et al* (1999) Immunization with amyloid-beta attenuates Alzheimer-disease-like pathology in the PDAPP mouse. *Nature* 400: 173-177
- Schlachetzki JC, Hull M (2009) Microglial activation in Alzheimer's disease. *Curr Alzheimer Res* 6: 554-563
- Schlepckow K, Monroe KM, Kleinberger G, Cantuti-Castelvetri L, Parhizkar S, Xia D, Willem M, Werner G, Pettkus N, Brunner B *et al* (2020) Enhancing protective microglial activities with a dual function TREM2 antibody to the stalk region. *EMBO Mol Med* 12: e11227
- Scholtzova H, Kascsak RJ, Bates KA, Boutajangout A, Kerr DJ, Meeker HC, Mehta PD, Spinner DS, Wisniewski T (2009) Induction of toll-like receptor 9 signaling as a method for ameliorating Alzheimer's disease-related pathology. *J Neurosci* 29: 1846-1854

- Sebastian Monasor L, Muller SA, Colombo AV, Tanriover G, Konig J, Roth S, Liesz A, Berghofer A, Piechotta A, Prestel M *et al* (2020) Fibrillar Abeta triggers microglial proteome alterations and dysfunction in Alzheimer mouse models. *Elife* 9
- Selkoe DJ (2001) Alzheimer's disease: genes, proteins, and therapy. *Physiol Rev* 81: 741-766
- Selkoe DJ, Hardy J (2016) The amyloid hypothesis of Alzheimer's disease at 25 years. *EMBO Mol Med* 8: 595-608
- Selkoe DJ, Schenk D (2003) Alzheimer's disease: molecular understanding predicts amyloid-based therapeutics. *Annu Rev Pharmacol Toxicol* 43: 545-584
- Serrano-Pozo A, Mielke ML, Gomez-Isla T, Betensky RA, Growdon JH, Frosch MP, Hyman BT (2011) Reactive glia not only associates with plaques but also parallels tangles in Alzheimer's disease. *Am J Pathol* 179: 1373-1384
- Sevigny J, Chiao P, Bussiere T, Weinreb PH, Williams L, Maier M, Dunstan R, Salloway S, Chen T, Ling Y *et al* (2016) The antibody aducanumab reduces Abeta plaques in Alzheimer's disease. *Nature* 537: 50-56
- Shaftel SS, Kyrkanides S, Olschowka JA, Miller JN, Johnson RE, O'Banion MK (2007) Sustained hippocampal IL-1 beta overexpression mediates chronic neuroinflammation and ameliorates Alzheimer plaque pathology. *J Clin Invest* 117: 1595-1604
- Shibata M, Yamada S, Kumar SR, Calero M, Bading J, Frangione B, Holtzman DM, Miller CA, Strickland DK, Ghiso J *et al* (2000) Clearance of Alzheimer's amyloid-ss(1-40) peptide from brain by LDL receptor-related protein-1 at the blood-brain barrier. *J Clin Invest* 106: 1489-1499
- Shie FS, Nivison M, Hsu PC, Montine TJ (2009) Modulation of microglial innate immunity in Alzheimer's disease by activation of peroxisome proliferator-activated receptor gamma. *Curr Med Chem* 16: 643-651
- Shirotani K, Tomioka M, Kremmer E, Haass C, Steiner H (2007) Pathological activity of familial Alzheimer's disease-associated mutant presenilin can be executed by six different gamma-secretase complexes. *Neurobiol Dis* 27: 102-107
- Shultz SR, Tan XL, Wright DK, Liu SJ, Semple BD, Johnston L, Jones NC, Cook AD, Hamilton JA, O'Brien TJ (2014) Granulocyte-macrophage colony-stimulating factor is neuroprotective in experimental traumatic brain injury. *J Neurotrauma* 31: 976-983
- Sierksma A, Lu A, Mancuso R, Fattorelli N, Thrupp N, Salta E, Zoco J, Blum D, Buee L, De Strooper B *et al* (2020) Novel Alzheimer risk genes determine the microglia response to amyloid-beta but not to TAU pathology. *EMBO Mol Med* 12: e10606
- Sierra A, de Castro F, Del Rio-Hortega J, Rafael Iglesias-Rozas J, Garrosa M, Kettenmann H (2016) The "Big-Bang" for modern glial biology: Translation and comments on Pio del Rio-Hortega 1919 series of papers on microglia. *Glia* 64: 1801-1840
- Sierra A, Encinas JM, Deudero JJ, Chancey JH, Enikolopov G, Overstreet-Wadiche LS, Tsirka SE, Maletic-Savatic M (2010) Microglia shape adult hippocampal neurogenesis through apoptosis-coupled phagocytosis. *Cell Stem Cell* 7: 483-495
- Sims R, van der Lee SJ, Naj AC, Bellenguez C, Badarinarayan N, Jakobsdottir J, Kunkle BW, Boland A, Raybould R, Bis JC *et al* (2017) Rare coding variants in PLCG2, ABI3, and TREM2 implicate microglial-mediated innate immunity in Alzheimer's disease. *Nat Genet* 49: 1373-1384
- Sisodia SS, Koo EH, Beyreuther K, Unterbeck A, Price DL (1990) Evidence that beta-amyloid protein in Alzheimer's disease is not derived by normal processing. *Science* 248: 492-495

## References

---

- Slooter AJ, Cruts M, Kalmijn S, Hofman A, Breteler MM, Van Broeckhoven C, van Duijn CM (1998) Risk estimates of dementia by apolipoprotein E genotypes from a population-based incidence study: the Rotterdam Study. *Arch Neurol* 55: 964-968
- Smith AM, Gibbons HM, Oldfield RL, Bergin PM, Mee EW, Curtis MA, Faull RL, Dragunow M (2013) M-CSF increases proliferation and phagocytosis while modulating receptor and transcription factor expression in adult human microglia. *J Neuroinflammation* 10: 85
- Sole-Domenech S, Cruz DL, Capetillo-Zarate E, Maxfield FR (2016) The endocytic pathway in microglia during health, aging and Alzheimer's disease. *Ageing Res Rev* 32: 89-103
- Soto C (2003) Unfolding the role of protein misfolding in neurodegenerative diseases. *Nat Rev Neurosci* 4: 49-60
- Spangenberg E, Severson PL, Hohsfield LA, Crapsier J, Zhang J, Burton EA, Zhang Y, Spevak W, Lin J, Phan NY *et al* (2019) Sustained microglial depletion with CSF1R inhibitor impairs parenchymal plaque development in an Alzheimer's disease model. *Nat Commun* 10: 3758
- Spangenberg EE, Green KN (2017) Inflammation in Alzheimer's disease: Lessons learned from microglia-depletion models. *Brain Behav Immun* 61: 1-11
- Spangenberg EE, Lee RJ, Najafi AR, Rice RA, Elmore MR, Blurton-Jones M, West BL, Green KN (2016) Eliminating microglia in Alzheimer's mice prevents neuronal loss without modulating amyloid-beta pathology. *Brain* 139: 1265-1281
- Spires-Jones TL, Hyman BT (2014) The intersection of amyloid beta and tau at synapses in Alzheimer's disease. *Neuron* 82: 756-771
- Srinivasan K, Friedman BA, Etxeberria A, Huntley MA, van der Brug MP, Foreman O, Paw JS, Modrusan Z, Beach TG, Serrano GE *et al* (2020) Alzheimer's Patient Microglia Exhibit Enhanced Aging and Unique Transcriptional Activation. *Cell Rep* 31: 107843
- Stalder M, Phinney A, Probst A, Sommer B, Staufenbiel M, Jucker M (1999) Association of microglia with amyloid plaques in brains of APP23 transgenic mice. *Am J Pathol* 154: 1673-1684
- Stark MR (2014) Vertebrate neurogenic placode development: historical highlights that have shaped our current understanding. *Dev Dyn* 243: 1167-1175
- Steiner H, Fukumori A, Tagami S, Okochi M (2018) Making the final cut: pathogenic amyloid-beta peptide generation by gamma-secretase. *Cell Stress* 2: 292-310
- Stevens B, Allen NJ, Vazquez LE, Howell GR, Christopherson KS, Nouri N, Micheva KD, Mehalow AK, Huberman AD, Stafford B *et al* (2007) The classical complement cascade mediates CNS synapse elimination. *Cell* 131: 1164-1178
- Streit WJ, Sammons NW, Kuhns AJ, Sparks DL (2004) Dystrophic microglia in the aging human brain. *Glia* 45: 208-212
- Sturchler-Pierrat C, Abramowski D, Duke M, Wiederhold KH, Mistl C, Rothacher S, Ledermann B, Burki K, Frey P, Paganetti PA *et al* (1997) Two amyloid precursor protein transgenic mouse models with Alzheimer disease-like pathology. *Proc Natl Acad Sci U S A* 94: 13287-13292
- Szepesi Z, Manouchehrian O, Bachiller S, Deierborg T (2018) Bidirectional Microglia-Neuron Communication in Health and Disease. *Front Cell Neurosci* 12: 323

- Tamboli IY, Barth E, Christian L, Siepmann M, Kumar S, Singh S, Tolksdorf K, Heneka MT, Lutjohann D, Wunderlich P *et al* (2010) Statins promote the degradation of extracellular amyloid {beta}-peptide by microglia via stimulation of exosome-associated insulin-degrading enzyme (IDE) secretion. *J Biol Chem* 285: 37405-37414
- Tay TL, Mai D, Dautzenberg J, Fernandez-Klett F, Lin G, Sagar, Datta M, Drougard A, Stempf T, Ardura-Fabregat A *et al* (2017) A new fate mapping system reveals context-dependent random or clonal expansion of microglia. *Nat Neurosci* 20: 793-803
- Thal DR, Rub U, Orantes M, Braak H (2002) Phases of A beta-deposition in the human brain and its relevance for the development of AD. *Neurology* 58: 1791-1800
- Thion MS, Garel S (2020) Microglial ontogeny, diversity and neurodevelopmental functions. *Curr Opin Genet Dev* 65: 186-194
- Tichauer JE, Flores B, Soler B, Eugenin-von Bernhardt L, Ramirez G, von Bernhardt R (2014) Age-dependent changes on TGFbeta1 Smad3 pathway modify the pattern of microglial cell activation. *Brain Behav Immun* 37: 187-196
- Tooyama I, Kimura H, Akiyama H, McGeer PL (1990) Reactive microglia express class I and class II major histocompatibility complex antigens in Alzheimer's disease. *Brain Res* 523: 273-280
- Tsai J, Grutzendler J, Duff K, Gan WB (2004) Fibrillar amyloid deposition leads to local synaptic abnormalities and breakage of neuronal branches. *Nat Neurosci* 7: 1181-1183
- Ulrich JD, Ulland TK, Mahan TE, Nystrom S, Nilsson KP, Song WM, Zhou Y, Reinartz M, Choi S, Jiang H *et al* (2018) ApoE facilitates the microglial response to amyloid plaque pathology. *J Exp Med* 215: 1047-1058
- van Dyck CH (2018) Anti-Amyloid-beta Monoclonal Antibodies for Alzheimer's Disease: Pitfalls and Promise. *Biol Psychiatry* 83: 311-319
- van Groen T, Kadish I, Funke A, Willbold D (2011) Staining of Amyloid Beta (Abeta) Using (Immuno) Histochemical Techniques and Abeta42 Specific Peptides. *Neuroimaging for Clinicians: Combining Research and Practice*: 59
- von Bernhardt R, Cornejo F, Parada GE, Eugenin J (2015) Role of TGFbeta signaling in the pathogenesis of Alzheimer's disease. *Front Cell Neurosci* 9: 426
- Wake H, Moorhouse AJ, Jinno S, Kohsaka S, Nabekura J (2009) Resting microglia directly monitor the functional state of synapses in vivo and determine the fate of ischemic terminals. *J Neurosci* 29: 3974-3980
- Walker DG, Lue LF (2013) Understanding the neurobiology of CD200 and the CD200 receptor: a therapeutic target for controlling inflammation in human brains? *Future Neurol* 8
- Walsh DM, Klyubin I, Fadeeva JV, Cullen WK, Anwyl R, Wolfe MS, Rowan MJ, Selkoe DJ (2002) Naturally secreted oligomers of amyloid beta protein potently inhibit hippocampal long-term potentiation in vivo. *Nature* 416: 535-539
- Wang ML, Motamed M, Infante RE, Abi-Mosleh L, Kwon HJ, Brown MS, Goldstein JL (2010a) Identification of surface residues on Niemann-Pick C2 essential for hydrophobic handoff of cholesterol to NPC1 in lysosomes. *Cell Metab* 12: 166-173
- Wang S, Wang R, Chen L, Bennett DA, Dickson DW, Wang DS (2010b) Expression and functional profiling of neprilysin, insulin-degrading enzyme, and endothelin-converting enzyme in prospectively studied elderly and Alzheimer's brain. *J Neurochem* 115: 47-57

## References

---

- Wang Y, Cella M, Mallinson K, Ulrich JD, Young KL, Robinette ML, Gilfillan S, Krishnan GM, Sudhakar S, Zinselmeyer BH *et al* (2015) TREM2 lipid sensing sustains the microglial response in an Alzheimer's disease model. *Cell* 160: 1061-1071
- Wilcock DM, Rojiani A, Rosenthal A, Levkowitz G, Subbarao S, Alamed J, Wilson D, Wilson N, Freeman MJ, Gordon MN *et al* (2004) Passive amyloid immunotherapy clears amyloid and transiently activates microglia in a transgenic mouse model of amyloid deposition. *J Neurosci* 24: 6144-6151
- Wilkinson BL, Landreth GE (2006) The microglial NADPH oxidase complex as a source of oxidative stress in Alzheimer's disease. *J Neuroinflammation* 3: 30
- Wisniewski HM, Narang HK, Terry RD (1976) Neurofibrillary tangles of paired helical filaments. *J Neurol Sci* 27: 173-181
- Wisniewski JR, Zougman A, Nagaraj N, Mann M (2009) Universal sample preparation method for proteome analysis. *Nat Methods* 6: 359-362
- Wlodarczyk A, Holtman IR, Krueger M, Yogev N, Bruttger J, Khorrooshi R, Benmamar-Badel A, de Boer-Bergsma JJ, Martin NA, Karram K *et al* (2017) A novel microglial subset plays a key role in myelination in developing brain. *EMBO J* 36: 3292-3308
- Wu J, Bie B, Yang H, Xu JJ, Brown DL, Naguib M (2013) Suppression of central chemokine fractalkine receptor signaling alleviates amyloid-induced memory deficiency. *Neurobiol Aging* 34: 2843-2852
- Wylot B, Mieczkowski J, Niedziolka S, Kaminska B, Zawadzka M (2019) Csf1 Deficiency Dysregulates Glial Responses to Demyelination and Disturbs CNS White Matter Remyelination. *Cells* 9
- Wyss-Coray T (2006) Inflammation in Alzheimer disease: driving force, bystander or beneficial response? *Nat Med* 12: 1005-1015
- Wyss-Coray T, Lin C, Yan F, Yu GQ, Rohde M, McConlogue L, Masliah E, Mucke L (2001) TGF-beta1 promotes microglial amyloid-beta clearance and reduces plaque burden in transgenic mice. *Nat Med* 7: 612-618
- Xiang X, Werner G, Bohrmann B, Liesz A, Mazaheri F, Capell A, Feederle R, Knuesel I, Kleinberger G, Haass C (2016) TREM2 deficiency reduces the efficacy of immunotherapeutic amyloid clearance. *EMBO Mol Med* 8: 992-1004
- Xu G, Ran Y, Fromholt SE, Fu C, Yachnis AT, Golde TE, Borchelt DR (2015) Murine Abeta over-production produces diffuse and compact Alzheimer-type amyloid deposits. *Acta Neuropathol Commun* 3: 72
- Yamasaki A, Eimer S, Okochi M, Smialowska A, Kaether C, Baumeister R, Haass C, Steiner H (2006) The GxGD motif of presenilin contributes to catalytic function and substrate identification of gamma-secretase. *J Neurosci* 26: 3821-3828
- Yankner BA, Lu T (2009) Amyloid beta-protein toxicity and the pathogenesis of Alzheimer disease. *J Biol Chem* 284: 4755-4759
- Yeh FL, Wang Y, Tom I, Gonzalez LC, Sheng M (2016) TREM2 Binds to Apolipoproteins, Including APOE and CLU/APOJ, and Thereby Facilitates Uptake of Amyloid-Beta by Microglia. *Neuron* 91: 328-340
- Yoshiyama Y, Higuchi M, Zhang B, Huang SM, Iwata N, Saido TC, Maeda J, Suhara T, Trojanowski JQ, Lee VM (2007) Synapse loss and microglial activation precede tangles in a P301S tauopathy mouse model. *Neuron* 53: 337-351

- Yuan P, Condello C, Keene CD, Wang Y, Bird TD, Paul SM, Luo W, Colonna M, Baddeley D, Grutzendler J (2016) TREM2 Haplodeficiency in Mice and Humans Impairs the Microglia Barrier Function Leading to Decreased Amyloid Compaction and Severe Axonal Dystrophy. *Neuron* 90: 724-739
- Zelcer N, Khanlou N, Clare R, Jiang Q, Reed-Geaghan EG, Landreth GE, Vinters HV, Tontonoz P (2007) Attenuation of neuroinflammation and Alzheimer's disease pathology by liver x receptors. *Proc Natl Acad Sci U S A* 104: 10601-10606
- Zhan Y, Lew AM, Chopin M (2019) The Pleiotropic Effects of the GM-CSF Rheostat on Myeloid Cell Differentiation and Function: More Than a Numbers Game. *Front Immunol* 10: 2679
- Zhan Y, Paolicelli RC, Sforazzini F, Weinhard L, Bolasco G, Pagani F, Vyssotski AL, Bifone A, Gozzi A, Ragozzino D *et al* (2014) Deficient neuron-microglia signaling results in impaired functional brain connectivity and social behavior. *Nat Neurosci* 17: 400-406
- Zhang F, Jiang L (2015) Neuroinflammation in Alzheimer's disease. *Neuropsychiatr Dis Treat* 11: 243-256
- Zhang S, Zhao J, Zhang Y, Zhang Y, Cai F, Wang L, Song W (2019) Upregulation of MIF as a defense mechanism and a biomarker of Alzheimer's disease. *Alzheimers Res Ther* 11: 54
- Zhang Y, Chen K, Sloan SA, Bennett ML, Scholze AR, O'Keefe S, Phatnani HP, Guarnieri P, Caneda C, Ruderisch N *et al* (2014) An RNA-sequencing transcriptome and splicing database of glia, neurons, and vascular cells of the cerebral cortex. *J Neurosci* 34: 11929-11947
- Zhao R, Hu W, Tsai J, Li W, Gan WB (2017) Microglia limit the expansion of beta-amyloid plaques in a mouse model of Alzheimer's disease. *Mol Neurodegener* 12: 47
- Zhong L, Chen XF, Wang T, Wang Z, Liao C, Wang Z, Huang R, Wang D, Li X, Wu L *et al* (2017) Soluble TREM2 induces inflammatory responses and enhances microglial survival. *J Exp Med* 214: 597-607
- Zhong L, Xu Y, Zhuo R, Wang T, Wang K, Huang R, Wang D, Gao Y, Zhu Y, Sheng X *et al* (2019) Soluble TREM2 ameliorates pathological phenotypes by modulating microglial functions in an Alzheimer's disease model. *Nat Commun* 10: 1365
- Zhou Y, Song WM, Andhey PS, Swain A, Levy T, Miller KR, Poliani PL, Cominelli M, Grover S, Gilfillan S *et al* (2020) Human and mouse single-nucleus transcriptomics reveal TREM2-dependent and TREM2-independent cellular responses in Alzheimer's disease. *Nat Med* 26: 131-142
- Zhou Y, Ulland TK, Colonna M (2018) TREM2-Dependent Effects on Microglia in Alzheimer's Disease. *Front Aging Neurosci* 10: 202
- Zuroff L, Daley D, Black KL, Koronyo-Hamaoui M (2017) Clearance of cerebral Abeta in Alzheimer's disease: reassessing the role of microglia and monocytes. *Cell Mol Life Sci* 74: 2167-2201

## List of Figures

Figure 1. AD brain atrophy compared to healthy brain.....	12
Figure 2. APP processing and A $\beta$ plaque formation. ....	13
Figure 3. Main types of extracellular A $\beta$ deposits in human AD brains. ....	15
Figure 4. Neurofibrillary tangles and dystrophic neurite pathology in AD brains.....	16
Figure 5. Microglia and astrocytes cluster around A $\beta$ plaques.....	18
Figure 6. Microglia present a ramified morphology in the adult healthy brain. ....	24
Figure 7. Experimental paradigm of short-term GM-CSF application.....	55
Figure 8. Experimental paradigm of long-term GM-CSF application.....	55
Figure 9. Immunohistological analysis of A $\beta$ burden in APPPS1 and APP-KI mice.....	67
Figure 10. Microglia isolation quality control by FACS.....	68
Figure 11. Consistent protein quantification by mass spectrometry-based proteomic analysis in APPPS1 and APP-KI microglia at 12 months. ....	69
Figure 12. Proteomic analysis of APPPS1 and APP-KI microglia during AD progression.....	71
Figure 13. Classification of MARPs and their dynamics in APPPS1 and APP-KI microglia. ....	73
Figure 14. Early, middle and advanced-MARPs and comparative analysis with the transcriptome. ....	75
Figure 15. Comparison of quantified proteins from APPPS1 and APP-KI microglia with identified single-cell microglial transcripts.....	76
Figure 16. Comparison of total regulated proteins in APPPS1 and APP-KI microglia and identified MARPs signatures with regulated single-cell transcripts.....	77
Figure 17. Gene ontology enrichment analysis of MARPs according to biological processes.....	79
Figure 18. Gene ontology enrichment analysis of MARPs according to cellular compartment and molecular function. ....	80
Figure 19. Selected MARPs were validated by western blot analysis.....	82
Figure 20. CLEC7a shows a greater increase in 3-month-old plaque-associated APPPS1 microglia. ....	83
Figure 21. TREM2 is markedly upregulated in 3-month-old plaque-associated APPPS1 microglia. ....	85
Figure 22. APOE shows a higher upregulation in 3-month-old plaque-associated APPPS1 microglia. ....	86
Figure 23. CLEC7a shows a similar upregulation in 12-month-old APPPS1 and APP-KI plaque-associated microglia. ....	88
Figure 24. TMEM119 shows a similar downregulation in 12-month-old APPPS1 and APP-KI plaque-associated microglia.....	89
Figure 25. APP-KI mice show higher A $\beta$ coverage at 3 months compared to APPPS1.....	90
Figure 26. APPPS1 mice show higher levels of fibrillar A $\beta$ compared to APP-KI mice.....	91
Figure 27. Microglial recruitment is higher in 3-month-old APPPS1 mice and triggered by fibrillar A $\beta$ . ....	93
Figure 28. (previous page) pE3-A $\beta$ is not responsible for microglial recruitment. ....	95
Figure 29. Dystrophic neurites do not correlate with microglial recruitment and proteomic changes.....	95

---

Figure 30. Phagocytosis deficiency correlates with the acquisition of MARP signatures. ....	96
Figure 31. GM-CSF induces A $\beta$ plaque clearance and microglia proliferation in an APP-KI <i>ex vivo</i> model.....	98
Figure 32. Proteomic changes upon short GM-CSF treatment in 5-month-old mice suggest induction of neuroprotective mechanism. ....	99
Figure 33. Short GM-CSF treatment of 5-month-old APP-KI mice did not induce changes in plaque load or proliferation. ....	100
Figure 34. Proteomic changes upon short GM-CSF treatment in 14-month-old mice indicate an induction of DNA reorganization and cell cycle.....	101
Figure 35. (previous page). Short GM-CSF treatment did not change A $\beta$ burden nor induced proliferation in 14-month-old mice. ....	103
Figure 36. Chronic GM-CSF treatment in 4-month-old mice induced only mild microglial proteomic changes related to substrate degradation systems.....	104
Figure 37. Long-term GM-CSF treatment does not induce A $\beta$ clearance or proliferation in 4-month-old APP-KI mice. ....	105
Figure 38. Biochemical analysis of A $\beta$ load confirms the lack of amyloid reduction upon GM-CSF long treatment. ....	106

## List of Tables

Table 1. Transgenic mouse models of AD.....	22
Table 2. List of laboratory equipment and consumables used in this study .....	38
Table 3. List of cell culture equipment and consumables used in this study .....	39
Table 4. Surgical tools used for the preparation of organotypic brain slices and microglia isolation .....	39
Table 5. List of microscopes used in this study .....	39
Table 6. List of mass spectrometry and FACS instruments, consumables and reagents.....	39
Table 7. List of mouse lines utilized in this study .....	40
Table 8. Primers used for genotyping of transgenic mouse lines .....	40
Table 9. Reagents used for genotypic of transgenic mouse lines .....	40
Table 10. Solutions used for genotyping of transgenic mouse lines.....	41
Table 11. Reagents and consumables utilized for <i>in vitro</i> and <i>ex vitro</i> procedures.....	42
Table 12. Solutions used for microglia isolation, culture and phagocytosis assay .....	43
Table 13. Solutions used for preparing, culturing and treating organotypic brain slices .....	43
Table 14. Reagents used for mouse procedures .....	44
Table 15. List of primary antibodies used for immunofluorescence .....	44
Table 16. Solutions utilized for mouse procedures including histology.....	45
Table 17. Reagents used for Western blotting .....	46
Table 18. List of primary antibodies used for protein detection by Western blotting .....	47
Table 19. Solutions used for sample lysis and western blotting .....	49
Table 20. Software tools used in this study.....	49
Table 21. PCR master mix recipe .....	50
Table 22. PCR program used to genotype the APPPS1 line .....	50
Table 23. PCR program used to genotype the APP <sup>NL-G-F</sup> line.....	51
Table 24. Information about mice used for <i>in vivo</i> GM-CSF application study .....	56
Table 25. Details of immunohistological analysis of <i>in vivo</i> GM-CSF treatments.....	59
Table 26. Proteomic data analysis from APPPS1 microglia.....	69
Table 27. Proteomic data analysis from APP-KI microglia.....	69
Table 28. AD risk genes are found altered in APPPS1 and APP-KI microglial proteome.....	81
Table 29. Significantly regulated microglial proteins upon short-GM-CSF treatment in 5-month-old APP-KI mice. ....	129
Table 30. Significantly regulated microglial proteins upon short-GM-CSF treatment in 14-month-old APP-KI mice. ....	133
Table 31. Significantly regulated microglial proteins upon long-GM-CSF treatment in 4-month-old APP-KI mice. ....	134

## List of Abbreviations

AACS	Acetoacetyl-CoA synthetase
A $\beta$	Amyloid- $\beta$ peptide
A2M	Alpha 2 macroglobulin
ABCA7	ATP-binding cassette, sub-family A, member 7
ABCD2	ATP-binding cassette sub-family D member 2
ABI3	ABI family member 3
ACE	Angiotensin I converting enzyme
ACOX3	Peroxisomal acyl-coenzyme A oxidase 3
ACSBG1	Long-chain-fatty-acid--CoA ligase ACSBG1
ACSS2	Acetyl-coenzyme A synthetase
ACTN1/4	Alpha actinin 1/4
ACTR3B	Actin-related protein 3B
AD	Alzheimer's disease
ADAD	Autosomal dominant Alzheimer's disease
ADP	Adenosine diphosphate
AICD	Amyloid precursor protein intracellular domain
ALDOA	Fructose-bisphosphate aldolase A
ALS	Amyotrophic lateral sclerosis
APC	Antigen-presenting cell
APH1	Anterior pharynx-defective 1
APOD	Apolipoprotein D
APOE	Apolipoprotein E
APP	Amyloid precursor protein
APS	Ammonium persulfate
ATP	Adenosine triphosphate
ATP6V	V-type proton ATPase
B2M	Beta 2 microglobulin
BACE1	$\beta$ -site APP-Cleaving Enzyme
BBB	Blood brain barrier
BCA	Bicinchoninic acid
BDNF	Brain-derived neurotrophic factor
BIN1/2	Myc box-dependent-interacting protein 1/2
BP	Biological processes
BrdU	5-Bromo-2'-deoxyuridine
BSA	Bovine serum albumin
C1q/3b	Complement component 1q/3b
CAA	Cerebral amyloid angiopathy

List of Abbreviations

---

CC	Celullar compartment
CCDC88A	Girdin
CCR5	C-C chemokine receptor type 5
CD	Cluster of differentiation molecule
CD11b	Cluster of differentiation molecule 11B
CD33/ SIGLEC3	Sialic acid-binding immunoglobulin (ig)-like lectin
CD200	OX-2 membrane glycoprotein
CD200R	Cell surface glycoprotein CD200 receptor 1
CDC42BPB	Serine/threonine-protein kinase MRCK beta
CDK6	Cyclin-dependent kinase 6
CFL1	Cofilin-1
CHI3L1	Chitinase 3 like 1
CLEC4a3/5a/7a	C-type lectin receptor 4a3/5a/7a
CLN3	Ceroid-Lipofuscinosis, Neuronal 3
CLU/APOJ	Clusterin
CNN2	Calponin-2
CNS	Central nervous system
COG2	Conserved oligomeric Golgi complex subunit 2
CR1	Complement receptor type 1
CSF	Cerebrospinal fluid
CSF1/M-CSF1	Colony stimulating factor 1/Macrophage colony stimulating factor
CSF1R	Colony stimulating factor 1 receptor
CST7	Cystatin F
CTF	C-terminal fragment
CTSB/D/H/Z	Cathepsin B/D/H/Z
CX3CL1	C-X3-C motif chemokine ligand 1
CX3CR1	C-X3-C motif chemokine receptor 1
CYBB/ NOX2	Cytochrome b-245 heavy chain
CytoD	Cytochalasin D
DAM	Disease-associated microglia
DAMPs	damage-associated molecular patterns
DDA	Data dependent acquisition
DEA	Diethylamine
DIA	Data independent acquisition
DMEM	Dulbecco's modified eagle medium
DMSO	Dimethylsulfoxide
DNA	Deoxyribonucleic acid
dNTP	Deoxynucleotide
E7.5	Embryonic day 7.5
E.coli	<i>Escherichia coli</i>

ECE1	Endothelin converting enzyme 1
ECHS1	Enoyl-CoA hydratase, mitochondrial
EDTA	Ethylenediaminetetraacetic acid
ELOVL1	Elongation of very long chain fatty acids protein 1
ENO1	Alpha-enolase
EOAD	Early-onset Alzheimer's disease
EPHX1	Epoxide hydrolase 1
FA	Formic acid
FABP3/5	Fatty acid-binding protein 3/5
FACS	Fluorescence-activated cell sorting
FAD	Familial Alzheimer's disease
FASN	Fatty acid synthase
FcR	Fc receptor
FCRLS	Fc receptor-like S
FCS	Fetal calf serum
FDR	False discovery rate
FER	FER tyrosine kinase
FSC-H/A	forward scatter height/area
FSCN1	Fascin
GAPDH	Glyceraldehyde 3 phosphate dehydrogenase
GCA	Grancalcin
GFAP	Glial fibrillary acidic protein
GLB1	Beta-galactosidase
GM-CSF	Granulocyte macrophage colony stimulating factor
GM-CSFR $\alpha/\beta$	Granulocyte macrophage colony stimulating factor receptor $\alpha/\beta$
GNG2/5/10	Guanine nucleotide-binding protein G(I)/G(S)/G(O) subunit gamma-2/5/10
GO	Gene ontology
GPI	Glucose-6-phosphate isomerase
GPR34	Probable G-protein coupled receptor 34
GVIN1	Interferon-induced very large GTPase 1
GWAS	Genome-wide association-studies
GYS1	Glycogen [starch] synthase, muscle
H2-D1	H-2 class I histocompatibility antigen, D-B alpha chain
H2-K1	H-2 class I histocompatibility antigen, K-B alpha chain
H3F3	Histone H3.3
HACD2	Very-long-chain (3R)-3-hydroxyacyl-CoA dehydratase 2
HEXA/B	Hexosaminidase subunit A/B
HBSS	Hanks's buffered salt solution
HIST1H2A	Histone H2A
HIST1H2B	Histone H2B

HOE	Hoechst
HPCAL1	Hippocalcin-like protein 4
HPF1	Histone PARylation factor 1
HRAS	GTPase Hras
HRP	Horse radish peroxidase
HSD17B12	Very-long-chain 3-oxoacyl-CoA reductase
HTRA1	High-Temperature Requirement A Serine Peptidase 1
IBA1/AIF1	Ionized calcium-binding adapter molecule 1
IDE	Insulin-degrading enzyme
IFI204	Interferon-activable protein 204
IFIT2/3	Interferon-induced protein with tetratricopeptide repeats 2/3
IFN	Interferon
IL-1 $\alpha$ / $\beta$	Interleukin-1 $\alpha$ / $\beta$
IL-6/34	Interleukin-6/34
INPP5D	Inositol polyphosphate-5-phosphatase D
i.p.	Intraperitoneal
IRF8	Interferon regulatory factor 8
ISG15	Ubiquitin-like protein ISG15
ITGAX /CD11c	Integrin alpha X
KDa	Kilodalton
KI	Knock-in
LFQ	label-free quantification
LGALS3	Galectin 3
LGALS3BP	Galectin 3 binding protein
LOAD	Late-onset Alzheimer's disease
LPL	Lipoprotein lipase
LRP1	Low density lipoprotein receptor-related protein 1
LYN	Tyrosine-protein kinase Lyn
MACS	Magnetic activated cell sorting
MAP	Microtubule-associated protein
MAPT	Microtubule-associated protein tau
MARCKS	Myristoylated alanine-rich C-kinase substrate
MARPs	Microglial A $\beta$ response proteins
MCM3/5	DNA replication licensing factor MCM3/5
MEM	Minimum essential medium
MF	Molecular function
MGnD	Microglial neurogenerative phenotype
MHC	Major histocompatibility complex
MHC-II	Major histocompatibility complex class II
MIF	Macrophage migration inhibitory factor

MMP9	Matrix metalloproteinase 9
MNDA	Myeloid cell nuclear differentiation antigen
MRAS	Ras-related protein M-Ras
MS	Multiple sclerosis
MS'	Mass spectrometry
MS4A	Membrane-spanning 4-domains, subfamily A
MYO5A	Unconventional myosin-Va
NADPH	Nicotinamide adenine dinucleotide phosphate
NCAN	Neurocan core protein
NCE	normalized collision energy
NCEH1	Neutral cholesterol ester hydrolase 1
NEP	Neutral endopeptidase, Neprilysin
NFT	Neurofibrillary tangles
NPC1/2	Niemann-Pick Disease Type C1/2
NRAS	GTPase NRas
n.s.	Not significant
OAS1A	2'-5'-oligoadenylate synthase 1A
O.C.T	Optimal cutting temperature
OLFML3	Olfactomedin like 3
P2RY12/13/6	Purinergic receptor 12/13/6
PBS	Phosphate-buffered saline
PAMPs	Pathogen-associated molecular patterns
PCNA	Proliferating cell nuclear antigen
PCR	Polymerase chain reaction
PDGF- $\beta$	Platelet-derived growth factor subunit $\beta$
PDLIM4/5	PDZ and LIM domain protein 4/5
pE3-A $\beta$	Pyroglutamate A $\beta$
PEN2	Presenilin enhancer 2
PET	Positron-emission tomography
PFA	Paraformaldehyde
PFKL	ATP-dependent 6-phosphofructokinase, liver type
PGAM1/2	Phosphoglycerate mutase 1/2
PGK1	Phosphoglycerate kinase 1
PGM1	Phosphoglucomutase-1
PHF	Paired helical filaments
PI	Propidium Iodide
PIK3R5	Phosphoinositide 3-kinase regulatory subunit 5
PKM	Pyruvate kinase PKM
PLCB3/G2	1-phosphatidylinositol 4,5-bisphosphate phosphodiesterase beta-3/ gamma-2

PreP	Presequence peptidase
PrP	Prion protein
PRRs	pattern-recognition receptors
PS1/2	Presenilin 1/2 (protein)
PSEN	Presenilin (gene)
PXN	PXN
RAC3	Ras-related C3 botulinum toxin substrate 2
RAGE	Receptors for advanced glycation end products
RNA	Ribonucleic acid
ROI	Region of interest
ROS	Reactive oxygen species
RPL38	60S ribosomal protein L38
RT	Room temperature
RUNX1	Runt-related transcription factor 1
SAD	Sporadic Alzheimer's disease
SALL1	Spalt like transcription factor 1
s.c.	Subcutaneous
SD	Standard deviation
SIGLECH	Sialic acid binding Ig-like lectin H
SMAD1/2/3	Mothers against decapentaplegic homolog 1/2/3
SNP	Single nucleotide polymorphism
snRNA	Single-nucleus RNA sequencing
SORL1	Sortilin-related receptor 1
SPARCL1	SPARC-like protein 1
SPI1/PU.1	Spi-1 proto-oncogene/ Transcription factor PU.1
SPP1	Secreted phosphoprotein 1
SR	Scavenger receptors
STAT1/2	Signal transducer and activator of transcription 1
SYK	Tyrosine protein kinase SYK
TAE	Tris-acetate EDTA
TAP2	Antigen peptide transporter 2
TAPBP	TAP binding protein/Tapasin
TBS	Tris base
TEMED	Tetramethylethylenediamin
TFE3	Transcription factor E3
TFEB	Transcription factor EB
TGF- $\beta$	Transforming growth factor- $\beta$
TGFBR1/2	Transforming growth factor- $\beta$ receptor 1
ThR	Thiazine red
Thy-1	Thy-1 membrane glycoprotein

---

TIGAR	Fructose-2,6-bisphosphatase TIGAR
TLR	Toll like receptors
TMEM119	Transmembrane Protein 119
TNF	Tumor necrosis factor
TPI1	Triosephosphate isomerase
TREM2	Triggering receptor expressed on myeloid cells 2
TRIOBP	TRIO and F-actin-binding protein
TTYH1	Protein tweety homolog 1
TYROBP	TYRO protein tyrosine kinase-binding protein
UDP	Uridine diphosphate
VAV2	Guanine nucleotide exchange factor VAV2
WT	Wild type

\* Protein abbreviation descriptions from the proteome dataset of microglia isolated from GM-CSF-treated mice can be found in appendix section 1.

## Acknowledgements

First of all, I would like to express my most sincere gratitude to my supervisor, Dr. Sabina Tahirovic, for trusting, supporting and guiding me throughout my PhD journey. Your contagious enthusiasm for research has been a great motivation and I have really enjoyed and learned doing and discussing science with you. Thank you for being always available for me, but also for letting and encouraging me to develop myself as a scientist.

I would also like to thank the members of my thesis advisor committee, Prof. Dieter Edbauer, Prof. Jürgen Bernhagen and Prof. Jochen Herms, for their support and input to my PhD project along these years. Special thanks to Prof. Dieter Edbauer for also reviewing my written thesis and evaluating my defense. Even if it has still not been approved at the time of printing this thesis, I would like to thank Dr. Annett Halle for agreeing on evaluating my thesis and defense, and Prof. Arthur Liesz for accepting to evaluate my defense.

I want to express my gratitude to the Graduate School of Systemic Neuroscience for providing a great structure for scientific enrichment and social interaction, and for their always warm support and help when was needed.

I would also like to thank all the collaborators that have contributed to this project, and from whom I have greatly learned. Special thanks to Prof. Stefan Lichtenthaler and particularly, to Dr. Stephan Müller, because without their expertise, this project would not have been so fruitful. Big thanks also to Dr. Stefan Roth, for being always willing to help and have the patient to teach me. I would also like to express my appreciation to Prof. Christian Haass and the people from his department, especially to Dr. Michael Willem, for our lively discussions and input to my project. Many thanks to the people from the animal facility, especially for all the help during my *in vivo* experiments. Also, many thanks to Benno, Sabine, Anke and Marcel for all the help during these years.

I feel tremendously grateful to have had such great colleagues during my PhD journey. Thank you, Alessio, for your endless advices and help and your (sometimes weird) sense of humor that made me always laugh. Thank you, Lina, for being the sweetest colleague, for all your help and support and for being the “happiness” of the lab. Thanks, Jasi, for being always willing to help and support and for making boring protocols fun. Also big thanks to my former colleague Anna Daria, for your patience teaching me during my first months as a PhD student. Thank you, Johannina and Mar, for our lunches and dinners of gossips and laughs. Thanks, Judit, for making

me laugh and being “my dramitas”. Many thanks to all my wonderful colleagues from the Lichtenthaler lab, Göki, Johannina, Georg, Ben, Andree (Chungo), Kathrin, Stephan, Hung-En, Anna, Juli, Jakob, Martina, Merav, Simo, Tobi, Fabi and many others, who adopted me as one more of them from my very first day in the lab, and made me feel always integrated and supported. Thanks for all the coffee and lunch breaks together and all the fun moments inside and outside the lab. I would also like to thank my colleagues from the Herms lab, especially to Jose, Tanja, Kathrin, Carmelo and Katharina, for being always nice and helpful. Special thanks to my dearest friend Jose, for being one of my pillars during my PhD time, for always cheering me up and caring for me, and for our “gordo” moments of chocolate and laughs.

Big thanks to my Spanish family in Munich, for making me feel like at home, specially to my good friend Julita, for always being there for me, cheering me up and for all the moments of joy and tears that we have shared together. Also special thanks to my friend Belén, with whom I started the PhD journey. Thank you for, even from the distance, always caring for me.

I have not enough words to thank my, now husband, Diego. Thank you for your infinite patience, for always being there for me and cheering me up in my toughest moments, but also, for sharing the happiness of my achievements. Your trust on me has always been my biggest support. Also, big thanks to my dearest friends in Spain, Inés, Tamara, Arantxa, Josefina, Estela y María, for your love and support that I always carry with me, even when living far away.

Finally, thanks to my family, for your unconditional support and love and for making me believe that I can achieve anything. Gracias familia, por vuestro apoyo incondicional, por estar siempre ahí para mí y por confiar en que puedo conseguir cualquier cosa que me proponga. Este triunfo os lo debo, en gran parte, a vosotros.

## Affidavit/Eidesstattliche Versicherung

I hereby confirm that the dissertation „**Proteomic characterization of microglial dysfunction and repair mechanisms in Alzheimer’s disease**“ is the result of my own work and that I have only used sources or materials listed and specified in the dissertation.

*Hiermit versichere ich an Eides statt, dass ich die vorliegende Dissertation „**Proteomic characterization of microglial dysfunction and repair mechanisms in Alzheimer’s disease**“ selbstständig angefertigt habe, mich außer der angegebenen keiner weiteren Hilfsmittel bedient und alle Erkenntnisse, die aus dem Schrifttum ganz oder annähernd übernommen sind, als solche kenntlich gemacht und nach ihrer Herkunft unter Bezeichnung der Fundstelle einzeln nachgewiesen habe.*

2.10.2020

Laura Sebastián Monasor

Munich, date/*München, den*

Signature/*Unterschrift*

## Author contributions

We hereby declare that the following authors contributed to the data presented in this study as following specified:

Dr. Sabina Tahirovic and Laura Sebastián Monasor, together with Dr. Stephan Müller and Prof. Stefan Lichtenthaler, designed the proteomic study from APPPS1 and APP-KI mice. Dr. Sabina Tahirovic and Laura Sebastián Monasor designed the GM-CSF *in vivo* study.

Dr. Stephan Müller, co-first author in (Sebastian Monasor *et al.*, 2020), performed the mass spectrometry-based proteomic analysis of microglia from APPPS1 and APP-KI mice and also from GM-CSF-treated APP-KI mice. In addition, he performed the GO analysis from proteomic data. Anna Berghofer assisted in the processing of microglial samples for the mass spectrometry analysis.

Dr. Alessio Colombo contributed to the isolation of microglia from the APPPS1 mouse model for proteomic analysis.

Dr. Stefan Roth assisted with the acquisition of FACS data from microglial phagocytosis assay and processed FACS acquired data with the FlowJo software.

Dr. Michael Willem with the assistance of Heike Hampel performed the western blot analysis of fibrillar A $\beta$  from APPPS1 and APP-KI mice.

Alison Morningstar isolated microglia from 14-15-month-old mice for proteomic candidate validation and assisted with the western blot analysis of SYK and p-SYK proteins.

All other experiments, including samples isolation, processing, imaging acquisition and data analysis were performed by Laura Sebastián Monasor.

Yours sincerely,

Place, Date

Munich, 2.10.2020

Laura Sebastián Monasor

Dr. Stephan Müller

Dr. Sabina Tahirovic